SCUOLA DI DOTTORATO
UNIVERSITÀ DEGLI STUDI DI MILANO-BICOCCA

Department of Earth and Environmental Sciences

PhD in Chemical, Geological and Environmental Sciences

Cycle XXXV

Curriculum: Geological Sciences

Sand provenance and dispersal in the Sahara and Kalahari deserts: fluvial aeolian interactions and climatic implications

Guido Pastore

Registration number 769265

Tutor: Prof. Eduardo Garzanti

Supervisor: Prof. Alberto Resentini

Coordinator: Prof. Marco Giovanni Malusà

ACADEMIC YEAR 2022

Abstract

This thesis presents a study of the composition of sand from desert dunes and adjacent rivers across the African continent to illustrate the effects of the interplay between fluvial and aeolian processes on sediment transport in desertic environments. Deciphering the role of wind and river transport in arid climates is an essential step not only for improving our knowledge on deserts formation and their development, but also for the study of sediment mixing from different sources and/or long-term recycling. The role of the desertic environment in the storage and supply of sediment is still poorly acknowledged in the study of present and past sedimentary systems. This work focuses on the Sahara and Kalahari deserts and Zambezi River and aims to: deductively reconstruct from a handful of detrital grains the sources of sediments by their distinctive mineralogical, geochemical or isotopic "fingerprints"; estimate the chemical and physical factors that can modify the provenance signal (source rock mineral fertility, weathering, grainsize, hydraulic sorting, dissolution in temporary storage environments). All this was made possible combining a wide array of provenance techniques and enquiring statistical analysis. The Sahara, Kalahari and Zambezi samples were analyzed by bulk-petrography, heavy-mineral, and detrital-zircon U–Pb geochronology. For the Zambezi case study, elemental geochemistry, Nd isotopes and clay minerals were also analyzed.

Saharan dune fields are, with a few local exceptions, composed of pure quartzose sand with very poor heavy-mineral suites dominated by durable zircon, tourmaline, and rutile. Some feldspar, amphibole, epidote, garnet, or staurolite occur closer to basement exposures, and carbonate grains, clinopyroxene and olivine near a basaltic field in Libya. Relatively varied compositions also characterize sand along the Nile Valley and the southern front of the Anti-Atlas fold belt in Morocco

Detrital zircon ages are dominated by Neoproterozoic Pan-African ages underlining that durability of zircon grains and their likelihood to be recycled from older sedimentary rocks argues against the assumption, that their age distribution reflects transport pathways existing at the time of deposition rather than inheritance from multiple and remote landscapes of the past.

Kalahari dune sand mostly consists of monocrystalline quartz associated with durable heavy minerals and thus drastically differ from coastal dune fields of Namibia and Angola, which are notably richer in feldspar, lithic grains, and chemically labile clinopyroxenes. Distinct is the dune field of south-eastern Namibia, where quartz-rich

feldspatho-quartzose dune sand indicates partly first-cycle provenance from the Damara Belt and Mesoproterozoic terranes. Composition varies only at the western and eastern edges of the desert, reflecting partly first-cycle fluvial supply from crystalline basements of Cambrian to Archean age in central Namibia and western Zimbabwe. Basaltic detritus from Jurassic Karoo lavas is dominant in dunes near Victoria Falls. Bulk-sediment petrography and geochemistry of northern and central Kalahari sands concur with heavy-mineral and clay-mineral assemblages to indicate extensive recycling in arid climate of sediment strongly weathered during previous humid climatic stages in subequatorial Africa. Distilled homogenized dune sand composition thus reverberates the echo of paleo-weathering passed on to the present landscape through multiple episodes of fluvial and eolian recycling.

The segmented morphology of Zambezi River is reflected by its mineralogy and geochemisty. Pure quartzose sand recycled from Kalahari Desert dunes in the uppermost tract is next progressively enriched in basaltic rock fragments and clinopyroxene. Sediment load is renewed first downstream of Lake Kariba and next downstream of Lake Cahora Bassa, documenting a stepwise decrease in quartz and durable heavy minerals. Composition becomes quartzo-feldspathic in the lower tract, where most sediment is supplied by high-grade basements rejuvenated by the southward propagation of the East African rift. Feldspar abundance in Lower Zambezi sand has no equivalent among big rivers on Earth and far exceeds that in sediments of the northern delta, shelf, and slope, revealing that provenance signals from the upper reaches have ceased to be transmitted across the routing system after closure of the big dams. Irumide ages predominate over Pan-African, Eburnean, and Neoarchean ages. Smectite, dominant in mud generated from Karoo basalts or in the equatorial/winter-dry climate of the Mozambican lowlands, prevails over illite and kaolinite. Elemental geochemistry reflects quartz addition by recycling (Uppermost Zambezi), supply from Karoo basalts (Upper Zambezi), and first-cycle provenance from Precambrian basements (Lower Zambezi). Mildly negative for sediments derived from mafic granulites, gabbros, and basalts, εNd values are most negative for sand derived from cratonic gneisses. Detrital Zircon, elemental geochemistry and Nd isotopes reveal that the Mazowe-Luenha river system contributes most of the sediment reaching the Zambezi delta today, with minor supply from the Shire River. On the plateau, mineralogical and geochemical indices testify to extensive breakdown of feldspars and garnet unjustified by the present dry climate. Detrital kaolinite is recycled

by incision of Cretaceous–Cenozoic paleosols even in the wetter lower catchment, where inefficient hydrolysis is testified to by abundant fresh feldspars and undepleted Ca and Na. Mud geochemistry and surficial corrosion of ferromagnesian minerals indicate that, at present, weathering increases only slightly downstream the Zambezi River.

Sahara and Kalahari case studies allow studying in situ sand generation by wind erosion versus external fluvial supply in arid environment. In the Sahara, most sand appears to be recycled from rocks with high sand-generation potential, such as sandstones, and is primarily composed of quartz and feldspars with generally very poor heavy-mineral suites largely consisting of ZTR minerals. The main transport mechanism is the wind saltation and dune movement, but, due to high homogeneity in composition, large scale pathways cannot be estimated in this case. In Kalahari, sediments are fed by rivers by first cycle erosion of exposed orogens at the flanks of the desert and therein homogenized. The contrasting effect of strong recycling by wind and fresh supply from rivers are identified in the literature as the key factors that define the peculiar composition of most. Their identification in terms of mineralogy and provenance proved to be precious for present and past climatic debate.

In addition, evaluating the results from the Kalahari and Zambezi studies allows to critically reconsider several dogmas, such as the supposed increase of mineralogical “maturity” during long-distance fluvial transport. This is strongly affected by provenance factors: quartz-rich recycled Kalahari dune sand is progressively diluted along the Zambezi River by sediment supplied by different crustal domains up to amphibole-dominated quartzo-feldspathic composition in the lower trunk. Inheritance of the “Kalahari paleo-weathering signal” by Zambezi River is highlighted also by geochemical indexes and mud composition, which, if recycling is not properly taken into account, would indicate more intense weathering in the arid Uppermost Zambezi catchment than in the wetter Middle and Lower Zambezi. This proves that deserts can be long-term deposits of polycyclic sand and archives of past climatic conditions that may be tapped by rivers transporting the inherited signal to distant sedimentary basins.

Index

Chapter 1: Introduction

1.1 Purpose of the thesis

The word defining "desert" is one of the oldest written terms, subsequently transcribed trough Egyptian hieroglyphs *Tésert* to Latin world *desertum* (place of abandoned wilderness), describing presumably the hot and vast dune field that the margin of the Nile valley (El-Baz, 1983). In modern times, the ancient definition has been progressively modified to imply aridity and lack of vegetation, which are a direct measure of the scarce amount of precipitation.

At the African tropics, we can find two of the most extended deserts of the world: Sahara and Kalahari that are actually the topics of this thesis (*Chapter 3 to 4*). The global mechanism to establish prolonged periods of suppressed precipitation is the downward branch of the Hadley cells, which promotes high pressure conditions at the tropics.

The environmental definition that, as geologists, we ascribe to a desert is of "a vast area of dune fields and arid land where wind blows dust in the air and moves sand grains across dune profiles". Due to wind action, sediments can be either transported and stored in dunes or eroded from them in a continuous and prolonged cycle. The process of sediment recycling is contrasted by the supply of freshly eroded sediment that can be sourced from local outcrops or from rivers draining both close and distant terranes. Deciphering the relative interplay of wind and river transport in arid environments is an essential step not only for improving our knowledge on desert formation and their development but also for the study of sediment mixing from different sources or long-term recycling. The desert environment is for this reason a peculiar sedimentary object, which can store huge amount of loose sediment and eventually provide it to reworked river-network systems. Some of the questions that this thesis aims to answer are: can the mineralogy of desert dunes reveal information of sediment circulation within and between ergs? How is sediment transported for long distance? Which is the interaction with big river systems? These questions require information from different kind of climatic, geological and morphological sources, that have to be weighted to decipher their relative interplay in the desert provenance system. To tackle this complexity Sahara and Kalahari are chosen for their peculiarities. These two deserts have experienced similar condition of extreme aridity and have no rivalry in extension, but, while Sahara Desert is at present day extremely arid and with only two main rivers at its edges (Nile and Niger), Kalahari is experiencing semi-arid condition, with vast areas of vegetated dunes and has a much more developed river network (Zambezi,

Okavango, Orange, Nossob, Molopo, Rietfontein, Gwai). To investigate the desert-river interactions, a of this thesis (*Chapter 7*) focuses on the sediment provenance of Zambezi River, which carves across the Kalahari dunes in its uppermost section and its interaction with dunes is second only to the Nile in the African continent. From the comparison of two major deserts and a crosscutting river this thesis aims to describe sediment transport concerning fluvio-aeolian interaction by the means of provenance studies. In conclusion the African laboratory is chosen for the availability of two large deserts that interact with large rivers and that have experienced different climatic condition in the recent past. The discussion will benefit both from similarity and dissimilarity from the two cases, ruling out and emphasizing different possible forcing factors.

1.2 Provenance studies in deserts

Provenance studies try to include in a sedimentological perspective both the sources and the transport mechanism (provenir, "to come from"). This kind of study aims to deductively reconstruct from a handful of detrital grains the sources of sediments by the distinctive mineralogical, geochemical or isotopic "fingerprints" that they can produce via erosion. Since the first linkage of mineralogy to tectonic setting proposed by Kyrnine (1948), assuming that the continental crust can be envisaged as consisting of sedimentary layers nonconformably overlying deformed metamorphic rocks intruded at depth by plutonic rocks, further importance and emphasis have been paid towards additional sources of complexities such as geological inheritance, volcanism, and diversity of geodynamic settings. A clear example is the introduction of chemical weathering by Folk who thus distinguished "climatic arkose," generated from basement rocks in dry climate even during stages of tectonic quiescence, from Krynine's "tectonic arkose". Following this evolution, modern provenance studies focus more on the chemical and physical modification that occurs before, during and after the transport to correctly reconstruct the dynamic path of sediment in the routing system. These controlling factors can be summarized as (i) source rock mineral fertility, (ii) weathering, (iii) grainsize, (iv) hydraulic sorting, (v) dissolution in temporary storage environments (Caracciolo et al. 2020). Balancing sediment signal by each of these factors is the only way of deducing correct information from the sedimentary cycle.

To describe regional wind circulation and sand transport early study on desert sediment transport developed on the observation of dune shape and pattern. The physical response of grain to the aeolian environment constitutes the basic knowledge of sediment dynamics

in deserts and it focuses on grain-size, grain shape and sorting effect over the dunes. The purpose of the majority of these studies is to progressively enlarge the scale of the subject, from grain motion to dune morphology, to dune dynamics, to sand sea patterns, with the aim of building generalised models of sediment dynamics.

The vast amount of knowledge concerning dune morphology and aeolian grain dynamics is mirrored by the lack of studies concerning the mineralogy of the dunes. Since the early study on dune colour and mineral content (Mckee, 1979), further studies have been made on desert sand provenance (El-Baz, 1998; Muhs, 2004; Pell et al., 1999; Muhs et al., 2013; Stevens et al., 2013, Garzanti et al., 2013; East et al., 2015; Rittner et al., 2016; Liang et al., 2019; Garzanti et al., 2022). Desert environment can be considered "ideal" for provenance studies because some of the aforementioned provenance biases are strongly reduced: extreme aridity prevents from chemical weathering of selected mineral species and hydraulic sorting is ruled by aeolian dune dynamics and can be clearly decoupled from the provenance signal. These beneficial factors are counterbalanced by the recycling of desert sand, which disrupts the direct link with the source rocks, introducing multiple events of erosion and transport from intermediate sedimentary rocks. In order to solve this provenance dilemma, this thesis proposes a "comparative provenance analysis" of sediments from the Sahara, Kalahari and Zambezi River. The same desertic environment, but with different geological framework, different geomorphological features and present day climatic conditions, will allow us to correctly balance the provenance bias and to estimate recycle vs fresh supply of the sediments in these settings.

1.3 Outline of the thesis

In this paragraph the author briefly summarizes the outline of the thesis to better convey the aim of understanding fluvio-aeolian interaction is large African deserts:

Chapter 2 gives a summarized description of the methodology applied in the thesis. Emphasis is placed on laboratory techniques to extract mineralogical, geochemical, and isotopic data, paired with the statistical and mathematical methods utilized for the interpretation of data. The applied laboratory parameters are exhaustively listed and commented on.

Chapter 3 presents the Sahara Desert case study within its geological, geomorphological, and climatic context. Here the dataset on Petrography, Heavy Minerals and Detrital Zircon dating of the Sahara Desert dunes are presented. A section is dedicated to the comparison with dataset from literature, which highlight the strong role of recycling in the provenance

of the Sahara.

Chapter 4 describes Kalahari Desert case study, with a geological, geomorphological, and climatic summary of southern Africa. Here the focus is on the comparison between dune and river sand samples to describe in detail the interplay of aeolian sediments with the fluvial network. Petrography, Heavy Minerals, Detrital Zircon dating, and geochemical analysis strongly suggest that recycling and supply of new sediment distinctively happens in different parts of the desert depending on the climatic condition. Geochemical data add important information in the preservation of inherited weathering signal by the dunes.

In chapter 5, the fluvio-aeolian interaction in the deserts is examined with joint conclusion from the two major African deserts coupled with the data from other provenance studies data on deserts around the world. Two classes of desert are clearly defined: wind-fed quartz-rich, and river-fed lithic-bearing deserts. Distinct behaviour of sediment transport is ruled by the fluvial-aeolian connectivity.

The joint conclusion of the previous chapters left some outstanding issues on the interaction of deserts with major rivers, and these are tackled in Chapter 6. For this reason, this chapter illustrates provenance analysis on the Zambezi River. Petrography, Heavy Minerals, Detrital Zircon dating, are coupled with geochemical, isotopic and clay mineralogy analysis to describe the Zambezi River course and its major tributaries. Strong differences in all the data suggest a present day (and possibly past) segmentation of the river. The multiple datasets presented enables suggestive intra- and inter- dataset comparison useful for sedimentological models and sediment budget of the catchment.

Chapter 7 focuses on the Zambezi River interaction with the Kalahari Desert with conclusive remarks on the recycling and weathering effect of sediments in rivers and deserts. The dataset comparison of these two cases describes in detail the preservation and mixing of the provenance signal of Kalahari dunes collected by Zambezi.

Chapter 2: Methods

2.1 Sampling strategy

Comparison between large number of samples relies on similar sampling strategies at first. Sediment composition can strongly be influenced by hydraulic sorting (Slingerland, 1984, Garzanti et al., 2008, Malusà et al., 2016), thus preventing robust statistical analysis of intra-samples variability. Samples presented in this thesis have been collected during different expeditions in various settings: dune fields, river bars, cores from the continental shelf. For this reason, strict rules could not be settled. Nevertheless, the majority of dune samples were collected at the crest of each dune, considering that finer sediment to be concentrated in the down-wind side where coarser grains concentrate in the inter-dunes (Lancaster, 1986, Hartmann & Christiansen, 1988). Sampling lots and lots of dune and river sands across such a vast area has not been straightforward, owing to the remoteness of many places. Various expeditions from many collaborations with different institutes allowed to gather all the required samples and for this reason, the work began when we estimated there was sufficient samples for each case study. For the Sahara, we aimed to have sufficient samples to represent the dune composition of major erg, with the addition of samples near the major reliefs and important geological structures (e.g Anti-Altas, Air Mountains, Haruj al Aswad Massif). The Kalahari case study focused more on the availability of samples from river bars close to dune field sample to describe the interaction of the two systems. Similarly to the previous case, additional samples were collected to describe composition of dunes with large geographical extension. The Zambezi case aimed, at first, to describe the sediment routing system, collecting samples from tributaries and the main trunk before and after the confluence. Samples GPS location is provided in the Appendix.

2.2 Analytical strategy

Likewise to the sampling strategy, the analytical strategy closely followed the development of the thesis, with adjustments and decisions that followed case study results. The essential analytical tools for provenance studies are considered by the author to be framework petrography and heavy mineral, which have been performed on the totality of the samples. These two techniques alone can give a clear provenance picture, describing source rocks composition, transport controlled textural characteristics, and identifying peculiar mineral phases diagnostic for some specific geological domains. As it will be inferred in the Sahara

case (*Chapter 3)*, these two techniques cannot characterize strongly recycled sediment being composed mostly of quartz and ultrastable heavy minerals. In this case Uranium-Lead (U-Pb) Detrital Zircon geochronology is a quick and reliable technique that univocally identifies the "protosource" of sediments. The choice of selected samples for U-Pb analysis (see Table 2.1) aimed to cover most of the analyzed deserts.

On the other hand, clay mineralogy and sediment geochemistry are largely controlled by factors other than provenance. If weathering is intense, then they reflect the lithology of source rocks only poorly, which explains why they have long been used to evaluate weathering rather than provenance (Nesbitt and Young 1982; Velde and Meunier 2008). As it was already questioned in Garzanti et al., 2014c, weathering indexes provided by clay mineralogy and geochemistry in Kalahari dunes and Zambezi and Okavango river bars, appear to be at odd with the current climatic condition and demanded further analysis and explanation. For this reason, *Chapter 4* and *6* benefited from the addition of these two datasets.

The nature of riverine samples of Zambezi case proved to be the most complex scenario, both because samples presented a wider range of grainsize (clay to sand) and because of the source terranes geological complexity, ranging from very old cratons to juvenile basalts. Individual samples have been selected for clay mineralogy, geochemistry, and Nd isotope geochemistry for the following reason. Geochemistry can be applied to bulk sediment samples of any size fraction from clay to granule. This allows us to investigate almost the entirety of the sediment flux, including clay and silt, which constitute the large majority of the detrital mass transported in river systems as suspended load (Johnsson 1993, Hay 1998; Milliman and Farnsworth 2011). This proved to be beneficial for the characterization of intra-sample and inter-sample variability for all spectrum of grainsizes. Isotope geochemistry do offer complementary information useful to augment the completeness and robustness of provenance analysis (McLennan et al., 1993), because it is best suited to tackle again a wider grainsize in respect to the millesimal fraction of zircon geochronology. Selected samples of tributaries and section of the main trunk foster the comparison with the sources.

	PT	HM	DZ	Clay	CHI_{sand}	CHI_{mud}	CHI_{Nd}
Sahara	44	44	32				
Kalahari	84	84	42	24			
Zambezi	39	39	18	17	31	18	28

Table 2.1 Number of analyses for each case study. PT: framework petrography, HM: heavy minerals, DZ: detrital zircon geochronology, CHI_{sand}: geochemistry of the sand fraction, CHI_{mud}: geochemistry of the mud fraction, CHI_{Nd}: geochemisty of the Neodymium isotope.

2.3 Petrography

Bulk sand samples were impregnated with araldite epoxy, cut into standard thin sections, stained with alizarine red to distinguish dolomite and calcite, and analysed by counting 400-500 points under the petrographic microscope (Gazzi-Dickinson method; Ingersoll et al., 1984). Sand classification was based on the relative abundance of the three main framework components quartz (Q), feldspars (F), and lithic fragments (L), considered if exceeding 10%QFL. According to standard use, the less abundant component goes first, the more abundant last (e.g., a sand is named litho-quartzose if Q > L > 10%QFL > F). Feldspar-rich feldspatho-quartzose (1 < Q/F < 2), feldspatho-quartzose (2 < Q/F < 4), quartz-rich feldspatho-quartzose (4 < Q/F < 9), quartzose (90% < Q/QFL < 95%), and pure quartzose compositions (Q/QFL > 95%) are distinguished (classification scheme after Garzanti, 2019). These distinctions are essential to discriminate among quartz-rich suites generated in anorogenic settings (Garzanti et al., 2001, 2018a). Metamorphic rock fragments were subdivided into very low to low-rank metasedimentary or metavolcanic, and medium to high-rank felsic or mafic categories (Garzanti and Vezzoli, 2003). The intrabasinal *versus* extrabasinal origin of carbonate and non-carbonate grains was established based on criteria illustrated in Zuffa (1985) and Garzanti (1991). Petrographic parameters used in this thesis include the plagioclase/total feldspar (P/F) ratio; feldspar identified by cross-hatch twinning is called microcline* through the text. Median grain size was determined in thin section by ranking and visual comparison with in-house standards composed of mounts of sieved Φ/4 classes. Key petrographic parameters are provided in Appendix.

2.4 Heavy Minerals

From the bulk sample or from a wide size-range obtained by wet sieving, heavy minerals were separated by centrifuging in Na-polytungstate (2.90 g/cm^3) and recovered after partial freezing of the test tube with liquid nitrogen (method described in detail in Andò, 2020). The dense fraction thus obtained was weighed, split with a micro-riffle box, and mounted on a glass slide with Canada balsam for counting. About 200 to 250 transparent heavy minerals were either counted by the area method or point-counted at suitable regular spacing to obtain real volume percentages (Galehouse, 1971). Aeolian dune sediments

presented as well sorted samples, for this reason were analysed in bulk. For moderately to poorly sorted samples (usually river bars), where the co-existence of detrital minerals with widely different sizes makes mounting and identification difficult (Mange and Maurer, 1992), this work analyzed size windows ranging from at least 3.5 ϕ (32–355 μm) to 5 ϕ (15–500 μm) or more (e.g. >15 μm or > 32 μm). Mineralogical analyses were carried out by routinely coupling observations under the microscope and the Raman spectroscope. Transparent-heavy-mineral concentration (tHMC; Garzanti and Andò, 2007b; 2019) ranges from extremely poor (tHMC <0.1), very poor (0.1 ≤ tHMC <0.5), poor (0.5 ≤ tHMC <1) and moderately poor (1 ≤ tHMC <2), to moderately rich (2 ≤ tHMC <5), rich (5 ≤ tHMC <10), very rich (10 ≤ tHMC <20), and extremely rich (20 ≤ tHMC <50). The sum of the percentages of zircon, tourmaline, and rutile (collectively called ZTR minerals throughout the text) expresses the mineralogical durability of the suite (ZTR index of Hubert, 1962; Garzanti, 2017). The "Amphibole Color Index" ACI varies from 0 in detritus from upper-greenschist/lower-amphibolite-facies metamorphic rocks yielding exclusively blue/green amphibole to 100 in detritus from granulite-facies or volcanic rocks yielding exclusively brown amphibole or oxyhornblende (Andò et al., 2014). Transparent-heavy-mineral assemblages are called "tHM suites" throughout the text and significant minerals are listed systematically in order of abundance (high to low). The complete heavy-mineral dataset including information on analyzed size classes is provided in Appendix.

2.5 Semi-automated Raman analysis

Raman spectroscopy is routinely applied in mineral identification because it measures the inelastic interaction of the vibrational or rotational mode of a molecule with an incident radiation (laser), returning an unique spectrum for each mineral phase. During this thesis, it has been developed a Semi-automated Raman analysis for identification of zircon grains. Photomosaics of grain mounts were referenced in Qgis (http://www.qgis.org) to match the Raman coordinate system. Grain outlines were obtained by using standard thresholding techniques and visually checked to avoid over-segmentation. For each grain, particle features such as perimeter, area, and long and short axes were extracted in Qgis. Grain size was determined as the equivalent diameter.

Coordinates of grain centroids determined by image analysis were passed over to a confocal Renishaw Qontor Raman spectrometer equipped with a Leica microscope, 532 nm solid state laser (~ 100 mW power), motorized stage, and autofocus. Raman

spectra were obtained using 50x LWD magnification applying 10% laser power for 0.5 s (repeated for 15 cycles) on each grain. Baseline correction and spectra normalization were performed using Renishaw Wire software. Grains were identified using a Matlab routine that matches the obtained spectra with an in-house-built reference database of known mineral spectra (Andò and Garzanti, 2014). Goodness of fit was assessed by the correlation coefficient r (0 = no match; 1 = perfect match), accepting only values ≥ 0.7. This procedure has become the standard procedure for zircon identification used in this work, also avoiding any operator-induced bias by hand picking. Zircon grains are in fact usually well recognizable for their optical features: high relief transparent bipyramidal elongated crystal. However, metamictization effects degrade the crystalline lattice down to a brownish and musky appearance and long transport and recycling can round even the most durable grains. This methodology allows to consider all zircon populations and to directly extract grainsize distribution of zircon for each sample.

2.6 Detrital Zircon Geochronology

Detrital zircons were concentrated from the heavy mineral suite with standard magnetic separation techniques with no additional dense liquids. The resulted amount of minerals was mounted in epoxy resin, grinded to maximize the exposed surface of the grains and polished. Zircon grains were later identified by Semi-automated Raman analysis with a Renishaw QONTOR Raman microscope without any operator selection by hand picking. U-Pb zircon ages were determined at the London Geochronology Centre with an Agilent 7900x LA-ICPMS (laser ablation inductively coupled plasma mass spectrometry) system, employing a NewWave NWR193 Excimer Laser operated at 10 Hz with a 25 μm spot size and ~2.2 J/cm^2 fluence. No cathodoluminescence imaging was done, and the laser spot was always placed "blindly" in the center of zircon grains in order to treat all samples equally and avoid bias in intersample comparison ("blind-dating approach", Garzanti et al. 2018). The mass spectrometer data were converted to isotopic ratios with the GLITTER 4.4.2 software (Griffin et al., 2008), employing Plešovice zircon (Sláma et al., 2008) as a primary age standard and GJ-1 (Jackson et al., 2004) as a secondary age standard. An NIST SRM612 glass was used as a compositional standard for the U and Th concentrations. GLITTER files were post-processed in R with IsoplotR 2.5 (Vermeesch, 2018a). Concordia ages were calculated as the maximum likelihood intersection between the concordia line and the error ellipse

of $^{207}Pb/^{235}U$ and $^{206}Pb/^{238}U$ (Ludwig, 1998). The discordance cutoff was set at -5/+15 of the concordia distance (Vermeesch, 2021). The complete geochronological data set is provided in Appendix .

2.7 Clay and Silt Mineralogy

The mineralogy of six mud samples (Chapter 6) from the Middle and Lower Zambezi main stem and tributaries (Kafue, Sangadze, Shire) was determined on both <32 μm and <2 μm fractions by X-ray powder diffraction (XRD) using PANalytical Aeris equipment with a Cu tube, at 15 kV and 40 mA. The <32 μm fraction was separated by wet sieving, and diffractograms were performed on randomly oriented powder in the range 2°–60° (2v angle). The <2 μm fraction, separated by centrifuging according to Stokes's law, was analyzed on oriented aggregates after air drying (analyzed 2v: 2°–30°), solvation with ethylene glycol, and heating at 550°C (analyzed 2v: 2°–15°). Mineral proportions were evaluated semi-quantitatively using diagnostic XRD peak areas (Moore and Reynolds, 1997; Kahle et al., 2002). Analyses were carried out by Prof. Pedro Dinis at the University of Coimbra, MARE (Marine and Environmental Sciences Centre), further technical information is provided in Dinis et al. (2020b).

2.8 Mud and Sand Geochemistry

Chemical analyses were carried out at Bureau Veritas Mineral Laboratories (Vancouver, Canada) of 51 samples from Zambezi case study (Chapter 6) and 25 samples from Kalahari case study (Chapter 4). A quartered aliquots of the <32 μm (for muds) and 63–2000 μm (for sands) fractions were obtained by wet sieving. Following a lithium metaborate/tetraborate fusion and nitric acid digestion, major oxides and several minor elements were determined by ICP emission spectrometry and trace elements by ICPMS (http://acmelab.com for detailed information on adopted procedures, standards used, and precision for elements of group 4A–4B and codes LF200 and LF300; apps. A and B are available online). Classic multielement chemical indices used to estimate weathering and calculated from molar proportions of mobile alkali and alkaline-earth metals include the WIP (weathering index of Parker, 1970) and the CIA (chemical index of alteration; Nesbitt and Young, 1982). The WIP, however, merely measures the amount of a set of mobile elements that decreases rapidly wherever quartz is added to the sediment, making it an index of quartz recycling more than an index of weathering. Because correcting the CIA for CaO in carbonates introduces uncertainties (Garzanti and Resentini, 2016), in this study

use the CIA* corrected only for CaO in apatite (CIA*= 100 x Al_2O_3/[Al_2O_3+(CaO-33.3 x P2O5)+Na_2O + K_2O]) . The weathering effect is best detangled from other controls on geochemical composition if mobile elements (Mg, Ca, Na, K, Sr, and Ba) are considered one by one. This can be done by using $\alpha^{Al}E$ values, defined as ((Al/E)sample/(Al/E)standard) (Garzanti et al. 2013a, 2013b), which compare the concentration of any mobile element E with reference to nonmobile Al in the samples to an appropriately selected standard composition (e.g., the UCC [upper continental crust] standard of Taylor and McLennan, 1995; Rudnick and Gao, 2003). Alluminium, hosted in a wide range of rock-forming minerals with diverse density, shape, and size, including phyllosilicates (concentrated in mud) and feldspars (concentrated in sand), is used as a reference for all elements rather than Ti, Nd, Sm, or Th (Gaillardet et al., 1999), which are hosted preferentially in ultradense minerals and thus may reach strongly anomalous concentrations as a result of hydrodynamic processes.

2.9 Nd Isotope Geochemistry

Sixteen samples from the Middle and Lower Zambezi catchments (*Chapter 6*) were treated with a sequential leaching procedure for quantitative removal of carbonates, Fe oxide phases, and organic matter (Bayon et al., 2002). Before geochemical analyses, about 80 mg of powdered samples were digested by a HF-HCl-HNO_3 mixture or alkaline fusion (for the 63–2000 μm fraction). Selected major and trace-element abundances were determined at the Pôle Spectrométrie Océan (PSO) with a Thermo Scientific Element XR sector field ICP-MS, using the Tm addition method (Barrat et al., 1996). Both the accuracy and the precision of measured concentrations were assessed by analyzing three certified reference materials (AN-G, AGV-1, BCR-1). Neodymium isotopes were measured at PSO with a Thermo Scientific Neptune multicollector ICP-MS, after Nd purification by conventional ion chromatography. Repeated analyses of a JNdi-1 standard solution gave $^{143}Nd/^{144}Nd$ of 0.512114 ± 0.000005 (2σ n=12), in full agreement with the recommended value of 0.512115 (Tanaka et al., 2000) and corresponding to an external reproducibility of 50.09ε (2σ). Epsilon Nd values were calculated with the present-day chondritic (chondrite uniform reservoir) value of $^{143}Nd/^{144}Nd$ = 0.512630 (Bouvier et al., 2008). Neodymium depleted-mantle model ages ($T_{Nd,DM}$) were calculated following the approach described in De Paolo (1981), using measured Sm and Nd concentrations ($^{147}Sm/^{144}Nd$ = (Sm/Nd) x 0.6049) and present-day depleted-mantle values of $^{143}Nd/^{144}Nd$ = 0.51315 and $^{147}Sm/^{144}Nd$ = 0.2145.

2.10 Statistical tools

One of the challenges of this thesis was to manage and combine multiple and large datasets. In order to fully understand a provenance model, one should gather as many pieces of information (i.e.reliable analyses) as possible, but this can make it difficult to see the full picture. Multivariate analysis can help to address this issue. It enables to visualize differences within a single dataset and identify peculiar samples, and also allows for the comparison and integration of information from different datasets in order to facilitate more informed discussions. Multidimensional Scaling (MDS; Kruskal and Wish, 1978; Vermeesch, 2013) is a multivariate ordination technique that takes a dissimilarity matrix as input and produces a map of samples as output, in which similar samples plot close together and dissimilar samples plot far apart. For detrital zircon U-Pb age spectra, a dissimilarity matrix can be constructed using the Kolmogorov-Smirnov statistic (i.e., the maximum vertical difference between two cumulative distribution functions; Feller, 1948). Correspondence Analysis (CA) is an ordination technique that is specifically tailored for count data such as petrographic and heavy-mineral point counts (Greenacre, 2017). This method can be shown to be a special case of MDS in which the dissimilarity matrix is populated with chi-square distances (Vermeesch, 2018b).

General Procrustes Analysis (GPA) and Individual Difference Scaling (INDSCAL) are higher-order data-mining techniques that combine several MDS maps together in order to simplify the interpretation of 'big' datasets (Vermeesch and Garzanti, 2015). In the case of GPA, this is achieved by mapping the different MDS configurations onto a common configuration by a number of affine transformations (reflection, rotation, scaling, and translation; Gower, 1975). INDSCAL, on the other hand, acts directly on the dissimilarity matrices. It is a higher order generalisation of the MDS method that aims to fit multiple dissimilarity matrices to a shared 'group configuration' by attaching different weights to the different datasets (Carroll and Chang, 1970). To illustrate heavy-mineral data the compositional biplot (Gabriel, 1971; Greenacre, 2017) is used, a statistical/graphical display that allows discrimination among multivariate observations (points) while shedding light on the mutual relationships among multiple variables (rays). The length of each ray is proportional to the variance of the corresponding variable in the dataset. If the angle between two rays is close to 0°, 90° or 180°, then the corresponding variables are directly correlated, uncorrelated, or inversely correlated, respectively.

In the Sahara case study (*Chapter 3*) dissimilarity matrices for multivariate ordination (for the different provenance proxies) were also used to construct hierarchical clustering

dendrograms with the normalised distance values obtained by chi-squared distance (for CA) and Kolmogorov-Smirnov distance (for MDS). This classification was able to assign the samples to different clusters, thereby augmenting further the visual interpretation (Fig. 3.8 A,B,C). The same method was applied to the GPA matrices of dissimilarities displayed in Fig. 3.8 E,F.

In the Zambezi case study (*Chapter 6*), the relative contribution from each tributary or geological domain to the sediment flux of the trunk river was quantified with forward-mixing models. This method relies on the fact that the compositional signatures of sediment in all potential sources are distinct and accurately determined (Weltje, 1997; Garzanti et al., 2012b). The forward-mixing model calculates a row vector of compositional data as a nonnegative linear combination between a matrix of fixed end-member compositions and a row vector of coefficients representing the proportional contribution of each end member to the observation. The accuracy of calculations depends on how distinct and precisely assessed the end-member signatures of all potential sources are. More accurate information is in the Appendix.

2.11 River Morphometry

The geomorphological properties of the Zambezi River and its major tributaries (Chapter 6) were quantified using TopoToolbox, a set of MATLAB functions for the analysis of relief and flow pathways in digital elevation models (Schwanghart and Scherler, 2014). The analysis of the longitudinal profile of bedrock channels was carried out on a 90-m-resolution DEM provided by Shuttle Radar Topography Mission Global (SRTM GL3; https://opentopography.org) to identify major knickpoints, defined as sites where the channel gradient changes abruptly owing to sharp local changes in bedrock strength and/or uplift rate. Channel concavity v and normalized channel steepness ksn (referenced to a fixed concavity 0.45 to facilitate comparison among channel slopes with widely varying drainage areas and concavities) are defined by the power-law relationship S= ksA2v between the local channel slope S and the contributing drainage area A used as a proxy for discharge (Flint 1974; Whipple 2004).

Chapter 3: Sahara Desert

This chapter has been published with modification as: "*Provenance and recycling of Sahara Desert sand*" by by Pastore, G., Baird, T., Vermeesch, P., Bristow, C., Resentini, A., & Garzanti, E. on Earth Science Reviews, 216, 2021.

3.1 Introduction

The Sahara is by far the largest hot desert on Earth, hosting several large dune fields. The provenance of these vast expanses of sand is gravely understudied. This chapter here present the first thorough and comprehensive multidisciplinary study aimed at understanding the nature of sand sources, how sand evolved during geological time, and under the action of which prevailing wind regimes and along which trajectories was it displaced and eventually accumulated in the sand sea.

The main purpose is to contribute to the ongoing debate in sedimentology and in Quaternary paleoclimatology concerning the production of sand and silt in arid landscapes. As far as quartzose sand is concerned (Dott, 2003; Muhs, 2004), one view is that sediment delivered from surrounding source rocks "matures" by essentially mechanical processes within the desert area (e.g., Dutta et al., 1993). Another is that the concentration of durable minerals is inherited from recycling of older sandstones that underwent extensive weathering in more aggressive climatic conditions, extensive intrastratal dissolution during diagenesis, or in general multiphase chemical leaching during multiple cycles of weathering and diagenesis (e.g., Garzanti, 2017).

Even more controversial are the generation mechanisms of "desert loess" (Smith et al., 2002; Lancaster, 2020). Throughout the Plio-Quaternary, the Sahara has represented a major source of fine particles, blown to as far as the other side of the Atlantic Ocean (Muhs et al., 1990, 2019; Prospero, 1996) and is currently the largest source of mineral aerosols globally (Tegen et al., 2013). Up to 85 megatons of dust are emitted into the atmosphere from the Sahara annually, with the Bodélé Depression representing the largest single area of dust production (Middleton and Goudie, 2001; Koren et al., 2006; Bakker et al., 2019). However, the precise mechanism behind the origin of mineral aerosol is debated. Studies have suggested the predominant genesis for dust emissions is the deflation of fine-grained sediments from depressed areas (e.g., Bristow et al., 2009), the abrasion of saltating sand grains within sand seas (e.g., Crouvi et al., 2012), or the accumulation of silt through hydrological factors, resulting in high emissions from alluvial deposits, desiccated lake beds, and palaeolakes (Bakker et al., 2019; Jewell et al., 2020). The need to identify major

sediment sources and clarify the process of sand and silt generation through tracing the main directions of aeolian transport within the Sahara are therefore much warranted.

This study investigates the origin, spatial variability, and transport pathways of aeolian sand in the Sahara by combining bulk-petrography, heavy-mineral, and detrital-zircon U–Pb geochronology analyses on 44 sediment samples. These samples have been collected in northern Africa across more than 20° degrees of latitude from the Sahel to the Mediterranean Sea and almost 50° degrees of longitude from the Nile River to the Atlantic Ocean (Fig. 3.1).

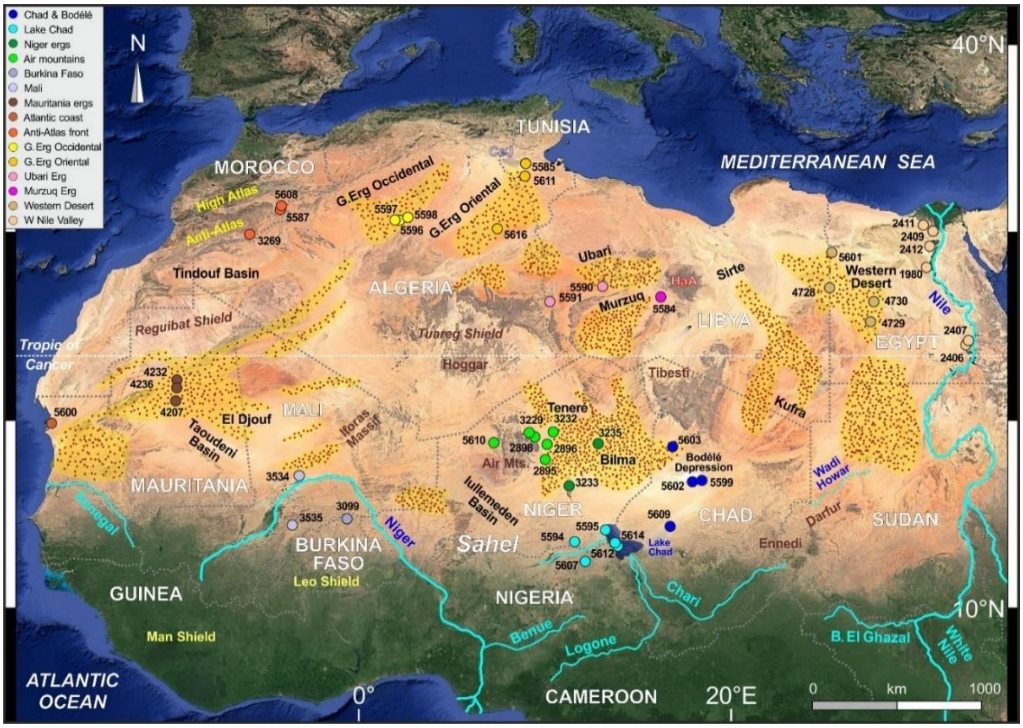

Figure 3.1. The Sahara Desert in northern Africa. Main dune fields, sedimentary basins, and geological domains are indicated. Sampling sites are shown with circles coloured by region. CeJ = Chott el Jerid (Tunisia); HaA = Haruj al Aswad (Libya).

Highly detailed provenance studies of desert sand have been carried out with the same multi-technique approach in diverse sand seas of Africa, Arabia, and Asia (e.g., Garzanti et al., 2012a, 2017, Stevens et al., 2013; Rittner et al., 2016) but not on the Sahara so far. Saharan dune sands have been broadly described as composed of quartz (e.g., El-Baz, 1998; Muhs, 2004; Abdelhak et al., 2014; Meftah and Mahboub, 2020) but their provenance has remained unknown. To identify the source regions, gain understanding of sand transport pathways, and extract all possible provenance information from a composition characterized by only a limited number of provenance-diagnostic minerals, this study

required the scrutiny of multi-proxy datasets using a full set of advanced statistical techniques. Multidimensional Scaling, Correspondence Analysis, Individual Difference Scaling, and General Procrustes Analysis were applied to provide both a highly robust statistical investigation and an unbiased visual representation of the relationships among the samples.

3.2 Geomorphological framework

3.2.1 Climate and wind patterns

The Sahara (in Arabic *sahra*, desert) covers an area of 9 million km^2 and extends from ~12°N to ~34°N (Fig. 3.1). The desert thus straddles the Tropic of Cancer and is influenced by the descending limb of the Hadley cell. The trajectory of air masses and rainfall are regulated by the strength of the subtropical high-pressure system and by the latitudinal shift of the Intertropical Convergence Zone (ITCZ). Average annual precipitation is <50 mm in most areas, which may not see rain in many consecutive years, and increases to ~160 mm in the semiarid Sahel to the south (from either the Arabic word *sahil*, shore, figurative for desert's edge, or *sahl*, plain).

During winter, the ITCZ shifts to the south and the Azores Anticyclone and the Sahara High are established, with only occasional disturbances by cyclonic systems from the Atlantic Ocean or by the polar front. Atmospheric circulation is dominated by westerly winds and by winds associated with the Mediterranean depression, and the only maritime air masses enter the Sahara from the Red Sea. In the spring, the *khamseen* wind (in Arabic *khamseen*, fifty, because the wind blows over ~50 days) moves hot tropical air towards the Mediterranean coast. In the summer, the northward displacement of the ITCZ allows air masses blown by recurved south-easterly trade winds to penetrate the continent, and the West African Monsoon brings moisture to the southern Sahara. In its northern position, the ITCZ represents a barrier for air masses blown by the hot and dry north-easterly trade winds (the *harmattan;* possibly derived indirectly from the Arabic word *haram*, evil), often regulated daily by the thermic inversion of near-surface air (Warner, 2009). Libya reaches one of the highest temperatures on Earth (58°C) with extreme diurnal variation (up to 50°C), whereas lower temperatures are recorded in the northwest influenced by the incursion of cold air from the Atlantic Ocean.

A climatic zonation distinguishes the northern Sahara, affected by the winter Mediterranean depression, and the southern Sahara, characterized by the West African Monsoon in summer. This zonation is strengthened by the position of the main topographic highs

(Hoggar, Tibesti, and Ennedi Mountains), hampering precipitations and southward sand transport from north to south (Wilson, 1971; Mainguet, 1978). Relief concentrates precipitation in summer and extreme events and flash floods occur when the monsoon pushes humid air against the Tibesti and Hoggar massifs.

Saharan sand-flow patterns are poorly constrained. Historically, the role of the subtropical high-pressure zone has been argued to split sand flows along a north-south divide (Wilson, 1971). In the northern zone, transport occurs mainly to the northeast, while the southern zone sees sand flow towards the coast of Mauritania and offshore into the Atlantic Ocean (Fig. 3.2). However, this theory relies on a short temporal sampling window and warrants revisiting.

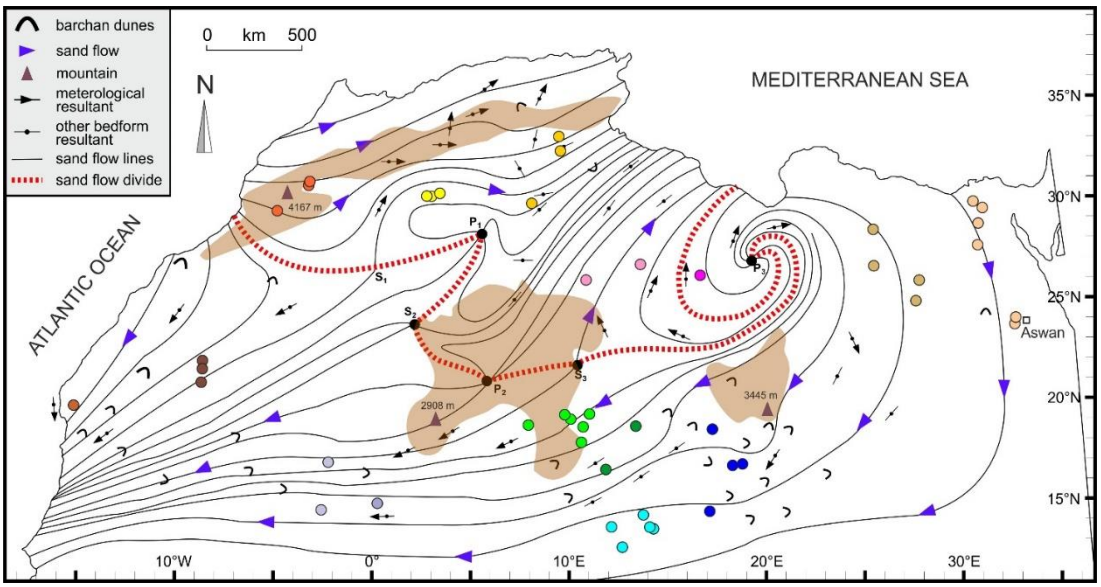

Figure 3.2. Sand flow patterns obtained by interpolation of metereological and bedform data (grain-size range 50-100 mm; modified after Wilson, 1971). The calculated divide (dashed red line) nearly corresponds to the southern boundary of the subtropical high-pressure zone; peaks P1 (Tademait), P2 (Hoggar), and P3 (Libyan) correspond to high-pressure centres from which sand flow radiates, and saddles S1 (Erg Chech), S2 (Tanezrouf), and S3 (Teneré) correspond to possible sand flow corridors. Mountain areas in brown, with indicated highest elevation for each; sample locations coloured as in Fig. 3.1.

3.2.2 Hydrology

Because of extreme aridity, river courses in the Sahara are transformed into desiccated dry valleys (in Arabic *wadi*, plural *widyan*), representing the remnants of the hydrological network inherited from wetter climatic stages in the past (Ghoneim et al., 2007; Abdelkareem and El-Baz, 2015; Abdelsalam, 2018). One example in the eastern Sahara is Wadi Howar (Fig. 3.1), sourced from the Ennedi and Darfur mountains and once draining northeastwards from the Chad/Sudan border to the Nile for 640 km but now marked only

by linear tree vegetation sustained by the groundwater table in the shallow subsurface (Pachur and Kröpelin, 1987). The major exception is the Nile River (basin area ~3 million km^2), which conveys across the desert the large volume of water received from East African lakes, augmented by monsoonal rains falling on the Ethiopian plateau in the summer (Sutcliffe and Parks, 1999).

The southeastern Sahara Desert receives water from the laterite-capped hilly plateau representing the water divide from the Congo and the source of several headwater branches of the Bahr El Ghazal, a western tributary of the Nile (in Arabic *bahr*, sea, figurative for big river). To the west, the Chari River and its major western Logone branch drain the Cameroon basaltic plateau to feed Lake Chad, a shallow body of water (depth mainly < 7 m) surrounded by seasonally inundated marshland (Fig. 3.1). Lake Chad is the only lake remaining in the desert, with a vast (2.5 million km^2) endorheic drainage basin that receives monsoonal rain falling during summer in the south. Climate change and increased water use for human activities make the lake vulnerable to drought events such as those of the 1970s and 1980s, which saw the lake surface area shrink by up to 90% (Birkett, 2000; Coe and Foley, 2001; Gao et al., 2011).

Farther west, the Niger River (basin area 2.3 million km^2), sourced in the Guinea plateau only ~250 km from the Atlantic coast, draws a wide arc across the southern Sahara passing through an inland delta in Mali and is eventually diverted southward towards the Gulf of Guinea (Gischler, 1976; Goudie, 2005). The Atlas Mountains collect precipitation also in the form of snow, recharging the large aquifers of the northwestern Sahara (Al-Gamal, 2011). In the eastern Sahara, subsurface water is stored in Nubian sandstone acquifers across the political borders of Libya, Egypt, Sudan, and Chad (Gossel et al., 2004).

3.2.3 Sand dunes

Sand dunes cover only a fifth of the immense surface of the Sahara. In order to understand the relationships with wind regimes, dune forms and distribution have long been studied with field expeditions (e.g., Bagnold, 1942; Capot-Rey, 1945) and satellite images (Breed et al., 1979; Lancaster, 1995; El-Baz, 2000; Pye and Tsoar, 2008; Baird et al., 2019). Mainguet and Chemin (1983) suggested that the central part of the desert, which is subjected to strong deflation, represents a major source of sand for dune fields along its margins, where more humid climate, vegetation, and decreased wind strength induce deposition especially close to the main topographic barriers.

In the western Sahara, linear dunes predominate from the coast inland, whereas crescentic

dunes are common to the south, associated with north-easterly anticyclonic circulation from the Sahara and Azores high-pressure cells. In Mali and Niger, most dunes are partially vegetated under the influence of monsoonal moisture. Two sets of dunes occur along the Niger River, one indicating northeastward drift induced by trade winds, and the other oriented E/W with more spaced and eroded ridges. Crescentic dunes and large isolated star dunes characterize the Erg de Bilma in Niger (Fig. 3.1; Mainguet and Callot, 1978).

In the Moroccan desert close to the Atlantic coast, barchan dunes form under the effect of prevailing winds from the northwest and moderate to low sand supply (Elbelrhiti, 2012). In the northern Sahara, large sand seas with star dunes occupy depressions bordered by elevated areas. Star dunes are the product of a complex, multi-directional wind regime (Lancaster, 1995; Zhang et al., 2012), resulting from the interaction of winter westerlies with summer north-easterly and south-westerly winds generated from cyclonic perturbations in Mediterrean and Atlantic depression systems. Star dunes occur in the northern part of the Grand Erg Occidental, grading southward into crescentic dunes, and are aligned in linear trends in the Grand Erg Oriental. A network of barchanoid dunes in southern Tunisia is generated by high-energy winds, whereas crescentic or linear dunes grown in response to unimodal or bimodal wind directions are more common south of 30°N (Breed et al., 1979).

3.2.4 Quaternary evolution

Dry and wet climate alternated repeatedly in northern Africa during the Quaternary. Wind strength fostering dune growth increased in the latest Pleistocene, followed by a humid early Holocene and eventually by the return to arid conditions since the mid-Holocene. The desert expanded during the Last Glacial Maximum, when the ITCZ was displaced towards the equator (Nicholson and Flohn, 1980; Arbuszewski et al. 2013) and dunes mobilized by stronger wind moved onto arid landscapes (Grove and Warren, 1968; Swezey, 2001; Bristow and Armitage, 2016). Arid to humid transitions seemingly occurred at 15-14.5 ka and 11.5-11 ka, in association with the reduction of polar ice-sheets, strengthened hydrological circulation (Gasse, 2000), and northward displacement of the ITCZ (Haug et al., 2001).

At the onset of the early Holocene African Humid Period (~14.5 ka), natural corridors opened to allow the displacement of humans and other animals (Kuper and Kropelin, 2006; Drake et al., 2011). The current aridity initiated between ~5.5 ka (deMenocal et al., 2000) and ~4.5 ka (Gasse, 2000), but the timing and rate of desiccation that affected the Sahara

and Sahel at the end of the African Humid Period, including Mega-Lake Chad, remain controversial (Sarnthein, 1978; Bristow and Armitage, 2016).

3.3 Geological framework

Four partially overlapping geological domains can be identified in the Sahara Desert (Fig. 3.3): 1) the West African Craton, representing the oldest core of the continent; 2) the Tuareg Shield, including different sub-domains from east to west; 3) the Sahara Metacraton in the east, where the Archean cratonic core was intensely remobilized during the Pan-African orogeny; 4) Phanerozoic cover strata in the northern part of the desert, accumulated during multistep episodes of basin subsidence, tectonic inversion, and volcanic activity.

3.3.1 West African Craton

The West African Craton comprises the Man Shield in the south and the Reguibat Shield in the north. These terranes include an Archean core, built during the Leonian (3.0-2.9 Ga) and Liberian (2.7-2.6 Ga) orogenic cycles (Feybesse and Milési, 1994), bordered by Proterozoic to Phanerozoic mobile belts and sedimentary basins. The eastern Reguibat Shield and the Man Shield were affected by the Eburnean orogeny (~2.0 Ga), when the high-grade Birimian basement formed (Abouchami et al., 1990). The Anti-Atlas Mountains in Morocco also contain Paleoproterozoic basement, including granites as well as metasedimentary and metavolcanic rocks (Thomas et al., 2002).

During the Pan-African orogeny (0.85-0.55 Ga), one of the most extensive mountain-building events of the Earth's history that assembled the Arabian-Nubian Shield and deeply affected the Sahara Metacraton, the 3000 km-long Trans-Sahara belt formed as a result of collisions among the West African Craton, the Congo Craton, and the Sahara Metacraton. High sediment influx caused the filling of the Taoudeni (in the south) and Tindouf (in the north) intraplate basins (Fig. 3.3; Nance et al., 2008). Low-grade metamorphism and granite intrusions took place along the margins of the West African Craton (Black et al., 1979), whereas volcanic sequences and transpressional deformation are documented in the Anti-Altas to the north (Ennih and Liégeois, 2001). In the east, the Pan-African event is responsible for the formation of thrust belts along the western side of the West Africa Craton (Villeneuve, 2008), which developed only minor tectonic structures in the foreland of the Paleozoic Variscan orogeny (Ennih and Liégeois, 2008). The Cenozoic Alpine orogeny affected only the northernmost part of the African continent forming the High Atlas of Morocco (Mattauer et al., 1977).

3.3.2 Tuareg Shield

The Tuareg Shield, located between the West African Craton in the west and the Sahara Metacraton in the east, developed during the Neoproterozoic by eastward subduction and closure of the Aoujej and Imira oceanic realms at 700 and 625 Ma, and consequent accretion of different terranes (Caby et al. 1981, 1989; Fabre et al., 1982). High-temperature N/S shear zones were interpreted to document post-collisional lateral escape of rigid tectonic blocks (Liégeois, 2019).

During the Pan-African orogeny, granulitic gneisses of Archean and Paleoproterozoic age in the central Hoggar (e.g., Unitè Granulitique de Iforas) were remobilized with development of amphibolite-facies mega-shear zones (Liégeois et al., 1994) and the Tuareg Shield was heavily reworked (Bertrand and Caby, 1978). To the southwest, the Adrar des Iforas Massif recorded several magmatic events, including emplacement of the Renatt leucogranite (Liégeois et al., 1994), the Kidal continental-arc andesites (Chikhaoui et al., 1978), alkaline plutons between 600 and 580 Ma (Fezaa et al., 2018), as well as late/post orogenic plutons, dykes, and volcanic rocks between 570 and 520 Ma (Liégeois and Black, 1987).

The Aïr Mountains in the southwestern Tuareg Shield include three N/S elongated terranes (Aouzegueur, Barghot, and Assodé) containing high-grade metasedimentary rocks and serpentinites (Boullier et al., 1991; Moreau et al., 1994). Granites cross-cutting the main deformation were intruded at 664±8 Ma in the Barghot domain and between 645 and 580 Ma in the Assodé domain (Liégeois et al., 1994). The Aouzegueur and Barghot terranes were thrust eastward over the Saharan Metacraton in the late Neoproterozoic (Liégeois et al., 2000). A ring complex including anorthosite was emplaced in the Aïr Mountains during the early Devonian (Black, 1965), whereas Cenozoic magmatism was volumetrically negligible.

The northeastern border of the Tuareg Shield was affected by a major intracontinental tectono-magmatic event at 575–555 Ma, associated with the indentation of the cratonic basement of the Murzuq Basin (Fezaa et al., 2010).

3.3.3 Sahara Metacraton

The Saharan Metacraton (Fig. 3.3), separated by a mega-shear from the Tuareg Shield in the west and from the Arabian-Nubian Shield in the east, consists of Archean and Paleoproterozoic continental crust profoundly remobilized during the Pan-African orogeny, when migmatitic gneisses and metasedimentary rocks were intruded by granitoids between 750 and 550 Ma (Abdelsalam et al., 2002). Various geodynamic processes,

including continental collision (Schandelmeier et al., 1988), delamination of subcontinental mantle (Bird, 1979), lithospheric extension (Denkler et al., 1994), and assemblage of exotic terranes (Rogers et al., 1978) have been invoked to explain the Neoproterozoic evolution of the metacraton (Ghuma and Rogers, 1978; Pinna et al., 1994). In the east, an ophiolitic suture contains low-grade volcaniclastic rocks possibly documenting the closure of a failed rift (Stern et al., 1994; Kuster and Liegeois, 2001).

3.3.4 Phanerozoic sedimentary and volcanic rocks

The northern part of the Sahara is largely covered by Paleozoic to Cenozoic rocks deposited in sedimentary basins formed in the wake of the Pan-African orogeny and subsequently by extensional reactivation of inherited tectonic structures (Echikh, 1998; Bumby and Giraud, 2005).

Between the mid-Cambrian and the Late Ordovician (520-440 Ma), quartz-rich sandstones where deposited all across northern Africa, possibly as a continuous blanket from Oman in eastern Arabia to Mauritania with an average thickness of ~1 km and a volume of ~10 million km^3 (Burke, 1999). Their deposition followed the Pan-African orogeny and post-Pan-African continental wrenching, and characterized the ensuing phase of cooling and thermal subsidence that generated the accommodation space for the widespread accumulation of sand sheets. At that time, quartz-rich sandstones were similarly deposited in other parts of Gondwana and in North America as well (e.g., St. Peter Sandstone; Dott, 2003). Quartz-rich composition is highly unusual for orogenic detritus (Dickinson, 1985; Garzanti et al., 2007), an anomaly that still needs understanding. If these sediments are indeed first cycle, then *ad hoc* explanations are required. Cambro-Ordovician landscapes still devoid of vegetation and supposedly characterized by low relief and low sedimentation rates are envisaged to have suffered very extensive chemical weathering, fostered by warm humid climate and by an unusually corrosive atmosphere following late Neoproterozoic volcanism (Burke, 1999; Avigad et al., 2005). This scenario is apparently at odds with the major glaciation that affected Gondwana in the Late Ordovician, which itself represents a geological paradox, having occurred within a long greenhouse period with high atmospheric CO_2 levels (Brenchley et al., 1994; Ghienne et al., 2014).

In the Silurian, tectonic subsidence favoured the accumulation of marine to lacustrine sediments, overlain by shallow-marine clastics in the Murzuq Basin of Libya, in western Algeria, and in southern Morocco (Fekirine and Abdallah, 1998). Failed rifts were inverted during the Carboniferous as a consequence of Variscan convergence, affecting mostly

Morocco and less intensely Algeria and Libya (Haddoum et al., 2001). The High Atlas graben system formed in the Triassic and Jurassic extending eastwards to northeastern Algeria and Tunisia (Coward and Ries, 2003). During the Cretaceous, the Sirte Basin developed as another horst-and-graben system filled by shale and evaporite (Thusu and Mansouri, 1995). In the northern Murzuq Basin, these strata are overlain by basaltic lavas of the Haruj al Aswad Massif, emplaced in multiple phases between 4 and 0.5 Ma and triggered by reactivation of Tibesti-Sirte basement faults (Cvetković et al., 2010; Elsahafi and Gudmundsson, 2016).

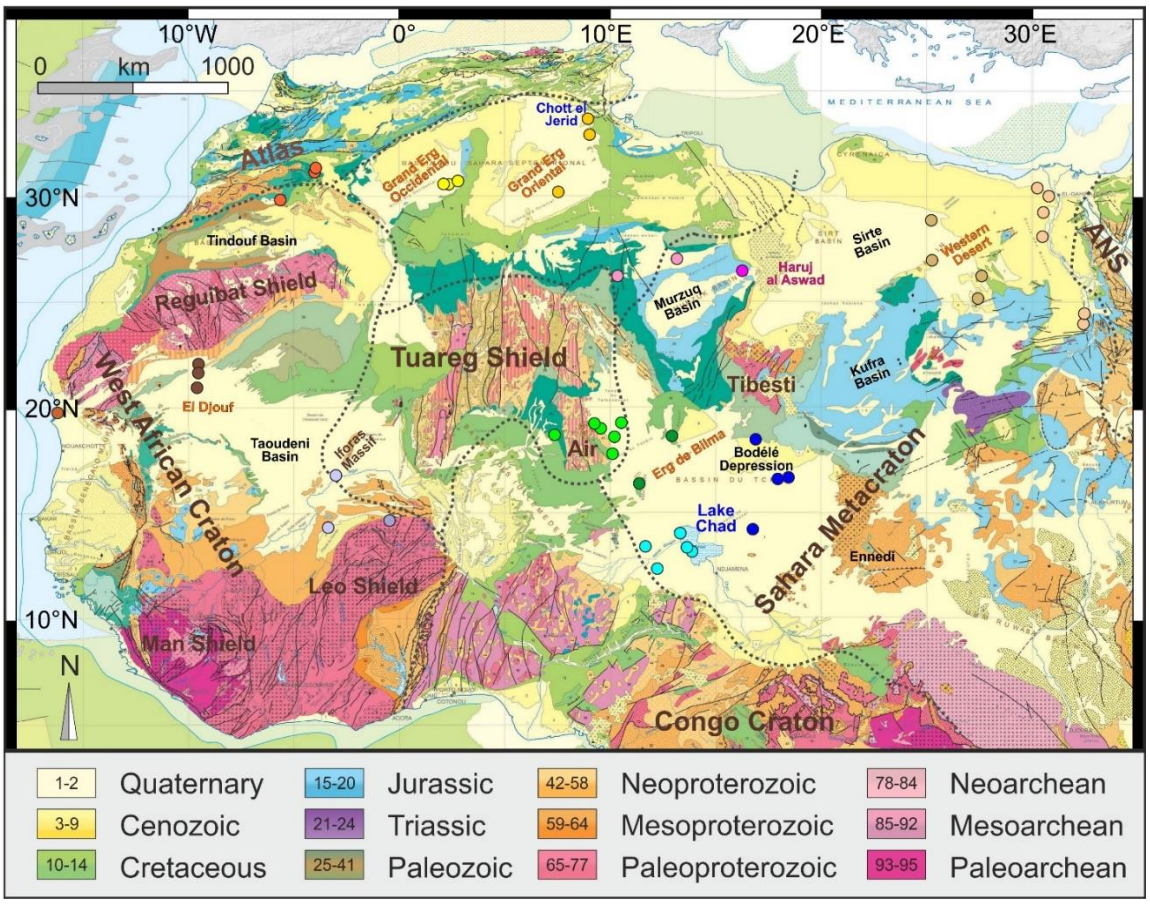

Figure 3.3. Geology of the Sahara (modified after CGMW-BRGM, 2016). Major tectonic domains are separated by dashed lines. Sample locations coloured as in Fig. 3.1. ANS = Arabian-Nubian Shield.

3.4 Sampling

This study analysed an archive of 45 sand samples of aeolian dunes, 36 collected between 2003 and 2019 by different operators across the Sahara Desert: 4 from Chad; 5 from Lake Chad, northern Nigeria, and southern Niger; 8 from central Niger; 1 from Burkina Faso; 2 from Mali; 4 from Mauritania; 3 from Morocco; 3 from Algeria; 2 from Tunisia; 3 from Libya; and 1 from western Egypt. Data are also provided for 9 additional aeolian dunes from Egypt: 3 from the Western Desert and 6 from the Nile Valley to the west of the Nile

River. Aeolian dunes to the east of the Nile River containing Nile-derived volcanic detritus (Muhs et al., 2013; Garzanti et al., 2015a) were considered as separated from the rest of the Sahara and thus not included in this study. GPS coordinates and further information on all sampling sites are provided in the Appendix.

3.5 Results

This section summarizes first the general petrographic, heavy-mineral, and detrital-geochronology signatures of Saharan dune sands. Next, highlights the characteristic compositional features of each region (Fig. 3.4).

3.5.1 Overview of detrital signatures

Most analysed sand samples (33 out of 44) are pure quartzose (Fig. 3.5), including all of those from the southeastern Sahara. In pure quartzose sands, orthoclase generally prevails over plagioclase and microcline*. The sum of lithic grains, micas and heavy minerals is <2% of total framework grains. The tHM suites of most samples (35 out of 44) are very poor to extremely poor and characterized by durable minerals (ZTR 25-96, anticorrelating with tHMC: r = 0.62, sign.lev. 0.1%) (Fig. 3.6). Zircon is most common, followed by tourmaline, epidote, amphibole, rutile, clinopyroxene, garnet, and staurolite.

Detrital zircon in Saharan dunes invariably yielded dominant Pan-African (Ordovician-Neoproterozoic) U-Pb ages, with a virtually continuous distribution between 0.48 and 1.1.Ga (77% of total ages), a prominent Cambrian-Ediacaran peak (0.5-0.6 Ga), a minor peak around 1.0 Ga, and an intervening broader cluster in the Cryogenian (0.65-0.8 Ga) (Fig. 3.7). Younger ages are Paleozoic (1.6%), Mesozoic (0.5%) and Cenozoic (0.2%). Older ages cluster between 1.8 and 2.2 Ga (11.7%) and between 2.47 and 2.7 Ga (2.8%). Zircon grains dated between 1.1 and 1.8 Ga and between 2.2 and 2.47 Ga represent 3.4% and 1.2% of total ages, respectively, whereas those older than 2.7 Ga represent 1.6%, with single ages as old as ~4 Ga.

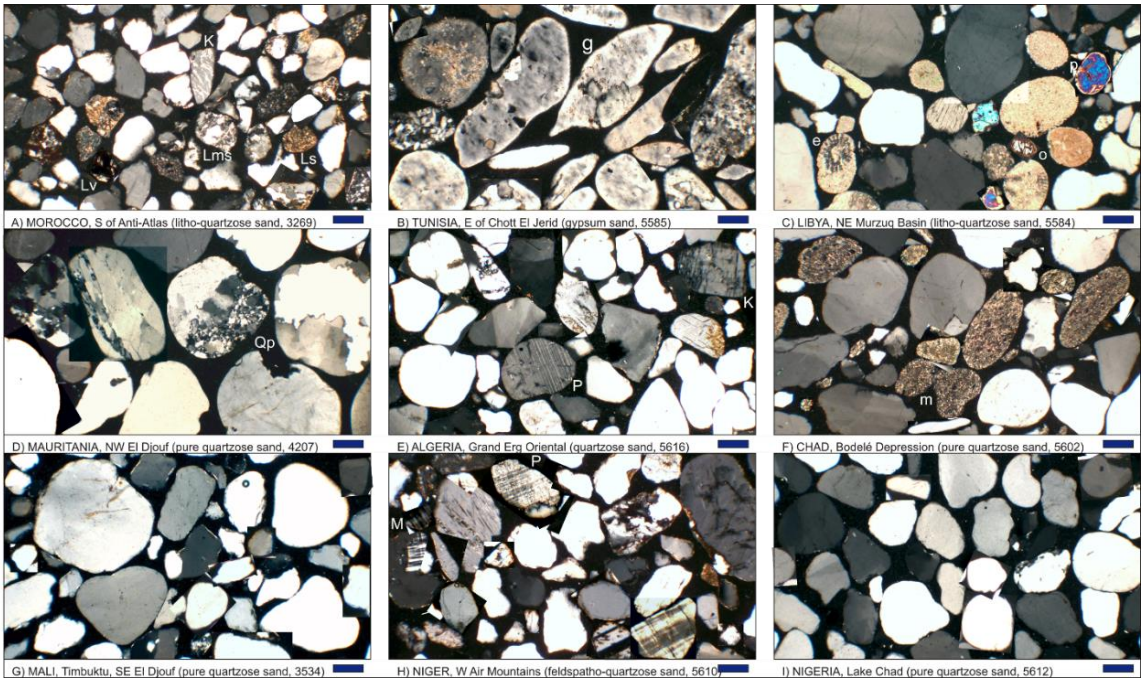

Figure 3.4. Compositional variability of Saharan dune sand (photos arranged in geographical order from NW to SE). **A**) Common sedimentary/low-rank metasedimentary lithics (*Ls*, *Lms*) with minor microlitic volcanic rock fragments (*Lv*) and perthitic K-feldspar (*K*) derived from nearby orogenic sources. **B**) Gypsum clasts (*g*) reworked from the adjacent salt lake. **C**) Common limestone grains (*e* = echinoid spine) with clinopyroxene (*p*) and olivine (*o*) derived from the Haruj al Aswad basaltic field. **D**) Common polycrystalline quartz (*Qp*) associated with up to well-rounded or etched monocrystalline quartz. **E**) Up to well-rounded or etched quartz associated with plagioclase (*P*) and K-feldspar (*K*). **F**) Up to well-rounded quartz with abundant mudclasts (*m*) reworked from the dry bed of once Mega-Lake Chad. **G**) Dominant, up to well-rounded monocrystalline quartz. **H**). Common K-feldspar (*M* = cross-hatched microcline) and plagioclase (*P*); quartz with abraded overgrowths (*arrow*) indicates recycled origin. **I**) Dominant, up to well-rounded monocrystalline quartz. All photos with crossed polars; blue bar for scale = 100 μm.

3.5.2 The southern Sahara

All across the southern Sahara, from Chad to the Atlantic Ocean, dune sand displays rather monotonous detrital signatures (Table 3.1). Both around the Bodélé Depression and in the Lake Chad region sand is pure quartzose with high ZTR indices (Fig. 3.4F, 4.4I). Minor K-feldspar occurs (sample 5609) and minor staurolite characterizes the Lake Chad region. Sample 5607 from Nigeria displays a sharp Ediacaran peak (44% of zircon grains).

In the ergs of central Niger, dune sand is pure quartzose with dominant durable minerals, locally associated with minor garnet or pyroxene (sample 3235). Closer to the eastern side of the Aïr Mountains, some grains of K-feldspar or plagioclase occur and tHM suites locally include common amphibole, epidote, and staurolite. Orosirian zircon ages are slightly more common in this region and Cambrian ages are also observed (3232) as well as one grain as

young as 6 Ma (3233). On the western side of the Aïr Mountains, sand is feldspatho-quartzose with significant polycrystalline quartz, orthoclase, microcline*, and sericitized plagioclase (Fig. 3.4H). The tHM suite is dominated by amphibole (mostly blue-green hornblende) associated with zircon and epidote. The zircon-age spectrum is also distinct, characterized by a sharp Ediacaran peak (47% of total ages), by secondary Orosirian (24%) and Silurian-Mississippian clusters (320-435 Ma; 19%), and by lack of ages older than the Orosirian.

Pure quartzose sand contains different amounts of ZTR minerals in Burkina Faso south of the Niger River (common epidote), Mali, and Mauritania (locally common epidote or pyroxene with minor garnet, staurolite, and amphibole) (Fig. 3.4D,G). Amphibole increases close to the Atlantic coast. Sand collected in Burkina Faso yielded a minor cluster of Early-Middle Jurassic detrital-zircon ages (4% of total grains). Zircon grains in Mali and Mauritania yielded a significant number of Orosirian (7-13% of total grains), Rhyacian (7-12%) and Archean ages (3-10%), and only minor Tonian (2-5%) and Stenian ages (≤ 4%).

3.5.3 The Northern Sahara

In the northern Sahara, sand composition is more varied. Sand collected along the southern and eastern front of the Anti-Atlas Mountains in Morocco ranges from pure quartzose to litho-quartzose with granitoid, mafic volcanic, sedimentary, or very-low-rank to medium-rank metasedimentary rock fragments (Fig. 3.4A). The tHM suite includes clinopyroxene associated with epidote, pumpellyite, prehnite, amphibole, and durable ZTR minerals. The obtained zircon ages are mostly Neoproterozoic and Orosirian, with one grain as young as 5 Ma (sample 3269).

Dune sand in the Grand Erg Occidental in Algeria is pure quartzose with dominant durable minerals, whereas dune sand of the Grand Erg Oriental in Algeria and Tunisia is quartzose (Fig. 3.4E), with K-feldspar including microcline* predominating over plagioclase, and locally dominant garnet (5616) or common amphibole and epidote (Table 3.1). Zircon grains yielded more Ediacaran ages in the Grand Erg Occidental and more Stenian ages in the Gran Erg Oriental.

In the Ubari Erg of Libya, dune sand is pure quartzose with dominant durable minerals associated with mainly actinolitic amphibole and epidote in the east. Dune sand collected in the Murzuq Erg near the Haruj al Aswad volcanic field (5584), instead, is litho-quartzose carbonaticlastic with a moderately poor tHM suite dominated by clinopyroxene and olivine (Fig. 3.4C). Orosirian ages of detrital zircon decrease, and Archean ages increase, from

west to east across the Libyan desert.

In pure quartzose sand of the Western Desert in Egypt, durable minerals are associated with epidote, garnet, and minor hornblende, staurolite and clinopyroxene. The zircon-age spectrum of sample 5601 in the northwest is similar to those of Libyan sands.

Detrital modes are varied in dune sand collected along the western side of the Nile Valley. In the Aswan area, litho-quartzose carbonaticlastic to quartzose sand contains a moderately poor tHM suite with epidote, amphibole, and clinopyroxene. Dune sand to the north ranges from quartz-rich feldspatho-quartzose, with K-feldspar including microcline* predominating over plagioclase, to litho-quartzose sedimentaclastic, quartzose, and pure quartzose. The very poor to moderately poor tHM suites include durable ZTR minerals associated with epidote, staurolite, hornblende, garnet, locally clinopyroxene, and minor kyanite (Table 3.1).

3.6 Data Analysis

All compositional datasets (petrography, heavy minerals, detrital-zircon geochronology) are remarkably homogeneous, indicating that most Sahara dune sands are either derived from similar sources or have been homogenized through multiple sedimentary cycles. Notable differences in compositional signals do occur, but only related to the local addition of volcanic, orogenic, or different sedimentary detritus (Fig. 3.4). Otherwise, identifying specific provenances, tracing sediment dispersal, and linking transport pathways with prevailing patterns of atmospheric circulation and wind regimes represents an arduous task. After this visual inspection of the data, we now turn to the multivariate ordination techniques to further investigate the presented results, in the anticipation that these tools may be able to detect hidden patterns and trends that the naked eye might have missed (Fig. 3.8).

3.6.1 Petrographic dataset

Correspondence Analysis of petrographic data (Fig. 3.8A) highlights the very limited variability of quartz content, with dominance of pure quartzose sand across the Sahara (Table 3.1). A significant variability is observed for K-felspar and plagioclase, which show a correlated behaviour. Quartz-rich feldspatho-quartzose samples from the western Aïr mountains, Grand Erg Oriental, and Nile Valley have low P/F ratio (24-29%) and low tHMC index, suggesting recycling of locally exposed sandstones ultimately derived from basement rocks rather than first-cycle supply from crystalline basement. Siltstone and metamorphic lithic grains are more common along the front of the Anti-Atlas in Morocco,

	n°	Q	F	Lv	Lc	Lsm	total	P/F	tHMC	ZTR	Ap	Ttn	Ep	P&P	Grt	St	Ky	Amp	Px	Ol	&tHM	total
CHAD & NIGERIA																						
Bodele Depression	4	99	0.8	0	0	0.1	100	0%	0.1	81	1	2	8	0	1	1	0.3	3	1	0	1	100
Lake Chad	4	98	1	0	0	0.5	100	54%	0.2	89	1	0.6	2	0	0.3	4	0.7	0.7	0	0	2	100
NIGER, BURKINA, MALI																						
Southern Niger	2	99	0.4	0	0	0.2	100	0%	0.3	94	0.2	1	1	0	0.2	1	0	0.2	0	0	1	100
Erg de Bilma	2	98	1	0	0	0.5	100	58%	0.2	60	0.5	1	13	0	7	2	0	6	9	0	0.2	100
E Air Mountains	2	99	0.7	0	0	0.3	100	0%	0.1	69	0.5	0.5	7	0	0	10	0	11	0.2	0	2	100
SE Air Mountains	2	96	4	0	0	0.1	100	31%	0.2	24	1	3	20	0	2	10	0	40	0	0	0.2	100
W Air Mountains	1	79	21	0	0	0	100	29%	0.2	23	4	1	16	0	1	1	1	52	0	0	0.5	100
Burkina Faso	1	100	0	0	0	0.2	100	n.d.	0.2	77	0	0	20	0	0	2	0	0.5	0	0	0	100
Mali	2	100	0.2	0	0	0	100	50%	0.1	91	0.2	0.5	3	0	0	3	1	0.5	0	0	0.5	100
MAURITANIA																						
Coastal Mauritania	1	97	3	0	0	0	100	33%	1.2	16	0.5	0.5	35	0	6	1	0	35	4	0	2	100
NW El Djouf	3	99	0.8	0	0	0.3	100	10%	0.1	50	1	0.4	21	0	4	4	0	5	13	0	1	100
MOROCCO & ALGERIA																						
Anti-Atlas	3	92	3	0.6	1	4	100	43%	0.3	19	1	3	11	12	2	2	0	9	38	0	3	100
Grand Erg Occidental	2	99	0.6	0	0	0	100	33%	0.1	93	0.2	0.4	5	0	2	0	0	0	0	0	0.2	100
Grand Erg Oriental	1	90	10	0	0	0.2	100	24%	0.6	20	0	1	7	0	64	1	1	0	0	0	5	100
TUNISIA & LIBYA																						
Grand Erg Oriental	1	94	5	0	0.5	0.5	100	25%	0.3	44	0.4	4	16	0	12	1	1	17	1	0	3	100
Ubari Erg	2	99	1	0	0	0	100	10%	0.3	72	0	1	11	0	3	1	0	10	1	0	1	100
NE Murzuq Erg	1	83	2	0.2	14	0.7	100	80%	1.1	2	0	0	2	0	0.5	0	0	0.5	56	38	1	100
EGYPT																						
Western Desert	4	97	3	0	0.3	0.2	100	39%	0.1	44	1	2	23	0	11	5	1	6	5	0	1	100
Aswan area	2	85	3	0.3	9	2	100	44%	1.5	11	0	0.2	30	0	2	3	0.7	29	23	0	1	100
Nile Valley	4	89	4	0.4	4	2	100	41%	0.8	36	0.1	1	26	0	7	10	4	9	6	0	0.2	100

Table 3.1. Petrography and heavy minerals in Sahara dune sands. Q = quartz; F = feldspars (P = plagioclase); L = lithic grains (Lv = volcanic; Lc = carbonate; Lsm = other sedimentary and metasedimentary). Transparent heavy minerals (tHMC) include: ZTR = zircon + tourmaline + rutile; Ap = apatite; Ttn = titanite; Ep = epidote; P&P = prehnite + pumpellyite; Grt = garnet; St = staurolite; Ky = kyanite; Amp = amphibole; Px = pyroxene; Ol = olivine; &tHM = others (anatase, sillimanite, andalusite, monazite, topaz, brookite).

reflecting orogenic contributions. Nile Valley and Murzuq Basin sands are enriched in carbonate grains derived from Cenozoic cover strata of the Sahara Metacraton.

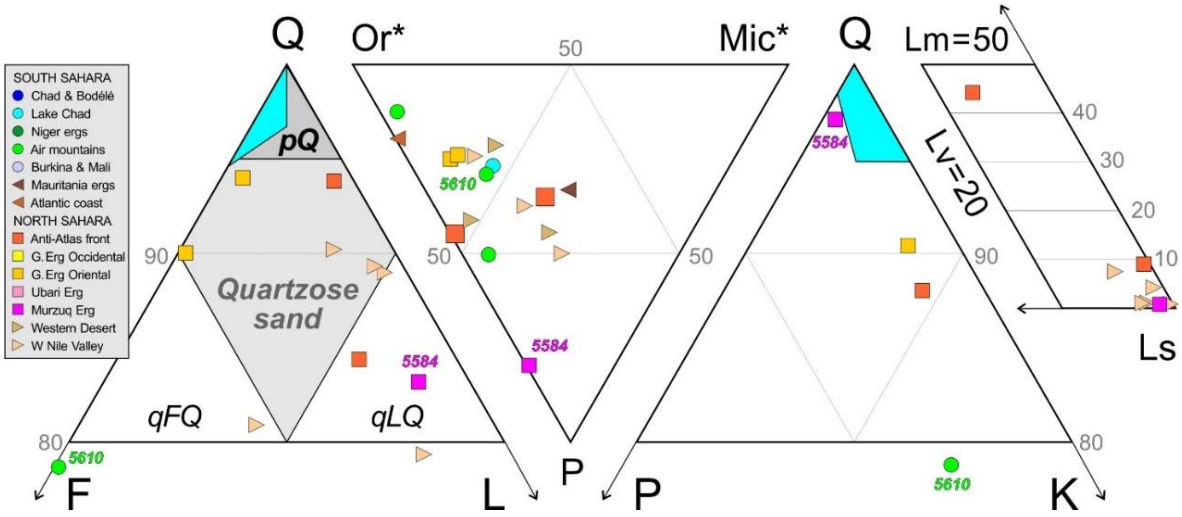

Figure 3.5. Petrography of Sahara dune sand. Most samples are monotonously pure quartzose (*pQ*; plotting in blue fields of QFL and QPK diagrams), with K-feldspar prevailing over plagioclase and negligible lithics. A few samples are quartzose, quartz-rich feldspatho-quartzose (*qFQ*) or quartz-rich litho-quartzose sedimentaclastic (*qLQ*; W of Nile Valley, S of Anti-Atlas in Morocco, and NE Murzuq Erg in Libya). Q = quartz; F = feldspars (P = plagioclase; Or* = untwinned K-feldspar: Mic* = cross-hatched microcline); L = lithic fragments (Lm = metamorphic; Lv = volcanic; Ls = sedimentary).

3.6.2 Heavy mineral dataset

Correspondence Analysis of heavy-mineral data (Fig. 3.8B) highlights the anti-correlation between durable ZTR minerals and epidote + garnet + amphibole, the triad forming the mineralogical suite typical of metamorphic basements (Garzanti and Andò, 2007a). The variability of the ZTR index matches that of quartz, indicating a concordant behaviour of all durable minerals typical of extensively recycled sediments. Epidote, amphibole and garnet are correlated (Fig. 3.6) and abundant both west and east of the Aïr Mountains, in the Western Desert of Egypt and along the Nile Valley, with maxima reached in coastal Mauritania and in the Grand Erg Oriental in Algeria. Sample 5616 is the only garnet-dominated sand. Clinopyroxene content varies widely, being most abundant in the NE Murzuq sample 5584, where it is associated with olivine (Fig. 3.4C), and in all three Moroccan samples also containing prehnite and pumpellyite (Table 3.1).

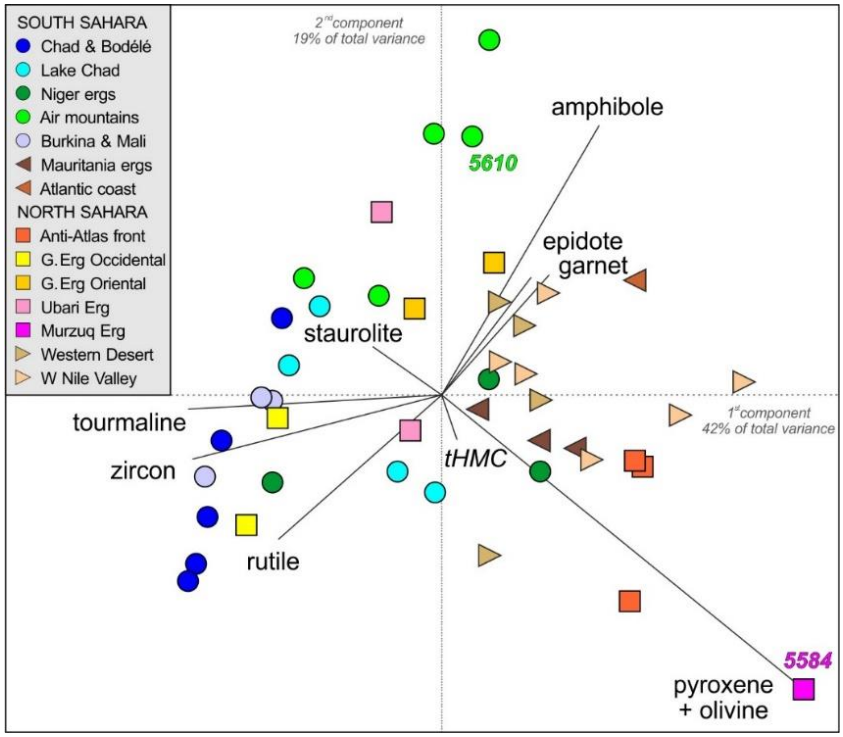

Figure 3.6. Heavy minerals in Saharan dune sand. The biplot highlights that tHM suites are mixtures of three main mineral groups: 1) largely recyled durable ZTR; 2) the orogenic triad amphibole, epidote and garnet; 3) volcanic-derived clinopyroxene and olivine. ZTR minerals are dominant in the southern Sahara, with amphibole and locally staurolite increasing close to the Aïr Mountains in Niger (5610). In the northern Sahara, clinopyroxene occurs more frequently and a clinopyroxene-olivine suite characterizes dunes near the Haruj al Aswad volcanic field in Libya (NE Murzuq Erg, 5584).

3.6.3 Detrital Zircon age dataset

Besides KDE plots — which basically highlight the ubiquitous Pan-African peak with lesser "Grenvillian" (~1 Ga) and "Eburnean" (~2 Ga) clusters (Fig. 3.7) thus underscoring the homogeneity of geochronological signatures across the Sahara —, the MDS map allows us to extract additional information from zircon-age distributions (Fig. 3.8C). Geographically closer samples tend to plot closer to each other, as in Chad and Mauritania. Hierarchical clustering analysis points to a systematic difference between southeastern Sahara samples, characterized by a more prominent ~1.0 Ga peak, and northwestern Sahara samples, yielding fewer Stenian zircons and characterized by a larger Paleoproterozoic peak and some Paleozoic and Mesozoic ages. Sample 5610 from west of the Aïr Mountains is singled out by the presence of a Paleozoic peak and the virtual lack of ~1.0 Ga grains.

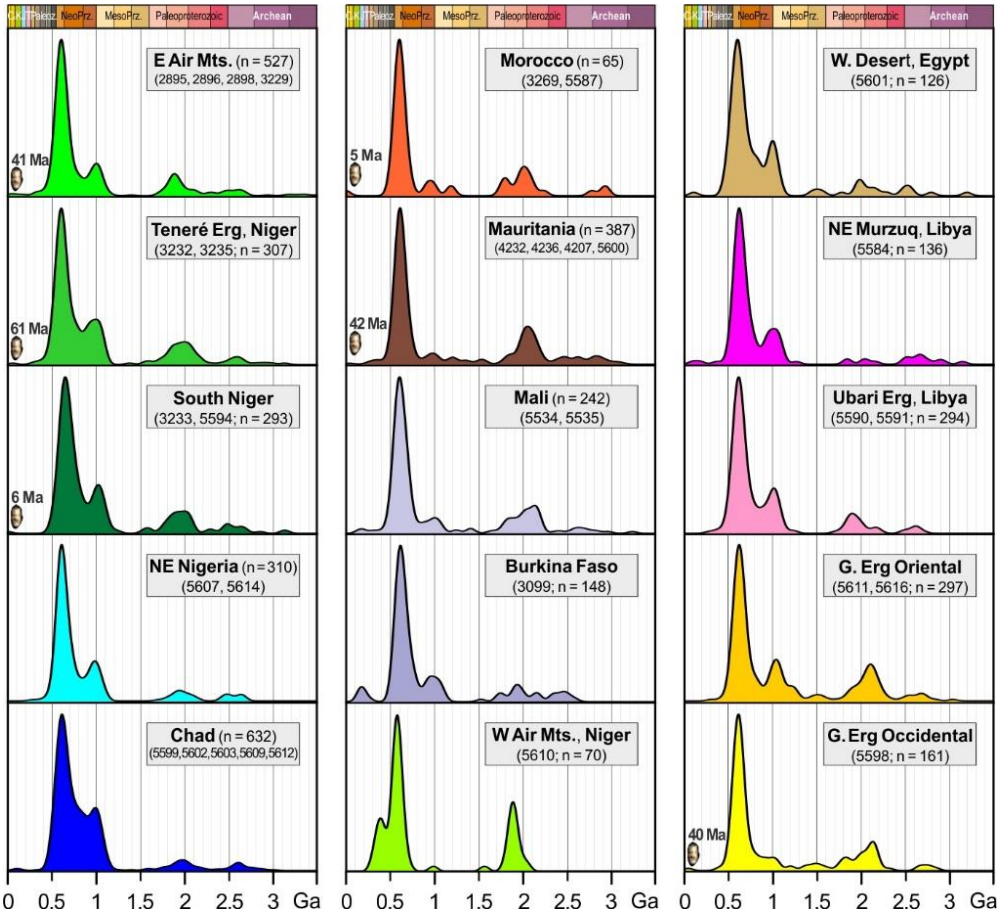

Figure 3.7. U-Pb age spectra of detrital zircons (age *vs.* frequencies plotted as Kernel Density Estimates using the *provenance* package of Vermeesch et al., 2016). All samples display the characteristic Neoproterozoic "double-peak", with minor Paleoproterozoic and Archean ages. Paleozoic and Mesozoic clusters occur west of the Air Mountains and in Burkina Faso, respectively. Cenozoic ages are found in Algeria and Mauritania and are locally as young as 5-6 Ma in Morocco and Niger.

3.7 Inferences based on combined dataset

Statistical analysis of single datasets meets only limited success in the attempt to highlight significant regional differences among the overall remarkably homogeneous provenance signatures of Sahara Desert sand. Within each dataset, dissimilarities are mostly small and clear only for the few samples documenting additional sediment contribution from local sources. In such a case of homogeneous data, statistical analysis may easily emphasize minor local anomalies and overstress their significance. Combining framework-petrography, heavy-mineral, and geochronological datasets with multivariate analysis produces visual plots (Fig. 3.8D, 4.8F) that helps us not only to increase discrimination power but also to verify the consistency of potential artefacts, thus leading to more robust results.

The INDSCAL plot (Fig. 3.8D) shows that three quarters of the samples have the same petrographic and heavy-mineral fingerprint, preventing any provenance discrimination among them. These samples are widely distributed from Chad to Tunisia and from the Western Desert of Egypt to Mauritania, thus failing to display a definite geographical distribution across the Sahara. Some significant differences are however confirmed, concerning samples collected along the Nile Valley in Egypt and the Anti-Atlas front in Morocco, or in the NE Murzuq Erg (5584) and the Aïr Mountains in western Niger (5610). Sample 5616 from Algeria is singled out by its garnet-dominated tHM suite.

In the GPA plot (Fig. 3.8F), clusters were based on the hierarchical clustering dendrogram (Fig. 3.8E), but addition of detrital-zircon ages does not change the overall picture substantially, maintaining the difference between NW Sahara and SE Sahara samples documented by MDS analysis of the zircon-age dataset. The distinctive local provenance of samples collected along the Anti-Atlas front in Morocco (3269), in the Grand Erg Oriental (5616) in the NE Murzuq Erg (5584), and west of the Aïr Mountains (5610) is confirmed. Other samples from Tunisia (5611), Mauritania (5600), have only minor peculiar petrographic or heavy-mineral fingerprint and they are singled out mainly by subtle differences in their zircon-age spectra This is thus considered either of local significance or as one case of artefact produced by the statistical algorithm which, in such homogeneous datasets, ends up emphasizing minor differences.

Even a thorough analysis conducted with sophisticated statistical techniques including Multidimensional scaling (MDS), Correspondence analysis (CA), Individual Difference Scaling (INDSCAL), and General Procrustes Analysis (GPA), therefore, could not break the compositional homogeneity of Sahara dune sands. Rather, the power of these techniques to reveal even the most subtle trend in a large dataset carries the risk of producing spurious results caused by local factors such as hydrodynamic sorting or bias in sampling or analytical procedures.

3.7.1 Local sediment sources

Petrographic, heavy-mineral, and geochronological signatures and their remarkable homogeneity indicate that Saharan sands have an overwhelmingly multicyclic origin, as discussed in detail below. Among the few differences highlighted by statistical analysis (Fig. 3.8), the two samples consistently displaying a distinct compositional fingerprint are those from the northeastern Murzuq basin (5584) and western Niger (5610).

The NE Murzuq sample is the richest in limestone grains, transparent heavy minerals,

clinopyroxene, and olivine of the entire sample set. The contrasting information provided by petrographic and heavy-mineral analyses represents an apparently paradoxical case, which is produced whenever recycled detritus generated by a heavy-mineral poor sedimentary source mixes with minor quantities of first-cycle detritus supplied by a heavy-mineral rich source (Garzanti and Andò, 2019). In this case, local sedimentary sources as young as Quaternary (Geyh and Thiedig, 2008) also supply limestone grains, whereas the Plio-Quaternary Haruj al Aswad basaltic field (Al-Hafdh and El-Shaafi, 2015) contributes clinopyroxene and olivine but very few basaltic grains.

The sample collected west of the Aïr mountains (5610) is most distinct in all respects. It is the richest in feldspars and amphibole and yielded only two zircon grains in the entire 654-1569 Ma age range. Rather than additional first-cycle contribution from basement rocks such as the Assodé-Issalane amphibolite-facies metamorphic rocks or Renatt granite, the low P/F ratio and very low heavy-mineral concentration point at recycling of (i.e., derivation from) Paleozoic to Mesozoic sandstones exposed nearby (e.g., Salze et al., 2018).

Moroccan samples document additional contribution from local orogenic sources represented by the High Atlas and adjacent Anti-Atlas Mountains, including clinopyroxene from volcanic rocks and epidote, prehnite, and pumpellyite from very-low to low-grade metavolcanic rocks. Prehnite and pumpellyite are peculiar of this region, and do not occur in the similar tHM suite characterizing the northwestern El Djouf Erg of central Mauritania, which includes more ZTR minerals and less clinopyroxene.

The enrichment in garnet in dune sample 5616 collected in the middle of the Grand Erg Oriental is puzzling (Table 3.1). This anomaly might be ascribed to local concentration of garnet by selective removal of lower-density minerals, a process that may occur in this dune field characterized by turbulent wind circulation. The widespread presence of star dunes in the erg (Telbisz and Keszler, 2018) lends support to this hypothesis.

Distinct composition also characterizes dunes along the Nile Valley, which include a few feldspars, carbonate rock fragments and a few other sedimentary, metasedimentary and volcanic lithics, together with a tHM suite ranging up to moderately poor and including epidote, amphibole, clinopyroxene, staurolite, and minor garnet and kyanite. This indicates sediment mixing from various sources, including the Saharan Metacraton, its Mesozoic to Cenozoic cover strata, and the Nile (Garzanti et al., 2015a).

3.7.2 Local sediment reworking

The considerations made above concern only sand derived from lithified source rocks. In desert environments, however, the incessant wind action causes repeated and extensive reworking of unconsolidated sediment, not only from the stoss side to the lee side of active dunes or from one active dune to the next, but also from locally exhumed fossil dune fields. Major sources of wind-reworked sediment are dry lake beds, found in diverse areas both within and at the periphery of the desert and representing the record of a recent wetter past (Drake et al., 2011). Examples include the active dunes dominated by gypsum grains found around Chott el Jerid at the northern edge of the Sahara in Tunisia (Fig. 3.4B) and the abundant rounded mudclasts mixed with monocrystalline quartz in dunes surrounding the Bodélé Depression in Chad (Fig. 3.4F). Sediment deflated from lake beds, however, dominantly consists of fine silt carried thousands of kilometers away as far as South America and the Caribbean (Swap et al., 1992; Prospero, 1996).

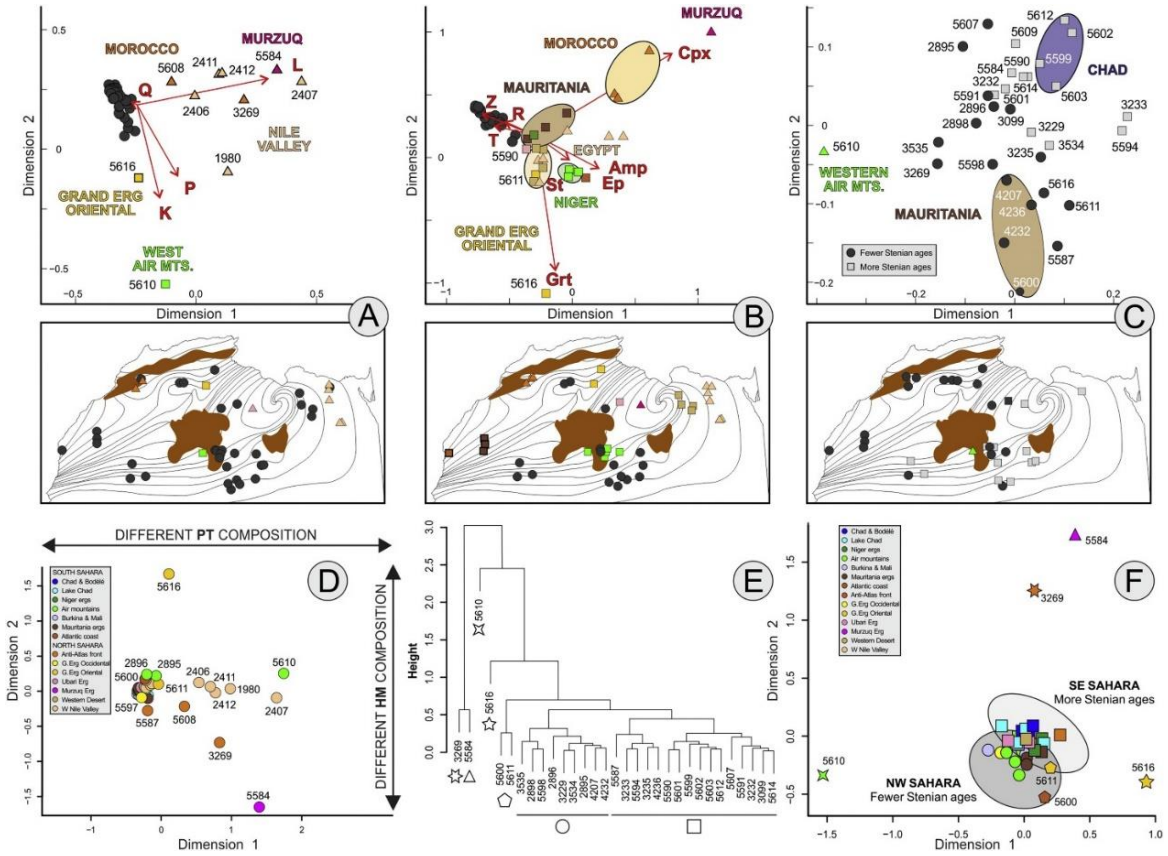

Figure 3.8. Multivariate statistical analysis **A**) CA for petrographic (PT) dataset. **B**) CA for heavy-mineral (HM) dataset. **C**) MDS for detrital-zircon (DZ) ages. **D**) INDSCAL for combined PT and HM datasets. Group configuration is expressed by perpendicular arrows and depict the direction of variability for each dataset. **E**) Hierarchical clustering dendrogram (height refers to normalised distance units produced by GPA of PT, HM, and DZ datasets; Garzanti and Vermmesch, 2015). **F**) Generalised Procrustes Analysis (GPA) of PT, HM and DZ datasets (symbol shapes refer to cluster

analysis in ***E*** and colours to geographical location). For ***A***, ***B***, and ***C***, sample locations are shown on the sand flow map below; clusters refer to hierarchical clustering;axes units are normalised values based on chi-square distance for ***A*** and ***B***, and on Kolmogorov-Smirnov distance for ***C***.

3.8 Polycyclic nature of Saharan sands

3.8.1 Sand derived from sandstone

Saharan dune sand is almost invariably pure quartzose with very poor tHM suites dominated by zircon, tourmaline, and rutile (Fig. 3.4, 3.5). Because these are the most mechanically and chemically durable common minerals, and hence those most likely to survive more than a single sedimentary cycle, quartz abundance and depleted tHM suites have long been used as indicators of the extent of recycling (e.g., Hubert, 1962; Blatt, 1967). The monotonous mineralogical signature of dune sand all across the Sahara thus points at provenance dominantly from siliciclastic rocks widely exposed throughout the region and ranging in age from Paleozoic (Avigad et al., 2005; Meinhold et al., 2011; Morton et al., 2011) to Mesozoic (e.g., "Nubian sandstone"; Selley, 1997; Carr, 2003), and Cenozoic (Swezey, 2009).

Detrital-zircon geochronology studies of these sandstones (Table 3.2) documented the widespread abundance of Neoproterozoic-aged zircon grains, indicating supply from the Pan-African orogen including the Trans-Sahara belt. A subordinate Paleoproterozoic cluster was inferred to indicate provenance from the West African Craton or perhaps Amazonia (Linnemann et al., 2011). A Tonian age cluster characterizes feldspar-bearing Cambrian sandstones in Morocco (Avigad et al., 2012). The common occurrence of ~1 Ga ("Grenvillian") zircons in Paleozoic to Mesozoic sandstones of southern Libya, lacking equivalents in igneous basements of northern Africa, has been emphasized (Meinhold et al., 2011).

3.8.2 Comparing compiled datasets

Statistical tools are here applied to compare zircon-age data obtained on modern sands (Fig. 3.9) with compiled age spectra from potential Paleozoic to Mesozoic parent sandstones exposed in northern Africa (Fig. 3.10). The stack of KDE plots highlights the recurrence of the most prominent Ediacaran (~0.6 Ga) peak in all compiled datasets (Fig. 3.10B). Among potential source rocks, most distinct is the spectrum from Paleozoic-Mesozoic sandstones of southern Libya (Meinhold et al., 2011), which display more prominent "Grenvillian" (~1 Ga), "Eburnean" (~2 Ga) and "Liberian" (Neoarchean) peaks. More and slightly older Eburnean-aged zircons characterize Cambrian sandstones from western Algeria (Wang et

al., 2020). Most striking is the similarity of zircon-age spectra between modern Saharan and Arabian dune sands. Besides the not many Mesozoic and Cenozoic zircons occurring in dune fields close to Arabian Gulf shores and derived from the Anatolia Plateau and the Zagros Mountains *via* the Euphrates-Tigris-Karun river system (Garzanti et al., 2016), differences are limited to a few more ages around 0.8 Ga (a feature common to Nile sand; Fig. 9) and a few more Neoarchean ages in Arabia.

The remarkable homogeneity of detrital-zircon age spectra all across Arabia and northern Africa is confirmed by Multidimensional Scaling analysis. The central position of Saharan sands in MDS maps (Fig. 3.10C,D) confirm that, as Arabian desert sands, they largely resulted from the homogenization of detritus recycled from Paleozoic to Mesozoic parent sandstones. The MDS maps highlight that this averaged zircon-age signal also characterizes Cambrian sandstones of southeastern Algeria, Morocco, and central-western Libya (Linnemann et al., 2011; Avigad et al., 2012; Altumi et al., 2013), whereas Paleozoic-Mesozoic sandstones of southern Libya (Meinhold et al., 2011) and Cambrian sandstones fromwestern Algeria (Wang et al., 2020) are distinct.

3.8.3 Paleozoic sandstones as a major sand supplier for modern dunes

Cambro-Ordovician and younger sandstones widely exposed across the Sahara represent a huge reservoir of quartz grains to be recycled through time, finally ending up in modern dune fields. In Saharan dune sand, zircon grains yielded mostly (77%) Neoproterozoic ages, consistently with ultimate origin from the Pan-African orogen and the Trans-Sahara belt. Virtually the same zircon-age spectra characterize dune sand across the Sahara, Nile River sand from Ethiopia and Sudan to Egypt, and Arabian sand seas from the Great Nafud in the north to the giant Rub' al Khali in the south (Fig. 3.9). Such a vast areal distribution of parent sandstones and daughter sands with the same mineralogical and geochronological fingerprints reflects multiple recycling and homogenization at the wide spatial scale of the whole northern Africa and Middle East throughout the Phanerozoic. After the major Pan-African mountain-building event and the tectonic activity that followed (e.g., Stern, 1985), the large volume of newly produced crustal material was extensively eroded and repeatedly recycled until the present day.

Besides the dominant Neoproterozoic double peak, Meinhold et al. (2013) noted that Grenvillian-aged zircons become more common from Morocco and Algeria to Libya, and from Cambrian to Middle Ordovician strata in Libya. Such an eastward trend is reflected in zircon-age spectra of dune sand, showing a southeastward increase in the relative

Study	Unit	Technique	concordant/ total ages	Age clusters	eHf(t) values
Linnemann et al., 2011	Cambro-Ordovician Tassili Ouan Hoggar, Algeria	U-Pb (LA-ICP-MS)	630/850	0.74–0.54 (61%), 2.2–2.0 (20%), 1.8–1.3 (7%), 0.98–0.75 (6%), 2.65–2.30 (3%)	
Meinhold et al., 2011	Paleozoic-Mesozoic Murzuq, Libya	LA-SF-ICP-MS	1257/1678	0.72–0.53 (39%), 1.06–0.92 (18%), 2.2–1.7 (16%), 2.75–2.50 (8%)	
Avigad et al., 2012	Lower and Middle Cambrian, Morocco	LA-ICP-MS/Lu-Hf	419/?	Mid.Cambrian: 0.63–0.54 (18%), 1.00–0.63 (61%), 1.2–1.0 (3%), 2.5–1.6 (16%) Lower Cambrian: 0.63–0.54 (71%), 1.00–0.63 (5%), 2.5–1.6 (23%)	Neoproterozoic zircons: LC: eHf(t) > 0; MC: eHf(t) < 0
Altumi et al., 2013	Cambrian Hasawnah Fm., Libya	LA-ICP-MS	329/720	0.70–0.54 (60%), 2.4–1.6 (18%), 3.4–2.5 (5%)	
Wang et al., 2020	Cambrian, Ougarta Mountains, Algeria	LA-ICP-MS/Lu-Hf	449/536	0.80–0.56 (49%), 1.47–0.89 (2.4%), 3.4–1.6 (48%)	0.6 Ga zircon: +12/-25 (avg -1) 2.3–1.7 Ga zircon: +6/-27 (avg -10)
Garzanti et al., 2013	Northern Arabia sand seas	LA-ICP-MS	1565/?	1.0–0.5 (74%), 1.1–1.0 (8%), 2.0–1.8 (3%), 2.6–2.5 (3%)	
Garzanti et al., 2017	Rub Al Khali, Saudi Arabia	LA-ICP-MS	3909/5454	1.10–0.49 (85%), 2.15–1.74 (5%), 2.73–2.40 (5%)	
This study	Sahara Desert	LA-ICP-MS	3996/5437	0.70–0.54 (51%), 1.1–0.9 (6%), 2.2–1.8 (11.7%) 2.70–2.47 (3%)	

Table 3.2. Compilation of ages of detrital zircons contained in Phanerozoic sedimentary rocks and modern dunes from Arabia and northern Africa. Age range is in Ga and percentage of grain ages are provided for each cluster.

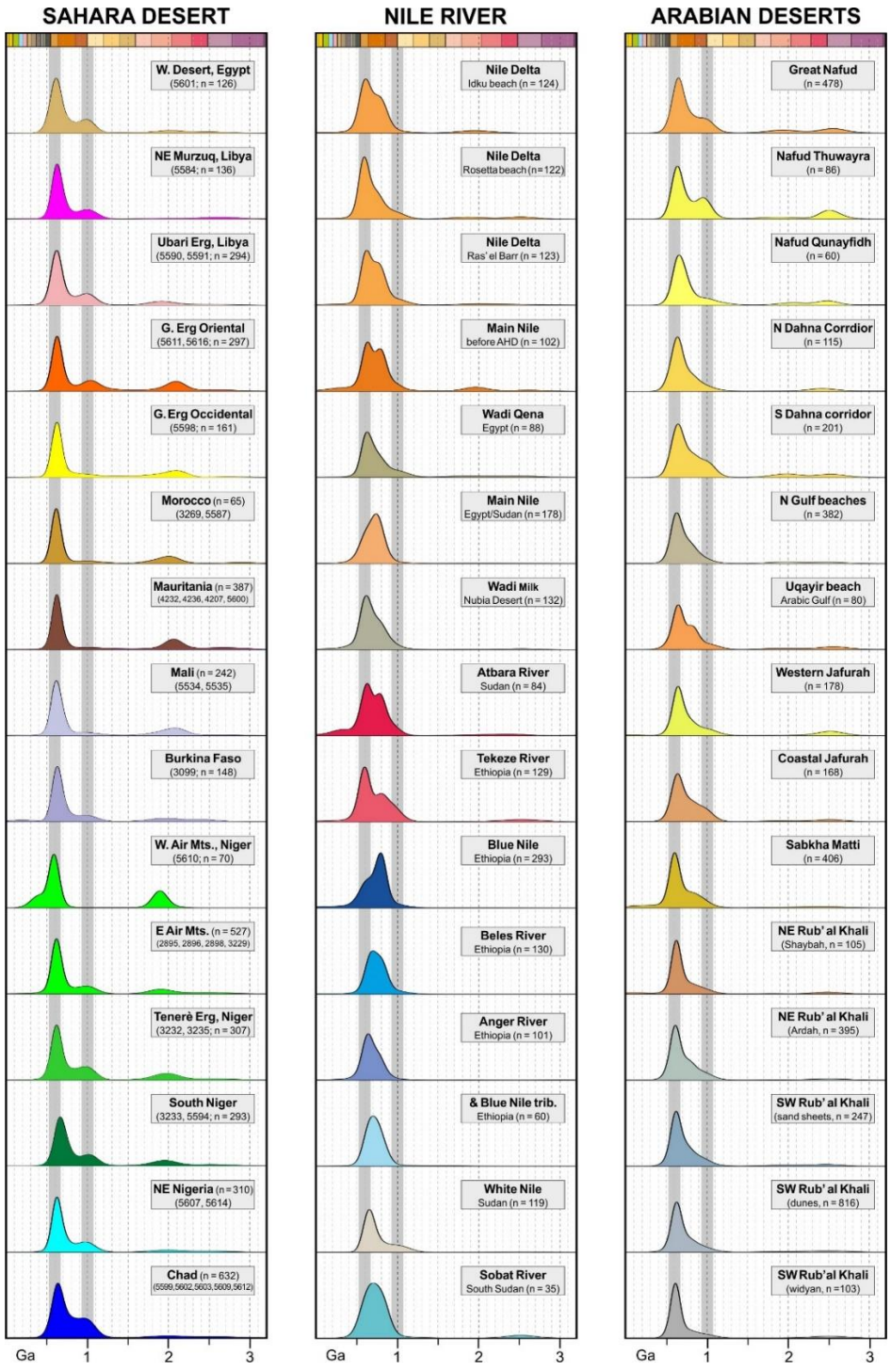

Figure 3.9. Statistical analysis based on compiled detrital-zircon ages presented in Table 3.2. **A)** Sample locations and sand flow map**. B**) Cumulative KDE plot of all concordant ages from this study (neon red) compared with KDE plots of compiled datasets (peak height normalized to maximum peak of each dataset; bandwidth maintained constant for all datasets). **C**, **D)** MDS maps comparing the cumulative age spectrum from this study (***C***), and age spectra for each sample group presented in Fig. 3.7 (***D***), with compiled datasets. Axes units are normalised values based on Kolmogorov-Smirnov distance, with 90% confidence polygons represented by dashed red lines. Shepard's plot shown in lower left corner.

abundance of Stenian-age zircons from Mali, Mauritania, western Niger and Morocco (≤5% of total ages) to central-eastern Niger, Chad, Libya, and Egypt (3-16% of total ages; Fig. 3.7).

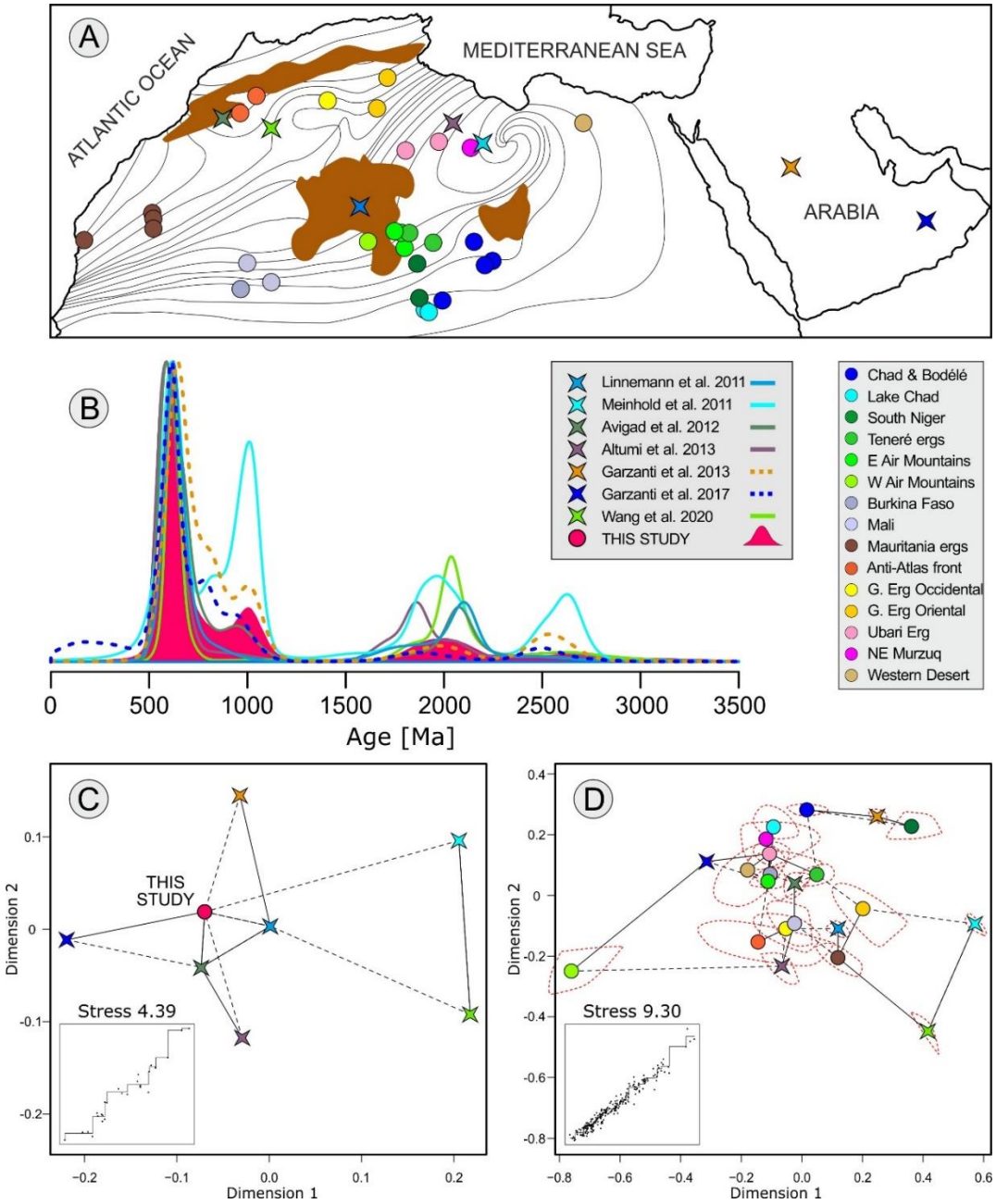

Figure 3.10. Statistical analysis based on compiled detrital-zircon ages presented in Table 3.2. **A)** Sample locations and sand flow map**. B**) Cumulative KDE plot of all concordant ages from this study (neon red) compared with KDE plots of compiled datasets (peak height normalized to maximum peak of each dataset; bandwidth maintained constant for all datasets). **C**, **D)** MDS maps comparing the cumulative age spectrum from this study (***C***), and age spectra for each sample group presented in Fig. 3.7 (***D***), with compiled datasets. Axes units are normalised values based on Kolmogorov-Smirnov

distance, with 90% confidence polygons represented by dashed red lines. Shepard's plot shown in lower left corner.

3.9 Conclusions

The Sahara is a vast desert. Its composite structure includes large dune fields hosted in sedimentary basins separated by elevated areas exposing the roots of Precambrian orogens or created by recent intraplate volcanism. Such an heterogeneity of landscapes and geological formations is contrasted by a remarkably homogeneous composition of dune sand, consisting almost everywhere of > 95% quartz and durable minerals such as zircon, tourmaline, and rutile. Exceptions are recorded only locally in the vicinity of volcanic fields (e.g., Haruj al Aswad in Libya), basement highs (e.g., Aïr Mountains in Niger), fold belts (Anti-Atlas in Morocco), or along the Nile Valley. Everywhere else, from Lake Chad and the Bodélé Depression to the great ergs of Algeria, and from the Western Desert of Egypt to the Atlantic coast of Mauritania, dune sand has almost the same, monotonous, pure quartzose composition. Besides U-Pb age spectra of detrital zircons, which reveal a significant difference between the southeastern part of the desert characterized by a more pronounced ~1 Ga peak *versus* the northwestern part where Paleoproterozoic ages are more common and some Paleozoic and Mesozoic ages occur, presented data do not show any compositional trend that could be compared with the main directions of present or past atmospheric circulation and wind transport.

The composition and homogeneity of Saharan dune sand reflect similar generative processes and source rocks, and extensive recycling repeated through geological time after the end of the Neoproterozoic, which zircon-age spectra indicate as the last major event of crustal growth in the region. Subsequently, the newly formed Arabian-Nubian Shield was covered by quartz-rich siliciclastic sediments extending all across the area from Oman to Mauritania and beyond. It is from this thick blanket of sandstone that large volumes of quartzose sand were generated and enriched progressively in durable minerals during the multiple cycles of erosion, sedimentation and diagenesis that took place in the long period of relative tectonic quiescence that characterized the entire Phanerozoic in this region. The geographic zircon-age distribution in daughter sands thus chiefly reflects the zircon-age distribution in parent sandstones (i.e., different patterns between southeast and northwest), and hence sediment dispersal systems existing at those times rather than present wind patterns (i.e., separation of sand flow between north and south).

Because zircon is durable, the larger part of zircon grains contained in most sediment

samples is likely to be recycled from sedimentary covers rather than derived first-cycle from basement rocks. In provenance studies based on detrital-zircon ages, the assumption that observed age patterns reflect transport pathways existing at the time of deposition rather than inheritance from even multiple and remote landscapes of the past thus needs to be carefully investigated and convincingly demonstrated rather than implicitly assumed.

Chapter 4: Kalahari Desert

This chapter has been published with modification as: "*Provenance of Kalahari Sand: Paleoweathering and recycling in a linked fluvial-aolian system*" by Garzanti, E.; Pastore, G., Stone, A., Vainer, S., Vermeesch, P., & Resentini, A. on Earth Science Reviews, 224, 2022.

4.1 Introduction

The intracratonic Kalahari sag basin hosts several dunefields that, largely inactive at present, represent the largest sand sea on Earth (Fig 4.1). The compositional signatures of such a vast expanse of aeolian sand and their provenance have not been systematically studied so far, and yet encrypted in them lies a bounty of information on the geological, geomorphological, and environmental history of the region. Formed as a consequence of the multistep break-up of Gondwana, the Kalahari Basin presently occupies the core of southern Africa, which experienced dynamic uplift in the Cenozoic and is currently cut across by the southwestward-propagating East African rift system (Haddon and McCarthy, 2005; De Wit, 2007). Complex landscape evolution during the Pleistocene and Holocene was punctuated by a high-frequency alternation of arid and humid climatic stages and consequent repeated changes in hydrology, drainage patterns, and interaction of fluvial and aeolian processes (Burrough et al., 2009a; Hürkamp et al., 2011; Moore et al., 2012; Matmon et al., 2015). Decrypting the Kalahari sedimentary archive is an essential step to improve the understanding not only of the evolution of tropical southern Africa but also of the interplay between tectonic and climatic forces that mould the Earth's surface. Clarifying the control exerted by key climate variables on arid landscapes can, in turn, help test the robustness of numerical models simulating dune field dynamics and improve model simulations that are used to predict the impact of future climate change on aeolian-dune remobilisation (Thomas et al., 2005; Mayaud et al., 2017; Vainer et al., 2021a). This article considers what is known about the Kalahari Basin and its hydrological systems and dunefields (Fig 4.2), including an overview of their Quaternary history. The geology of the region is first outlined in the wider context of southern Africa (Fig.4.3), before reviewing what was currently known about the provenance of the dunefields and potential fluvial feeder systems. To date, much of the information on provenance has been inferred from likely palaeowind directions (e.g., Thomas, 1987) or by applying a limited number of techniques (mostly sediment textures and heavy minerals) to some parts of this vast basin. Several sedimentological issues have thus remained controversial, including the relative role played by fluvial processes *versus* aeolian reworking and the origin of weathering.

Quantitative petrographic data were obtained only on a few aeolian-dune sands in the north and west, and detrital-zircon ages only on fluvial sands in the north (Gärtner et al., 2014; Garzanti et al., 2014a). For these reasons, this chapter present new results from bulk-petrography, heavy-mineral, and detrital-zircon U–Pb geochronology analyses on 100 aeolian-dune and river-bar sands collected across 17 degrees of latitude from Zambia to South Africa and over 13 degrees of longitude from Angola to Zimbabwe. A set of statistical techniques was applied to this multi-proxy dataset to adequately illustrate the compositional variability of aeolian sand across the Kalahari Basin, reveal meaningful mineralogical patterns, identify the original sediment sources, and gain insight into sand dispersal pathways. In particular, this chapter investigates inheritance from past climatic conditions, buffering of environmental signals through linked fluvial and aeolian systems, and progressive compositional homogenization and concentration of most durable minerals acquired through multiple cycles of erosion, transport, deposition, and diagenesis. The new provenance data are integrated and reviewed in terms of what is known about fluvial-aeolian interactions, chemical weathering, and drainage evolution in the Kalahari. Understanding the complexities of sediment transport systems, and particularly how sediment-routing connectivity regulates the transmission of environmental signals from source areas to depositional sinks over spatial and temporal scales, is essential for a realistic interpretation of the stratigraphic record (Romans et al., 2016; Allen, 2017; Caracciolo, 2020).

4.2 Geology of Southern Africa

Southern Africa was amalgamated through multiple tectono-magmatic events dating back to the Archean and culminated with the Neoproterozoic Pan-African orogeny (Fig 4.3; Hanson, 2003). The Archean core consists of the Kaapvaal and Zimbabwe Cratons, welded by the Limpopo Belt. The Kaapvaal Craton, progressively amalgamated between 3.7 and 2.7 Ga, was stabilized by 2.6 Ga, and eventually intruded by the Bushveld Complex at 2.06 Ga (Eglington and Armstrong, 2004). The Zimbabwe Craton, comprising 3.5–2.95 Ga gneisses non-conformably overlain by volcanic and sedimentary rocks and 2.7 Ga greenstone belts, was eventually sealed by the Great Dyke Swarm at ~2.6 Ga (Kusky, 1998; Jelsma and Dirks, 2002). The ~200 km-wide Limpopo Belt includes high-grade orthogneisses, retrograde amphibolite-facies metasedimentarary rocks, and granitoids with ages clustering at 3.3–3.2, 2.7–2.6, and 2.1–2.0 Ga (Zeh et al., 2007). This composite Archean core grew progressively during Proterozoic orogenic cycles that generated the

discontinuously exposed mid- Paleoproterozoic Magondi-Okwa-Kheis Belt in the west and the latest Mesoproterozoic Namaqua–Natal Belt in the south. In the northwest, the Angola Block represents instead the southern part of the Congo Craton, cored by largely mid-Paleoproterozoic (~2 Ga) mid-crustal granitoid gneisses (De Carvalho et al., 2000; McCourt et al., 2013; Jelsma et al., 2018). Stabilization of the Proto-Kalahari Craton by 1.75 Ga was followed by intraplate magmatism at 1.4–1.35 Ga and again at 1.1 Ga (Hanson et al., 2006). Amalgamation of the Kalahari Craton was completed by 1.0 Ga (Jacobs et al., 2008), when the Namaqua–Natal Belt was generated by arc accretion and continental collision. This orogen extends from SW Namibia to NE South Africa and includes Paleoproterozoic basement and up to high-grade metasedimentary rocks intruded by voluminous granitoids dated at 1.2–1.0 Ga (Eglington, 2006). The Mesoproterozoic volcano-sedimentary Sinclair Group of southern Namibia underwent only low-grade deformation and was intruded by numerous granitoids (Becker et al., 2006). Cratonic southern Africa was finally welded to the Congo Craton in the north during the major Neoproterozoic Pan-African orogeny, testified by the Damara–Lufilian–Zambezi Belt stretching from coastal Namibia in the west and across Botswana and southern Zambia to connect with the Mozambique Belt in the east (Frimmel et al., 2011; Goscombe et al., 2020). The Damara Belt in Namibia includes 2.0–1.2 Ga basement gneisses overlain by Neoproterozoic metasediments intruded by 570–460 Ma granitoids (Miller, 2008). A 3 km-thick succession of Neoproterozoic to Cambrian sandstone, mudrock and limestone was deposited in the foreland of the Damara Orogen in southern Namibia (Nama Group; Blanco et al., 2011). The Lufilian Arc consists of metasedimentary and metaigneous rocks hosting Cu-Co-U and Pb-Zn mineralizations (Kampunzu and Cailteux, 1999; Eglinger et al., 2016). The Zambezi Belt contains a volcano-sedimentary succession deformed under amphibolite-facies conditions at 0.9–0.8 Ga (Hanson, 2003), whereas eclogite-facies metamorphism dated as 592 Ma constrains the timing of subduction and thrust emplacement as 550–530 Ma (Hargrove et al., 2003; John et al., 2004). Initial disruption of the Gondwana supercontinent was recorded by the several km-thick Upper Carboniferous to Lower Jurassic Karoo Supergroup, covering almost two-thirds of southern Africa. Basin subsidence in the southern retroarc basin was induced by subduction of paleo-Pacific lithosphere, while transtensional stress propagated southwards from the Neotethyan rift in the north (Catuneanu et al., 2005). The Karoo succession begins with diamictite, turbidite, and coal-bearing fluvio-deltaic strata, followed by braidplain sandstone, mudrock, and aeolian sandstone (Johnson et al., 1996). Permian sandstones contain andesitic-dacitic

volcanic detritus (Johnson, 1991) and interlayered tuffs yielding ages mainly between 270 and 260 Ma (Lanci et al., 2013; McKay et al., 2016). Karoo sedimentation was terminated by flood-basalt eruptions recorded throughout southern Africa around 183 Ma (Svensen et al., 2012; Greber et al., 2020). A vast network of dolerite dykes and sills suggests that tholeiitic lavas originally covered an area of ~2.5 million km^2. The passive margins surrounding Africa developed after rifting of the Indian and Atlantic Oceans in the Late Jurassic and Early Cretaceous, respectively. Widespread intrusion of pipe-like bodies, including diamond-bearing kimberlites, took place in the Cretaceous to Paleogene (Moore et al., 2008). In the Kalahari Basin, stretching ~2200 km in the hinterland from the Congo to South Africa, up to 450 m-thick sediments were deposited since the Late Cretaceous (Haddon and McCarthy, 2005). The Plio- Pleistocene consists of gravel, clay, and aeolian sand with calcrete and silcrete (Thomas and Shaw, 1990; Vainer et al., 2018a). In the Quaternary, the East African rift propagated along a network of unconnected basins extending from Lake Tanganyika to the Okavango Graben and central Namibia farther west (Modisi et al., 2000; Kinabo et al., 2007; Vainer et al., 2021b).

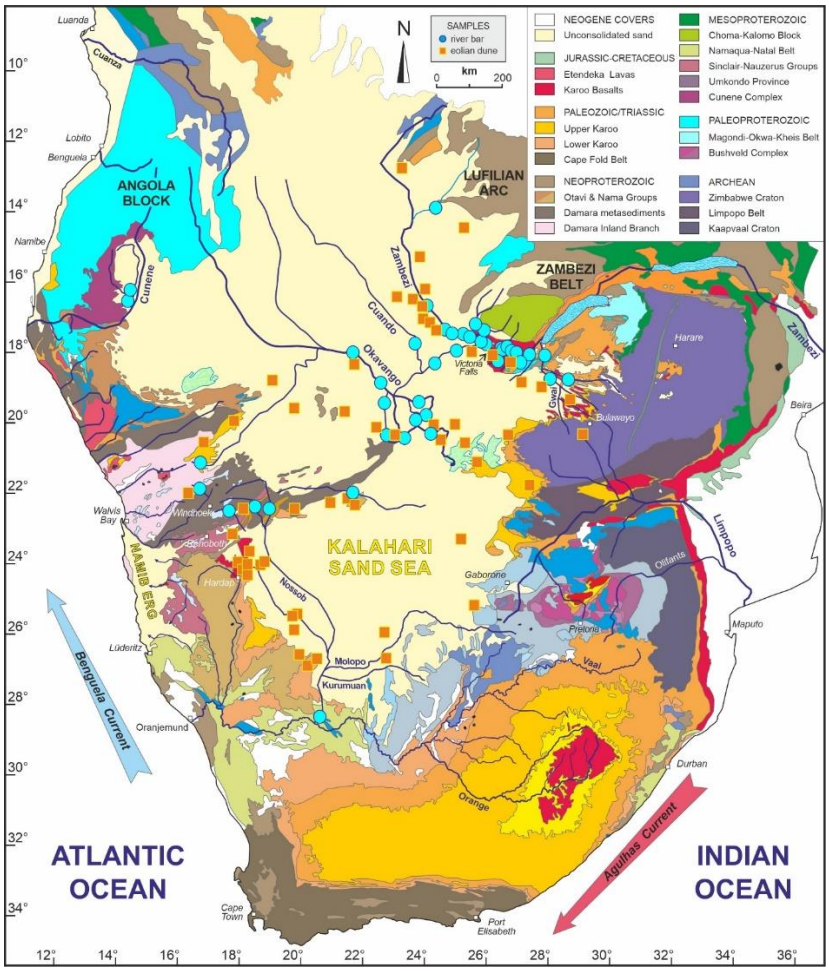

Figure 4.3. Geology of southern Africa (compiled after Schlüter, 2008 and other sources cited in text).

4.3 The Kalahari Basin

The intracratonic Kalahari sag basin comprises the largest continuous sand sea on Earth, which extends for over 2.5×10^6 km^2 (Fig 4.2). The interior of the Kalahari is an elevated plateau with flat topography (average altitude 1200 m), delimited by relatively steep escarpments down to the Atlantic Ocean in the west and to the Indian Ocean in the east. Kalahari Group sediments — including basal gravel and conglomerate, sandstone with calcrete, and unconsolidated sand —stretch north from the Orange River in South Africa (~29◦S) to the Democratic Republic of Congo (~6◦S; Haddon and McCarthy, 2005). The landscape across the Kalahari is varied, encompassing spatially discrete dunefields dominated by linear dunes, the Okavango alluvial fan (delta) and wetlands in northern Botswana, and aligned drainage and pans (Lancaster, 1981; Thomas and Shaw, 1991; Shaw and Goudie, 2002; Goudie and Viles, 2015). The erg is traversed by rivers that were initially mostly endorheic but were progressively captured from both sides by rivers eroding headwards from the coast (e.g., Moore and Larkin, 2001). Development of endorheic drainage and expansion of a landlocked sand sea in this arid tropical region was favored by multiple phases of tectonic activity in bordering areas since the Mesozoic, promoted by asthenosphere upwelling during the rifting stage and maintained during the passive-margin stage by flexuring associated with sediment loading of the continental terrace, or rejuvenated by isostatic processes or buoyancy forces in the mantle (Moucha and Forte, 2011; Blenkinsop and Moore, 2013).

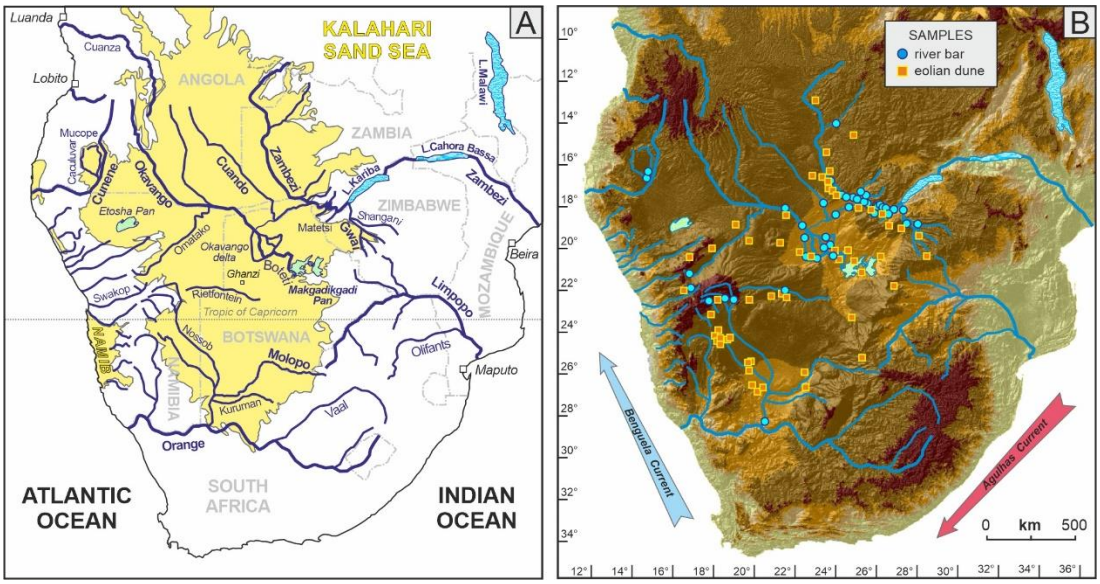

Figure 4.2. The vast Kalahari Basin in southern Africa. A) Main regions and river courses are indicated. B) Sampling sites are shown.

4.3.1 Climate

Climate in southern Africa results from the disturbance by a great land mass of quasi-stationary anticyclones over the Atlantic and Indian Oceans, corresponding to the descending limb of the Hadley Cell (Schulze, 1972). A major influence is exerted by the Intertropical Convergence Zone and associated Tropical Rain Belt (Nikulin and Hewitson, 2019), by the Congo Air Boundary, and by temperate frontal systems within the southern hemisphere westerlies in the west and south. The Indian Ocean is a major source of water vapor for the sub-continent via easterly winds (Fig 4.3A), and climatic changes within southern Africa have been linked to the variability of Indian Ocean surface temperature (Partridge, 1993; Tyson and Preston-Whyte, 2000; Washington and Preston, 2006; Vigaud et al., 2009). The South Indian Convergence Zone may extend its influence on the sub-continent via synoptic systems known as Tropical Temperate Troughs, which connect the mid-latitudes to the tropics (Cook, 2000; Todd et al., 2002). Oceanic currents also affect climate in the continental interiors (Walker, 1990). The warm Agulhas current flows southward along the coast of Mozambique (Fig 4.2C), allowing humid air masses to enter the continent from the Indian Ocean, thus causing heavy rains onto orographic barriers (e.g. Drakensberg Mountains of Lesotho) and a marked westward decrease in precipitation across southern Africa (Reason, 2001) (Fig 4.3B, C). The Agulhas current is retro-deflected at 16–20°E longitude when encountering the cold Benguela current (Lutjeharms and Van Ballegooyen, 1988), which displaces Antarctic water along the Atlantic coast of South Africa, Namibia and southern Angola, causing low sea-surface temperatures, low humidity of southerly winds, and very little rain through the year (Rogers and Bremner, 1991). Rainfall occurs mainly during winter in the southwestern corner of the sub-continent and during summer in the rest of the region. The aridity center is situated in southern Botswana. Annual rainfall increases from 150 mm in the southwest to 400 mm in Zimbabwe, and climate becomes sub-humid and less seasonal northward (Fig 4.3B, C). The wind regime in the Kalahari is more complex than expected in areas of linear dune development (Fig 4.3A), being influenced by the seasonal fluctuation of the high-pressure cells (Tyson and Preston- Whyte, 2000). The dry winter season is characterized by southeasterly winds associated with the South Atlantic anticyclone (Bultot and Griffiths, 1972). In the summer, winds blow mainly from the north in the eastern Kalahari and from the west in the western Kalahari (Nicholson, 1996). The southwestern Kalahari is dominated by southwesterly winds (Wiggs et al., 1996).

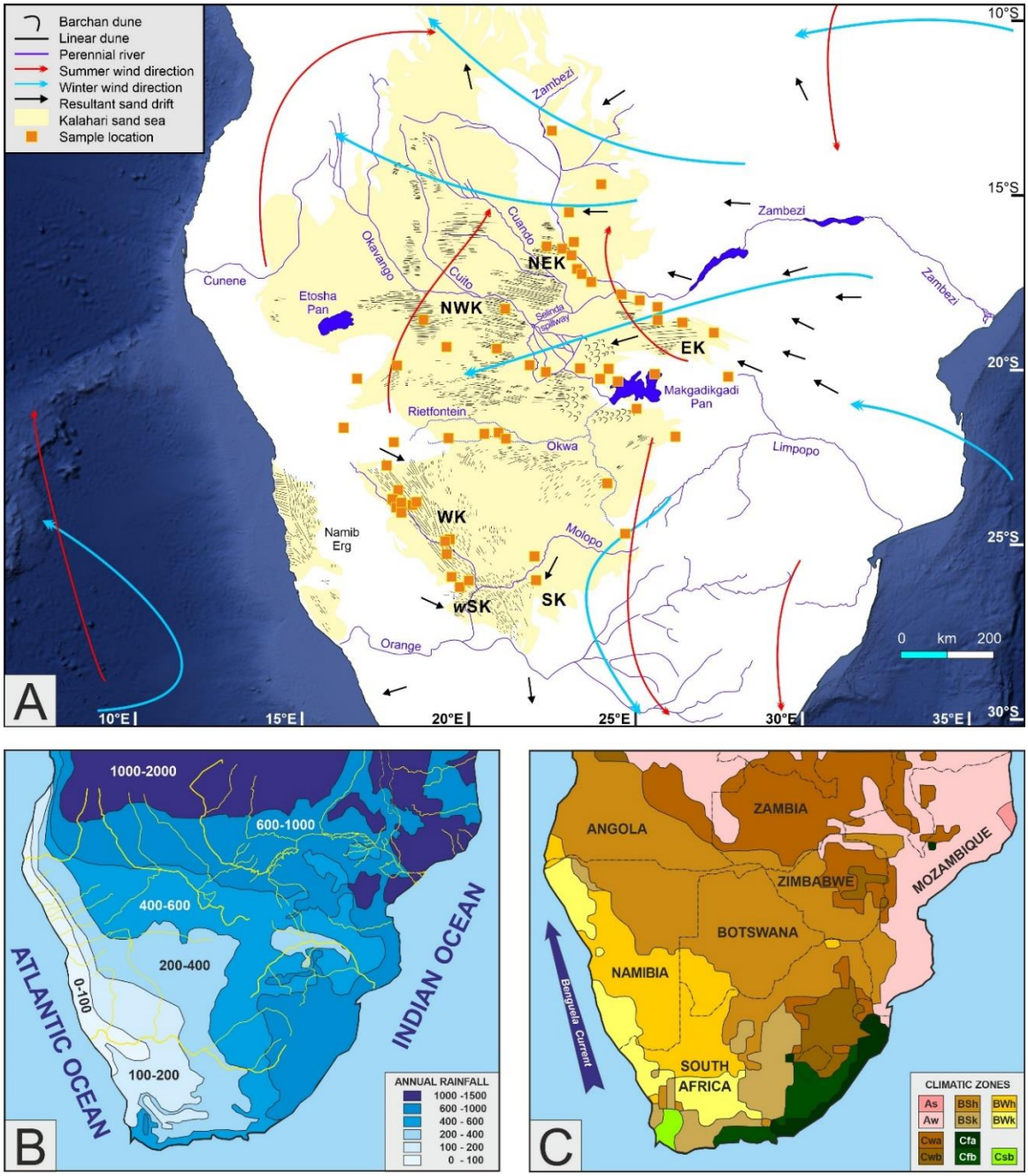

Figure 4.3. The Kalahari sand sea. **A**) Dune types, wind directions, and sandflow patterns (compiled after Thomas and Shaw, 1991, Nicholson, 1996, and Haddon, 2005). **B**) Rainfall map, showing increase in precipitation from south to north and from west to east across southern Africa. **C**) Distribution of climatic zones (Köppen–Geiger classification; Kottek et al., 2006): A = equatorial; B = arid; C = warm temperate. Precipitation: W = desert; S = steppe; f = fully humid; s = summer dry; w = winter dry. Temperature: h = hot arid; k = cold arid; a = hot summer; and b = warm summer.

4.3.2 Hydrology

Three major rivers flow from humid Angola and western Zambia across the northern Kalahari: the Cunene, the Okavango, and the Zambezi (Fig 4.2). The Cunene, sourced in Angolan highlands uplifted in the Plio-Quaternary (Klöcking et al., 2020; Vainer et al.,

2021b), runs along the westernmost edge of the sand sea drained by the Caculuvar and Mucope tributaries (Fig 4.2A; Shaw and Goudie, 2002). Once endorheic and emptying into what is today Etosha Pan (Miller et al., 2010), the Cunene was captured by a headward eroding coastal stream and its youthful terminal tract now debouches into the Atlantic Ocean (Goudie and Viles, 2015). The Okavango, the main endorheic river of the Kalahari, is fed from humid Angola, where the southward migration of the Congo Air Boundary brings heavy rains between December and March (annual rainfall ≤1400 mm). The flood-wave takes until August to filter through the anastomosing channels and swamps of the Okavango, the largest wetland in southern Africa and the largest inland delta on Earth (McCarthy and Ellery, 1998). Suspended sediments supplied annually to the Okavango Delta amount to only ~19% of total load (McCarthy et al., 2012), suggesting that weathering intensity is presently quite low even in the northern Kalahari Basin. Sedimentation of fine sand dominates the upper delta, whereas chemical sedimentation in the form of calcrete and silcrete prevails in the lower delta (McCarthy and Metcalfe, 1990). Finally reunited in the Boteti River, the drastically reduced flood waters traverse another stretch of the Kalahari, ending endorheically in the Makgadikgadi Pan. The main source of water for the pan is the ephemeral Nata River, sourced in Zimbabwe to the east. The Zambezi and its major Cuando tributary (named Kwando, Linyanti, and next Chobe after entering the Okavango Graben in the Caprivi strip) also flow across the northern Kalahari. Downstream of Victoria Falls, the Zambezi plunges into deep gorges carved in Karoo basalt, heading towards the Indian Ocean (Moore et al., 2007). The Gwai River drains the eastern edge of the sand sea in Zimbabwe, along with its tributaries once directed westwards toward the central Kalahari (Thomas and Shaw, 1988). In Namibia, three ephemeral rivers draining into the Kalahari flow only in case of exceptionally heavy and continuous precipitation. The Omatako in the north is an Okavango tributary, the Rietfontein dries up in central Botswana as a former tributary of the fossil Okwa River (Fig 4.3A), and the Nossob in the south joins the Molopo River. The occasional floods in the Nossob and Molopo are absorbed along the way and recharge groundwater aquifers with water losses up to 90% and 80%, respectively (van Veelen et al., 2009). The flow of the Nossob and Auob (its major western tributary) typically ceases between 24◦S and 25◦S, respectively, and the Molopo seldom flows west of 23◦40′ E (Nash, 2015). The Molopo has continuous river flow and reaches the Orange River — thus becoming exorheic — only during extreme events, which have a return period of between 20 and 50 years (Nash and Endfield, 2002). The Kuruman, the major Molopo tributary in South Africa, is also dry

except for flash floods, but has permanent flow over its first 10 km owing to its famous dolomite spring source (*Die Oog*, the 'Eye of the Kalahari'), which has yielded a constant ~750 m^3/h flux during the last two centuries at least (Shaw et al., 1992). The southern and western Kalahari rivers are misfit streams within wider, flat-bottomed channels reaching 0.5 to 1.8 km in width (Bullard and Nash, 2000). They contain gorge-like sections with varying steepness (typical incision depth ~ 25 m) and show evidence of groundwater processes (sapping and deep weathering; Shaw and de Vries, 1988; Bullard and Nash, 1998; Stone, 2021a). Pans (endorheic basins that temporarily host water and deposit mostly salt and clay) are widespread in the Kalahari, found in depressed areas where an integrated fluvial system is lacking and surface geology is suitable (soluble duricrusts or regions with deflatable loose silt and sand). They occur in many interdune corridors of the linear dunefields and in higher concentration along the western watershed of the southern dunefield (Goudie and Thomas, 1985; Lancaster, 1978, 1986).

4.3.3 Dunefields

The five dunefields identified in the Kalahari Basin (NWK, northwestern; NEK, northeastern; EK, eastern; WK, western; SK southern; Fig 4.3A) are all dominated by linear dunes (Thomas and Shaw, 1991; Shaw and Goudie, 2002). Other morphologies include topographically constrained dunes occurring at hill and mountain fronts (Tyson, 1999) and lunette dunes fringing the widespread pans (Telfer and Thomas, 2006; Hürkamp et al., 2011). There are also areas with sand sheets (e.g., southwestern Kalahari; Bateman et al., 2003) and areas of degraded dune patterns resembling barchanoid ridges on the eastern edge of the western Kalahari near the Botswana/Namibia border (McFarlane et al., 2005; Stone, 2021a). Kalahari dunefields may have started to accumulate in the early Pleistocene (Partridge, 1993; Miller, 2014; Vainer et al., 2021a). In the western Kalahari, dunes superimposed over a megafan are inferred to be younger than the 4-Ma-old mainly vertebrate fossils that lie below the sand (Miller, 2008; Miller et al., 2010), whereas dunes in the east lie below Middle Stone Age artifacts, constraining the youngest possible age for sand deposition as >200 ka (McFarlane and Segadika, 2001). In the southern Kalahari, Vainer et al. (2018b) simulated a range of scenarios of sand exposure and burial based on cosmogenic nuclides and luminescence constraints and suggested there may have been 22 overturning cycles since sand was available for aeolian distribution, at 1.5–2.2 Ma and/or 4.2–5.2 Ma (in agreement with Miller, 2014). Reworking of the initially produced sand occurred throughout the Quaternary, and burial ages for the most recent of any dune

recycling and accumulation episodes are determined by luminescence dating (see compilation spanning ~190 ka for the INQUA Dune Atlas by Thomas and Burrough, 2016). Finite luminescence ages for basal sediments of linear dunes range from 1.1 ± 0.1 ka to 104 ± 8 ka (including samples in saturation, i.e., at the upper limit of the dating technique that can be extended if integrated with cosmogenic-nuclide dating; Vainer and Ben Dor, 2021). Today, precipitation levels, vegetation cover, and insufficient wind energy hamper aeolian activity even in the driest area of the erg, excepting some blowing sand on dune crests in the western and southern Kalahari (Wiggs et al., 1995; Bhattachan et al., 2013). The cover of grasses and savannah bush increases on a broad north-south gradient, with increasing concentrations of woodland north of ~21oS (Van Rensburg, 1971; Thomas and Shaw, 1991). Therefore, Kalahari dunes are currently largely inactive, sometimes pedogenically modified and in places extensively degraded, with a higher proportion of silt and clay than normally found in active dune fields (Thomas, 1984; Wiggs et al., 1995; McFarlane et al., 2005). The extent of this alteration by slope and locally tectonic processes (McFarlane and Eckardt, 2007) increases northwards and eastwards as the woodland vegetation cover increases, and in western Zambia eroded dune crests largely stabilized by vegetation may rise only ~5 m from the vegetated interdunes (O'Connor and Thomas, 1999). The trend of linear dunes changes from ESE/WNW to E/W and then to ENE/WSW from west to east in the northern Kalahari (NWK, NEK, and EK), it is NE/SW south of Makgadikgadi and NW/SE to NNW/SSE in the southern Kalahari (WK and SK) (Fig 4.2A). These patterns have been ascribed to wind circulation around, and shifts in the position of, the southern African anticyclone (Lancaster, 1979, 1981; Thomas, 1984). However, the accompanying idea that there were discrete periods of formation for each dunefield has been overturned by the large number of compiled luminescence ages, indicating multiple accumulation phases in each region over the last ~190 ka. Five different classes of linear dunes are identified in the southern Kalahari (WK, SK; Bullard et al., 1995; Bullard and Nash, 1998): 1) simple and discontinuous; 2) simple and continuous; 3) compound with common Y-junction branches; 4) compound with more-obtuse angles between branches; 5) no preferred orientation and discontinuous. The tallest and most closely spaced dunes are found in the southeast of this region, as shown by detailed morphometric analysis using ASTER global digital-elevation-model data (White et al., 2015). This contradicts the often-reported relationship of bigger dunes with wider spacing, suggesting that these dunes have experienced a reduction in sediment supply through time and/or post-depositional modification (Kiss et al., 2009; White et al., 2015).

4.3.4 Duricrusts

Duricrusts that act as cement and stabilize sand's potential movement are widespread below, within, and above Kalahari sands, covering most of the surface in the southern part of the basin (Botha, 2000). Studies based on their minerology, micromorphology, bulk geochemistry, isotopic signature, chronology, and geomorphological context have suggested several formation mechanisms dependent on hydrology and climate. Semi-arid to arid conditions under alternating dry and humid stages are generally considered as suitable for their precipitation (Kampunzu et al., 2007; Ringrose et al., 2009), but their paleoenvironmental interpretation is not straightforward (Summerfield, 1983; Nash and McLaren, 2003). Duricrusts are chemical precipitates that form under saturation of the host sediment through a combination of lateral and vertical transfer mechanisms. Therefore, they are not restricted to one phase within a chronological stratigraphy and occur in both vadose and phreatic environments. Alternating conditions (e.g., moisture availability, temperature, vegetation) promote changes in pH that commonly result in mixed compositions of cements, which range from pure carbonate to pure silica and may include Fe-oxy-hydroxides and clays (Shaw and Nash, 1998; Nash et al., 2004; Kampunzu et al., 2007; Vainer et al., 2018b). Multi-phase accumulation through repeated dissolution and re-precipitation occurs at varied subsurface and surficial settings, including paleolakes, pans, and marginal pools (McCarthy and Ellery, 1995; Ringrose et al., 2002; Thomas et al., 2003), valley-fills (Nash and McLaren, 2003), and pedogenic profiles (Watts, 1980), where flora and fauna may be involved in their generation. Varied formation settings and processes, with consequently diverse textures ranging from dispersed powder to nodular and hardpan, has led to different classification criteria (Goudie, 2020). These include geomorphological and hydrological conditions as well as macro- and micromorphological characteristics (size, structure, mineralogy, porosity, biological components, secondary filling and coating) and chronological relationships between the precipitating phases (Nash and Shaw, 1998; Nash and McLaren, 2003). In the Kalahari, indurated layered carbonate characterizes weathering profiles in NW Botswana and could be widespread throughout the basin but covered by unconsolidated sand (McFarlane et al., 2010). Based on Sr isotopic ratios, chemical precipitation is inferred to have occurred from solutions migrating laterally from dolomitic rocks when aquifer levels dropped shortly after clastic deposition (Vainer et al., 2018b). A source other than underlying bedrock for the cementing agents was similarly inferred for duricrusts in southern and central Botswana based on geochemical differences with the underlying bedrock (Nash et al., 2004). U-Pb dating of carbonates

deposited in a mega-fan environment in the Etosha sub-basin reaches back to the early Eocene (Houben et al., 2020), much earlier than the establishment of dunefields in the Kalahari. Because of intrinsic difficulties in radiometric dating of calcrete (Geyh and Eitel, 1997), the age of duricrusts is mainly constrained by the association with fossils and artefacts, indicating formation since the early Pleistocene and throughout the Quaternary (Haddon, 2005). Over the last decades, luminescence dating has allowed to establish when quartz grains within calcrete were last exposed to light, confirming duricrust formation spanning at least from the middle and late Pleistocene (Ringrose et al., 2002) to the Holocene (Burrough et al., 2009a).

4.3.5 Quaternary climate change

In the Kalahari dryland, Quaternary environmental and climatic changes are documented by different proxies in a range of archives, including aeolian sand dunes, former lake shorelines, pan deposits and fringing lunette dunes, fluvial sediments, tufa carbonates, speleothems, groundwater and rock shelter deposits (animal and human middens and rock art) (Stone, 2021b). The Quaternary dynamics of aeolian-fluvial interactions can be put into context by combining these different archives. Given the size and current climatic heterogeneity of the Kalahari Basin it is pragmatic to consider three broad sub-regions: i) northern (including the NWK, NEK and EK dunefields); ii) southern (including the WK and SK dunefields); iii) eastern, with no major dunefield. Over the past ~150 ka, at least seven wetter intervals are identified in these sub-regions, which are not paced consistently with precession and whose onset and end do not align with global marine oxygen isotope stages. Some appear to be widespread, but others display opposing meridional trends. Data compiled from the INQUA Dune Atlas by Thomas and Burrough (2016) indicate relatively continuous aeolian-dune accumulation across most of the Kalahari over the past 190 ka, with only a few gaps (174–107 ka, 96–87 ka, and 38–42 ka) possibly ascribed to a lack of preservation. The implication of this dataset of ~400 ages is that the pattern of episodic aeolian-dune formation and aridity proposed by Stokes et al. (1998) is an artefact driven by low sampling density across space and to only shallow depths within a dynamic and heterogeneous landscape (Stone and Thomas, 2008). A first wetter interval at ~140 to 120 ka is seen in the northern sub-region, when diverse isolated basins became interconnected in mega-lake Makgadikgadi reflecting changed hydroclimatic conditions in humid Angola (Burrough et al., 2009b). Speleothem growth reflects instead more localised climate conditions (133 ± 27 ka; Brook et al., 1998). In the southern sub-region, presence of

palygorskite suggests semi-arid climate from 156 ± 11 to 121 ± 6 ka (Lukich et al., 2019, 2020). In the southern Kalahari, the only preserved evidence of linear-dune accumulation between ~174 and 107 ka is a mottled sandstone unit dated by luminescence as between 160 and 108 ka (Bateman et al., 2003). A second wetter interval between ~112 and 90 ka is recorded by mega-lake Makgadikgadi phases (105 ± 4 ka and 92 ± 2 ka; Burrough et al., 2009b) and speleothem growth (112 ± 5 to 108 ± 7 ka and 93 ± 6 ka: Brook et al., 1998). Evidence for aeolian-dune accumulation is lacking in the southern sub-region during this period, when there was locally abundant re-surging groundwater (111 ± 3 to 102 ± 2 ka; Wilkins et al., 2021) and increased moisture availability at Kathu Pan (Lukich et al., 2020). A third wetter interval is recorded between ~80 and 70 ka at Etosha Pan (Hipondoka et al., 2014) but not in the mega-lake Makgadikgadi system, whereas semi-arid conditions are recorded at 74 ± 5 ka in the south at Kathu Pan (Lukich et al., 2020). In contrast, a fourth interval is documented between ~63 and 43 ka by a mega-lake Makgadikgadi phase at 64 ± 2 ka, and by speleothem growth (~61 ka; Brook et al., 1998; ~51–43, Holmgren et al., 1995; 58–46 ka, Holzkämper et al., 2009; from 56.8 ± 0.4 to 43 ± 7 ka, Pickering et al., 2007). The southern sub-region recorded semi-arid conditions at 55 ± 3 ka (Lukich et al., 2020) and aeolian dunes continued to accumulate (Thomas and Burrough, 2016). A following drier interval is documented in the eastern sub-region by a lack of speleothem growth between ~43 and 27 ka (Holmgren et al., 1995) and groundwater record (Kulongoski et al., 2004). However, wetter conditions are testified between ~43 and 30 cal ka B.P. in the western part of the southern Kalahari (Schüller et al., 2018). Aeolian dunes accumulated consistently, suggesting sufficient windiness and perhaps inadequate moisture availability to keep vegetation cover below a limiting threshold. A fifth wetter interval is documented in the northern sub-region at 39 ± 2 ka and 27 ± 1 ka by two mega-lake Makgadikgadi phases (Burrough et al., 2009a, 2009b) and at 36–32 and 27–22 ka (Thomas et al., 2003). Evidence includes aquifer recharge at ~36–33 ka (Stute and Talma, 1998), speleothem growth at ~33 ka (Brook et al., 2010), and pan-floor flooding at 32 ± 5 ka (Telfer et al., 2009). In contrast, dry conditions are documented in the southern sub-region (~30–25 cal ka B. P.; Schüller et al., 2018), where aeolian dunes continued to accumulate (Thomas and Burrough, 2016). Wetter conditions started later in the eastern sub-region, as indicated by speleothem growth from 27 to 21 ka (Holmgren et al., 1995), 24.3–12.7 ka (Holmgren et al., 2003), and 16.5 ± 0.2 ka (Pickering et al., 2007). A sixth wetter interval is documented between ~23 and 16 ka as a mega-lake Makgadikgadi phase (17 ± 2 ka; Burrough et al., 2009b) and as lake phases at Etosha Pan (23–21 and 18–16 ka; Hipondoka

et al., 2014). In the southern sub-region, fluvial units were dated at 23 ka and 18 ka in the lower Molopo basin (Hürkamp et al., 2011), pan flooding at ~20 ka (Telfer et al., 2009), and speleothem growth at 32–17 ka (Brook et al., 2010). In contrast, drier conditions are indicated at 22 ± 1 ka by a hardpan unit at Kathu Pan indicating a strongly negative moisture balance (Lukich et al., 2020), but wet enough at the eastern fringes of the Kalahari for speleothem growth through to 21 ka (Holmgren et al., 1995). A seventh wetter interval is recorded in the northern sub-region at 16–12 ka (Thomas et al., 2003) and in the southern sub-region at 15–13 cal ka B.P. (Schüller et al., 2018). This episode is not documented in the mega-lake Makgadikgadi system and aeolian dunes continued to accumulate in the southern sub-region (Thomas and Burrough, 2016). At the start of the Holocene, wetter conditions are indicated by a mega-lake Makgadikgadi phase at 8 ± 5 ka (Burrough et al., 2009b), by an Etosha Pan lake phase at ~10 ka (Hipondoka et al., 2014), and by speleothem growth at ~8.2 ka (Brook et al., 1998), consistently with an absence of age evidence for aeolian-dune activity since ~8 ka in the northeastern Kalahari (Thomas and Burrough, 2016). In contrast, only episodic flash-flood events are documented in the lower Molopo from ~9.5 to 6.5 ka (Schüller et al., 2018) and aeolian dunes were active in the southern-sub-region during this time (Thomas and Burrough, 2016). Speleothem growth ceased before the Holocene in the eastern sub-region (Holmgren et al., 1995) but continued from ~5 ka onwards in the north (Brook et al., 1998). A wet phase is recorded at ~5.5 cal ka B.P. in the south (Schüller et al., 2018), whilst aeolian-dune activity continued in the southern sub-region (Thomas and Burrough, 2016). Overall, the spacing of wetter intervals does not demonstrate a regular periodicity, suggesting an interplay of factors more complex than solely global glacial-interglacial cycles or precession-paced forcing of hydroclimate.

4.4 Overview of previous work on the provenance of Kalahari sands

The provenance of Kalahari sands has not been investigated thoroughly by a multi-technique approach so far. Previous surveys recognized the highly quartzose composition of aeolian sands, but their compositional variability has been only broadly evaluated, and the origin of Kalahari dunefields was mostly ascribed to either reworking of older sediments (e.g., Du Toit, 1954; Baillieul, 1975; Thomas, 1987) or dominant fluvial processes (e.g., De Ploey et al., 1968; Verboom, 1974; Moore and Dingle, 1998). Petrographic, mineralogical, geochemical, and geochronological results from aeolian and river sediments collected in the Kalahari Basin and illustrated in Garzanti et al. (2014b, 2014c) complement the new dataset obtained in this study and will be summarized and

discussed later on. The earliest heavy-mineral study of Kalahari sands was carried out by Poldervaart (1957), who identified tourmaline as a ubiquitous component, associated with zircon increasing eastwards at the expense of staurolite and kyanite. In his survey across Botswana, Baillieul (1975) distinguished four different types of Kalahari sands according to their texture, composition, and origin: 1) pure quartz sand reworked from older longitudinal dunes in northwestern Botswana; 2) finer-grained feldspar-bearing sand largely derived from recycling of the feldspatho-quartzose Neoproterozoic Ghanzi Sandstone in central-western Botswana; 3) pure quartz sand inferred to be recycled from Upper Triassic/Lower Jurassic sandstones of the Karoo Supergroup in central to soutwestern Botswana (Boocock and Van Straten, 1962); 4) various sands of fluvial origin in eastern Botswana, locally containing micas or basaltic rock fragments and largely derived from diverse exposed bedrocks. Thomas (1987) emphasized the remarkable homogeneity of textural and compositional features, held to testify an overriding importance of aeolian activity across the Kalahari. In their textural and mineralogical study of the Kalahari Erg in NW South Africa, central Botswana and NE Namibia, Schlegel et al. (1989) distinguished between sand collected from the crest of modern aeolian dunes and 'mixed sands' collected in interdune areas or close to ephemeral rivers or pans. They found that tourmaline and staurolite are most abundant in dune-crest samples, whereas garnet, zircon, amphibole, pyroxene, rutile, sillimanite, andalusite, and opaque oxides (magnetite, ilmenite, and hematite) are more abundant in the 'mixed' samples. In South Africa, aeolian sand resulted to yield subrounded to very well-rounded tourmaline, staurolite, kyanite, and opaque oxides. In Botswana and Namibia, more heterogeneous suites consist of mostly well-rounded tourmaline with subordinate staurolite, epidote, and zircon. Heavy minerals were observed to be denser, less spherical and less rounded in 'mixed samples', garnet commonly occurring as broken angular fragments. Main source rocks were held to be Nama and Karoo Group siliciclastics in South Africa and Botswana. In their textural and mineralogical study of central Botswana cover sands, Moore and Dingle (1998) failed to find a correspondence between the variability of sediment textures and wind patterns, and thus inferred a dominance by fluvial processes. Ephemeral streams and sheetwash were inferred to produce heavy-mineral enrichment in coarser proximal sands passing to finer sediments with fewer heavy minerals in distal settings. Tourmaline (mainly in the southwest), staurolite (mainly in the north), and kyanite were confirmed as the most common heavy minerals. More recently, Haddon and McCarthy (2005) recognized the major role played by both fluvial and aeolian processes and identified local reworking from

older deposits as a major source of Kalahari sand. In a most recent study, Vainer et al. (2018a) used detrital mineralogy, elemental geochemistry, and Sr, Nd and Pb isotopic ratios to detect provenance changes through a complete Quaternary section of Kalahari Group sediments in South Africa. Provenance from distant Angolan highlands *via* a trans-Kalahari palaeo-drainage system was inferred for the basal part of the section, overlain by strata containing detritus derived locally from volcano-sedimentary rocks of the Archean Kaapvaal Craton exposed in the east and south. The more recent aeolian sands indicated instead sediment supply from Paleoproterozoic source rocks in the west and northwest. Chemical proxies suggested that weathering intensity was typical of humid areas for the basal part of the section at a time of relatively dense hominin occupation of the area, but limited to groundwater alteration and precipitation of duricrusts in the overlying strata. Based on geochemical data, sediments of the Okavango Basin were considered to represent a mixture of detritus derived from Proterozoic basement rocks exposed in Angola, Namibia, and NW Botswana with locally recycled aeolian sand and calcareous soils (Huntsman-Mapila et al., 2005). Using elemental geochemistry complemented by Nd, Sr, and Pb isotopes, Vainer et al. (2021b) outlined a more complex provenance pattern, with detritus derived from multiple sources including the Angola Shield in the northwest, the Archean Kasai Craton in the north, Mesoproterozoic granitoids of the Choma-Koloma Block in the east, and the Ghanzi-Chobe and Damara Belts in the west, with possible contribution also from the Lufilian Belt and Karoo basalts. Gärtner et al. (2014) used U-Pb detrital-zircon geochronology and groundwater alteration and precipitation of duricrusts in the overlying strata. Based on geochemical data, sediments of the Okavango Basin were considered to represent a mixture of detritus derived from Proterozoic basement rocks exposed in Angola, Namibia, and NW Botswana with locally recycled aeolian sand and calcareous soils (Huntsman-Mapila et al., 2005). Using elemental geochemistry complemented by Nd, Sr, and Pb isotopes, Vainer et al. (2021b) outlined a more complex provenance pattern, with detritus derived from multiple sources including the Angola Shield in the northwest, the Archean Kasai Craton in the north, Mesoproterozoic granitoids of the Choma-Koloma Block in the east, and the Ghanzi-Chobe and Damara Belts in the west, with possible contribution also from the Lufilian Belt and Karoo basalts. Gärtner et al. (2014) used U-Pb detrital-zircon geochronology and zircon morphology from sand carried by the Cunene, Okavango, Cuando, and uppermost Zambezi Rivers to pinpoint the protosources of sediment recycled from and fed into the northern Kalahari Basin. They suggested that most sediment originated from the Lufilian and Kibaran Belts with westward increasing input

from the Damara Belt. Zircons derived from the Angola Block were detected only in the Cunene and westernmost part of the Okavango drainage basins.

4.5 Sampling

In this provenance study, 57 samples of aeolian dunes have been analysed, collected across the vast Kalahari sand sea in the frame of diverse research projects (Stone and Thomas, 2008; Matmon et al., 2018; Burrough et al., 2019; Stone et al., 2019; Wittmann et al., 2020; Vainer et al., 2021a). Another 43 sand samples collected from exposed sandbars or dry riverbeds in Angola, Botswana, Zambia, Zimbabwe, Namibia and South Africa, and previously studied with similar and complementary methodological approaches (Garzanti et al., 2014b, 2018a), were considered to monitor changes in sediment composition associated with fluvial-aeolian interactions. Aeolian-dune samples are mostly fine to lower medium sand (average 2.3 ± 0.5 ϕ), whereas river sands range more widely from fine to coarse (average 1.8 ± 0.8 ϕ). Full information on sampling sites is provided in Appendix.

4.6 Mineralogy of river sand

The main rivers that drain into the Kalahari Basin are sourced in the humid regions of Angola and Zambia in the north. The Caculuvar and Mucope tributaries of the Cunene River, draining the western edge of the Kalahari Erg in Angola (Fig 4.1A), carry pure quartzose sand with a few K-feldspar grains. The extremely poor, zircon-rich tHM suite includes epidote, tourmaline, and minor andalusite, staurolite and rutile (Table 4.1). The Okavango and Cuando Rivers, which are also sourced in Angola and drain the northern Kalahari Basin towards the Caprivi Strip and Botswana, carry pure quartzose sand (Fig 4.4I) with extremely poor, tourmaline-zircon-epidote-staurolite-kyanite-rutile tHM suites. Sand carried by the upper Zambezi River in Zambia is also pure quartzose (Fig 4.4K) with a poor tHM suite dominated by ZTR minerals with common kyanite, staurolite, and minor epidote. Clinopyroxene appears downstream of Ngonye Falls, increases towards Victoria Falls, and becomes rapidly predominant along the gorges downstream. Zambezi tributaries in Zimbabwe include the Matetsi, which carries quartzo-lithic basalticlastic sand (Fig 4.4M) with extremely rich tHM suites containing clinopyroxene exclusively, and the Gwai, which carries feldspatho-quartzose sand (Fig 4.4O) with a poor tHM suite containing amphibole, subordinate epidote and garnet, and minor clinopyroxene, kyanite, and sillimanite. The Shangani, a Gwai tributary (Fig 4.1A), carries quartzose sand with basaltic rock fragments, a few plagioclase grains, and a moderately rich tHM suite dominated by

clinopyroxene. In northern and central Namibia, the Omatako carries feldspatho-quartzose sand with K-feldspar ≫ plagioclase and a very poor tourmaline-amphibole-garnet tHM suite. The Okakongo (a northern tributary of the Swakop River draining towards the Atlantic Ocean) carries feldspar-rich feldspatho-quartzose sand (Fig 4.4A) with moderately rich hornblende-dominated tHM suite. The Rietfontein carries pure quartzose sand (Fig 4.4C) with a very poor staurolite-tourmaline tHM suite. The White Nossob and Black Nossob (western and eastern branches of the Nossob River) carry feldspatho-quartzose sand containing granitoid and high-rank metamorphic rock fragments (Fig 4.4E) with a moderately poor amphibole-garnet-staurolite-epidote tHM suite, and quartz-rich feldspatho-quartzose sand containing low-rank metasedimentary rock fragments with a moderately poor staurolite-epidote-garnet-zircon tHM suite, respectively. The Molopo River, which drains the southern Kalahari, carries quartz-rich feldspatho-quartzose sand with common monocrystalline quartz displaying abraded overgrowths, plagioclase > K-feldspar, and a few shale/slate or quartzose sedimentary and metasedimentary rock fragments (Fig 4.4G). The moderately poor tHM suite includes epidote, amphibole, ZTR minerals, garnet, clinopyroxene, and minor staurolite and kyanite.

4.7 Mineralogy of aeolian-dune sands

Dune sand is quartz-rich over most the vast Kalahari Basin: out of the 57 studied samples, 31 are pure quartzose, 12 quartzose, and 10 quartz-rich feldspatho-quartzose (Fig 4.5). Throughout the northern Kalahari, in Angola, northeastern Namibia, Caprivi Strip, northern Botswana and western Zambia, sand consists virtually exclusively of monocrystalline quartz commonly showing rounded to subrounded outline and abraded overgrowths (Fig 4.4L). Aeolian sand in the Caprivi Strip contains abundant red iron-oxide particles. Pure quartzose sand also characterizes the eastern edge of the Kalahari in Zimbabwe as well as the central part of the sand sea from eastern Namibia to southeastern Botswana. In all these regions, K-feldspar prevails among the few feldspar grains, lithics are rare or lacking, and tHM assemblages are very poor to extremely poor and dominated by ZTR minerals. Staurolite is widespread, most common in the Ghanzi area (Fig 4.4D) and generally associated with kyanite and minor andalusite. Kyanite increases progressively southwards in westernmost Zambia and is most abundant to the west of the Cuando/Zambezi confluence, where it is associated with minor garnet. Epidote is common south of the Okavango inland delta, where a few amphibole grains occur. Garnet is rare or lacking altogether (Table 4.1). Basaltic detritus including rock fragments, plagioclase and

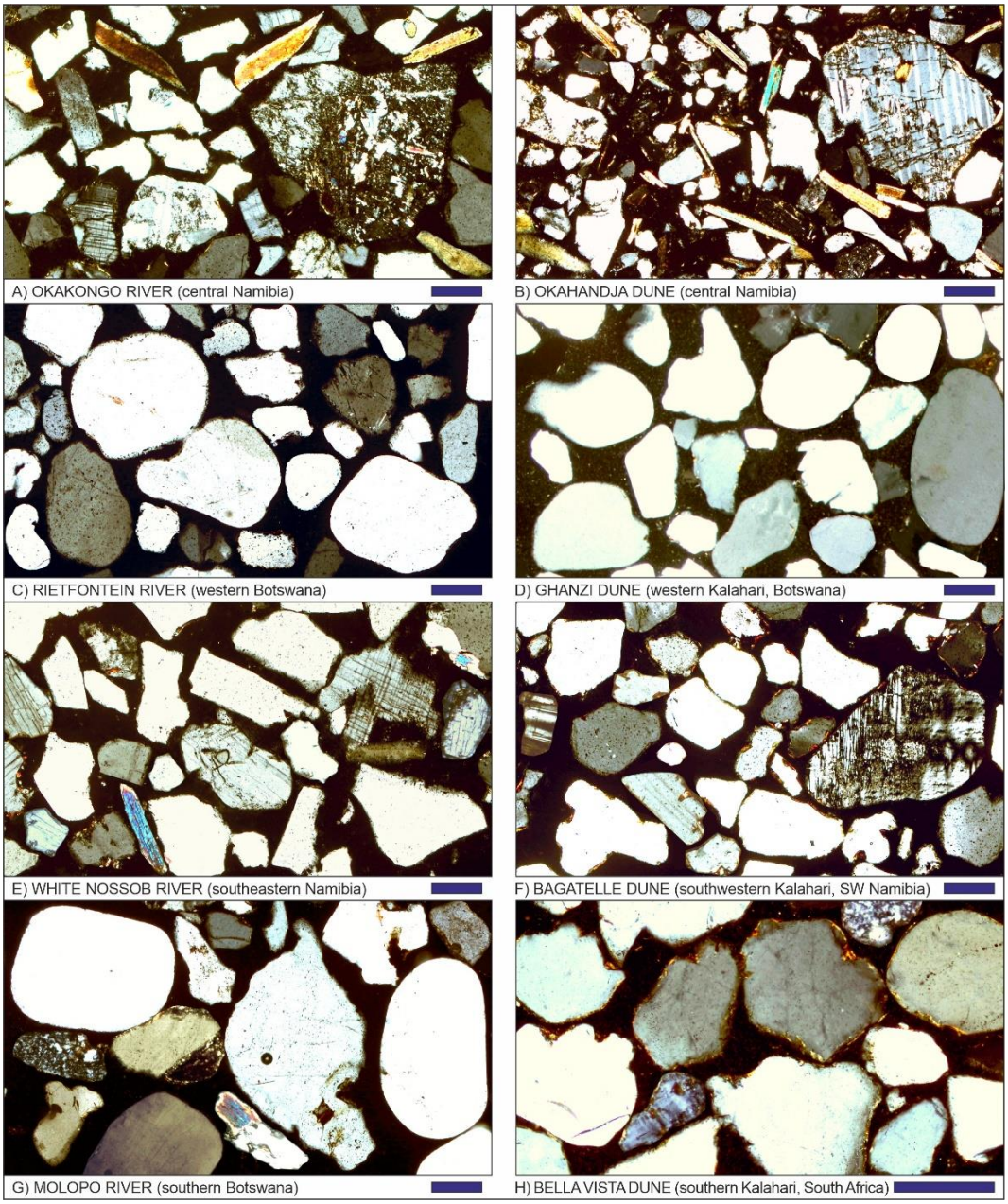

Figure 4.4. Comparison between the petrographic composition of fluvial and associated eolian-dune sands in the Kalahari Basin (photos arranged in geographical order: A to H from NW to SE in the west; I to P from W to E in the east). A, B: feldspar-rich feldspatho-quartzose sands (S4364 and E4875). C, D: pure quartzose sands (S4309 and E4889). Feldspatho-quartzose (E: S4313) and quartz-rich feldspatho-quartzose sands (F: NAM6/4/2). Quartz-rich feldspatho-quartzose (G: S5145) and pure quartzose sands (H: E5540). Pure quartzose sands (I: S4299, note weathered quartz to the right; J: NKALB, note ooids). K, L: pure quartzose sands (S4297 and E5481). Quartzo-lithic volcaniclastic (M: S4287) and litho-quartzo-feldspathic volcaniclastic sands (N: E4881, note rounded clinopyroxene). O, P: feldspatho-quartzose sands (S4284 and E4882). All photos with crossed polars; blue bar for scale = 100 μm.

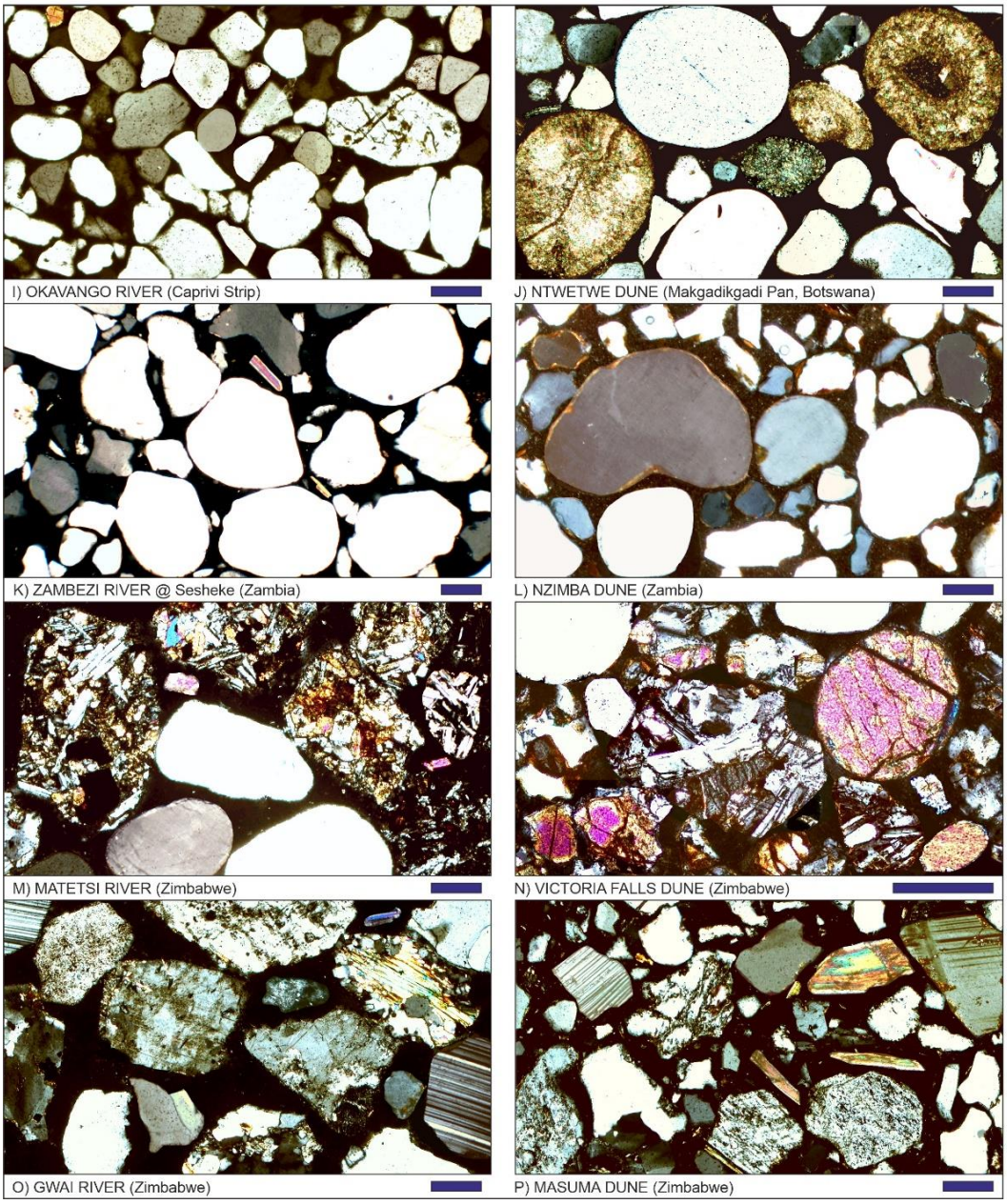

Figure 4.4 continued

clinopyroxene is significant in dune sand NW of Victoria Falls, and dominant in litho-quartzo-feldspathic dune sand close to the Zambezi gorges downstream (Fig 4.4N). In western Zimbabwe, dunes are markedly enriched in feldspars. In the NW near Masuma, aeolian sand is feldspatho-quartzose (Fig 4.4P) with plagioclase > K-feldspar, quartz-rich siltstone/sandstone and medium-rank metamorphic rock fragments, biotite, and a moderately rich garnet-epidote tHM suite. In the SE near Bulawayo, aeolian sand is quartzo-feldspathic with K-feldspar > plagioclase and a poor amphibole-epidote suite. In eastern Botswana around the Makgadikgadi Pan, aeolian sand is quartzose, with K-feldspar

> plagioclase and a very poor tHM suite with common epidote, ZTR minerals, amphibole and/or clinopyroxene, and minor kyanite, garnet and staurolite. Polycrystalline quartz, a few felsic volcanic, and quartz-rich siltstone/sandstone rock fragments are locally significant. Calcareous grains including common ooids occur in mounds on the surface of the Ntwetwe (western Makgadikgadi) Pan (Fig 4.4J; McFarlane and Long, 2015). Straddling the Botswana/South Africa border, aeolian dunes consist of quartzose to pure quartzose sand (Fig 4.4H) with K-feldspar > plagioclase, and very poor tHM suites dominated by ZTR minerals with locally common epidote or staurolite. The Koppieskraalpan dune is quartz-rich feldspatho-quartzose with a few basaltic rock fragments, plagioclase > K-feldspar, and a moderately rich tHM suite including dominant clinopyroxene and subordinate garnet. In the western Kalahari, SW of the Nossob River, aeolian-dune sand is relatively homogeneously quartzose to quartz-rich feldspatho-quartzose with K-feldspar ≫ plagioclase (Fig 4.4F). The mostly poor and epidote-dominated tHM suite includes ZTR minerals and staurolite. Amphibole with minor clinopyroxene are significant in the northern Hardap region, staurolite with subordinate kyanite most common in SW Namibia, and garnet common in South Africa. In northern Namibia, mineralogy is more varied. The Okahandja dune is feldspar-rich feldspatho-quartzose (Fig 4.4B) with plagioclase > K-feldspar, up to high-rank metasedimentary rock fragments, common biotite, and a moderately rich tHM suite dominated by hornblende with clinopyroxene, ZTR minerals, apatite, and epidote. In the central region, aeolian sand is quartzose to pure quartzose, with K-feldspar ≫ plagioclase and poor tHM suites including mainly ZTR minerals, epidote, kyanite associated with either staurolite or garnet, and locally clinopyroxene. Quartzose sandstone and shale rock fragments may occur. In northwesternmost Botswana, the Qangwa dune is quartz-rich feldspatho-quartzose with plagioclase > K-feldspar and a moderately poor, epidote-dominated tHM suite including ZTR minerals.

	n°	Q	F	Lvm	Lsm		P/F%	MI*	tHMC	ZTR	Ap	Ep	Grt	St	Ky	Amp	Px	&tHM	
RIVERS																			
Cunene tributaries	2	99	1	0	0	100	13	-	0.04	69	2	16	1	4	2	1	0	6	100
Okavango	9	99	0.5	0.1	0	100	-	-	0.06	57	0.4	15	0.3	14	6	5	0.2	2	100
Cuando	3	99	0.6	0.1	0	100	-	-	0.08	61	0.3	3	0	16	16	2	0	1	100
Uppermost Zambezi	7	97	3	0	0.1	100	32	-	0.2	58	0.1	6	0.4	7	21	2	4	2	100
Upper Zambezi	1	85	5	9	0.3	100	50	-	2.7	0	0.6	0	0	0	0	0.6	96	3	100
Matetsi	1	37	3	60	0.3	100	100	-	33.3	0	0	0	0	0	0	0	100	0	100
Shangani	1	91	2	6	0	100	86	-	4.7	1	0	0	0	0.5	0	0.5	98	0	100
Gwai	1	71	27	1	0.7	100	54	414	0.5	2	2	17	17	0	3	48	8	3	100
Omatako	1	79	21	0	0.3	100	21	-	0.1	44	0	9	22	0	0	26	0	0	100
Okakongo	1	55	44	0	1	100	53	419	3	10	5	4	13	0.5	0	61	4	2	100
Rietfontein	1	98	0.7	0	1	100	-	-	0.2	46	0	1	0	43	8	3	0	0	100
Nossob	3	81	18	0	1	100	56	333	2.8	10	2	21	19	14	5	28	0	0.7	100
Molopo	1	85	11	0.3	4	100	69	200	0.9	14	2	28	14	4	2	28	8	0	100
DUNES																			
N Botswana	6	99	1	0.1	0.2	100	29	-	0.1	58	1	16	0.3	16	7	1	0	1	100
Serondela	1	100	0	0	0.3	100	-	-	0.1	40	0	5	4	11	35	1	0	2.4	100
W Zambia	11	98	2	0.3	0	100	22	-	0.4	72	0.3	0.1	0.1	10	10	0	7	0.2	100
Victoria Falls	1	35	49	15	0.4	100	99	-	24.3	0.5	1	0	0	0	0.5	0	98	0	100
Masuma	1	64	32	0	4	100	71	296	3	3	5	24	64	0.5	2	1	0	0	100
Bulawayo	1	41	58	0	0.6	100	37	400	0.6	9	1	37	0	0	2	51	0	0.4	100
Zimbabwe	2	99	0	0.7	0	100	-	-	0.1	74	0.3	1	0.6	17	6	1	0	0.2	100
Makgadikgadi	3	93	6	0.6	0.2	100	25	143	0.2	28	0.6	40	2	2	4	8	13	2.1	100
Ghanzi area	4	99	0.4	0.1	0.3	100	-	-	0.2	43	0.2	1	0	48	7	0.5	0	0.3	100
N Namibia	3	98	2	0.1	0	100	0	-	0.3	60	0	16	0.5	17	6	0	0	0.3	100
Qangwa	1	90	10	0	0	100	60	-	1.6	15	3	78	0	1	0	2	0	0.5	100
Otjiwarongo	1	90	8	0	2	100	6	-	0.7	55	1	3	24	1	11	1	0	3.9	100
Okahandja	1	63	34	0	2	100	60	367	3	11	9	7	2	0.5	0	60	10	0.5	100
C Namibia	1	95	4	1	0	100	21	-	1	16	0.5	24	1	14	20	5	20	0	100
SE Namibia	14	86	13	0.4	0.5	100	10	250	0.7	18	0.3	54	4	12	3	5	2	0.6	100
SE Botswana	2	98	2	0	0	100	17	-	0.1	87	0.2	0.7	0.2	9	1	0	1	0.2	100
Mokgomane	1	91	9	0	0	100	31	-	0.3	57	0	40	1	0.5	1	0	0	0.5	100
S Botswana	2	97	3	0	0	100	43	-	0.1	69	0.5	7	0.5	19	3	0.2	0	0.5	100
Koppieskraalpan	1	79	19	1	1	100	62	125	3.4	4	0	6	27	1	1	0	61	0.5	100

Table 4.1. Petrography and heavy minerals in river and dune sands of the Kalahari. Q = quartz; F = feldspars (P = plagioclase); L = lithic grains (Lvm = volcanic to very low-rank metavolcanic; Lsm = sedimentary and metasedimentary); tHMC = transparent heavy minerals; ZTR = zircon + tourmaline + rutile; Ap = apatite; Ep = epidote; Grt = garnet; St = staurolite; Ky = kyanite; Amp = amphibole; Px = pyroxene; &tHM = other transparent heavy minerals (mostly andalusite, titanite, anatase, sillimanite, and locally olivine or monazite).

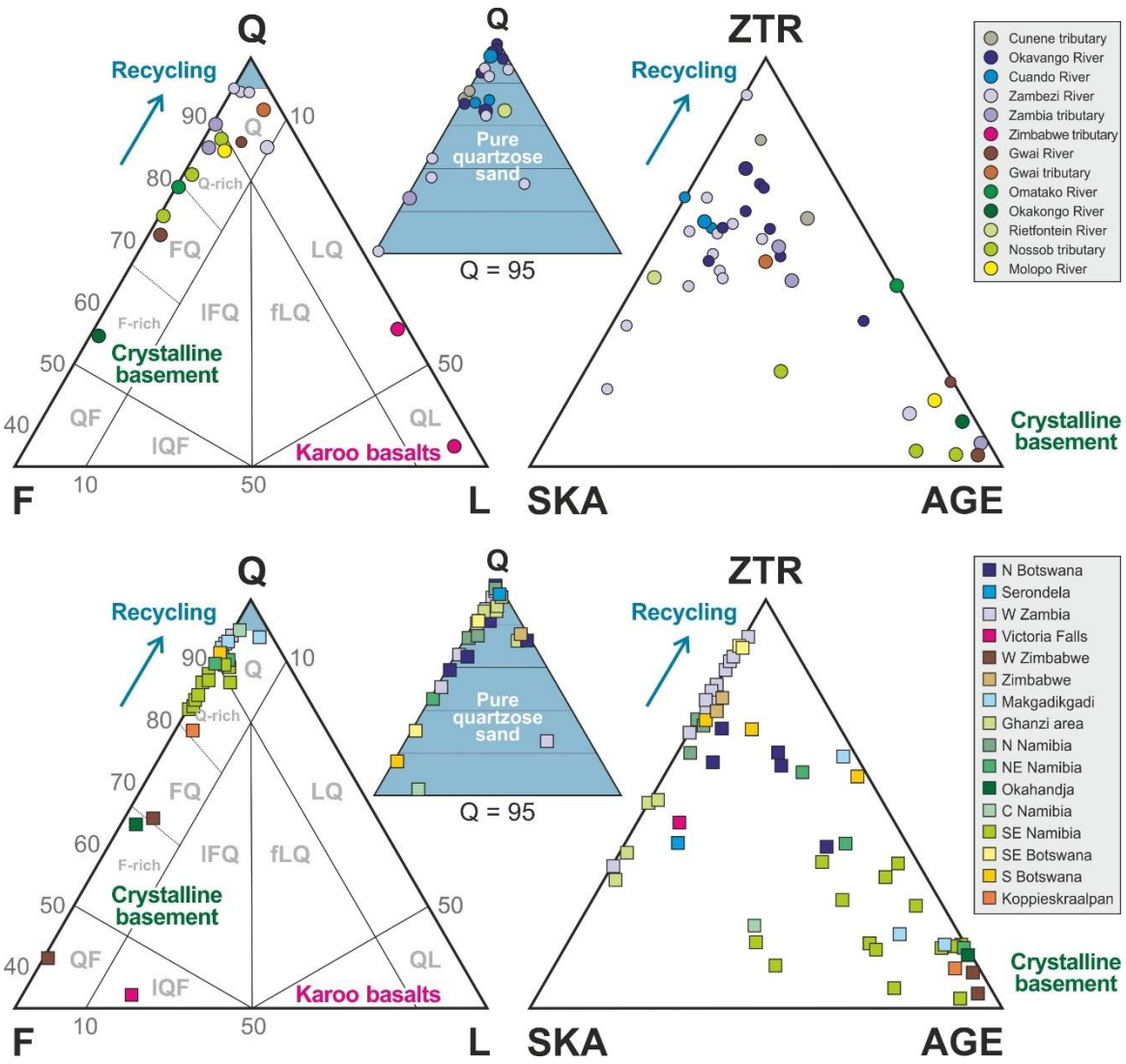

Figure 4.5. Petrography and heavy minerals in river (circles, above) and dune sands (squares, below). Q = quartz; F = feldspars; L= lithic fragments; ZTR = zircon + tourmaline + rutile; SKA = staurolite + kyanite + andalusite + sillimanite; AGE = amphibole + garnet+ epidote. Besides sands largely derived from Karoo basalts in western Zimbabwe, samples plot along the Q/F leg of the triangle, with compositions ranging from quartzo-feldspathic (QF) and feldspatho-quartzose (FQ), to quartzose (Q) and pure quartzose (pQ) (compositional fields after Garzanti, 2019b). The Q/F ratio and ZTR index are indicators of selective chemical breakdown of less durable feldspars (preferentially plagioclase) and heavy minerals (preferentially garnet, amphibole, and epidote) integrated through repeated sedimentary cycles. Symbols for upstream samples in the same river system are smaller.

4.8 Age of detrital zircons

Five age ranges recur among the analyzed samples (Fig 4.6), corresponding to main orogenic episodes in southern Africa (Hanson, 2003; Dirks et al., 2009; Andersen et al., 2016, 2018): I) Limpopo (2.5–2.8 Ga, Neoarchean; peak at 2720 Ma); II) Eburnean (1.8–2.05 Ga, Orosirian; peak at 1893 Ma); III) Sinclair-Kibaran (1.2–1.4 Ga, Ectasian; peak at 1312 Ma); IV) Namaqua-Irumide (1.0–1.1 Ga, Stenian; peak at 1056 Ma); V) Damara-

Lufilian (0.45–0.65 Ga, Ordovician-Cryogenian; peak at 581 Ma). Younger ages include a minor 'Karoo' cluster (220–320 Ma, Triassic-Pennsylvanian; peak at 266 Ma) and some Early Cretaceous ages (120–135 Ma) associated with magmatism related to South Atlantic rifting (e.g., Trumbull et al., 2004). Even younger grains (59–70 Ma, Paleocene-latest Cretaceous) associated with post-rift alkaline magmatism (Moore et al., 2008) sporadically occur in Botswana. In provenance interpretation, it must be kept in mind that the ages of zircon grains in sediments reflect their crystallization age, which may not — and in general does not — necessarily correspond to the age of the source rock, because zircon is a durable mineral that can be recycled even multiple times. The U-Pb age spectra of detrital zircons, therefore, only allow us to discriminate among the different ages of the original crystalline source rocks (i.e., proto-sources *sensu* Andersen et al., 2016), whereas the proportion of first cycle *versus* even multiply recycled zircon grains can be evaluated qualitatively for each sample based on petrographic composition and heavy-mineral concentration (Garzanti, 2016). An additional approach would be to consider other geochronometers (e.g., Fission tracks on Apatite and Zircon or U-Pb on Rutile and Titanite) that rely on lower closure temperatures of the isotopic system, in order to discriminate by comparison with the Zircon U-Pb (crystallization) age. This approach is certainly more precise but introduces time consuming analyses and may exacerbate the issue of different mineral fertility in extremely depleted heavy mineral suites. The author aims to apply this methodology for smaller case study (e.g. small river catchment scale or small dune field). For the Kalahari case it will be proved that petrography and heavy mineral analysis are an expeditive and accurate method to infer the "recycling grade" of sand. Data obtained in this study are compared with previously obtained radiometric ages on diverse crustal domains across southern Africa compiled from numerous literature sources (Fig 4.7). The age compilation is summarized in Table 4.2. Further extensive information on bedrock ages in the region are contained in Gärtner et al. (2014) and Goscombe et al. (2020).

4.8.1 River sands

The zircon-age spectrum in sand of the Mucope River, draining entirely within the northwestern Kalahari dunefield in Angola, displays a unimodal Orosirian peak at ~1.96 Ga, identifying the Eburnean Angola Block as the main protosource (Fig 4.6). Detrital-zircon U-Pb age patterns in Okavango and Cuando sands are characterized by Ediacaran-Cryogenian and Stenian peaks, with a major Orosirian cluster and a minor Neoarchean cluster. Upper Zambezi sand is similar but with notably less Neoarchean ages, and both

Orosirian and Neoarchean ages become rarer in its Zambian tributaries (Fig 4.6). These rather homogeneous zircon-age signatures across the northern part of the Kalahari Basin reflect extensive recycling of sediment originally derived from mainly Eburnean, Irumide, and Damara protosources. In contrast, Gwai River sand in Zimbabwe yielded a polymodal zircon-age spectrum indicating major Neoarchean and Eburnean, and minor Irumide and Pan-African protosources.

4.8.2 Aeolian-dune Sands

Pure quartzose dune sands in the Okavango region, from the inland delta to the Makgadikgadi Pan, yielded multimodal zircon-age spectra characterized by Ediacaran, Stenian, and Orosirian peaks. Similar spectra, with more Cryogenian to Stenian ages and less Paleoproterozoic to Neoarchean ages, are displayed by pure quartzose aeolian-dune sand along the upper Zambezi valley, reflecting more Damaran and Irumide, and somewhat less Eburnean protosources (Fig 4.7). In Zimbabwe, pure quartzose aeolian sand at the eastern edge of the Kalahari Basin is characterized by similar age spectra with major Ediacaran and Stenian peaks, subordinate Orosirian, and minor Neoproterozoic clusters. In western Zimbabwe, instead, the feldspatho-quartzose Masuma dune yielded a few Stenian, Orosirian-Rhyacian, and Archean zircon ages, whereas Archean-aged zircons occur in quartzo-feldspathic dune sand near Bulawayo (Fig 4.6). In Botswana south of Makgadikgadi Pan, Paleozoic ages increase slightly, and Orosirian ages decrease. Farther south, the quartzose Mokgomane dune near Gaborone is singled out by the common Neoarchean to Mesoarchean zircons pointing at cratonic protosources (Fig 4.7A, B), whereas Stenian and subordinate Cryogenian zircons increase progressively westwards in pure quartzose to quartz-rich feldspatho-quartzose dune sand along the Molopo River course in the southern Kalakari (Fig 4.6). In Namibia, Ordovician to Ediacaran ages predominate in feldspar-rich feldspatho-quartzose to quartzose dune sand, reflecting prominent Damara protosources (Fig 4.6). Along a SW/NE traverse in northern Namibia, pure quartzose aeolian sand yielded multimodal, Permo- Triassic, Cambrian to Ediacaran, Stenian, Orosirian and minor Neoarchean clusters. The quartz-rich feldspatho-quartzose Qangwa dune located near the Aha Hills in NW Botswana is singled out by its nearly unimodal spectrum with early Tonian age peak at 956 Ma (Fig 4.6). Along a W/E traverse between Windhoek in central Namibia and the Ghanzi Ridge in Botswana, pure quartzose aeolian sand yielded mainly Orosirian, Statherian, and Stenian zircon ages in the west, mainly Stenian to Ectasian ages in the center, and mainly Cambrian to Ediacaran ages in

the east (Okahandja dune). Quartzose to quartz-rich feldspatho-quartzose aeolian sand in the western Kalahari (WK in Fig 4.6) yielded mostly Mesoproterozoic (Ectasian and subordinately Stenian) zircon ages and no ages younger than 500 Ma, indicating mainly Sinclair and Namaqua protosources.

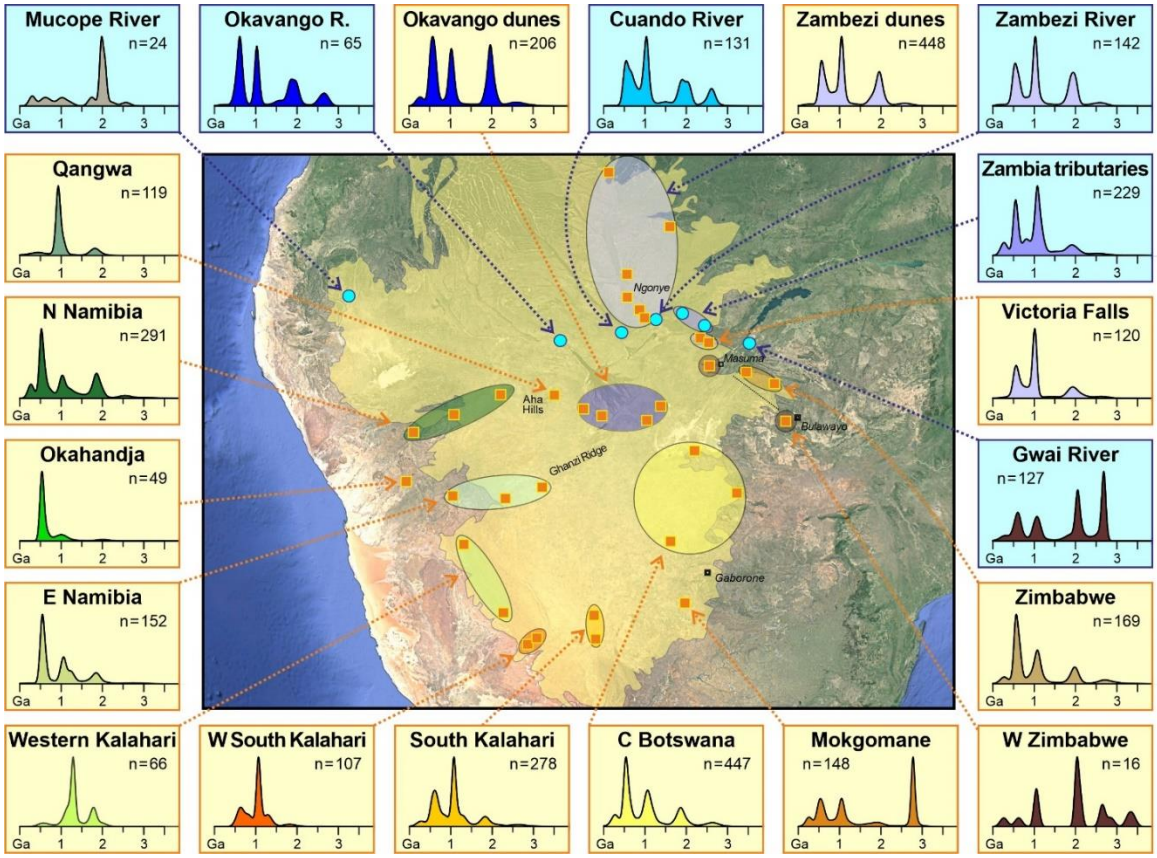

Figure 4.6. Mineralogy of Kalahari dune sands discriminated with the compositional biplot (drawn with CoDaPack software by Comas-Cufí and Thió-Henestrosa, 2011). Pure quartzose sand strongly depleted in all other detrital components besides durable ZTR minerals, staurolite, kyanite, and andalusite dominates through the northern Kalahari and across the central erg in Botswana. Detritus from Precambrian rocks, significant in SE Namibia, is locally dominant at opposite edges of the erg in central Namibia and SW Zimbabwe. Detritus from Karoo basalts, abundant near Victoria Falls, is only locally significant elsewhwere. Lvm = volcanic and metavolcanic lithics; Lsm = sedimentary and metasedimentary lithics; tHMC =transparent heavy-mineral concentration; ZTR = zircron + tourmaline + rutile.

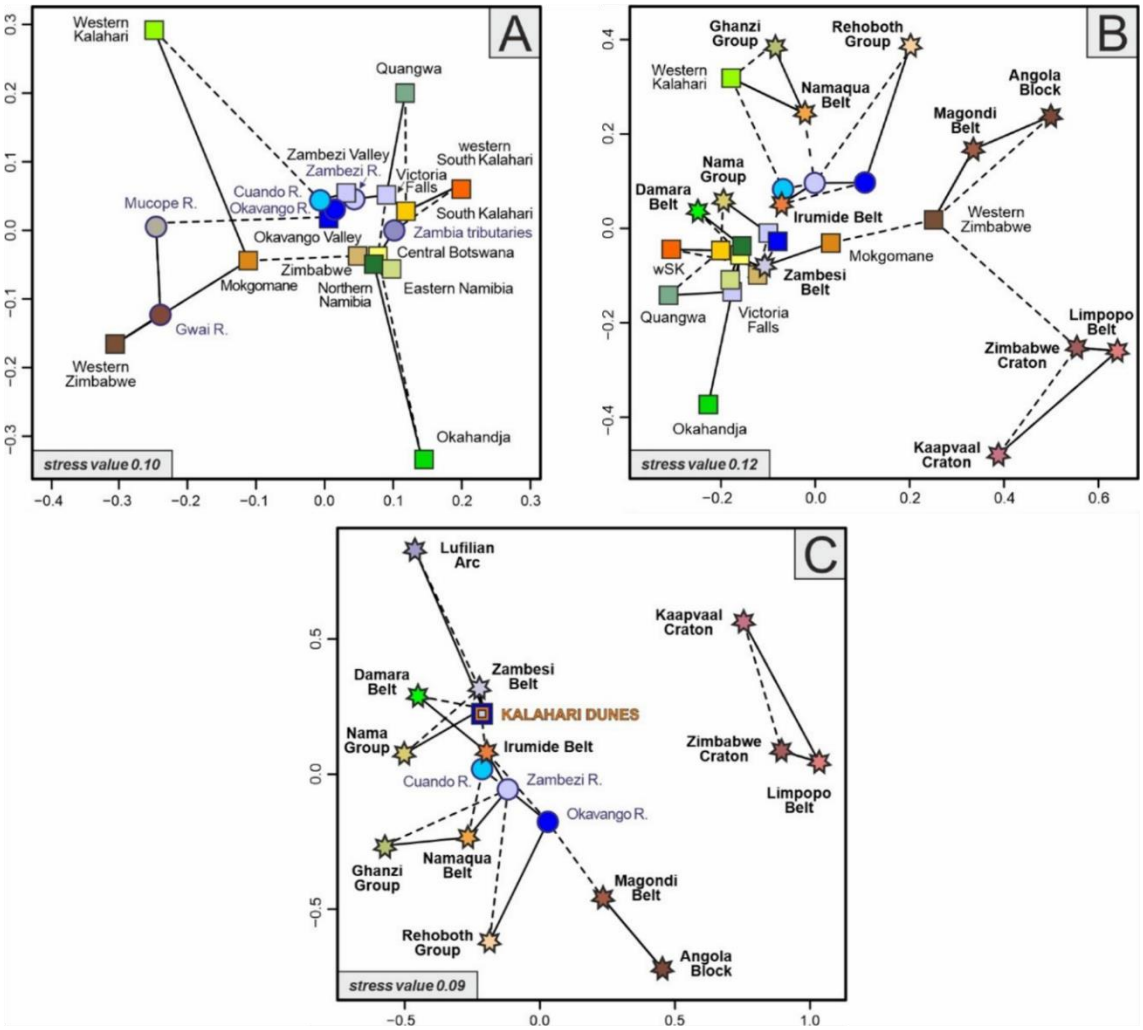

Figure 4.7. Multidimensional scaling maps based on U-Pb age spectra of detrital zircons highlight the different degree of sand homogenization across various parts of the Kalahari Basin (axes units are normalised values based on Kolmogorov-Smirnov distance). A) Comparison among age spectra of aeolian-dune (squares) and river (circles) sands presented in Fig. 6. Distinct provenance signatures are documented locally (69% of ages ≥ 2 Ga in western Zimbabwe dunes; 54% Orosirian-Rhyacian ages in Mucope sand; 55% Tonian ages in Qangwa dune; 67% of Cambrian-Ediacaran ages in Okahandja dune; 61% of Stenian-Ectasian ages in western and western southern Kalahari). B) Comparison among age spectra of aeolian-dune and major river sands from this study and literature data (stars) compiled in Table 4.2. C) Comparison among the cumulative age spectrum of aeolian-dune and major river sands analysed in this study and all potential sources and protosources (stars; data compiled in Table 4.2). Closest and second closest neighbours are linked by solid and dashed lines, respectively. The goodness of fit is evaluated using the "stress" value of the configuration (0.2 = poor; 0.1 = fair; 0.05 = good; Table 1 in Vermeesch, 2013).

	Population 1	*Frequency*	Population 2	*Frequency*	Population 3	*Frequency*	Population 4	*Frequency*	Population 5	*Frequency*
MODERN SANDS										
Cunene River	1394 ± 5	*28.6%*	1746 ± 4	*31.9%*	1948 ± 4	*36.7%*	2456 ± 10	*2.8%*		
Okavango River	96 ± 1	*2.1%*	545 ± 2	*23.8%*	1040 ± 4	*13.3%*	1971 ± 2	*49.6%*	2607 ± 5	*11.2%*
Cuando River	29 ± 2	*0.8%*	590 ± 2	*23.7%*	1024 ± 3	*30.9%*	1902 ± 3	*38.8%*	2648 ± 6	*5.8%*
Zambezi River	646 ± 5	*19.2%*	1023 ± 6	*27.4%*	1193 ± 5	*45.2%*	2570 ± 8	*8.2%*		
ANCIENT SANDSTONES										
Nama Group	616 ± 1	*20.8%*	1010 ± 1	*26.0%*	1181 ± 1	*38.3%*	1891 ± 2	*14.9%*		
Ghanzi Group	1118 ± 1	*50.3%*	1259 ± 1	*32.4%*	1881 ± 1	*17.3%*				
Rehoboth Group (Langberg and Billstein Fms.)	1221 ± 2	*22.5%*	1858 ± 2	*61.0%*	2023 ± 3	*16.5%*				
CRUSTAL DOMAINS										
Damara Belt (+ Cretaceous granite)	131 ± 1	*3.2%*	523 ± 1	*33.6%*	794 ± 1	*16.6%*	1464 ± 1	*35.8%*	2096 ± 2	*10.8%*
Lufilian Arc	555 ± 1	*41.6%*	826 ± 1	*43.1%*	1125 ± 6	*15.3%*				
Zambesi Belt	485 ± 2	*16.8%*	827 ± 5	*26.1%*	1104 ± 1	*34.1%*	1794 ± 16	*15.4%*	2860 ± 4	*8.0%*
Irumide Belt (+ Pan-African rejuvenation)	597 ± 1	*20.4%*	1065 ± 1	*28.7%*	1140 ± 1	*5.6%*	1958 ± 1	*27.7%*	2354 ± 2	*17.5%*
Namaqua Belt	1119 ± 1	*47.8%*	1662 ± 1	*30.3%*	2003 ± 7	*11.9%*	2360 ± 1	*9.9%*		
Magondi Belt (+ Pan-African rejuvenation)	569 ± 7	*7.1%*	2080 ± 93	*92.9%*						
Angola Block	1935 ± 1	*100.0%*								
Limpopo Belt (+ PPz tectono-thermal event)	1953 ± 1	*54.0%*	2594 ± 1	*29.1%*	3284 ± 2	*16.9%*				
Zimbabwe Craton (+ PPz tectono-thermal event)	1881 ± 1	*11.7%*	2411 ± 1	*44.8%*	2580 ± 1	*43.6%*				
Kaapvaal Craton (+ Vredefort magmatic rocks)	977 ± 4	*8.8%*	2845 ± 1	*7.3%*	3467 ± 2	*83.9%*				

Table 4.2. Compilation of detrital zircon ages in modern sands and crustal domains of southern Africa.Age peaks and relative frequencies calculated with Density Plotter (Vermeesch, 2012).

4.9 Provenance of Kalahari aeolian-dune sand

In most of the Kalahari Basin, including the NWK and NEK dunefields in Angola, Namibia and Zambia, much of Botswana, and part of the EK dunefield in Zimbabwe, dune sand is dominated by monocrystalline quartz associated with very poor tHM suites including durable ZTR minerals, staurolite, and kyanite (Figs. 4.8, 4.9, and 4.10). Such a homogenized mineralogical signature reveals multiple recycling of older quartzose sandstones through geological time. A local exception is the quartz-rich feldspatho-quartzose sand of the Qangwa dune collected near the Aha Hills, which contains a moderately poor, epidote-dominated tHM suite with zircon grains yielding mostly Tonian-Stenian ages (Fig 4.6). This suggests recycling of Neoproterozoic siliciclastic rocks exposed nearby (e.g., Ghanzi Group; Baillieul, 1975; Hall et al., 2018), whereas the few Statherian-Orosirian ages point at minor protosources in the Angola Block to the north (McCourt et al., 2013). At the other extreme, aeolian dunes situated at the opposite margins of the Kalahari, near exposures of crystalline basement in central Namibia or of Karoo basalts in Zimbabwe, reveal mainly first-cycle provenance and limited mixing with recycled aeolian sand of the erg (Fig 4.10). Litho-quartzo-feldspathic composition with dominant plagioclase, clinopyroxene, and mafic volcanic rock fragments derived from Karoo lavas characterizes aeolian-dune sand near the basaltic gorges carved by the Zambezi River downstream of Victoria Falls, where less than a fourth of the bulk sediment is represented by aeolian monocrystalline quartz (i.e., less than in local right-bank Zambezi

tributaries draining into the Karoo volcanic rocks; cf. Fig 4.4M and N). The aeolian dune located on the Zimbabwe Craton near Bulawayo (Fig 4.3) is singled out by its quartzo-feldspathic composition with high-rank metamorphic rock fragments, amphibole-epidote tHM suite, and Archean-aged zircon grains, reflecting provenance from local cratonic basement. The feldspatho-quartzose Masuma dune yielded a moderately rich garnet-dominated tHM suite with subordinate epidote and most zircon grains dated between 2.0 and 3.4 Ga (Fig 4.6), indicating largely local provenance from the metamorphic basement of the Dete/Kamativi Inlier belonging to the Paleoproterozoic Magondi Belt (Fig 4.7B; Glynn et al., 2020). On the western side of the Kalahari, the Okahandja dune has feldspar-rich feldspatho-quartzose composition with moderately rich amphibole-dominated tHM suite (Figs. 4.8 and 4.9) and mainly Cambrian- Ediacaran zircon grains, indicating provenance dominantly from amphibolite-facies metamorphic rocks exposed in the inland branch of the Damara orogen (Jung et al., 2007). Consistently quartz-rich feldspatho-quartzose to quartzose composition and poor tHM suite including common epidote associated with ZTR minerals and staurolite characterize sand in the western Kalahari dunefield, where detrital-zircon ages are mostly Mesoproterozoic (Ectasian to Stenian with peak around 1.3 Ga, and subordinately late Paleoproterozoic with peak around 1.8 Ga). Aeolian sand is inferred to have been fed from Damara, Nama, and Karoo sedimentary and metasedimentary rocks, together with arc-related low-grade metasedimentary and magmatic rocks of the Rehoboth terrane in the northwest (Fig 4.3; Becker et al., 2006). Clinopyroxene occurs in the northern Hardap region, reflecting minor contribution from locally exposed Karoo basalts (Fig 4.3). Petrographic composition is similar in the adjacent western southern Kalahari (wSK) dunefield, where garnet notably increases (Fig 4.10) and detrital-zircon ages are mainly Stenian (peak around 1.07 Ga), indicating extensive recycling of the Nama Group (Blanco et al., 2011; Andersen et al., 2018). The moderately rich, clinopyroxene tHM suite of the Koppieskraalpan dune in the wSK dunefield (Fig 4.2A) reveals minor local supply from Karoo lavas. Transitional quartzose sand containing mostly K-feldspar with locally dominant microcline* and mostly very poor tHM suites — including ZTR minerals as well as epidote, kyanite, staurolite, and locally common clinopyroxene or some amphibole — characterizes aeolian dunes in parts of Zambia (upper Zambezi valley), Botswana (e. g., Makgadikgadi and Gaborone areas), northern South Africa, and central-northern Namibia (Fig 4.10). Clinopyroxene dominates the tHM suite of the aeolian dune in the Zambezi valley shortly upstream of Victoria Falls, testifying to minor local first-cycle supply from Karoo basalts. Garnet is relatively common in central-

northern Namibia, where half of zircon grains yielded Ordovician-Ediacaran ages indicating contribution from the northern Damara Belt nearby (Fig 4.7B; Lehmann et al., 2016).

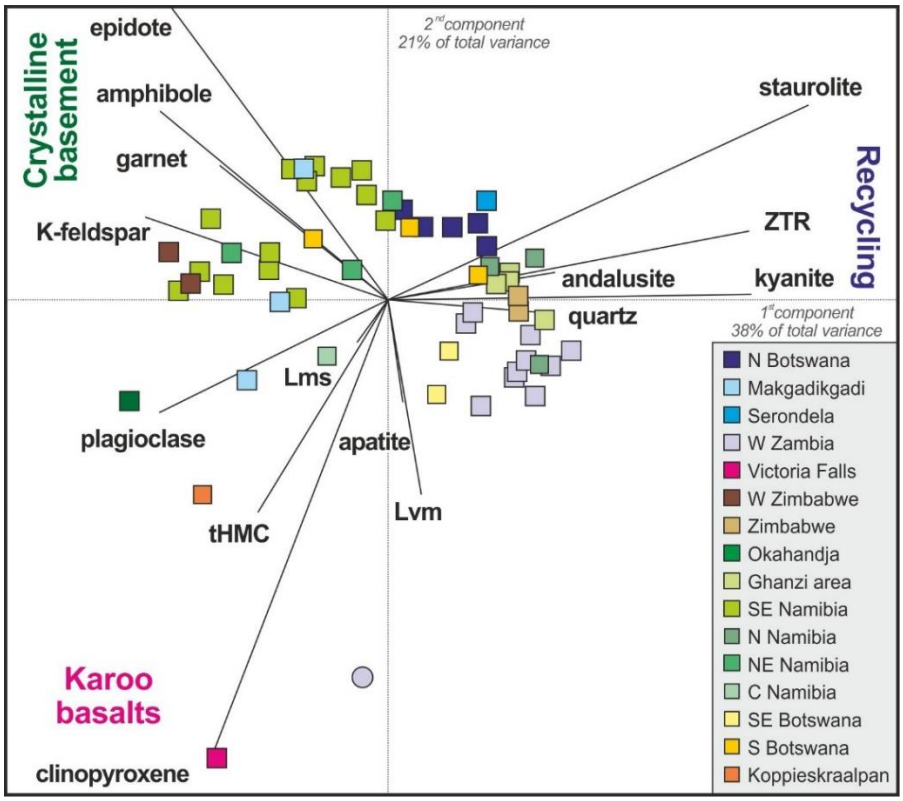

Figure 4.8. Mineralogy of Kalahari dune sands discriminated with the compositional biplot (drawn with CoDaPack software by Comas-Cufí and Thió-Henestrosa, 2011). Pure quartzose sand strongly depleted in all other detrital components besides durable ZTR minerals, staurolite, kyanite, and andalusite dominates through the northern Kalahari and across the central erg in Botswana. Detritus from Precambrian rocks, significant in SE Namibia, is locally dominant at opposite edges of the erg in central Namibia and SW Zimbabwe. Detritus from Karoo basalts, abundant near Victoria Falls, is only locally significant elsewhwere. Lvm = volcanic and metavolcanic lithics; Lsm = sedimentary and metasedimentary lithics; tHMC =transparent heavy-mineral concentration; ZTR = zircron + tourmaline + rutile.

4.10 Multistep recycling in Kalahari

The Mega-Kalahari — which extends over more than twenty degrees of latitude, is characterized by a pronounced increase in precipitation from the tropical south to the subequatorial north, and has seen repeated changes in climatic conditions through the recent and less recent past — provides both end-member examples, as well as a series of intermediate situations. Sand mineralogy is rather homogeneously pure quartzose in the more humid north, from Angola to western Zambia and parts of Zimbabwe (NWK, NEK,

and EK dunefields), but presents peculiar feldspar-rich or even lithic-rich composition at both eastern and western margins of the erg, where detrital modes with more abundant and varied tHM suites indicate largely first-cycle supply from local rivers or creeks (Fig 4.9).

Intermediate is the case of the WK dunefield in southeastern Namibia, where sand is quartz-rich but with a significant amount of mostly K-feldspar, a few lithic fragments, and an up to moderately poor tHM suite including not only epidote and staurolite but also amphibole and pyroxene locally, thus reflecting supply from deflation of fluvial sediments (cf. Figs. 4.4E and 4.4F).

In the NWK and NEK dunefields, as in Botswana, the coexistence of pure quartzose sand in both rivers (Mucope, Okavango, Cuando, Upper Zambezi, Rietfontein) and adjacent dunes (cf. Figs. 4.4C, 4.4I, and 4.4K with 4.4D, 4.4J, and 4.4L) makes it hard to discern how much river sand has ended up in the dunes and, *vice versa*, how much of the river sand has been supplied by erosion and reworking of the dunes. Anyway, the bulk of the sand in all the above-mentioned rivers must have been ultimately derived from reworking of Kalahari Group sediments, as most reliably assessed for Angolan rivers that drain entirely within the erg (e.g., Mucope and Cuando). It is noteworthy that both river and dune sands along the final Chobe tract of the Cuando River get notably enriched in kyanite. This reveals mixing with sand originally fed by the Upper Zambezi and reworked by the Cuando from the toe of the alluvial fan previously built by the Zambezi across the Okavango rift, between Lake Liambezi in the west and the Chobe depression in the east (Lake Caprivi of Shaw and Thomas, 1988).

In the opposite case, feldspar-rich or lithic-rich dune sand with similar mineralogy as river sediments nearby points to chiefly first-cycle origin and fluvial supply, followed by eolian deflation and accumulation at the margins of the erg with limited mixing with eolian quartz (cf. Figs. 4.4A, 4.4M, and 4.4O with 4.4B, 4.4N, and 4.4P, respectively). The proportion of eolian Kalahari sand reworked in river sediments is readily identified by commonly rounded to subrounded monocrystalline quartz and thus readily calculated. Overwhelming in the Caculuvar, Mucope, Okavango, Cuando, and Rietfontein Rivers (Figs. 4.4C and 4.4I), reworked eolian quartz represents more than 90% of bulk sand in the Upper Zambezi (Fig 4.4K) and still ~85% upstream of Lake Kariba despite progressively increasing volcaniclastic supply across the basaltic gorges downstream of Victoria Falls. In Zambezi tributaries of western Zimbabwe, eolian quartz is estimated to range from a minimum of 35-50% in Masuie and Matetsi sand up to 80-85% in Upper Gwai and Shangani sand

(Garzanti et al., 2014b). Recycled eolian monocrystalline quartz with rounded outlines or abraded overgrowths accounts for a large majority of the sand in the Molopo River (Fig 4.4G).

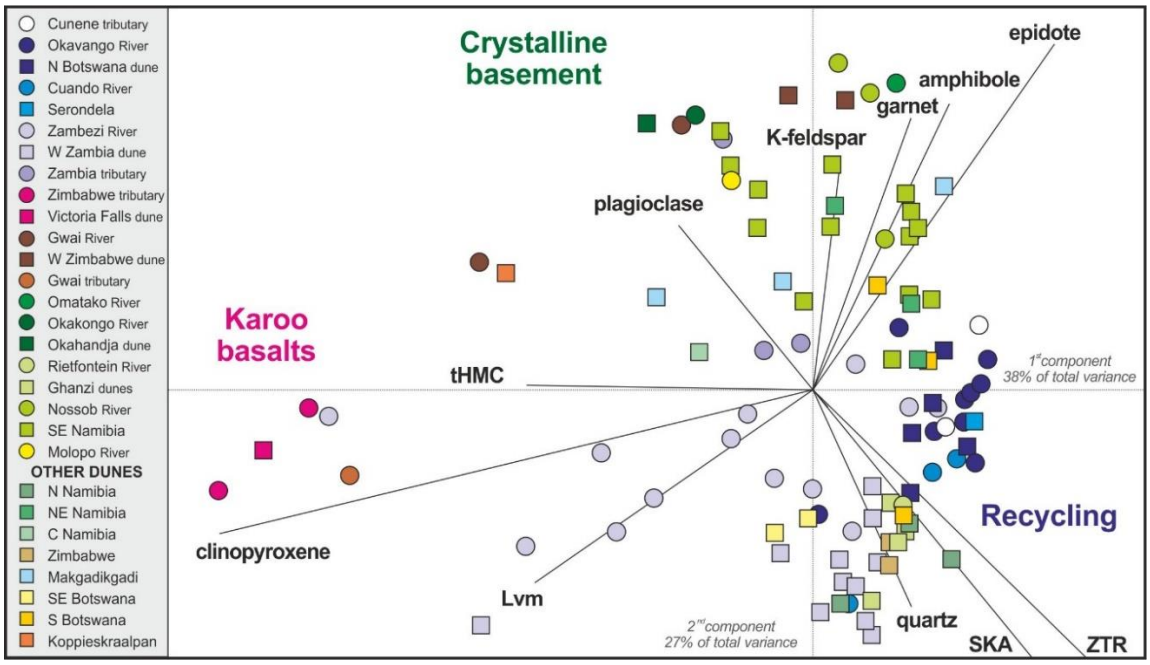

Figure 4.9. Comparison between the mineralogy of river (circles) and dune (squares) sands. The correspondence between the mineralogical signatures of river and dune sand in the same region indicates that pure quartzose polycyclic Kalahari sand mixes locally with first-cycle detritus from Archean to Cambrian basements, as in western Zimbabwe and central Namibia. Because of arid conditions and high-frequency climatic fluctuations, exchange of sediment from river channels to dunefields and back has taken place repeatedly across the erg during the Quaternary. Parameters as in Figs. 4.5 and 4.6.

4.11 Paleoweathering in the Kalahari

The extent to which a sediment has been subjected to chemical weathering, integrated over a series of sedimentary cycles, can be evaluated by combining evidence from petrographic, heavy-mineral, clay-mineral, and geochemical data. Distilled multicyclic sand of northern Kalahari aeolian dunes and of the Okavango, Cuando, and upper Zambezi Rivers is composed dominantly of quartz with strongly depleted tHM suites including zircon, tourmaline, rutile, staurolite, and kyanite but virtually no garnet or apatite (both invariably ≤1%tHM; Table 1). The scarcity of garnet relative to staurolite, kyanite, andalusite, and sillimanite [G/(G + SKA) < 5% in both aeolian and fluvial sands; Fig. 4.10] is anomalous, because these minerals are associated in amphibolite-facies metapelites and unweathered detritus derived from them, where garnet is typically dominant [G/(G + SKA) = 70 ± 20%;

Garzanti et al., 2006, 2010a]. The Okavango and Zambezi Rivers carry mud containing ~40% kaolinite (i.e., more than most other rivers in tropical southern Africa; Garzanti et al., 2014c). Northern Kalahari aeolian dunes are strongly depleted in virtually all chemical elements but Si. Even Zr and Hf are low in both aeolian and fluvial sands (83 ± 55 and 2 ± 1 ppm *versus* 190 and ~ 6 ppm in the Upper Continental Crust standard; Taylor and McLennan, 1995), suggesting that all minerals including zircon are depleted relative to most durable quartz. Among chemical indices of weathering, $\alpha^{Al}Na$ is >3 in Okavango, Cuando, and upper Zambezi fluvial sands, reaches >5 in aeolian-dune sand, and is ~20 in mud Garzanti et al., 2014b, 2014c). The traditional WIP and CIA indices (Parker, 1970; Nesbitt and Young, 1982) reach down to 0 and up to ≥80 in aeolian sand (down to 1 and up to ≥90 in fluvial sand), with consequently extreme CIA/WIP ratio reflecting extensive recycling (Garzanti et al., 2019b).

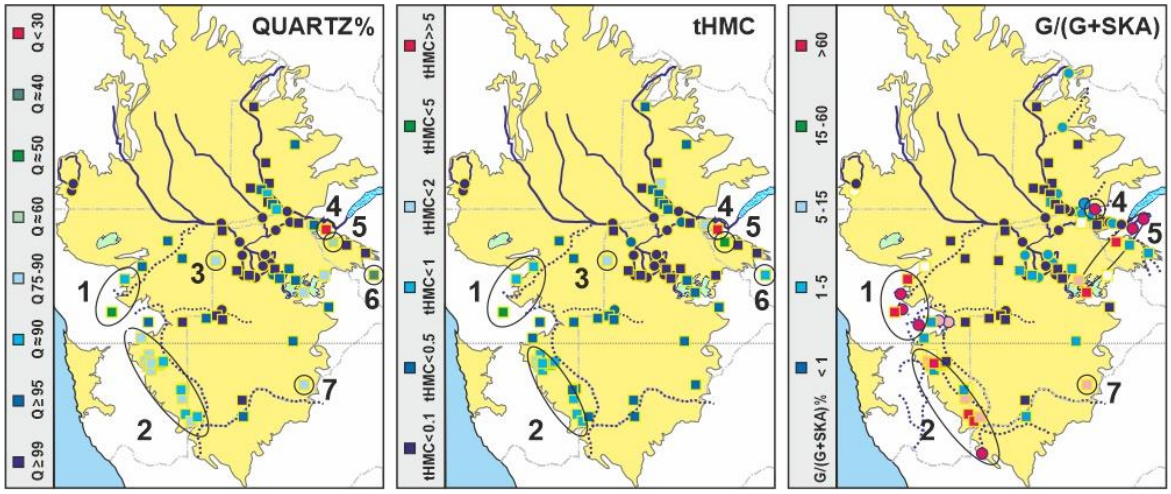

Figure 4.10. Provenance maps of the Mega-Kalahari. Across most of the erg, dune sand has homogenized pure quartzose composition with depleted tHM suites lacking garnet. Mixing in various degrees with locally supplied detritus including significant amounts of feldspars, rock fragments and heavy minerals including garnet occurs in seven areas: 1) inland branch of the Damara Belt; 2) SE Namibia; 3) near Aha Hills; 4) near Karoo basalts; 5) near Magondi Belt; 6) Zimbabwe Craton; 7) near Kaapvaal Craton. Lack of garnet from north to south across the erg indicates inherited weathering from previous more humid climatic stages.

Pure quartzose sand lacking garnet in presence of common staurolite and kyanite, abundance of kaolinite in mud, and chemical indices pointing at high weathering intensity cannot be the product of a single sedimentary cycle in the current climatic setting. They require widespread recycling of sediments affected by extensive weathering in chemically

much more aggressive hot-humid climates of the past. All these pieces of evidence combined cannot be explained with breakdown of all but the most durable minerals by grain-to-grain aeolian impacts, which prove to be effective enough to round sand-sized silicate grains but far from efficient enough to systematically destroy them mechanically (Garzanti et al., 2015b; Rittner et al., 2016; Resentini et al., 2018). Detrital components of northern Kalahari aeolian sand must have undergone very extensive weathering in humid subequatorial climate before being recycled during repeated episodes of alternating fluvial and wind erosion, leading to their accumulation in the erg. In other words, they represent the echo of paleo-weathering stages passed on to the present landscape through multiple recycling episodes.

4.12 Conclusions

Aeolian dunes of the Kalahari are homogeneously pure quartzose in Angola, Zambia, and over much of Botswana and parts of Zimbabwe and Namibia, where they also contain a few K-feldspar grains and strongly depleted heavy-mineral assemblages dominated by ZTR minerals and including common staurolite in Botswana and kyanite in Zambia, but virtually no garnet. Composition varies markedly only at the western and eastern edges of the erg, ranging from feldspar-rich feldspatho-quartzose and hornblende-rich in the Damara Belt of central Namibia to quartzo-feldspathic and hornblende-rich in the Zimbabwe Craton or litho-quartzo-feldspathic and clinopyroxene-rich beside the Zambezi basaltic gorges near Victoria Falls. Compositionally distinct is the partially active western Kalahari dunefield of SE Namibia, where sand is quartzose to quartz-rich feldspatho-quartzose with common epidote, indicating partly first-cycle but largely polycyclic provenance from Mesoproterozoic crustal domains, Damara Belt, and Nama and Karoo Groups. U-Pb age spectra of detrital zircons allow discrimination among protosources of different ages in various parts of the erg. Damara ages (0.45–0.65 Ga) are widespread and most abundant in aeolian dunes of central Namibia but quite rare in the western Kalahari dunefield to the south. Namaqua-Irumide Stenian ages (1.0–1.1 Ga), also widespread, are particularly common in aeolian dunes along the Botswana/South Africa border, increasing southward towards the Namaqua Belt. Sinclair Ectasian ages (1.2–1.4 Ga) are most abundant in the western Kalahari dunefield of SE Namibia. Eburnean Orosirian ages (1.8–2.05 Ga) are most frequent in Angola and northernmost Botswana. Neoarchean ages characterize aeolian dunes at the edge of the Zimbabwe and Kaapvaal Cratons in SW Zimbabwe and SE Botswana. The compositional fingerprints of aeolian-dune sand and their processes

across the sand sea. In northern Kalahari dunefields adjacent to humid subequatorial regions, widespread monocrystalline quartz commonly showing abraded overgrowths combined with strongly depleted ZTR-rich heavy-mineral assemblages lacking garnet but containing staurolite and kyanite, common kaolinite in river muds, and geochemical indices reveal that the sediments have undergone very extensive weathering in humid subequatorial climate before being stored into the erg. The composition of aeolian-dune sand thus reverberates the echo of paleo-weathering passed on to the present landscape through multiple recycling episodes. Intracratonic sag basins such as the Kalahari, straddling the arid tropical belt, contain vast amounts of quartz-rich polycyclic sand. Whenever tectonic or climatic conditions favor the development of an integrated drainage system connecting the continental interiors with the coast, tapping into such a huge sediment reservoir may induce a sudden pulse of quartz-rich sand to the oceans and thus a significant mineralogical change in continental-embankment successions. Such an event, recorded in post-Tortonian sediments of the Zambezi Delta, may occur again in the future if development of the Okavango rift will lead to the incorporation of the entire Okavango River to the Zambezi drainage system.

Chapter 5: Fluvial-Aeolian interaction in Deserts

The origin of sand in large dune fields still represents a controversial issue. In many Earth's deserts, aeolian sand is enriched in most durable quartz and ZTR minerals (Muhs, 2004), but such a simple monotonous compositional signature hardly facilitates interpretation, because it is the resultant of the combined effects of diverse processes accumulated through geological time (Dott, 2003). Prominence of physical factors or of chemical processes? Selective break-down of less durable grains by mechanical abrasion, pre-depositional weathering, or inherited intrastratal dissolution? This is the crux of the "quartzarenite problem" (Basu, 2020).

Sahara and Kalahari case studies proved to be of crucial importance for this thesis to discuss *in situ* sand generation by wind erosion *versus* external fluvial supply. In the Sahara, most sand results from disaggregation of rocks with high sand-generation potential, such as sandstones or locally granites, and will thus be primarily composed of quartz and feldspars with generally very poor heavy-mineral suites largely consisting of ZTR minerals. In Kalahari, sediments are fed by rivers into the desert by first cycle erosion of exposed orogens at the flanks of the basins and therein homogenised. Here are presented also desert sand composition from literature where mineralogy is variable, with larger percentages of first-cycle detritus derived from a wide range of source rocks, including lithic fragments as well as amphibole, epidote, garnet, or pyroxene, fed by major river systems.

5.1 Wind-fed quartz-rich sand seas

Sand seas consisting of pure quartzose sands are well documented in the Paleozoic (e.g., Dott et al., 1986), Mesozoic (e.g., Bertolini et al., 2020), and Cenozoic (e.g., Vainer et al., 2018a). Although the Sahara has several predecessors in geological history, characterized by the same monotonous compositional signature dominated by the most durable minerals, the Sahara cannot be considered the rule in this respect, but rather an end-member case (Fig. 5.1). The debate on the existence of first-cycle quartzarenites went on for long (Krynine, 1941; Suttner et al., 1981; Johnsson, 1993), until the modern-sand lesson indicated unambiguously that sand consisting virtually entirely of quartz and ZTR minerals cannot be the result of mechanical or weathering processes even in the most aggressive climatic conditions met in modern Earth, but that the final cleansing of less stable minerals requires extensive intrastratal dissolution, i.e., inheritance from previous sedimentary cycles of weathering and diagenesis (Garzanti et al., 2019a). Pure quartzose composition

thus implies that sand is originated from homogenization of detritus chiefly produced by physical disaggregation of quartz-rich parent sandstones, possibly derived in turn from older "grand-parent" sandstones, along a line of ancestry rooted in the deep past.

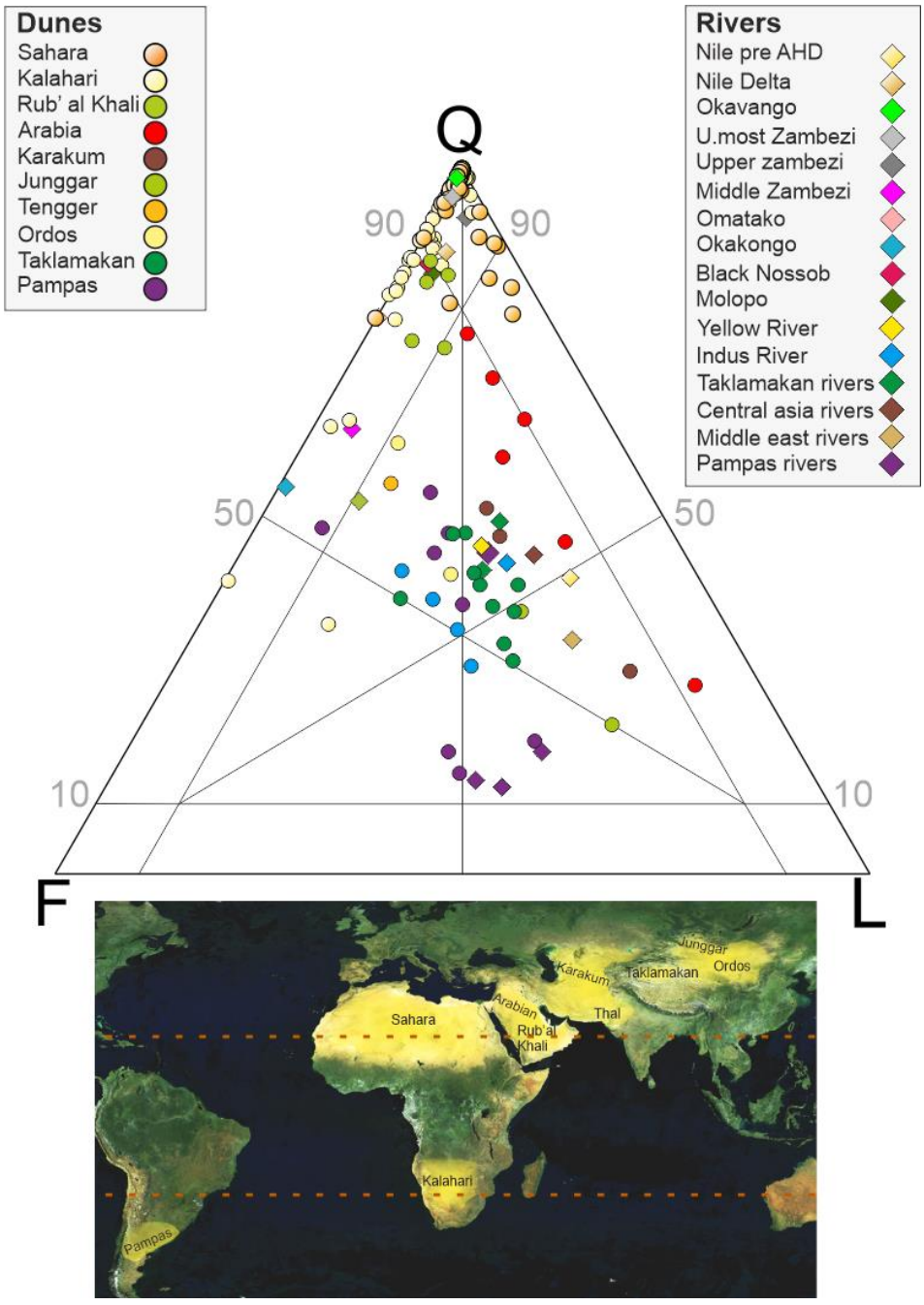

Figure 5.1 Sand composition in deserts of Asia, Africa and South America compared with their fluvial feeder systems (modified after Garzanti et al., 2019b). Note general consistency of detrital modes in eolian (circles) and river sands (rombs of corresponding colour. Data sources: Taklamakan and Junggar (Rittner et al. 2016); Tengger, Ordos (Pan et al. 2016; Pang et al. 2018); Thal (Liang et al. 2019); Arabia (Garzanti et al. 2003, 2013, 2017), Pampas (Garzanti et al., 2022); Sahara (*Chapter 3*); Kalahari (*Chapter 4*); Zambezi (*Chapter 6*) Q = quartz; F = feldspars; L = lithics. In the lower part, geographical map of the location of world desert, tropics are drawn by red dashed lines.

The Sahara is an example of a vast desert hosting sand purified during multiple steps through Phanerozoic time. No clear trace is left of sediments supplied by rivers draining towards the desert, with the exception of Moroccan dunes at the foot of the Anti-Atlas Mountains and of pyroxene-enriched Egyptian dunes near Aswan and east of the Nile (Garzanti et al., 2015a). Conversely, aeolian sand is overwhelming. Rather than the river supplying sand to the desert, it is the dune field that commonly invades and chokes the dry river valleys, as seen in northeastern Egypt and Sinai (Garzanti et al., 2015a). In hyperarid climate, river action may be weakened to the point that fluvial contribution to the dune field becomes insignificant, as documented in northern Arabia, where sand is dominantly supplied by disaggregation of Cambro-Ordovician quartzarenites and no river influences the mineralogy of dune sand, if not minimally (< 5%), and only locally where it empties into the desert (Garzanti et al., 2013a).

5.2 River-fed lithic-bearing sand seas

The opposite end-member is represented by sand seas fed by a major rivers, as indicated by sand mineralogy maintaining the same characteristic fingerprints of the fluvial system through distances up to a thousand kilometers (Fig. 5.1). These deserts can be considered as wind-reworked inland or coastal deltas. An emblematic case is represented by the coastal ergs of southwestern Africa, which are mostly fed *via* northward littoral drift from the Orange River mouth. Dune sand of the coastal Namib Erg (southern Nambia) is estimated to be 99% derived from the Orange River even at its farthest northern edge, the main mineralogical and textural differences being a slightly enrichment in quartz at the expense of most easily destroyed sedimentary and metasedimentary lithics, a dearth of mica, and a markedly higher degree of grain roundness (Garzanti et al., 2012a, 2015b). Because of hyperarid climate, additional fluvial supply is limited along the coast. Consequently, coastal ergs in northern Nambia to southern Angola are still dominantly derived (~80% and ~60%, respectively) from the Orange River mouth after a multistep longshore transport up to 1800 km (Garzanti et al., 2014a, 2018c). All along, composition of dune sand remains constantly feldspatho-quartzose with common basaltic rock fragments and rich tHM suites containing high, although progressively diluted, percentages of clinopyroxene.

Fluvial-dominated dune fields tend to be the rule in orogenic settings, with several examples documented in arid inland areas across Asia, where river sediments are trapped in subsiding troughs adjacent to the front of active orogens such as the Kopeh-Dagh, Kun Lun, Altyn Tagh, Tian Shan, or western Himalaya (East et al., 2015). The Karakum Desert

in Turkmenistan contains feldspatho-litho-quartzose dune sand with varied lithic population and moderately rich epidote-amphibole-garnet tHM suite, which closely matches sand of the Amu Darja River draining the western Pamir mountains of Tajikistan (Garzanti et al., 2019b). Dune sand of the Thal Desert in central Pakistan contains subequal amounts of quartz, feldspars, and mostly metamorphic and sedimentary lithic fragments, as well as a very rich amphibole-epidote-garnet-pyroxene tHM suite (Liang et al., 2019). This low-quartz signature indicates supply from the upper Indus River at latest Pleistocene/ealy Holocene times, when erosion was focused on the high mountains of northern Pakistan (Garzanti et al., 2020).

The large Taklamakan Desert of northwestern China contains feldspatho-litho-quartzose sand with mainly sedimentary and metamorphic lithics and moderately rich amphibole-epidote-pyroxene tHM suite, a composition virtually indistinguishable from sand of the Yarkhand River draining the northern Karakorum and Kun Lun Mountains (Rittner et al., 2016). In South America Pampean the high fluvial discharge of the past is testified by high volcanic detritus composition in dunes (Garzanti et al., 2022). First cycle supply is transported from the Adean volcanic province by paleo-rivers and stored into distant dunes, preserving unstable minerals from chemical weathering. Present day arid condition and river desiccation could not allow such long transport, testifying that the Pampean Desert was river fed in the past.

5.3 Fluvial/aeolian connectivity in arid environments

The interaction between fluvial supply and wind reworking is documented at the periphery of all sand seas. Excellent examples are represented by the eastward landward side of Namibian deserts, where the conflict between persistent wind action and episodic river floods produces spectacular sedimentary features (Stanistreet and Stollhofen, 2002; Svendsen et al., 2003; Feder et al., 2018). In the Kalahari Desert dune sand is also largely pure quartzose but composition is not equally homogeneous, and distinct mineralogy in different areas reflects a greater role of fluvial supply (Garzanti et al., 2014b). Kalahari dune fields are best developed west of river channels, suggesting deflation of fluvial sediments by easterly winds during drier periods (Shaw and Goudie 2002). Conversely, rivers have inundated interdune areas and incised their course across dune ridges during wetter periods (Thomas et al. 2000). Quartz grains are commonly well rounded in both dune and river sands, documenting aeolian abrasion at one or more stages of their multistep transport history. Climate-controlled cycling of quartzose sand from the fluvial to the

aeolian environment and back has taken place repeatedly in the Kalahari (Thomas and Shaw 2002).

In Saudi Arabia, dune sand remains homogeneously quartz-rich feldspatho-quartzose to quartzose across the Rub'Al Khali, the largest continuous sand sea on Earth, but compositional variations are observed along the desert's rims. Dune sand becomes lithic carbonaticlastic close to the Hadhramaut carbonate tableland in Yemen to the south and quartzo-lithic carbonaticlastic along the Gulf shores of the Emirate of Abu Dhabi to the northeast (Garzanti et al., 2001, 2003). Fluvial interactions are documented at the southwestern edge of the sand sea, where dune sand is less quartz-rich than in Cambro-Ordovician parent sandstones, has distinctly higher heavy-mineral concentration, higher amphibole, and lower ZTR indices, indicating that *wadi*-derived first-cycle detritus from the crystalline basement accounts for ~20% of aeolian sand (Garzanti et al., 2017).

Fluvial-aeolian connectivity is well documented in the Thar Desert of southern Pakistan, where sand was exchanged over spatial scales of hundreds of kilometers between the Indus River and the desert. Summer monsoon winds recycle sediment from the lower Indus River and delta downwind and upstream. Large volumes of sediment were thus stored inland since the mid-Holocene, when the desert expanded as the summer monsoon rainfall decreased, buffering the sediment flux to the ocean (East et al. 2015).

Another renowned example of fluvial-aeolian interaction is provided by the sand seas and loess plateau of northern China, where the accumulated sand and dust have been largely transported originally by the Yellow River from the northern Tibetan Plateau (Stevens et al., 2013; Nie et al., 2015). Contrariwise, aeolian sediment is widely supplied to the Yellow River in Inner Mongolia, where the river course is largely incised within loess deposits and flanked by a wide desert area from where aeolian sand is blown periodically toward the fluvial channel by the winter monsoon (Pang et al., 2018). Such a multistep, back-and-forth sediment mixing contributes to extensive homogenization of compositional fingerprints of fluvial sand, dune sand, and loess deposits.

5.4 Aeolian processes able to modify sand composition and texture

Distinguishing end-member types of deserts may appear as a largely conceptual exercise, because landscapes evolve through time under the complex effects of climate change, which controls wind strength, fluvial runoff, water-table level, and vegetation cover. Despite Nature's complexities, however, a basic distinction holds between river-fed sand seas with varied mineralogy including first-cycle detritus (most typical of orogenic

settings) *versus* sand seas fed in *situ* by recycling of older sandstones and characterized by distilled composition dominated by quartz and ZTR minerals (most typical of anorogenic settings).

Because arid climate hampers the effectiveness of chemical reactions, processes that can alter sediment composition within a desert are essentially physical, including abrasion and wind sorting. Recycling *per se* can only replicate the mineralogy of parent clastic units in the daughter sand, but by this fundamentally physical mechanism the effects of selective chemical and mechanical breakdown of labile grains can be accumulated through multiple sedimentary cycles, and inherited in the next (Garzanti, 2017). As a most evident effect of mechanical abrasion and comminution, softer detrital grains effectively increase their roundness in aeolian dunes as a consequence of repeated impacts with harder grains in air (Resentini et al., 2018). Clear examples are seen in the Rub'al Khali, where carbonate grains are most readily rounded with transport distance, progressively reduced in size, and finally removed. Other minerals, cleaved or softer than quartz or garnet like feldspars, rock fragments or ferromagnesian silicates, may also be selectively comminated and concentrated in finer size fractions (Garzanti et al., 2017). Selective entrainment and winnowing are other physical processes that can affect sand mineralogy even markedly. Deflation by strong winds selectively removes slow-settling detrital components, leaving behind coarser layers (e.g., granule ripples) or laminae enriched in ultradense minerals such as garnet and magnetite. Contrary to mechanical abrasion and comminution, these modifications are largely temporary and reversible.

5.5 Fluvio-Aeolian transport in deserts

The conclusion of "desert chapters" of the thesis indicates that Sahara and Kalahari are substantially dominated by different sediment transport processes of fluvial-aeolian interaction. In the case of the Sahara, the Nile is the only river that, before the building of the Aswan High Dam in 1964, possessed sufficient discharge and competence to carry as far as the sea Saharan sand and silt (estimated as ~10% of total sediment load, which used to vary between ≤50 and ≥ 300 million tons/year; Inman and Jenkins, 1984; Garzanti et al., 2015a). This is between one and two orders of magnitude less than the volume of dust blown off the Sahara towards and beyond the Atlantic Ocean and the Mediterranean Sea, estimated to range between 130 and 460 and 1400 million tons/year overall (Goudie and Middleton, 2006; Stuut et al., 2009). Aeolian process dominates the movement of dunes sediment and given that minor particulate dust can travel long distances (Bagnold, 1974),

first cycle detritus transport is detected only in dunes at limited range from the source (e.g. Air Mountains, Murzuq province, Anti-Atlas Belt). Past condition of higher fluvial discharge (e.g perennial river during African Humid Period, Blanchet et al., 2021) may also have not influenced substantially the dune composition because of ubiquitous presence of highly quartzose Paleozoic sandstone.

In comparison, the amount of dust emissions from the Kalahari is much lower (Crouvi et al., 2010; Bhattachan et al., 2013) and sediment exported to the ocean notably less even though diverse major rivers draining the dryland reach the coast. To the west, Kalahari sand supply to the Atlantic Ocean cannot be estimated with forward-mixing calculations for the Congo River because it carries sediment overwhelmingly recycled from multiple quartzose sandstone units. Kalahari supply may represent up to 30% of Cuanza River sand (annual sediment load 0.6 ± 0.1 million tons, 43% mostly fine sand; Holisticos, 2012), but it is very minor for the Cunene River (although recycled aeolian sand accounts for ~15% of Cunene sand at the western edge of the Kalahari) and negligible for the Orange River (based on petrographic and heavy-mineral data in Garzanti et al., 2014b, 2018a). To the east, Kalahari sand is conveyed towards the Indian Ocean almost exclusively by the Zambezi River (annual sediment flux between 20 and 100 million tons; Hay, 1998). Kalahari aeolian quartz grains representing ~85% of upper Zambezi sand are all trapped in Lake Kariba at present, but Kalahari sand accounted for no more than 10% of total Zambezi bedload even before dam construction (Chapter 6). The total volume of Kalahari sand exported towards the oceans is thus of the same order of magnitude as the endorheic Okavango sediment flux (between 0.2 and 2 million tons of mostly bedload sand recycled from Kalahari aeolian dunes; Shaw and Thomas, 1992). Hence, less than half of the sand eroded from Kalahari dunes is exported towards the ocean today. This budget, however, may have changed drastically and repeatedly in the past, and may change again in the future depending on climatic conditions as well as on the balance between rejuvenated subsidence in the Okavango Graben *versus* rejuvenated uplift of the African superswell (Kinabo et al., 2007; Al-Hajri et al., 2009). River piracy plays a fundamental role too, as emblematically documented on both flanks of the Kalahari Plateau by the recent capture of formerly endorheic Cunene and Zambezi drainage by headward eroding coastal rivers. Capture of the Upper Zambezi by the middle Zambezi is generally held to have occurred around early Pleistocene time (Moore et al., 2007) but the upper Zambezi returned to be at least partly endorheic in the mid- Pleistocene, as inferred from diverse mega-lake Makgadikgadi phases through the late Pleistocene (Burrough et al., 2009b; Moore et al., 2012). During

this period of partly endorheic Zambezi floods (Burrough and Thomas, 2008), repeated drainage changes were induced by the evolution of the Okavango Graben (Vainer et al., 2021b). This tectonic depression finally diverted the Cuando River towards the Zambezi and is presently favoring the capture of the Okavango as well, conveyed eastward along the Selinda spillway (Gumbricht et al., 2001). In a deeper past, a marked increase in monocrystalline quartz grains with rounded to subrounded outline and abraded overgrowths is documented in post-Tortonian strata of the Zambezi Delta subsurface (Chanvry et al., 2018), pointing to a sudden flux of recycled quartz-rich Kalahari sand from the continental interiors.

Chapter 6: The Zambezi River

This chapter has been published with modification as: "The Segmented Zambezi Sedimentary System from Source to Sink: 1. Sand Petrology and Heavy Minerals" by Garzanti, E.; Pastore, G., Resentini, A., Vezzoli, G., Vermeesch, P., Ncume, N., Van Niekerk, H. J., Jouet, G. & Dall'Asta, M., on The Journal of Geology, 129, vol. 4, 2021. And as: "The Segmented Zambezi Sedimentary System from Source to Sink: 2. Geochemistry, Clay Minerals, and Detrital Geochronology" by Garzanti, E.; Bayon, G., Dinis, P., Vermeesch, P., Pastore, G., Resentini, Barbarano, M., Ncume, N. & Van Niekerk, H. J., on The Journal of Geology, 130, vol. 3, 2022.

6.1 Introduction

The Zambezi is one of the most fascinating river systems on Earth, flowing across wild landscapes from Barotseland to Victoria Falls and next plunging into deep gorges carved in basalt and along ancient rift valleys to finally reach the Indian Ocean (Fig 6.1; Main 1990; Moore et al. 2007). The relatively recent, complex, and controversial natural evolution of its drainage basin ended in the Anthropocene with its drastic subdivision into separate segments by man's construction of two big dams and associated reservoirs. This is the first of a series of articles aiming at characterizing, by a multitechnique approach, the composition of sediment generated in the diverse tracts of the vast Zambezi catchment and the present and inherited factors that influence compositional variability from the headwaters to the Mozambican coast and beyond.

Figure 6.1. Zambezi drainage basin (base map from Google Earth). White circles indicate sampling locations (more information in file Zambezi.kmz). VF = Victoria Falls.

This study, based on framework petrography and heavy-mineral data, focuses specifically on: (1) the relative effects of source-rock lithology and chemical weathering on sand mineralogy in a subequatorial climate, (2) the transmission of compositional signals along the sediment-routing system from source to sink, and (3) the use and misuse of current petrological models to infer sediment provenance and of mineralogical parameters to infer climatic conditions. A complementary dataset is composed of data from sand and mud geochemistry, clay mineralogy, and detrital zircon geochronology on the same sample set. The ultimate purpose is to build up a solid knowledge of the modern sedimentary system that can be applied to trace fluvial transport from the land to the deep sea and, eventually, to investigate provenance changes recorded in stratigraphic successions accumulated in marine depocenters through time and thus unravel the complex evolution of the Zambezi River since the late Mesozoic.

6.2 Geology

6.2.1 The Precambrian

The Archean core of southern Africa includes the Zimbabwe Craton, welded by the Limpopo Belt to the Kaapvaal Craton in the south and bounded by the mid-Paleoproterozoic Magondi Belt in the west (Fig. 6.2). The Zimbabwe Craton comprises a central terrane flanked by greenstone belts. Gneisses of the central terrane are nonconformably overlain by volcanic rocks and conglomerates. The craton was stabilized in the mid-Neoarchean and finally sealed by the Great Dike Swarm at ~2575 Ma (Kusky 1998; Jelsma and Dirks 2002; Söderlund et al. 2010). The composite Archean core grew progressively during the Paleoproterozoic and Mesoproterozoic. The Proto-Kalahari Craton was established by the late Paleoproterozoic and affected by widespread intraplate magmatism at 1.1 Ga (Hanson et al. 2006), not long before the Kalahari Craton was formed during the orogenic event when Rodinia was assembled (Jacobs et al. 2008). Orogens developed in the Paleoproterozoic and reworked in the Neoproterozoic at the southern margin of the Tanzania Craton include the northwest southeast-trending Ubendian metamorphic belt, bounding the Bangweulu Block to the north (Boniface and Appel 2018) and the southwest-northeast striking Usagaran Belt to the east (Collins et al. 2004). In northern Zimbabwe, the Orosirian Magondi Belt contains arc-related volcano-sedimentary and plutonic rocks metamorphosed at amphibolite facies along the northwestern margin of the Zimbabwe Craton (Majaule et al. 2001; Master et al. 2010). The Angola Block, far to the west, represents instead the southern part of the Congo Craton. It comprises a central

zone in the east, a central Eburnean zone, and the Lubango zone extending southward into Namibia, which recorded several distinct magmatic events between 2.0 and 1.77 Ga (De Carvalho et al. 2000; McCourt et al. 2013; Jelsma et al. 2018). Orogens generated in the Mesoproterozoic include the Kibaran Belt in the north (Kokonyangi et al. 2006; Debruyne et al. 2015) and the Irumide Belt, which stretches from central Zambia in the southwest to northern Malawi in the northeast, is delimited by the largely undeformed basement of the Bangweulu Block in the north and was largely affected by the Neoproterozoic orogeny in the west (Fig. 6.2). The Irumide Belt includes a Paleoproterozoic gneissic basement overlain by siliciclastic and minor carbonate strata deposited during the late Orosirian (Muva Supergroup), as well as granitoid suites emplaced in the earliest, middle, and latest Mesoproterozoic. Granitoid suites were emplaced at 1.65–1.52, 1.36–1.33, and 1.05–0.95 and during the orogeny, metamorphic grade increased from greenschist facies in the northwest to upper amphibolite and granulite facies in the southeast (De Waele et al. 2006, 2009).

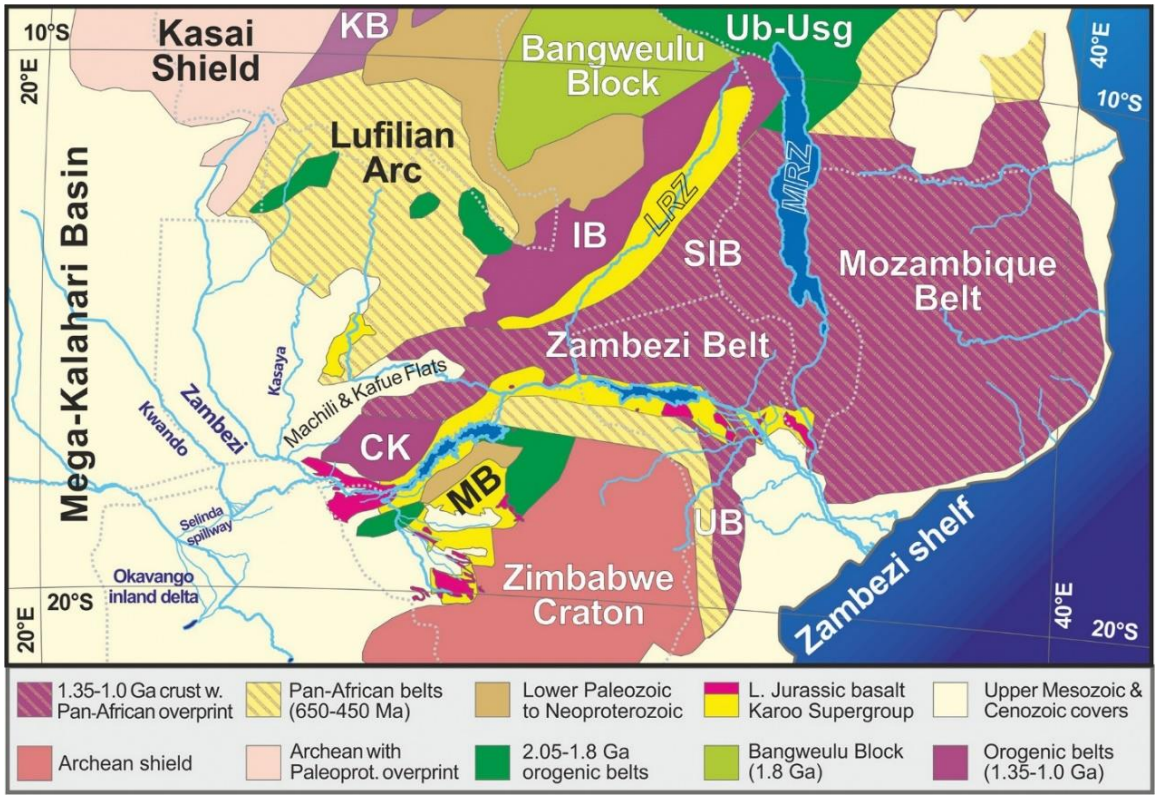

Figure 6.2. Geological domains in Zambezi catchment and adjacent regions (after Hanson 2003 and Thiéblemont et al. 2016). CK=Choma-Kalomo Block; IB=Irumide Belt; KB=Kibaran Belt; LRZ=Luangwa Rift Zone, activated in the Permian and reactivated in the Neogene; MB p Magondi Belt; MRZ p Malawi Rift Zone; SIB p South Irumide Belt, deeply affected by the Pan-African orogeny; UB=Umkondo Belt; Ub-Usg=Ubendian-Usagaran Belts; L. Jurassic=Lower Jurassic; Paleoprot. = Paleoproterozoic.

The high-grade internal zone is exposed to the north of the lower Zambezi Valley between the Luangwa and Shire Rivers (southern Irumide Province; Alessio et al. 2019) and includes the The Choma-Kalomo Block, in southwestern Zambia, consists of crystalline basement covered by amphibolite facies paragneiss and schist yielding zircon grains of Paleoproterozoic age, intruded by two generations of Mesoproterozoic granitoid plutons (1.37 and 1.18 Ga; Bulambo et al. 2006) and documenting a thermal event between 1.02 and 0.98 Ma (Glynn et al. 2017). The Kalahari Craton of southern Africa was eventually welded to the Congo Craton during the major Neoproterozoic Pan-African orogeny, testified by the Damara-Lufilian-Zambezi Belt stretching from coastal Namibia in the west and across Botswana and southern Zambia to finally connect with the Mozambique Belt in the east (Frimmel et al. 2011; Fritz et al. 2013; Goscombe et al. 2020). The Lufilian Arc, located between the Congo and Kalahari Cratons, consists of Neoproterozoic low-to-highgrade metasedimentary and metaigneous rocks hosting Cu-Co-U and Pb-Zn mineralizations (Kampunzu and Cailteux 1999; John et al. 2004; Eglinger et al. 2016). The Zambezi Belt contains a volcano-sedimentary succession deformed under amphibolite facies conditions at 0.9–0.8 Ga (Hanson 2003), whereas eclogite facies metamorphism dated at 592 Ma constrains the timing of subduction and basin closure (John et al. 2003), with thrust emplacement dated as 550–530 Ma (Hargrove et al. 2003).

6.2.2 Gondwana break-up

A major tectono-magmatic event straddling the Paleozoic/Mesozoic boundary is widely documented across southern Africa (Jourdan et al. 2005; Manninen et al. 2008), when the several kilometer-thick Upper Carboniferous to Lower Jurassic Karoo Supergroup was deposited, including glacial sediments, shale, and volcaniclastic sandstone followed by fluvial sediments (Johnson et al. 1996). Karoo basins include the elongated Gwembe and Luangwa troughs that control the drainage of the Middle Zambezi and Luangwa Rivers, respectively (Nugent 1990). Sedimentation was influenced by changing climate, from initially cold to warmer since the mid-Permian and finally hot with fluctuating precipitation in the Triassic, when braid plain sandstone and floodplain mudstone were capped by eolian sandstone (Catuneanu et al. 2005). Karoo-type basins formed in intra-land intercratonic settings by rift-related extension. In the Tuli and mid-Zambezi basins of Zimbabwe, glacial deposits are overlain by Permian sandstones and coal-bearing mud rocks, followed by ~0.5-km-thick Triassic red beds and pebbly sandstones (Bicca et al. 2017). Karoo sedimentation was terminated by flood-basalt eruptions recorded throughout southern

Africa in the Early Jurassic around 183 Ma (Svensen et al. 2012, Greber et al. 2020). Finally, rifting and breakup of Gondwana in the mid-Jurassic was followed by opening of the Indian Ocean in the Early Cretaceous, an event associated with formation of sedimentary basins (Salman and Abdula 1995; Walford et al. 2005), strike-slip deformation (Klimke et al. 2016), and extensive volcanism in the Mozambique Channel (Vallier 1974; König and Jokat 2010). In the Cenozoic, fluvial and lacustrine sediments were deposited inland in the Mega-Kalahari rim basin (in Tswana language Kgalagadi, "waterless place"), which comprises the largest sand sea on Earth, extending across the southern Africa plateau for more than 2.5 x 10^6 km^2 (Haddon and McCarthy 2005, Burrough et al. 2019). Repeated phases of eolian deposition took place during Quaternary dry stages, separated by depositional hiatuses corresponding to more humid stages (Stokes et al. 1998; Thomas and Shaw 2002). The East African rift developed throughout the Neogene (Ebinger and Scholz 2012; Roberts et al. 2012; Maselli et al. 2019), until along-axis propagation reached the Kalahari region in the Quaternary, through a network of unconnected basins extending southwest of Lake Tanganyika (Kinabo et al. 2007), where fault related subsidence in the Okavango Rift is exerting a major control on drainage patterns (McCarthy et al. 2002; Vainer et al. 2021). Since the late Pleistocene, faulting and subsidence in the incipient Okavango Rift Zone has exerted a major control on drainage reorganization.

6.3 The Zambezi River

6.3.1 Climate

Southern Africa, with its largely rural population dependent on rain-fed subsistence agriculture, is particularly vulnerable to climate variability and extreme events. These include severe droughts affecting much of Zambia, Malawi, Zimbabwe, or northern South Africa, alternating with devastating floods such as those periodically striking Mozambique. Cyclones occur in the wet season, and in 2019 two cyclones caused floods and destruction in the same year for the first time (Siwedza et al. 2021). Climate variability has a multitude of forcing factors that interact with each other and wax and wane in their importance through time (Reason et al. 2006; Howard and Washington 2019). Overall, rainfall increases from west to east at subtropical latitudes and from south to north at subequatorial latitudes, the principal sources of humidity being the Indian Ocean in the east and the Atlantic Ocean in the northwest (Fig. 4.3B).

The African continent divides the tropical high-pressure zone into the Indian Ocean and South Atlantic anticyclones, particularly during the austral summer, when heating of the

landmass reaches its maximum. Moisture derived primarily from air masses moving inland from the warm Indian Ocean is reduced by orographic effects along the eastern escarpment and declines progressively westward, resulting in increasing aridity. Descending, divergent air masses occur throughout the year along the west coast, where the temperature inversion is reinforced by the northward-flowing Benguela current and upwelling of cold Antarctic waters offshore. Dominant southwesterly winds are dry and thus contribute to the marked westward decrease in rainfall across the subcontinent. A sharp contrast thus exists between humid coastal Mozambique (maximum annual rainfall of 1.5 m) and the Kalahari Plateau inland, where quasistationary anticyclonic conditions prevail (Fig 4.3C). Mozambique is characterized by a tropical climate, with a wet season from October to March and a dry season from April to September (average annual rainfall of ~0.65 m at Tete).

In subequatorial southern Africa, atmospheric circulation is complex. Moist South Atlantic air moved inland by westerly winds converges with Indian Ocean air along the Congo Air Boundary, frequently associated with development of pressure lows and widespread rains across the Kalahari Plateau. Annual rainfall, chiefly associated with the southward shift of the Intertropical Convergence Zone, reaches 1.4 m in Angola during summer (Jury 2010). In winter, when the Intertropical Convergence Zone and the Congo Air Boundary migrate northward, interior southern Africa remains generally dry under the influence of the Indian Ocean anticyclone.

6.3.2 Zambezi River morphology

The Zambezi (from either the Bantu term *mbeze*, "fish," or the M'biza people of central–eastern Zambia), 2575 km in length and with a catchment area of ~1.4 x 10^6 k km^2, is the largest river of southern Africa, extending from 11° to 20°S and from 19°E to 36.30°E (Fig. 6.1). Annual water discharge is ~100 km^3, and suspended load amounts to 50–100 million tons (Hay 1998). Annual rainfall in the basin increases from <600 mm in the south to >1200 mm in the north. The largest contribution to runoff, therefore, comes from the headwater branches in Zambia and Angola. Mean monthly flows at Victoria Falls remain more than 1000 m^3/s from February to June, with maxima of 3000 m^3/s in April and minima of 300 m^3/s in October to November; 9000 m^3/s were reached during the 1958 flood, while the Kariba Dam was under construction (Moore et al. 2007). The natural course of the Zambezi River has been modified profoundly by the great dams that have created since 1959 Lake Kariba, marking the border between Zimbabwe and Zambia, and since 1974 Lake Cahora Bassa in northern Mozambique (the former site of the frightful impassable rapids named

kebrabassa, "end of work," by slaves who could proceed no farther upstream). Because the sediment-routing system is strictly partitioned by these two major reservoirs, it is here convenient to distinguish four reaches: (1) an Uppermost Zambezi headwater tract as far as the Kwando confluence, (2) an Upper Zambezi that includes Victoria Falls and the Batoka Gorge as far as Lake Kariba, (3) a Middle Zambezi between the two reservoirs, and (4) a Lower Zambezi downstream of Lake Cahora Bassa (Fig. 6.3).

Sourced among low ridges of the Kasai Shield in the Mwinilunga District of northernmost Zambia and undecided at first whether to head toward the Atlantic or Indian Ocean, the Uppermost Zambezi cuts across Precambrian basement in easternmost Angola. Back to Zambia, the river traverses unconsolidated Kalahari sands and widens in a ~180-km-long floodplain reaching 30 km in width during peak flood (O'Connor and Thomas 1999). Tree growth is inhibited by the persistently high-water table, and river waters slowly filter through the wetland, where clay accumulates in soils enriched in humus. The major Uppermost Zambezi tributary is the Kwando River. Sourced in humid Angola, which receives an annual precipitation up to 1400 mm concentrated between December and March, when the southward migration of the Congo Air Boundary brings heavy rains, the river chiefly drains the vegetated Mega-Kalahari dune field (Shaw and Goudie 2002). After entering the Okavango Rift (Modisi et al. 2000; Kinabo et al. 2007), the Kwando (here named Linyanti, and next Chobe) deviates sharply eastward along the Linyanti and Chobe Faults, forming a tectonic depression that favored the recent capture of the Kwando by the Zambezi and is currently favoring the capture of Okavango waters as well, conveyed eastward along the Selinda spillway (Gumbricht et al. 2001). The depression, hosting large swamps and once large paleolakes (Shaw and Thomas 1988), continues into Zambia, where it includes the low-gradient Kasaya and Ngwezi Rivers. These west-bank tributaries of the Zambezi, as the Kabombo (Kabompo) to the north, are sourced in the Lufilian Arc and the Choma-Kalomo Block. Downstream of the Kwando confluence, the Upper Zambezi and its local tributaries (e.g., Sinde from Zambia) incise into Karoo basaltic lavas, where the gradient steepens, forming local rapids. Suddenly, the river plunges some 100 m along the 1.7-km length of the Victoria Falls (in Lozi language Mosy-wa-Tunya, "the-Smoke-that-Thunders"), and the turbulent waters downstream carve an amazing zigzag into the deep Batoka Gorge of black Karoo basalt, the result of progressive retreat of the waterfalls during the Quaternary (Derricourt 1976). After receiving tributaries draining Karoo lavas overlain by a veneer of Kalahari dune sand (Masuie and Matetsi from Zimbabwe), the river reaches Lake Kariba shortly downstream of the confluence with the Gwai River. Sourced in the

Zimbabwe Craton, the low-gradient senile upper course of the Gwai River is incised, as are its east-bank tributaries Umguza and Shangan, in Karoo basalt and sedimentary rocks surrounded by Kalahari dune sand (Thomas and Shaw 1988; Moore et al. 2009a). In the youthful lower tract, the Gwai cuts steeply across the Dete-Kamativi Inlier of the Paleoproterozoic Magondi Belt (Glynn et al. 2020) and receives the eastern Tinde tributary, mainly draining Pan-African molasse (Goscombe et al. 2020).

In the lower 1400 km, the Zambezi skirts around the Zimbabwe Craton, flowing through a rift zone formed on top of the Pan-African (Kuunga) suture zone (Goscombe et al. 2020) and hosting a thick infill of basalt-capped Permian–Triassic sedimentary rocks overlying Ordovician–Devonian siliciclastic strata (Nyambe and Utting 1997). The major north-bank Zambian tributaries of the Middle Zambezi are the Kafue and the Luangwa Rivers. The Kafue drains southward into the Lufilian Arc and next turns sharply eastward, cutting across the Zambezi Belt to eventually reach the Zambezi main stem (Fig 6.3). The Kafue, the longest Zambezi tributary (length: 1576 km, basin area: 154.200 km^2), is sourced in the Lufilian arc, flows across a 240-km-long, swampy, flat floodplain, and next drops 550 m into a 60-kmlong gorge carved in gneiss and metasedimentary rocks of the West Zambezi Belt to join the Zambezi∼75 km downstream of Lake Kariba. The Luangwa (length: 770 km, basin area: 151.400 km^2), sourced in the Ubendian Belt of northernmost Zambia, flows for most of its course along a Karoo rift basin filled with an 8-km-thick Permo-Triassic sedimentary succession (Banks et al. 1995), separating the external nappes of the Irumide Belt in the north from the high-grade southern Irumide Province in the south and finally traverses the Zambezi Belt before joining the Zambezi just upstream of Lake Cahora Bassa. The Lower Zambezi in Mozambique receives tributaries from the west (Sangara, Mufa) and north (Luia, Morrunguze) that largely drain high-grade southern Irumide rocks. The largest tributary is the Shire (from chiri = steep banks), the outlet of Lake Malawi, which drains largely garnet-free mafic granulites of the Blantyre domain (southern Malawi-Unango Complex), where middle-lower crust at the southern margin of the Congo Craton underwent high-grade metamorphism at ∼920 Ma (Goscombe et al. 2020). From the west, the Mazowe and Luenha Rivers drain well into the Archean Zimbabwe Craton in the headwaters. Downstream, the two rivers cut across the polymetamorphic Mudzi migmatitic gneisses remobilized during the Pan-African orogeny and next across the Neoproterozoic Marginal Gneiss. Lowermost-course tributaries include the Sangadze and Zangue Rivers, sourced in the Pan-African Umkondo Belt, comprising greenschist facies to lower amphibolite facies schists thrust onto the margin of the Zimbabwe Craton and upper

amphibolite facies to granulite facies gneisses in the core (Stenian Barue Complex). The northern Minjova tributary largely drains the Moatize-Minjova Basin filled by coalbearing Permian–Triassic Karoo clastic rocks (Fernandes et al. 2015).

Finally, the Lower Zambezi traverses the Cretaceous and Cenozoic sedimentary covers of the Mozambique lowlands (Fig. 6.2). Here the river forms a large floodplain with multiple meandering channels, oxbow lakes, and swamps before emptying into the Indian Ocean, where it feeds a wide shelf extending beyond Beira in the south and Quelimane in the north (e.g., Praia da Madal). The flatness of the shelf, reaching 150 km in width offshore Beira, contributes to the highest tidal range around Africa (up to 6.4 m). The finest sediment fractions of the river suspended load settle far off the shelf, forming a wide mud apron on the slope between 300and 2000-m water depth. A considerable fraction of Zambezi sediment, however, is not deposited today offshore of the mouth, but transported toward the northeast, a direction opposite to the mean flow within the Mozambique Strait (Schulz et al. 2011; van der Lubbe et al. 2014). Longshore currents are confined to the inner shelf, whereas the outer shelf is largely covered by palimpsest sand with heavy-mineral lags formed by winnowing by strong oceanic, tidal, and wave-induced currents (Beiersdorf et al. 1980; Miramontes et al. 2020). The multisourced Zambezi deep-sea fan, one of the Earth's largest turbidite systems active since the Oligocene (Droz and Mougenot 1987), is mainly fed via the ~1200-km-long, curvilinear, and exceptionally wide Zambezi Valley starting at the shelf break offshore Quelimane ~200 km northeast of the Zambezi mouth (Fig. 6.1). In the more than 1000-km-long fan, up to very coarse-grained sand occurs from the upper canyon to the distal lobes (Kolla et al. 1980; Fierens et al. 2019, 2020).

6.3.3 Drainage evolution

The history of the Zambezi River reflects the multistep changes of African landscape caused by the progressive breakup of Gondwana (Partridge and Maud 1987; Key et al. 2015; Knight and Grab 2018). The Zimbabwe craton it is demonstrated to be already a topographic high during the Neoproterozoic (Doucuré and de Wit, 2003) and to have come under progressive denudation ever since (Mackintosh et al., 2017), acting as a constant source of detritus. Extensional phases in eastern southern Africa started in the Permian (Macgregor 2018). The entire Middle Zambezi and its major tributary the Luangwa River flow along Permo-Triassic rift zones (Fig. 6.2). The eastward slope, instead, originated in the Early Cretaceous by domal uplift related to incipient rifting of the South Atlantic and emplacement of the Paranà-Etendeka large igneous province in the

west (Cox 1989; Moore and Blenkinsop 2002). Superposed onto Precambian mobile belts and Permo-Triassic rifts, or intersecting them, the southward propagation of the East African Rift during the Neogene has created further tectonic depressions, including those occupied by Lake Malawi in the east and by the Okavango inland delta in the west (Ebinger and Scholz 2012).

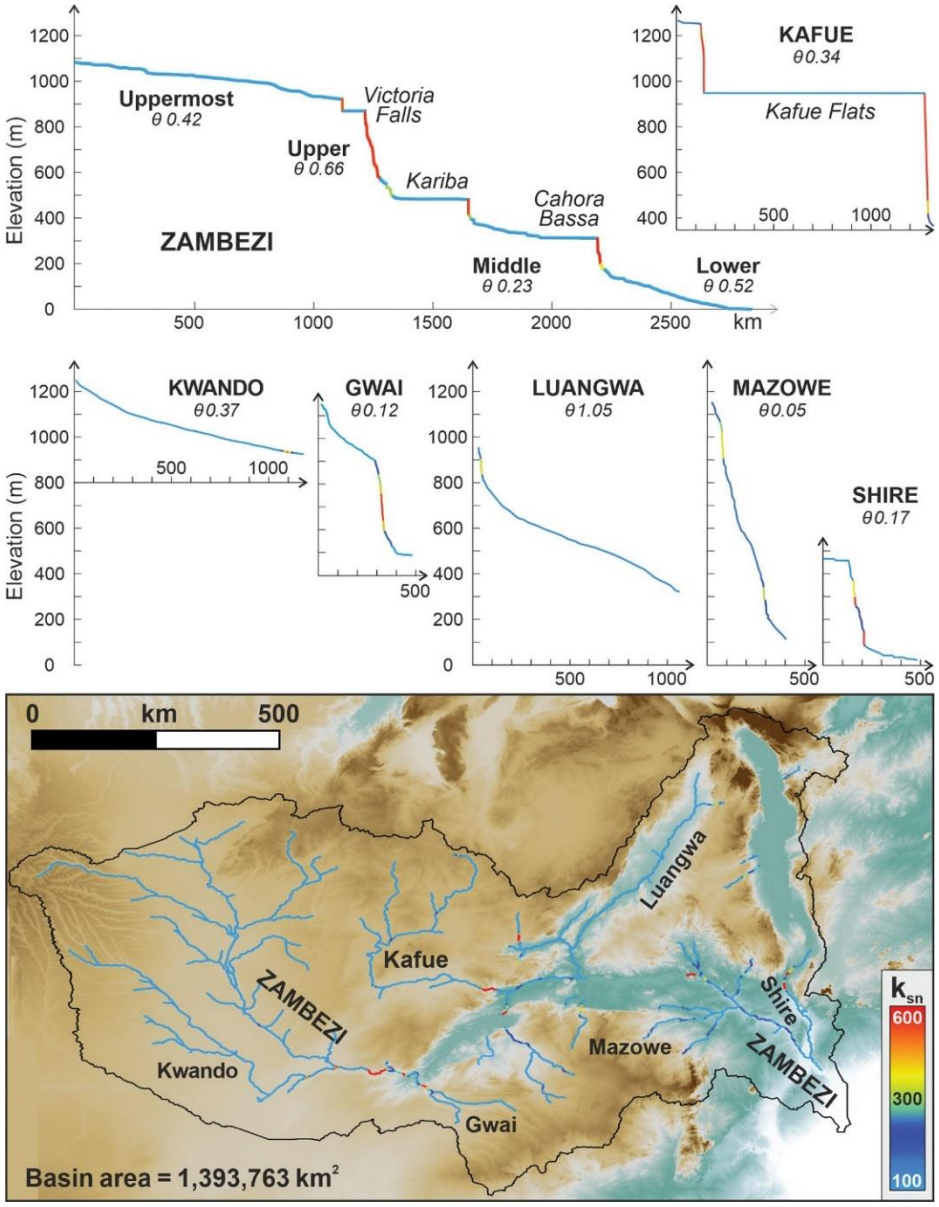

Figure 6.3. River morphometry (same vertical scale for all profiles; same horizontal scale for tributaries). Besides the concave equilibrium profile of the Kwando, longitudinal channels are highly irregular, as highlighted by extreme variations in both steepness and concavity indices k_{sn} and θ. As with most rivers in southern Africa, the Zambezi and several tributaries (e.g., Gwai, Kafue, Shire) display youthful, staircase profiles with long flat segments separated by very steep tracts, reflecting the presence of stepped planation surfaces separated by escarpments, a characteristic feature of southern African landscape (Knight and Grab 2018).

The modern Zambezi drainage is thus the result of inheritance from multiple Permo-Mesozoic extensional events on both sides of Africa combined with rifting inside Africa that is still ongoing. Successive events of river capture and drainage reversal, indicated by sharp changes in direction of its major Kwando, Kafue, and Luangwa tributaries, and the genetic similarities of fish populations between the Kafue and Upper Zambezi and between the Middle Zambezi and the Limpopo, have long suggested that the Zambezi, Okavango, and Limpopo originally formed a single transcontinental river following uplift associated with Early Cretaceous rifting of the South Atlantic (Thomas and Shaw 1988; Moore et al. 2007). In the Paleogene, uplift of the Ovamboland-Kalahari-Zimbabwe axis resulted in endorheic drainage of the Okavango and Upper Zambezi (Moore and Larkin 2001). The then-isolated Lower Zambezi initiated headward erosion, leading to the sequential capture of its middleand upper-course tributaries. Both Kafue and Luangwa Rivers once drained southwestward, the former joining the Upper Zambezi in the Machili Flats and the latter flowing across the Gwembe trough currently occupied by Lake Kariba (Thomas and Shaw 1991). Linking with the upper course in the Plio-Pleistocene was followed by the capture of the Kwando River, and by the currently occurring capture of the Okavango as well (Wellington 1955; Moore et al. 2007). In northwest Zimbabwe, drainage is largely controlled by an old pre-Karoo surface, tilted westward during domaluplift in the Early Jurassic (Moore et al. 2009b). The present east-bank tributaries of the Gwai River all drained westward toward Botswana, until they were captured by headward erosion of the Gwai River after establishment of the modern Zambezi River course (Thomas and Shaw 1988).

6.3.4 The Zambezi in the Anthropocene

The course of the Zambezi has been profoundly modified by man since the second half of the twentieth century. The Kariba and Cahora Bassa Dams built on the main stem, as well as others built on major tributaries, have substantially altered the hydrological regime of the Zambezi River and its delta and have disrupted the natural sediment-routing system, efficiently trapping detritus generated upstream (Davies et al. 2000; Beilfuss and dos Santos 2001; Calamita et al. 2019). Lake Kariba (length: 223 km, storage capacity: 185 km^3) is the world's largest artificial reservoir, whereas Lake Cahora Bassa (length: 292 km, storage capacity: 73 km^3) is Africa's fourth largest (Vörösmarty and Moore 1991). Since Zambia's independence, two big dams have been built also on the Kafue River, at Itezhi-Tezhi ("slippery rock") and in the Kafue Gorge. The Itezhi-Tezhi Dam (storage capacity: 6 km^3,

completed in 1977) closes the gap through a ridge of ~100-m-high hills where the paleo-Kafue (once flowing southward toward Lake Makgadikgadi and the Limpopo River) was captured and started to flow eastward as part of the Zambezi drainage (Thomas and Shaw 1991; Moore and Larkin 2001). Downstream, the river flows sluggishly in the maze of swampy channels and lagoons of the Kafue Flats and next plunges into the Kafue Gorge, where other dams have been constructed (Upper Kafue Gorge; storage capacity: 0.8 km^3, operational since 1973) or are under construction (Lower Kafue Gorge). Other dams were built (e.g., Nkhula, Tedzani, Kapichira), or are planned, on the Shire River in southern Malawi. Besides human intervention, the Zambezi sediment-routing system is segmented by natural processes as well, much sediment being retained in large wetlands such as the Barotse floodplain and Chobe swamps on the Uppermost Zambezi, the Kafue Flats, or the Elephant Marsh on the Shire River (Bolton 1984; Moore et al. 2007).

6.3.5 Sediment Fluxes

Regional long-term sediment fluxes and denudation rates, estimated by fission track analysis, testify to a Cretaceous and Early Cenozoic increase in sediment flux with up to 3km of basement exhumation (Gallager and Brown, 1999, Walford, 2005) with subsequent regional uplift in the Oligocene and Early Miocene (Wildman et al.,2020). Information on sediment loads transported both before and after the construction of the big dams is largely missing throughout the Zambezi drainage basin. In the lack of accurately gauged sediment fluxes, estimates on annual solid transport range widely between 20 million and 100 million tons (Hay 1998), with a median value around 50 million tons (Milliman and Meade 1983; ERM 2011; Milliman and Farnsworth 2011). These figures correspond to an average annual sediment yield and erosion rate between 15 and 70 tons/km^2 and between 0.005 and 0.03 mm, respectively (median values: ~35 tons/km^2 and ~0.01 mm). On the basis of cosmogenic nuclide data, the annual Uppermost Zambezi sediment flux was estimated as 5.5 ± 0.6 million tons (Wittmann et al. 2020), corresponding to a sediment yield and erosion rate of 16 ± 2 tons/km^2 and 0.006 ± 0.001 mm. An annual sediment volume of only 100,000 m^3, ascribed to a low topographic gradient and the presence of vast wetlands on the Kalahari Plateau, was estimated at Victoria Falls, whereas nearly half of the sediment flux (22 million out of 51 million m^3) was considered as generated in the Lower Zambezi catchment (FFEM 2005; van der Lubbe et al. 2016). After closure of the Kariba and Cahora Bassa Dams, annual sediment supply to the Zambezi Delta may have been reduced to as low as 0.8 million m^3, between 1% and 7% of which is bedload (Ronco et al. 2010; ERM 2011).

Uncertain by an order of magnitude are also the estimates of sediment accumulation in Lake Kariba (between 7 million and 70 million tons, according to Bolton 1984, but only ~4 million tons, according to Kunz et al. 2011) and Lake Cahora Bassa (between 20 million and 200 million tons, according to Bolton 1984, and 28.6 million m^3, according to Ronco et al. 2010). From sparse data on sediment concentration, annual sediment yields of 40 and 200 tons/km^2 were estimated for the Gwai and Luangwa catchments, respectively, corresponding to average erosion rates of 0.015 and 0.075 mm (Bolton 1984). Similar values were evaluated for minor tributaries in Zambia and Mozambique (200 tons/km^2) and for the Luangwa and the rest of the Middle Zambezi (170– 250 tons/km^2, from sediment volumes of 14.0 million and 14.6 million m^3, respectively; Ronco et al. 2010). Very high annual rates of soil loss (up to 2900 tons/km^2) are reported from the Shire catchment in southern Malawi (Mzuza et al. 2019).

6.4 Sampling

Between 2011 and 2019, 71 sediment samples were collected from active sand bars (57), levees (2), and freshly deposited muds (12) of the Zambezi River and its major tributaries, from the source in northwesternmost Zambia to the delta in Mozambique. To cover the entire Zambezi system from source to sink, this work also studied four fine sands from the Bons Sinais Estuary and adjacent beaches in the Quelimane area of the northern Zambezi delta, and five sandy silts collected offshore of Quelimane (core MOZ4-CS14, 181 m below sea level [b.s.l.]) and of the Zambezi delta (core MOZ4-CS17; 550 m b.s.l.) during the PAMELA-MOZ04 IFREMER-Total survey (Jouet and Deville 2015). Offshore sediments, collected by Calypso piston corer within 25 m below the sea floor, were deposited during the last glacial lowstand (MOZ4-CS17-2402-2407cm, 24.1 ka), the postglacial warming and sea-level rise (MOZ4-CS14-16021607cm, 15.9 ka; MOZ4-CS17-702-707cm, 14.6 ka), and the Holocene highstand (MOZ4-CS14-21-26cm, 4.3 ka; MOZ4-CS17-52-57cm, 4.0 ka). These sediments were dated using accelerator mass spectrometer standard radiocarbon methods on marine mollusk shells and bulk assemblages of planktonic foraminifera by applying a local marine reservoir correction of mean $\Delta R = 158 \pm 42$ y. Analyses, calibrated dates, and interpolated age models are illustrated in detail in Zindorf et al. (2021). The oceanographic PAMELA-MOZ04 cruise was part of the PAMELA (Passive Margin Exploration Laboratories) scientific project led by IFREMER and TOTAL in collaboration with the Université de Bretagne Occidentale, Université Rennes 1, Université Pierre and Marie Curie, Centre national de la recherche scientifique (CNRS), and Institut Français du

Pétrole et des Energies Nouvelles (IFPEN). Estuary and beach samples from the Quelimane area were kindly provided by C. de Carvalho Matsinhe (Tongji Univeristy, Shanghai). Between 2011 and 2019, 71 sediment samples were collected from active sand bars (57), levees (2), and freshly deposited muds (12) of the Zambezi River and its major tributaries, from the source in northwesternmost Zambia to the delta in Mozambique. The XRD data previously obtained on the <32 μm fraction of mud samples collected from the Upper Zambezi catchment and main tributaries, including the Kwando and the Gwai (Garzanti et al. 2014a; Setti et al. 2014), were also considered. For mud and sand geochemistry was considered a quartered aliquots of the <32 μm (18 river muds) and 63–2000 μm (31 river sands) fractions obtained by wet sieving. Two levee silty sands were analyzed in bulk. Geochemical data are summarized in table 2. For Nd isotopes was 80mg of powdered samples was taken from seven <32 μm fractions, nine 32–63 μm classes, 14 63–2000 μm fractions and two bulk samples. Isotope data, including results previously obtained on muds from the upper part of the Zambezi catchment (Garzanti et al. 2014a), are summarized in table 3. Petrographic, geochemical, isotope and geochronological data, including full information of samples location is provided in the Appendix.

6.5 Data

In the partitioned Zambezi sediment-routing system, sand compositional signatures are radically different upstream and downstream of both Lake Kariba and Lake Cahora Bassa (Table 6.1), indicating that no sand can pass across each reservoir. In the Uppermost Zambezi main stem, as in some of its major tributaries including the Kwando and the Kafue, another factor hampering the continuity of downstream sediment transport is the occurrence of densely vegetated flat lowland occupied by numerous pans commonly aligned with shallow grassy valleys (*dambos*) acting as natural sediment traps (Moore et al. 2007).

6.5.1 The Uppermost Zambezi

Near the source, close to the political boundaries of Zambia, Congo, and Angola, sand is pure quartzose with K-feldspar >> plagioclase and a very poor tHM suite dominated by zircon with tourmaline, minor rutile, and staurolite (Fig. 6.4A). Kyanite increases downstream and clinopyroxene is significant upstream of the Kwando confluence. The Kwando River from Angola contributes pure quartzose sand with a very poor tHM suite including zircon, tourmaline, kyanite, and staurolite (Fig 6.5A). Sand of west-bank tributaries from Zambia ranges from quartz-rich feldspatho-quartzose with K-feldspar > plagioclase (Kabombo, Ngwezi) to pure quartzose with K-feldspar >> plagioclase

	n°	Q	F	Lvm	Lsm	Lmfb	QFL_{tot}	P/F	Mica	tHMC	ZTR	Ap	Ttn	Ep	Grt	St	Ky	Sil	Amp	Cpx	Hyp	&tHM	HM_{tot}	ACI
Kwado	3	99	1	0	0	0	100	-	0	0.1	61	0.3	0.3	3	0	16	16	0	2	0	0	1	100	39
Uppermost tributaries	3	90	9	0.2	0.5	0	100	36	2	0.4	31	1	1	38	2	5	6	1	7	5	2	2	100	0-5
Uppermost Zambezi	6	96	3	0	0	0	100	32	0.1	0.4	60	0	0.4	5	0.3	7	18	0	2	4	0	2	100	0
Uppermost pre Victoria Falls	1	91	1	7	1	0	100	-	0	0.3	5	0.4	0	0.4	0	1	0	0	0.4	92	0	0	100	-
Upper pre Victoria Falls	4	96	2	1	0	0.2	100	47	0	0.4	34	0	0	8	0.2	3	23	0.5	3	27	0	1	100	0-39
Uppermost Zambezi pre Kwado	2	46	2	52	0	0	100	-	0	10.5	0	0	0	3	0	0	0	0	0	97	0	0	100	-
Upper Zambezi pre Kwado	4	93	3	4	0	0	100	60	0	1.3	3	0.3	0	2	0.2	2	6	0	1	84	0	1	100	-
Gwai	3	74	22	3	1	1	100	61	4	1.6	3	1	0	18	7	0.3	1	1	35	30	0.2	1	100	11-37
Gwai Tributaries	5	83	11	5	0.5	0	100	60	0	3.5	12	1	2	27	2	1	0.2	0	12	43	0	0.4	100	8-34
Kafue	2	67	29	0.4	0.5	3	100	41	6	6.7	8	2	3	10	2	1	4	1	67	1	0	1	100	9-16
Middle Zambezi	2	63	32	1	2	2	100	36	4	4.8	12	1	4	14	2	0	6	0.2	51	6	1	2	100	9-16
Luangwa	1	74	25	0	0	1	100	39	0.3	2.9	11	1	4	18	6	4	11	7	35	1	0	2	100	46
Sangara	2	49	48	0.3	3	0.5	100	44	0.1	3.2	4	2	0.2	4	3	0	1	0	20	41	21	4	100	13-24
Morrunguze	1	46	50	0	1	4	100	51	1	14.7	2	1	3	12	4	0	0	0	30	36	12	0	100	41
Minjova	1	70	26	1	3	0	100	55	0	0.4	6	1	1	7	25	0	0	0.5	26	24	9	0.5	100	91
Mufa	2	47	50	1	1	0.2	100	44	1	12.1	2	2	3	2	2	0	0.5	0	71	9	8	1	100	45-50
Mazowe-Luhena	2	45	26	1	0	1	100	38	1	9	3	1	4	12	3	0	2	1	73	1	0.5	0	100	31-38
Lower Zambezi	2	48	50	1	0.4	0.2	100	58	5	16.4	5	1	1	9	25	0	0.2	0.5	43	7	5	2	100	14-63
Shire	1	33	67	0	0	0.4	100	72	3	14.1	4	4	0.4	6	4	0	1	0	76	2	2	0	100	41
Sangadze	2	64	35	0	1	0.2	100	28	0	1.2	2	2	1	5	58	7	4	3	18	1	0.2	0.5	100	27-80
Lower Zambezi (final)	2	49	49	1	0	1	100	45	3	6.9	3	1	4	21	3	2	1	0.2	58	3	3	0	100	26-38
Zambezi upper slope	3	63	35	0.2	1	1	100	52	11	3.1	4	2	4	23	3	0.2	1	3	46	11	2	1	100	4-7
Quelimane coast	4	69	28	1	2	0.4	100	53	2	4.5	5	2	4	17	4	0.5	1	2	53	8	3	0.2	100	2-11
Quelimane outer shelf	2	58	40	1	1	0.5	100	46	29	2.2	5	3	2	24	0.2	0	0.2	4	47	14	1	1	100	4-8

Table 6.1. Key Petrographic and Heavy-Mineral Signatures. Q = quartz; F = feldspars (P = plagioclase); L = lithic grains (Lvm = volcanic to low-rank metavolcanic; Lsm = sedimentary to low-rank metasedimentary; Lmfb = high-rank felsic metamorphic and metabasite); tHMC = transparent

heavy-mineral concentration; ZTR = zircon + tourmaline + rutile; Ap = apatite; Ttn = titanite; Ep = epidote; Grt = garnet; St = staurolite; K = Lake Kariba; Ky = kyanite; Sil = sillimanite; Amp = amphibole; Cpx = clinopyroxene; Hyp = hypersthene; &tHM = other transparent heavy minerals (mainly anatase and andalusite with monazite, olivine, or enstatite locally); ACI = amphibole color index; n.d. = not determined; Ust. Z. = Uppermost Zambezi; U.Z. = Upper Zambezi; VF = Victoria Falls. Boldface indicates Zambezi main stream.

(Kasaya). Muscovite occurs. The tHM suites vary from poor with tourmaline, rutile, epidote, and kyanite (Kabombo) to very poor and including epidote, zircon, tourmaline, staurolite, and green augite (Kasaya), or epidote dominated with amphibole and minor garnet (Ngwezi). Smectite prevails over kaolinite and mica/illite in mud of the Zambezi main stem and is dominant in Ngwezi and Kwando muds (Fig 6.6). In Zambezi and Kwando sands, SiO_2 is overwhelming (98%; Fig 6.8A) and other elements very low, including Zr (62–114 ppm) and REEs (Fig 6.5). The CIA* is ≥77, the WIP is <1, $\alpha^{Al}Ca \geq 3$, and $\alpha^{Al}Na \sim 4$. Ngwezi sand is less SiO_2 rich, with higher Al, Ca, Na, K, Rb, Sr, and Ba but very low Mg (Fig 6.4B). Kasaya sand has an intermediate composition. Chemical indices are CIA* = 83, $\alpha^{Al}Ca = 4$, $\alpha^{Al}Na = 21$ for Zambezi mud and CIA* = 77 ± 1, $\alpha^{Al}Ca = 2.9 \pm 0.5$, and $\alpha^{Al}Na = 11 \pm 4$ for Kasaya and Ngwezi muds. Kwando mud has anomalously low $\alpha^{Al}Ca$, $\alpha^{Al}Mg$, $\alpha^{Al}Sr$, and $\alpha^{Al}Ba$ (Table 6.2). The general observed order of element mobility is $Na \gg Sr > Ca > Mg \approx K$ for mud and $Na \approx Ca > Sr$ for sand. In mud samples, REE patterns normalized to CI carbonaceous chondrites (Barrat et al. 2012) display classical shapes with higher light-REE (LREE) than heavy-REE (HREE) fractionation and moderately negative Eu anomaly. Pure quartzose sands display slightly stronger LREE enrichment, negative Ce anomalies, more strongly negative Eu anomalies, and low HREE fractionation. The ε_{Nd} values vary between -14 and -17 (-15.5 for Uppermost Zambezi mud; Table 6.4). Ages of zircon grains in Uppermost Zambezi, Kwando, and Kasaya sands display polymodal spectra, with mostly Cambrian to Stenian ages, including a main Irumide and subordinate Pan-African populations (Fig 6.10). Orosirian ages are common in Uppermost Zambezi and Kwando sands and minor in Kasaya sand. Kwando sand is distinguished by a Neoarchean age cluster, whereas Kasaya sand yielded several zircon grains with Devonian to Triassic ages.

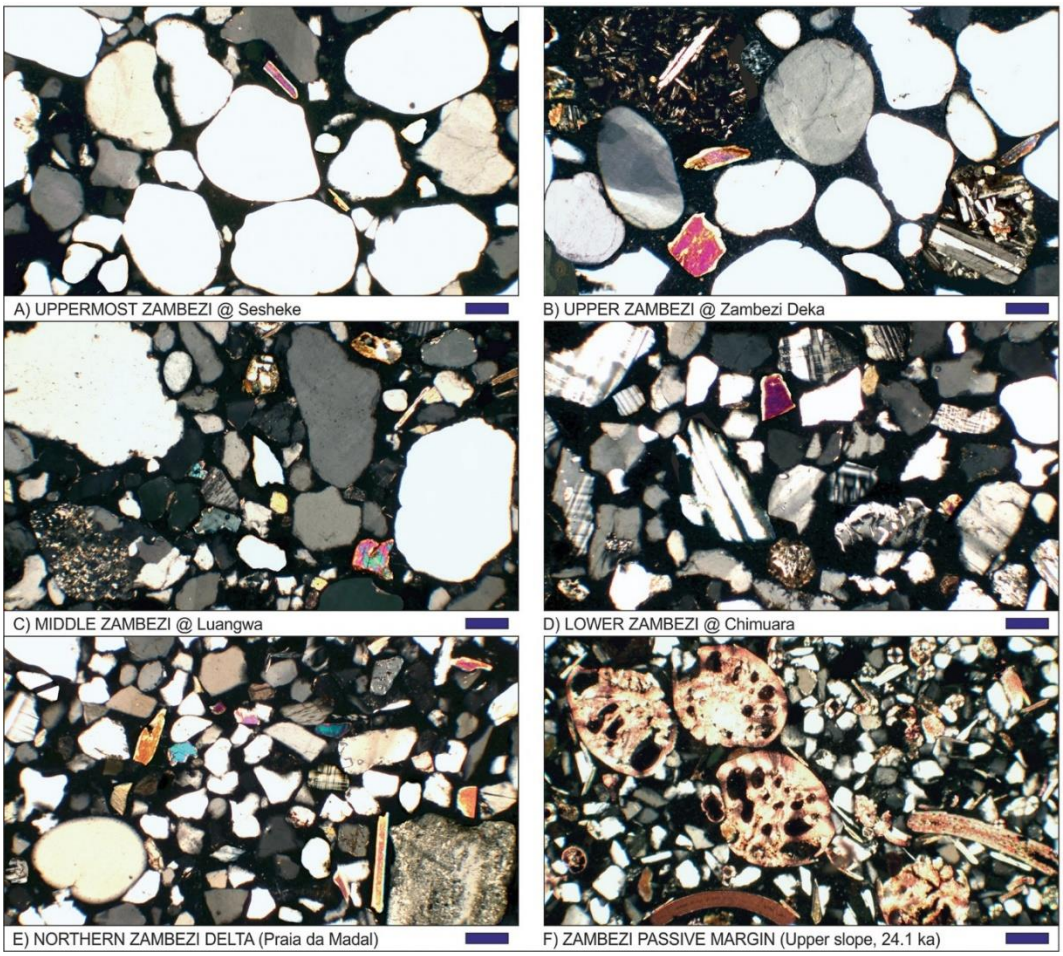

Figure 6.4. Petrographic changes along Zambezi sediment-routing system from source to sink. A, Pure quartzose sand recycled from the Mega-Kalahari Desert. B, Marked enrichment in lathwork to microlitic volcanic rock fragments and clinopyroxene in quartzose sand downstream of Victoria Falls. C, Reconstituted feldspatho-quartzose metamorphiclastic bedload downstream of Lake Kariba. D, Sharp increase in feldspars in reconstituted bedload downstream of Lake Cahora Bassa. E, Feldspatho-quartzose beach sand in the Quelimane area. F, Very fine-grained feldspar-rich feldspatho-quartzose sand containing benthic foraminifera (stained by alizarine red) and deposited during the last glacial lowstand on the upper slope offshore of the Zambezi mouth. All photos with crossed polars; blue bar for scale = 100 μm.

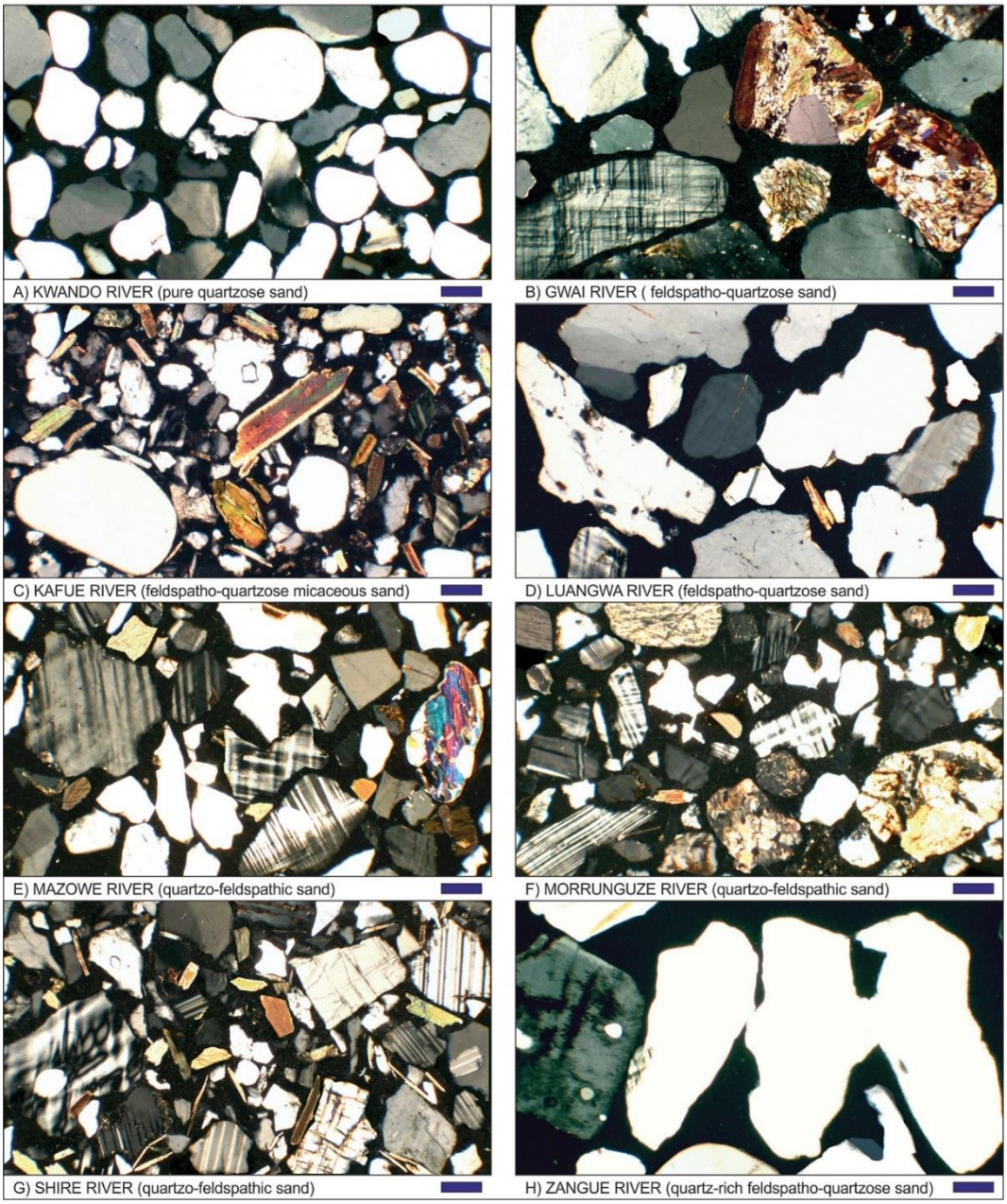

Figure 6.5. Sand composition in major Zambezi tributaries. A, Up to well-rounded monocrystalline quartz grains recycled from Mega-Kalahari dunes. B, High-rank metamorphic rock fragments and microcline derived first-cycle from the Magondi Belt. C, Biotite-rich metamorphic detritus from the Lufilian Arc and Zambezi Belt mixed with rounded recycled quartz. D, Deeply corroded quartz and feldspar grains derived from the Irumide Belt and recycled from Karoo strata. E, Abundant microcline with high-rank metamorphic rock fragments from the Archean Zimbabwe Craton and Proterozoic gneisses. F, Microcline, gabbroic rock fragments, pyroxene, and amphibole from the southern Irumide Belt and Tete gabbro-anorthosite complex. G, Dominant feldspar derived from orthogneisses and granulites of the Blantyre domain. H, Skeletal quartz and weathered K-feldspar grains in Mozambican lowlands. All photos with crossed polars; blue bar for scale = 100 μm.

6.5.2 The Upper Zambezi

Basaltic detritus from Karoo lavas mixes with quartz as the river approaches Victoria Falls, and in steadily increasing proportions across the gorges downstream of the falls. Upstream of Lake Kariba, bedload sand and levee silty sand include mafic volcanic rock fragments with lathwork and microlitic textures (Fig 6.4B) and are, respectively, quartzose with plagioclase ≈ K-feldspar and litho-feldspatho-quartzose with plagioclase > K-feldspar. The moderately rich tHM suite consists almost entirely of green augite with a few olivine grains. Upstream of Victoria Falls, the Sinde tributary from Zambia carries quartzose sand with mafic volcanic grains and a poor tHM suite dominated by brown and green augite. Basaltic detritus increases in tributary sand downstream of the falls. Masuie and Matetsi sands are, respectively, lithic-rich lithoquartzose and quartzo-lithic basalticlastic, with rich and very rich tHM suites consisting almost exclusively of augite and augite-bearing rock fragments. River bars and levees of the Gwai River from Zimbabwe consist of feldspatho-quartzose sand with plagioclase > K-feldspar (Fig 6.5B). Mostly biotitic mica is concentrated in levee silty sand. The moderately rich tHM suite consists of amphibole with subordinate epidote, garnet, and clinopyroxene. The Deka River carries quartz-rich litho-quartzose basalticlastic sand with a very rich tHM suite dominated by clinopyroxene with some epidote.

Smectite predominates over mica/illite and kaolinite in Zambezi mud and is overwhelming in muds of the Sinde and Matetsi tributaries, which contain kaolinite (Fig 6.6). Silica decreases progressively along the Upper Zambezi, with corresponding increases in most other elements, including Fe, Mg, Ca, Na, Sr (Fig 6.8G, H), and REEs (Fig 6.9C) but not Zr, Hf, and Nb. Chemical indices upstream of Lake Kariba are CIA* = 59 ± 6, $\alpha^{Al}Ca$ = 0.9 ± 0.3, and $\alpha^{Al}Na$ = 3.9 ± 0.9 for mud; CIA* = 45, $\alpha^{Al}Ca$ = 0.5, and $\alpha^{Al}Na$ = 1.5 for silty sand; and CIA* = 49, $\alpha^{Al}Ca$ = 0.9, and $\alpha^{Al}Na$ = 1.2 for sand (Table 6.2). Tributaries draining progressively larger portions of Karoo basalts display an even sharper trend from west to east. Masuie and Matetsi sands have much lower SiO_2 than Sinde sand and higher concentrations of all other elements (Fig 6.4A). In these rivers, both mud and sand are markedly enriched in Mg, Ca, Sc, Ti, V, Cr, Fe, Mn, Co, Ni, and Cu (Fig 6.9B) and display regular chondritenormalized REE patterns lacking an Eu anomaly (Fig 6.9A,D, and G). The ε_{Nd} value is around -12 in Zambezi mud between Victoria Falls and Lake Kariba and is much less negative for Matetsi (-4) and Sinde (-5) muds (Table 6.4). Sinde sand yielded a zircon age spectrum with a dominant Irumide peak, common Neoproterozoic ages, and minor Permian–Triassic, Eburnean, and Neoarchean ages. Upper Zambezi sand upstream of Lake Kariba yielded a polymodal spectrum with main Pan-African and Irumide peaks

and minor Orosirian and Neoarchean clusters (Fig 6.10). Lower Gwai sand is feldspathoquartzose, with biotite and amphibole. Smectite predominates in upper Gwai and Umguza muds, whereas mica/illite prevails over kaolinite and smectite in mud of the lower-course Tinde tributary (Fig 6.6). Chemical indices are CIA* = 73, $\alpha^{Al}Ca$ = 1.9, and $\alpha^{Al}Na$ = 10 for upper Gwai mud and CIA* = 54, $\alpha^{Al}Ca$ = 2.9, and $\alpha^{Al}Na$ = 1.4 for lower Gwai sand. Umguza mud is similar to upper Gwai mud, whereas Umguza sand is much richer in Fe, Mg, Ca, Ti, Mn, Sr, V, Co, Ni, and Cu than lower Gwai sand (Fig 6.8C, D). Tinde mud is richer in Si, Na, K, Rb, Ba, Y, REEs, Th, U, Zr, Hf, Nb, and Ta and poorer in Fe, Mg, Ca, P, Mn, Sc, V, Cr, Co, Ni, and Cu (table 2). The ε_{Nd} value ranges between -12 and -15 in upper Gwai, Umguza, and Tinde muds, but it is strongly negative in Gwai sand upstream of lake Kariba (-25), which yielded a polymodal zircon age spectrum with major Neoarchean and Eburnean peaks and minor Irumide and Pan-African peaks (Fig 6.10).

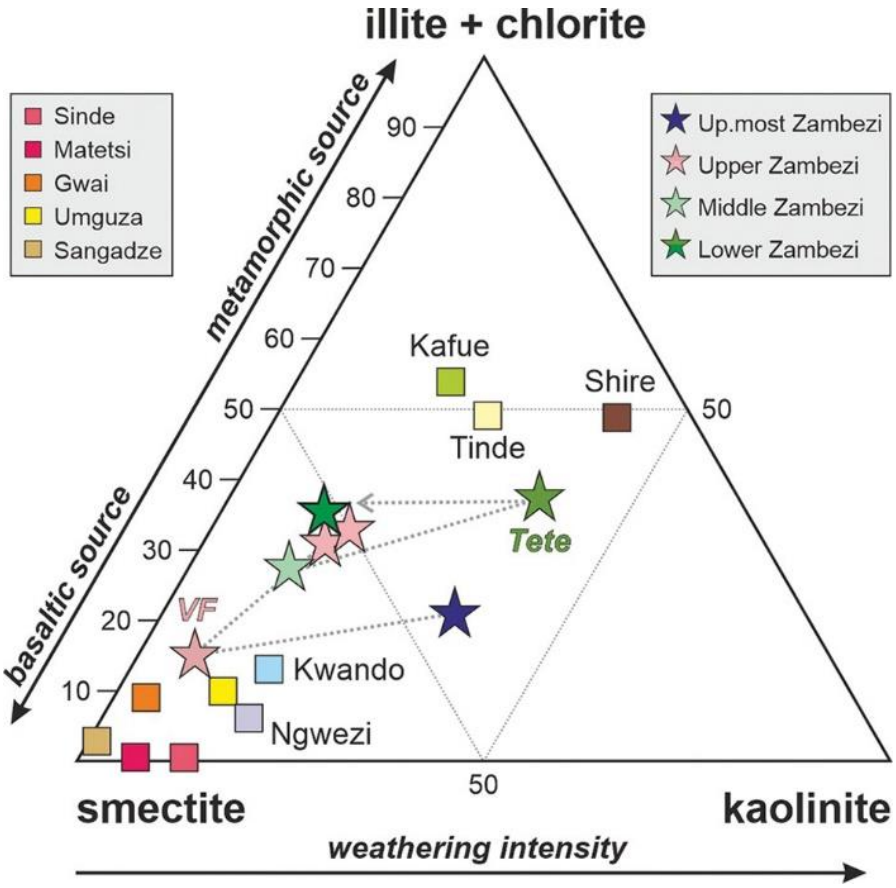

Figure 6.6 Clay mineralogy. Multiple controls explain erratic trends (dotted arrow) downstream the Zambezi River (stars). Recycled kaolinite occurs in both Uppermost (Up.most) Zambezi and Lower Zambezi catchments (e.g., Shire mud). Smectite is derived from Karoo basalt around Victoria Falls (VF) but is also produced on the Kalahari Plateau and Mozambican lowlands (e.g., Sangadze mud). Illite is derived from metasedimentary and siliciclastic rocks of the Irumide and Pan-African belts (e.g., Kafue and Tinde muds).

6.5.3 The Middle Zambezi

Downstream of Lake Kariba, Zambezi sand has the same feldspar-rich feldspatho-quartzose composition as Kafue River sand, with K-feldspar >> plagioclase, some metamorphic rock fragments, and micas (biotite ≥ muscovite; figs. 4C and 5C). The rich tHM suite includes amphibole (blue-green to green-brown hornblende and actinolite) and subordinate epidote, kyanite, and clinopyroxene. Amphibole decreases and zircon increases slightly downstream on the mainstream. The Luangwa River carries feldspatho-quartzose sand with K-feldspar >> plagioclase and granitoid to gneissic rock fragments, with a moderately rich tHM suite including mainly amphibole (greenbrown to blue-green hornblende), kyanite, zircon, and prismatic or fibrolitic sillimanite (Fig 6.5D).

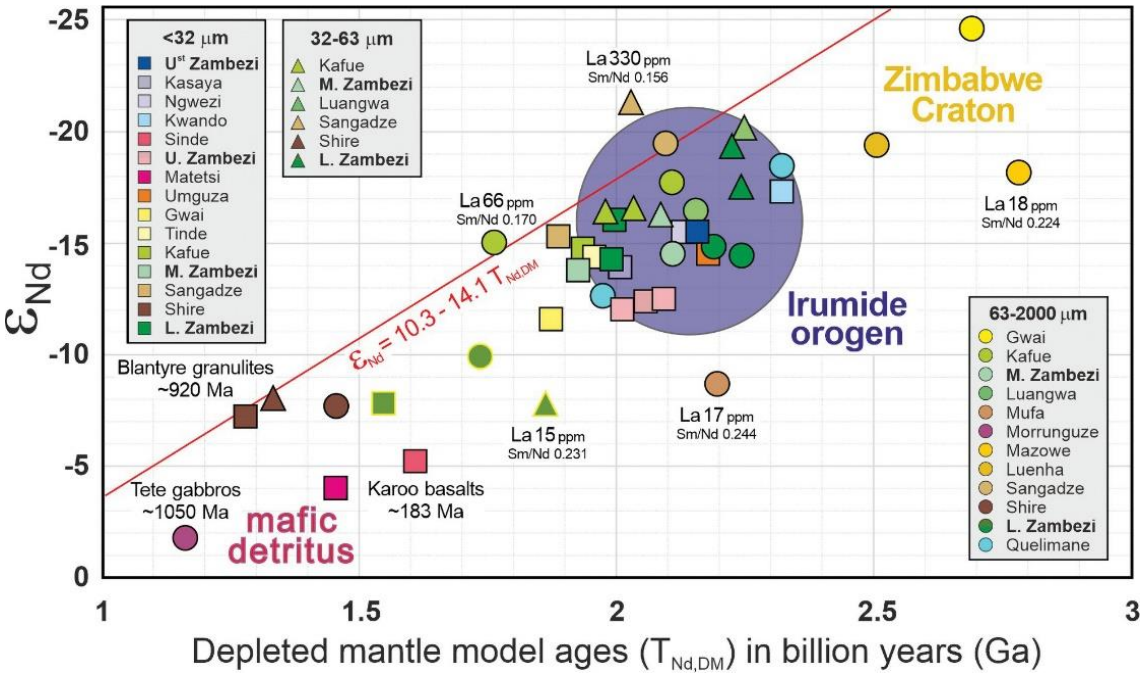

Figure 6.7 Relationship between εNd(0) and depleted-mantle model ages (TNd,DM) for the Zambezi main stem and tributaries. The εNd and TNd,DM values are least negative and youngest for detritus from Karoo basalt, Tete gabbro, and Blantyre mafic granulite (emplacement ages after Svensen et al. 2012, Westerhof et al. 2008, and Goscombe et al. 2020, respectively) and most negative and oldest for detritus from Neoarchean cratonic gneiss. Most samples have higher Sm/Nd ratios than the upper continental crust and thus plot to the right of the red line (based on (Sm/Nd)UCC=0.1735(Sm/Nd)UCC=0.1735). The 32–63-μm size class of sand samples, representing the fine tail of the size distribution, where ultradense monazite is concentrated, has high LREEs (light rare earth elements) and a steeper LREE pattern (lower Sm/Nd) than the 63–2000-μm fraction. Instead, the 32–63-μm size class of the Lower Zambezi silt collected at Tete (yellow outline) has low LREEs and a high Sm/Nd because it represents the coarse tail of the size distribution depleted in ultradense minerals. Ust = uppermost; U. = upper; M. = middle; L. = lower.

Smectite predominates over mica/illite and kaolinite in mud of the Zambezi main stem, whereas mica/illite predominates over smectite and kaolinite in Kafue mud (Fig 6.6) Chemical indices are CIA* = 67 ± 3, $\alpha^{Al}Ca$ = 2.1 ± 0.6, and $a^{Al}Na$ = 5.2 ± 0.2 for mud and CIA* = 51 ± 3, $\alpha^{Al}Ca$ = 2.1 ± 1.3, and $\alpha^{Al}Na$ = 1.6 ± 0.2 for sand (Table 6.2). The observed order of element mobility is Na > Sr > Ca > K > Ba for mud and Ca > Na > Sr for sand. Luangwa sand is higher in SiO_2, K, and Ba and lower in most other elements (especially Mg, Ti, and Sc; Fig 6.8C). The finer-grained of the two Kafue sand samples is notably enriched in Zr, Hf, REEs, Th, U, Nb, and Ta (Table 6.2). Kafue and Middle Zambezi muds have virtually identical chemical compositions (Fig 6.8D, H). All ε_{Nd} values range between -14 and -18, reaching -20 only in the 32–63-μm size class of Luangwa sand (Fig 6.7).

The zircon age spectrum of Kafue sand displays a dominant Irumide peak with a minor Pan-African cluster and a few Triassic and Paleoproterozoic to Neoarchean ages. Luangwa sand is characterized by a trimodal spectrum with major Irumide, subordinate Pan-African, and minor Eburnean peaks and a few Permian ages (Fig 6.10).

6.5.4 The Lower Zambezi

In Mozambique, Zambezi sand ranges from quartzo-feldspathic to feldsparrich feldspatho-quartzose with K-feldspar ≥ plagioclase (Fig 6.4D). Mica (mostly biotite) is common in very fine sand. The rich tHM suite includes mostly amphibole (blue-green to green-brown hornblende and actinolite), subordinate epidote, locally strongly enriched garnet, and minor titanite, zircon, clinopyroxene, and hypersthene. Most tributaries contribute quartzo-feldspathic sand with K-feldspar ≥ plagioclase and a rich tHM suite (figs. 5E–5G). An exception is represented by the Minjova and Zangue tributaries, which carry feldspatho-quartzose and quartz-rich feldspathoquartzose sand with a poor tHM suite (Fig 6.5H). Feldspars (mostly plagioclase) are twice as abundant as quartz in Shire sand from Malawi. Metabasite grains are significant in Morrunguze sand (Fig 6.5F). Chacangara sand includes gabbroic, quartzose sandstone/metasandstone, and shale/slate rock fragments. The tHM suites are diverse. Amphibole (mainly green-brown and blue-green hornblende) is dominant in Mufa, Mazowe, Luenha, and Shire sand (ACI 31–50), and common in most other tributaries (ACI 13–27 in Sangara, Chacangara, and Zangue sand but up to 80–91 in Sangadze and Minjova sand). Clinopyroxene and hypersthene are most abundant in Chacangara sand and also characterize Sangara, Morrunguze, Minjova, and, to a lesser extent, Mufa sand (Table 6.1). Epidote is invariably present in moderate amounts. Garnet is dominant in Sangadze sand and common in Zangue and Minjova sand. Staurolite is

	Major elements %wt										
	SiO_2	Al_2O_3	Fe_2O_3	MgO	CaO	Na_2O	K_2O	TiO_2	P_2O_5	MnO	LOI
	Sand (63-2000 μm)										
Uppermost Zambesi	98.5	0.4	0.2	0.0	0.0	0.0	0.1	0.1	0.02	<0.01	0.8
Kasaya	99.2	0.9	0.1	0.0	0.1	0.1	0.4	0.1	<0.01	<0.01	0.9
Ngwezi	93.4	3.2	0.4	0.0	0.5	0.4	1.7	0.0	<0.01	0.03	0.5
Kwando	99.3	0.2	<0.04	<0.01	<0.01	<0.01	<0.01	0.0	0.01	<0.01	0.5
Chobe	98.0	0.3	0.9	0.0	0.0	<0.02	0.0	0.1	<0.00	<0.01	0.7
Upper Zambezi	98.9	0.3	0.1	0.0	0.0	0.0	0.1	0.1	<0.00	<0.01	0.9
Sinde	94.8	1.3	1.6	0.3	0.5	0.2	0.2	0.4	0.02	0.02	0.9
Zambezi above Victoria Falls	98.0	0.6	0.4	0.1	0.1	0.1	0.1	0.2	0.03	<0.01	0.6
Zambezi rapid #19	99.2	0.8	0.3	0.1	0.1	0.1	0.2	0.2	<0.01	<0.01	0.8
Zambezi rapid #10	99.4	0.3	0.3	0.1	0.1	0.1	0.1	0.1	<0.01	<0.01	1.0
Masuie	61.8	8.3	12.9	3.1	4.9	1.5	0.9	2.8	0.19	0.15	2.4
Upper Zambezi	99.7	0.4	0.4	0.1	0.2	0.1	0.1	0.1	<0.01	<0.01	0.8
Matetsi	63.1	8.4	11.7	3.1	5.0	1.7	0.8	2.8	0.23	0.14	2.9
Zambezi above Kariba	89.7	3.9	2.0	0.6	1.1	0.8	0.9	0.5	0.05	0.02	0.5
Umguza	85.4	5.4	2.0	0.4	3.2	1.1	1.6	0.2	0.03	0.07	3.2
Lower Gwai	88.3	7.1	0.9	0.2	0.6	1.3	2.6	0.1	0.0	0.0	0.9
Kafue (FS)	81.1	6.5	4.4	1.0	1.5	1.2	1.6	1.3	0.13	0.05	1.0
Kafue (VFS)	83.0	6.2	3.5	1.0	1.2	1.0	1.7	0.9	0.10	0.04	1.1
Middle Zambezi	80.6	8.0	3.3	1.1	1.3	1.5	2.3	0.8	0.11	0.04	0.9
Luangwa	89.9	4.7	1.2	0.1	0.3	0.6	2.4	0.2	0.05	0.02	0.3
Mufa	71.3	11.8	3.9	1.8	3.7	2.4	2.9	0.8	0.18	0.06	0.9
Lower Zambezi and Tete	68.2	14.0	2.1	0.9	3.2	3.2	2.8	0.5	0.16	0.04	4.8
Morrunguze	52.4	12.5	15.1	3.9	5.5	2.4	1.5	5.5	0.08	0.17	0.7
Mazowe	78.7	10.2	2.2	0.6	1.7	2.2	3.3	0.4	0.1	0.0	0.5
Luenha	74.5	10.7	5.1	0.8	2.2	2.4	2.8	1.4	0.08	0.08	-0.3
Sangadze	82.1	8.5	1.5	0.2	0.9	1.3	4.2	0.5	0.07	0.04	0.6
Shire	68.3	14.7	3.8	1.3	3.9	3.7	2.1	0.8	0.20	0.06	0.9
Lower Zambezi (VFS)	80.2	9.3	2.1	0.6	1.8	2.0	2.6	0.5	0.10	0.03	0.7
Lower Zambezi (FS)	78.1	10.4	2.3	0.7	2.1	2.3	2.6	0.6	0.11	0.04	0.7
	Mud (<32 μm):										
Uppermost Zambesi	55.4	15.0	7.0	0.7	1.1	0.2	1.0	0.9	0.1	0.1	18.1
Kasaya	53.5	16.1	5.8	0.8	1.8	0.3	1.7	1.0	0.4	0.0	n.d.
Ngwezi	51.1	18.6	8.5	1.5	1.6	0.6	2.1	1.1	0.1	0.1	14.5
Kwando	43.3	5.9	3.1	3.3	10.6	0.1	0.5	0.4	0.1	0.2	30.0
Sinde	45.5	14.6	14.2	2.0	3.0	1.0	0.9	3.5	0.2	0.2	14.7
Zambezi above Victoria Falls	54.0	10.6	7.3	1.4	2.7	0.6	0.8	1.8	0.1	0.1	20.1
Matetsi	44.4	14.2	12.2	3.7	6.2	1.7	0.9	2.0	0.4	0.2	13.9
Zambezi above Kariba	51.0	11.6	10.2	2.4	3.4	0.8	0.9	2.0	0.2	0.2	17.1
Umguza	51.0	15.0	8.8	2.0	3.0	0.6	1.2	1.4	0.2	0.1	16.4
Upper Gwai	48.6	16.3	8.9	1.7	2.3	0.4	1.5	1.2	0.2	0.2	18.3
Tinde	67.5	13.3	4.0	0.8	0.7	0.7	2.5	0.9	0.1	0.1	9.2
Kafue(VFS)	46.8	16.5	9.5	3.2	2.7	0.8	2.9	1.3	0.2	0.1	15.3
Middle Zambezi	49.5	16.4	9.5	3.2	1.8	0.8	2.9	1.3	0.2	0.1	13.6
Lower Zambezi and Tete	46.4	17.7	10.4	2.0	2.2	1.0	2.1	1.2	0.3	0.2	16.2
Sangadze	47.1	16.8	6.9	3.0	3.1	0.4	1.9	0.8	0.2	0.1	19.2
Shire	42.2	19.3	12.1	2.6	2.2	0.9	1.9	1.3	0.4	0.2	16.5
Lower Zambezi (VFS)	48.3	16.3	11.6	2.9	2.4	1.0	2.4	1.5	0.2	0.2	12.5

Table 6.2. Sand and Mud Geochemistry in the Zambezi Catchment. FS = fine sand; VFS = very fine sand; LOI = loss on ignition; ND = not determined. CIA∗CIA* (chemical index of alteration) values are corrected only for CaO in apatite. The α values are defined as $(Al/E)_{sample}/(Al/E)_{UCC}$, where UCC = upper continental crust.

	Rb	Sr	Ba	Sc	Y	Th	Zr	Hf	V	Nb	Ni
					Sand (63-2000 μm)						
Uppermost Zambesi	2	3	29	<1	2	1	81	2	14	1	1
Kasaya	11	18	124	<1	4	2	128	3	<8	2	1
Ngwezi	47	50	419	<1	5	1	38	1	11	2	3
Kwando	1	2	21	<1	1	0	62	2	<8	2	0
Chobe	2	4	29	<1	2	1	114	3	15	2	1
Upper Zambezi	2	4	31	<1	2	0.7	232	6	<8	2	1
Sinde	3	51	58	2	4	1	68	2	57	2	8
Zambezi above Victoria Falls	3	11	52	<1	2	0.7	73	2	21	3	1
Zambezi rapid #19	5	18	81	<1	2	0.7	62	2	14	3	1
Zambezi rapid #10	2	7	157	<1	1	1	31	1	11	2	2
Masuie	18	268	295	22	23	2	168	4	414	10	45
Upper Zambezi	1	13	25	<1	2	0.4	37	1	16	1	2
Matetsi	16	365	296	20	22	2	182	5	356	13	40
Zambezi above Kariba	24	85	235	4	7	3	65	2	57	2	6
Umguza	52	186	476	3	12	2	57	2	51	3	16
Lower Gwai	69.3	87.5	483.5	2.0	10.7	3.8	72.5	2.1	15.0	2.2	4.5
Kafue (FS)	52	92	316	8	28	16	596	16	84	24	8
Kafue (VFS)	58	80	325	7	18	10	334	9	61	16	9
Middle Zambezi	74	122	415	7	18	8	294	8	58	15	9
Luangwa	59	107	620	1	7	3	83	2	18	5	4
Mufa	76	315	626	10	18	9	459	12	78	11	10
Lower Zambezi and Tete	70	313	695	6	15	4	125	3	39	5	14
Morrunguze	27	285	424	26	15	2	181	4	471	7	27
Mazowe	76.3	143.1	560.0	4.5	10.0	3.6	130.3	3.5	38.5	8.9	7.1
Luenha	74	168	552	8	21	32	348	9	89	25	6
Sangadze	103	237	1093	3	10	6	212	5	24	10	2
Shire	35	585	995	10	14	2	268	7	78	11	10
Lower Zambezi (VFS)	67	199	621	5	10	4	165	5	40	8	6
Lower Zambezi (FS)	69	200	616	6	15	6	153	4	41	9	7
					Mud (<32 μm):						
Uppermost Zambesi	53	54	301	17	34	11	246	8	134	15	19
Kasaya	147	84	459	16	37	22	372	9	122	19	25
Ngwezi	163	101	555	24	41	18	232	6	157	17	42
Kwando	44	339	707	6	14	6	170	5	82	8	18
Sinde	26	194	362	32	40	4	321	10	348	17	55
Zambezi above Victoria Falls	37	125	251	18	32	10	623	19	171	19	29
Matetsi	22	291	332	31	33	3	201	6	259	11	52
Zambezi above Kariba	45	135	318	22	36	10	450	13	235	18	34
Umguza	55	147	303	22	25	6	175	4	196	10	59
Upper Gwai	75	125	410	22	30	10	200	6	174	13	56
Tinde	119	83	607	10	39	18	466	14	73	19	16
Kafue(VFS)	188	125	497	22	54	30	389	11	139	27	94
Middle Zambezi	184	113	512	22	57	31	489	13	144	28	87
Lower Zambezi and Tete	118	170	614	24	59	13	210	6	142	16	53
Sangadze	86	166	523	17	30	11	144	4	98	15	51
Shire	84	231	807	30	44	11	194	5	187	15	98
Lower Zambezi (VFS)	157	148	536	23	51	28	665	18	164	26	106

Table 6.2 continued

	CIA*	$\alpha^{Al}Mg$	$\alpha^{Al}Ca$	$\alpha^{Al}Na$	$\alpha^{Al}K$	$\alpha^{Al}Rb$	$\alpha^{Al}Sr$	$\alpha^{Al}Ba$
	Sand (63-2000 μm)							
Uppermost Zambesi	77	1.8	3.0	4.1	1.2	1.0	3.1	0.5
Kasaya	55	4.5	2.5	2.1	0.4	0.5	1.1	0.3
Ngwezi	49	12.3	1.8	1.9	0.4	0.4	1.4	0.3
Kwando	>89	> 2.3	> 4.4	> 4.1	> 3.6	1.4	2.1	0.3
Chobe	78	2.1	3.4	> 6.9	1.4	0.9	1.6	0.4
Upper Zambezi	75	2.5	4.2	3.9	1.1	1.1	1.9	0.4
Sinde	47	0.7	0.6	1.5	1.6	2.5	0.5	0.8
Zambezi above Victoria Falls	63	1.7	1.4	2.1	1.0	1.2	1.1	0.4
Zambezi rapid #19	58	1.9	1.6	2.0	0.8	1.0	1.1	0.4
Zambezi rapid #10	50	0.7	0.7	1.5	1.3	1.2	1.0	0.1
Masuie	41	0.4	0.4	1.3	1.9	2.9	0.7	1.1
Upper Zambezi	47	0.6	0.6	1.4	1.5	1.8	0.6	0.6
Matetsi	41	0.4	0.4	1.2	2.0	3.4	0.5	1.1
Zambezi above Kariba	49	1.1	0.9	1.2	0.9	1.0	1.0	0.6
Umguza	37	1.9	0.4	1.2	0.7	0.7	0.6	0.4
Lower Gwai	54.4	6.2	2.9	1.4	0.6	0.7	1.8	0.5
Kafue (FS)	52	1.0	1.2	1.4	0.9	0.9	1.6	0.7
Kafue (VFS)	53	0.9	1.5	1.5	0.8	0.7	1.8	0.7
Middle Zambezi	53	1.1	1.7	1.4	0.8	0.7	1.5	0.7
Luangwa	54	5.7	3.9	1.9	0.4	0.5	1.0	0.3
Mufa	47	0.9	0.9	1.3	0.9	1.0	0.9	0.7
Lower Zambezi and Tete	50	2.2	1.2	1.1	1.1	1.4	1.0	0.7
Morrunguze	45	0.5	0.6	1.4	1.8	3.2	1.0	1.1
Mazowe	50.3	2.7	1.7	1.2	0.7	0.9	1.6	0.7
Luenha	50	1.9	1.3	1.1	0.9	1.0	1.5	0.7
Sangadze	51	8.2	2.7	1.7	0.4	0.6	0.8	0.3
Shire	50	1.6	1.0	1.0	1.5	2.9	0.6	0.5
Lower Zambezi (VFS)	51	2.3	1.4	1.2	0.8	0.9	1.1	0.5
Lower Zambezi (FS)	51	2.1	1.4	1.2	0.9	1.0	1.2	0.6
				Mud (<32 μm):				
Uppermost Zambesi	82.9	2.9	3.7	21.4	3.3	1.9	6.4	1.8
Kasaya	77.9	3.0	2.5	14.2	2.1	0.7	4.4	1.3
Ngwezi	75.8	1.8	3.3	8.2	1.9	0.8	4.2	1.2
Kwando	23.1	0.3	0.2	21.7	2.9	0.9	0.4	0.3
Sinde	65.9	1.1	1.4	3.7	3.4	3.8	1.7	1.5
Zambezi above Victoria Falls	62.3	1.1	1.1	4.6	3.1	1.9	2.0	1.5
Matetsi	50.3	0.6	0.6	2.2	3.3	4.4	1.1	1.5
Zambezi above Kariba	58.9	0.7	0.9	3.9	3.0	1.8	2.0	1.3
Umguza	67.3	1.1	1.4	6.4	2.8	1.9	2.4	1.8
Upper Gwai	73.1	1.4	1.9	10.5	2.4	1.5	3.0	1.4
Tinde	73.4	2.4	5.2	5.2	1.2	0.8	3.7	0.8
Kafue(VFS)	64.7	0.7	1.7	5.3	1.3	0.6	3.0	1.2
Middle Zambezi	69.3	0.7	2.6	5.0	1.3	0.6	3.4	1.2
Lower Zambezi and Tete	71.0	1.3	2.3	4.4	1.8	1.0	2.4	1.0
Sangadze	68.3	0.8	1.5	9.8	2.0	1.3	2.3	1.2
Shire	74.7	1.1	2.5	5.6	2.2	1.6	1.9	0.9
Lower Zambezi (VFS)	67.2	0.8	1.9	4.3	1.5	0.7	2.5	1.1

Table 6.2 continued

	BULK SAMPLE (< 32 µm fraction, wet sieved)								CLAY MINERALS (< 2 µm)					
	Qz	Kf	Pl	Carb	Amp	Hem	Phyll	Total	Sme	Ill	Chl	Kao	Total	Kao / (Ill+Chl)
Uppermost Zambezi	49	15	1	0	0	0	35	100	43	21	0	36	100	1.7
Ngwezi	33	11	6	0	0	0	50	100	76	6	0	18	100	3.0
Kwando	89	0	0	4	0	0	7	100	70	13	0	17	100	1.3
Sinde	14	6	17	0	0	10	53	100	87	0	0	13	100	∞
Zambezi at Victoria Falls	75	8	2	0	0	0	15	100	78	15	0	7	100	0.5
Matetsi	7	20	15	4	0	9	45	100	93	0	0	7	100	∞
Upper Zambezi	41	12	15	0	0	5	27	100	54	31	0	15	100	0.5
Upper Zambezi	43	11	19	0	0	4	23	100	50	33	0	17	100	0.5
Umguza	26	8	7	3	0	0	56	100	87	4	5	4	100	0.4
Gwai	20	4	4	3	0	0	69	100	77	5	5	13	100	1.3
Tinde	34	24	5	0	0	0	37	100	25	40	9	26	100	0.5
Kafue	9	7	11	2	2	1	69	100	27	54	1	19	100	0.3
Middle Zambezi	10	7	11	6	1	0.2	64	100	60	27	0	12	100	0.4
Zambezi at Tete	19	5	19	0	2	0	54	100	25	37	0	38	100	1.0
Sangadze	12	8	10	3	0	0	67	100	96	3	0	1	100	0.4
Shire	14	7	16	0	2	0	61	100	9	49	0	42	100	0.9
Lower Zambezi	17	14	20	0	0	0	49	100	52	35	0	12	100	0.4

Table 6.3. Silt and Clay Mineralogy in the Zambezi Catchment Determined by X-Ray Powder Diffraction Qz = quartz; KF = K-feldspar; Pl = plagioclase; Carb = carbonate; Amp = amphibole; Hem = hematite; Phyll = phyllosilicate; Sme = smectite; Ill = mica/illite; Chl = chlorite (including vermiculite); Kao = kaolinite.

	ε_{Nd}			T_{DM} (Ma)		
	< 32 µm	*32-63 µm*	*63-2000 µm*	*< 32 µm*	*32-63 µm*	*63-2000 µm*
Uppermost Zambezi	-15.5	-	-	2162	-	-
Kasaya	-14.0	-	-	2006	-	-
Ngwezi	-15.6	-	-	2128	-	-
Kwado	-17.3	-	-	2320	-	-
Sinde	-5.3	-	-	1608	-	-
Zambeziat Victoria Falls	-12.5	-	-	2056	-	-
Matemsi	-4.1	-	-	1454	-	-
Upper Zambezi	-12.0	-	-	2010	-	-
Upper Zambezi	-12.5	-	-	2092	-	-
Umguza	-14.7	-	-	2177	-	-
Upper Gwai	-11.6	-	-	1872	-	-
Tinde	-14.4	-	-	1953	-	-
Gwai	-	-	-24.6	-	-	2690
Kafue (FS)	-	-16.4	-15.0	-	1976	1762
Kafue (VFS)	-14.8	-16.5	-17.7	1935	2029	2107
Middle Zambezi	-13.8	-16.2	-14.5	1925	2084	2106
Luangwa	-	-20.1	-16.5	-	2244	2155
Mufa	-	-	-8.8	-	-	2195
Lower Zambezi at Tete	-7.8	-7.7	-10.0	1552	1864	1735
Morrunguze	-	-	-1.9	-	-	1162
Mazowe	-	-	-18.2	-	-	2781
Luenha	-	-	-19.4	-	-	2504
Sangadze	-15.3	-21.1	-19.5	1887	2028	2094
Shire	-7.3	-8.0	-7.7	1279	1333	1455
Lower Zambezi (FS)	-16.0	-19.3	-14.8	1995	2221	2188
Lower Zambezi (VFS)	-14.3	-17.4	-14.5	1990	2242	2242
Quelimane (estuary)	-	-	-18.3	-	-	2319
Quelimane (beach)	-	-	-12.7	-	-	1968

Table 6.4. Neodymium Isotope Values and Sm-Nd Model Ages for Cohesive-Mud (<32-µm), Very Coarse Silt (32–63-µm), and Sand (63–2000-µm) Fractions of Zambezi Sediments. Except as noted, data are from sand samples. FS = fine sand; VFS = very fine sand; ND = not determined.

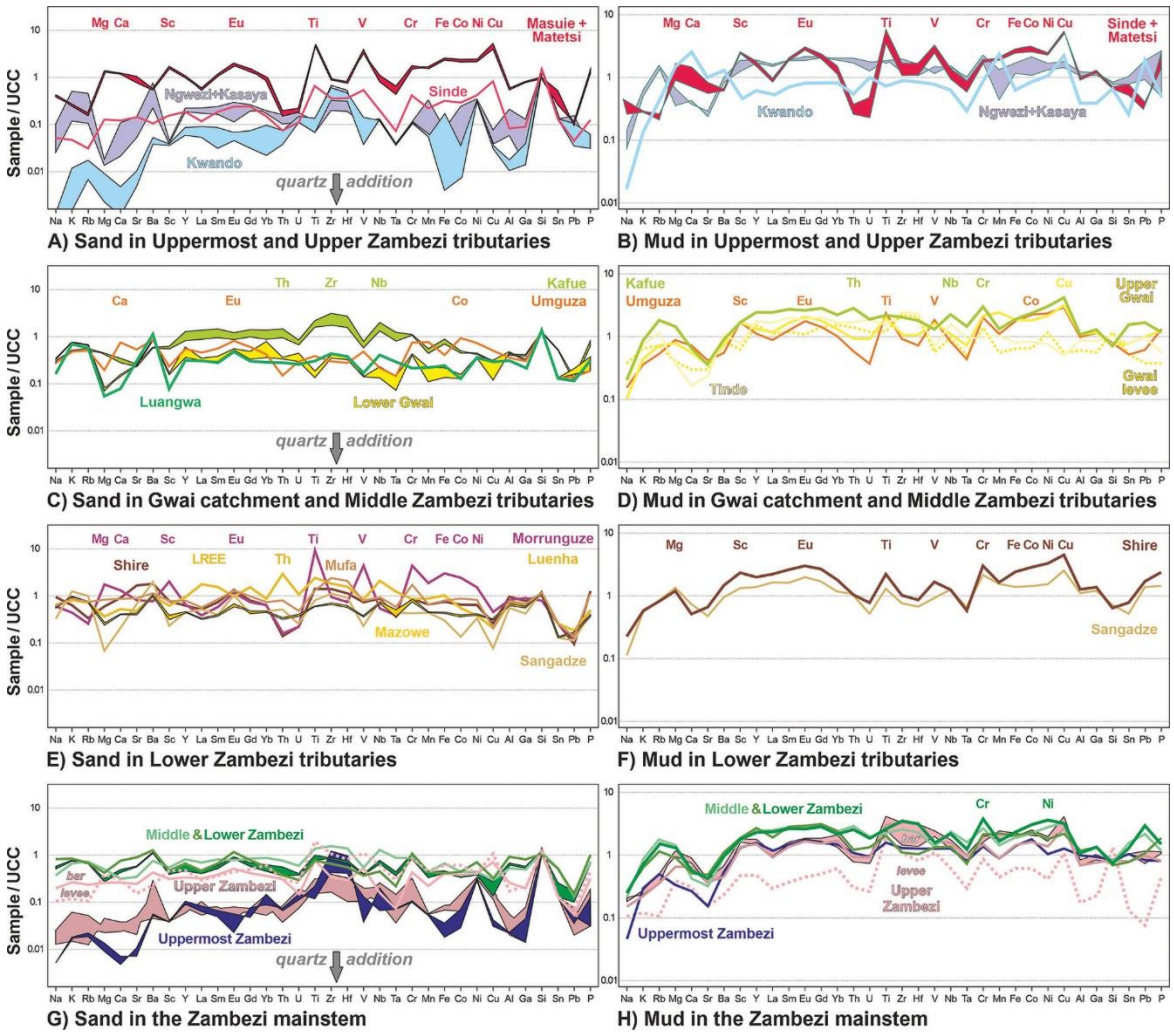

Figure 6.8 Sand and mud geochemistry (in UCC [upper continental crust]-normalized diagrams, chemical elements are arranged following the periodic table group by group). *A*, *B*, In Zambezi headwaters, extensive quartz addition by recycling explains relative depletion of most elements other than Si in sand. Supply from Karoo basalt leads to marked increase in ferromagnesian metals and lack of an Eu anomaly. High Ca, Sr, Mg, and Ba in Kwando mud reflect reworking of calcrete soils. *C*, *D*, Kafue samples are slightly enriched in elements hosted in ultradense minerals. Umguza and Upper Gwai sediments include minor detritus from Karoo basalt. Luangwa sand is partly recycled from Karoo siliciclastic strata. *E*, *F*, Most Lower Zambezi tributaries carry sediment that is undepleted relative to the UCC. In Morrunguze sand, high ferromagnesian metals and lack of an Eu anomaly reflect supply from the Tete gabbro-anorthosite. High light rare earth elements (LREE) and Th in Luenha sand suggest presence of monazite. *G*, *H*, Recycled quartz decreases downstream the Zambezi main stem. Lower Zambezi sand is only moderately depleted relative to the UCC, and mud is undepleted.

associated with kyanite and prismatic or fibrolitic sillimanite in Zangue sand. Kyanite and sillimanite also occur in Luenha sand. Zircon and other durable minerals, as well as titanite and apatite, are minor (ZTR up to eight in Sangara sand). Rare olivine was detected in

Sangara, Chacangara, and Mufa sands. Kaolinite, mica/illite, and smectite occur in subequal amounts in Zambezi mud collected at Tete, whereas smectite predominates over mica/illite and kaolinite is subordinate upstream of the delta (Fig 6.6). Sangadze mud consists almost exclusively of smectite, whereas Shire mud contains mica/illite and kaolinite in subequal proportions (Table 6.3).

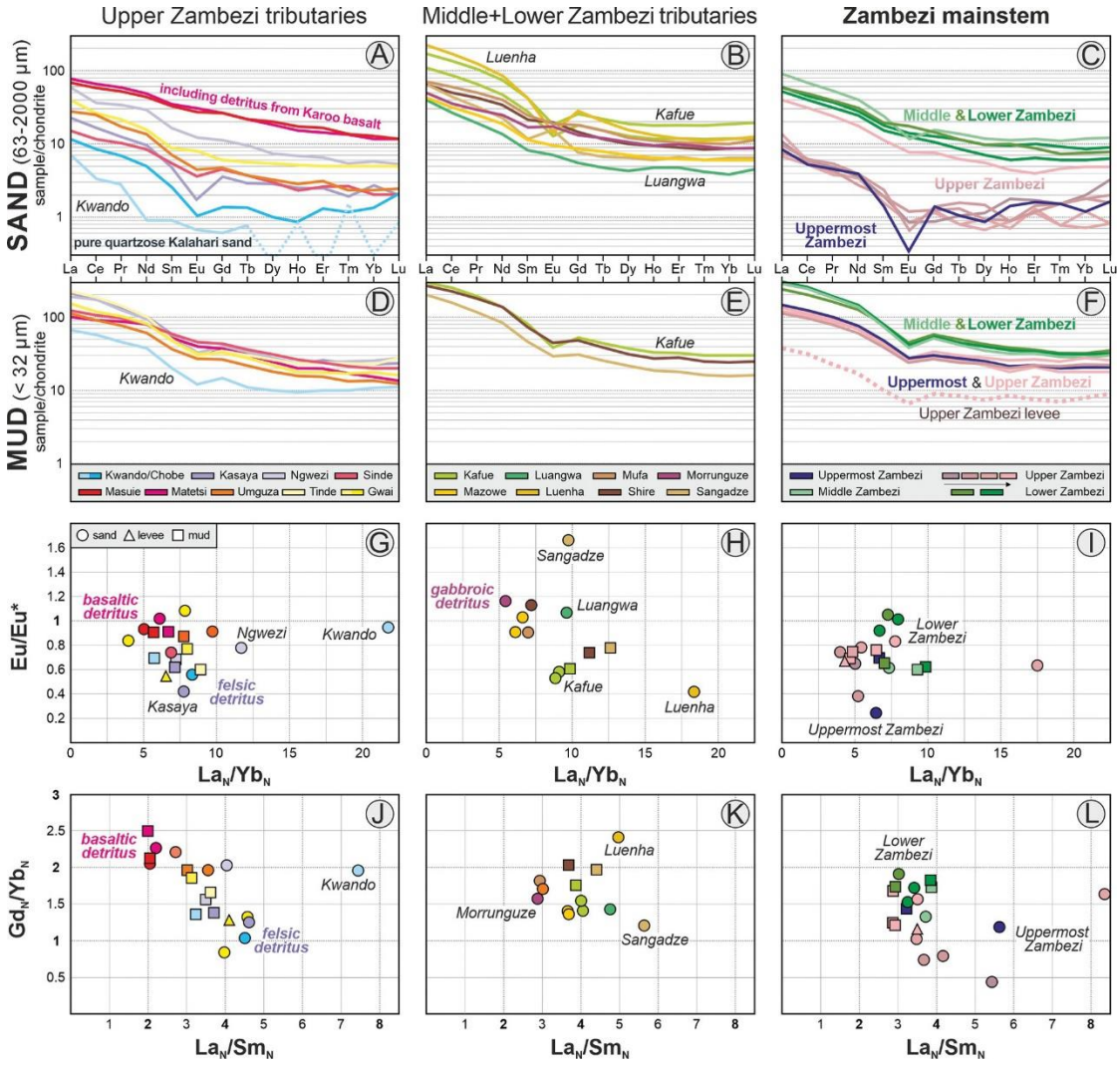

Figure 6.9 Rare earth elements (REEs). *A–C*, Chondrite-normalized REE patterns for sand. HREE (heavy-REE) trends are ill defined in pure quartzose sand because of very low concentration of elements with odd atomic numbers (Tb, Ho, Tm, Lu). *D–F*, Chondrite-normalized REE patterns for mud. *G–I*, La_N/Yb_N versus Eu anomaly. *J–L*, LREE (light-REE) versus HREE fractionation. Mafic detritus, conspicuous in Matetsi, Masuie, and Morrunguze sediments and present in Sinde, Umguza, and Upper Zambezi sediments, has higher REE concentration, lower LREE fractionation, no Eu anomaly, and higher HREE fractionation. Absence of an Eu anomaly in most Lower Zambezi sands reflects abundance of Ca-bearing feldspar. The steepest REE patterns with a strongly negative Eu

anomaly in Luenha sand indicate the presence of monazite, whereas the strongly positive Eu anomaly in Sangadze sand reflects abundant feldspar with lesser quantities of heavy minerals.

Chemical indices are remarkably constant in sediments of the Zambezi main stem and most of its main tributaries (CIA* = 70 ± 3, $\alpha^{Al}Ca$ = 2.0 ± 0.4, and $\alpha^{Al}Na$ = 6.0 ± 2.6 for mud; CIA* = 50.4 ± 0.4, $\alpha^{Al}Ca$ = 1.6 ± 0.5, and $\alpha^{Al}Na$ = 1.2 ± 0.2 for sand; Table 6.2). Plagioclase abundance explains why an Eu anomaly is not shown (Fig 6.9H, 5I). The observed order of element mobility is Na > Sr > Ca > K > Rb for mud and Ca > Na > Sr for sand. In all grain-size fractions of Lower Zambezi sediments, ε_{Nd} values become much more negative from Tete to upstream of the delta, where the very-fine-sand sample yielded a less negative value than the fine-sand sample (Table 6.4). Sand of the Morrunguze River, draining gabbroic rocks of the Tete Complex, is low in SiO_2 (52%), K, and Rb and notably rich in Fe, Mg, Ca, Ti, Mn, Sc, V, Cr, Co, Ni, and Cu (Fig 6.8E) and yielded the least negative ε_{Nd} value (Fig 6.7). Mufa sand, enriched in the same elements but to a much lesser extent, yielded high Zr and Hf concentrations (Table 6.2) and a more negative ε_{Nd} value. Luenha sand is relatively rich in Zr, Hf, U, Nb, Ta, and REEs, is the richest in Th (Fig 6.8E), displays the steepest REE patterns with the largest negative Eu anomaly (Fig 6.9H, K), and is the only sample with negative loss on ignition (LOI; 20.3). Mazowe and Luenha sands have ε_{Nd} values of -18 and -19, respectively. Shire sand is highest in Al, Na, Sr, and P and shows a much less negative ε_{Nd} value (Fig 6.7). Sangadze sand is the richest in K, Rb, and Ba and displays a strongly positive Eu anomaly (Fig 6.9H), reflecting abundant feldspar fewer heavy minerals, and a strongly negative ε_{Nd} value. Shire mud is low in SiO_2 (42%) and highest in Al, Fe, Sr, Ba, P, Sc, V, and Cu (Fig 6.4F). Zambezi mud upstream of the delta is high in Zr, Hf, REEs, Th, U, Nb, Ta, Cr, Mo, W, Co, and Ni (Fig 6.4H) and displays a negative Eu anomaly (Fig 6.9I). The U-Pb age spectrum of zircon grains supplied by the Zambezi River to the delta displays a dominant Irumide peak, with common Neoproterozoic, some Orosirian, and a few Neoarchean and late Paleozoic ages (Fig 6.10). Sangara and Morrunguze zircons show a unimodal Irumide peak, which is associated with minor Neoproterozoic ages in Mufa sand. Luenha and Mazowe sands yielded nearly identical bimodal zircon age spectra with Neoproterozoic and Neoarchean peaks (Table 6.5). The spectrum of Shire sand is also bimodal but with Irumide and Pan-African peaks. Pan-African ages are more common than Irumide ages in Zangue sand (Fig 6.10).

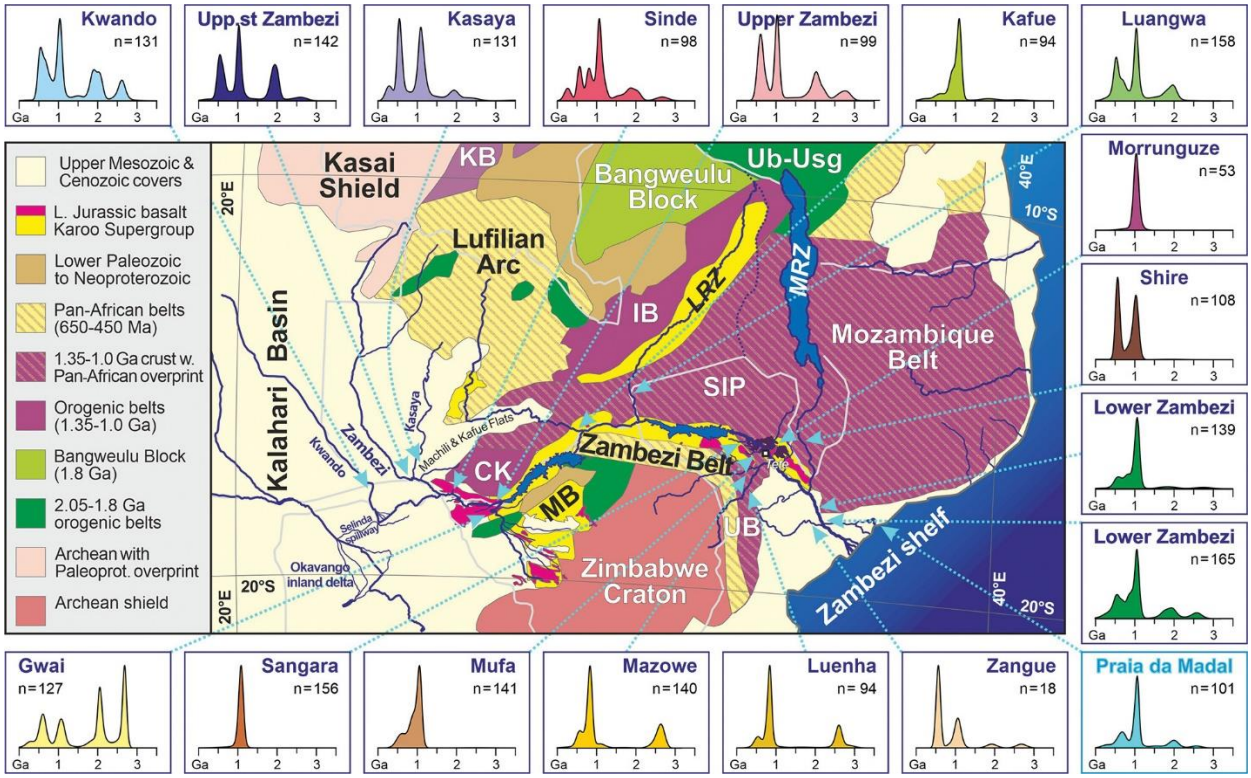

Figure 6.10 U-Pb age spectra of detrital zircons. Archean ages are common in Gwai, Mazowe, and Luenha sands sourced in the Zimbabwe Craton. Orosirian ages are common in Kwando and Uppermost (Upp.st) Zambezi sands recycling Kalahari dunes and in Gwai sand largely derived from the Paleoproterozoic (Paleoprot.) Magondi Belt. Irumide ages are widespread, overwhelming in Sangara and Morrunguze sands and dominant in Lower Zambezi sand. Pan-African zircons are also widespread, but only locally prevalent (Shire and Zangue sands). Geological domains are after Hanson (2003) and Thiéblemont et al. (2016). CK = Choma-Kalomo Block; IB = Irumide Belt; KB = Kibaran Belt; LRZ = Luangwa Rift Zone; MB = Magondi Belt; MRZ = Malawi Rift Zone; SIP = southern Irumide Province; UB = Umkondo Belt; Ub-Usg = Ubendian-Usagaran Belts; L. Jurassic = Lower Jurassic.

6.5.5 The Northern Coast, the Shelf, and the Slope

Sand in the Bons Sinais Estuary near Quelimane and adjacent beaches, located between 100 and 130 km north of the Zambezi mouth, is feldspathoquartzose with plagioclase ≥ K-feldspar and a rich tHM suite including mainly blue-green amphibole, subordinate epidote, clinopyroxene, and minor titanite, garnet, hypersthene, and mostly prismatic sillimanite (Fig 6.4E). Very fine-grained sand to coarse silt, cored on the upper continental slope ~85 km offshore of the Zambezi delta and close to the shelf break ~80 km to the east-northeast of the Bons Sinais mouth, is feldspar-rich feldspatho-quartzose with K-feldspar ≈ plagioclase and a moderately rich tHM suite including blue-green amphibole, epidote, clinopyroxene, and minor prismatic sillimanite, titanite, tourmaline, apatite, hypersthene,

and garnet. Benthic foraminifera are abundant (Fig 6.4F). No major mineralogical difference is observed either between samples cored offshore of the Zambezi mouth and Quelimane area or among sediments deposited during the last glacial lowstand, the postglacial sea-level transition, and the Holocene highstand in both areas. The ε_{Nd} value of bulk sand ranges between -13 and -18. The U-Pb zircon age spectrum displays a dominant Irumide peak with common Neoproterozoic, some Orosirian, and a few Neoarchean and Permian ages, similar to Lower Zambezi sand (Fig 6.10).

6.6 Provenance Insights from Petrography and Heavy Minerals

6.6.1 The Uppermost Zambezi: Polycyclic Sand from the Kalahari

Sand generated in southeastern Angola and westernmost Zambia and carried by the Uppermost Zambezi and its Kwando tributary consists almost entirely of monocrystalline quartz with very poor, ZTR-dominated tHM suite including staurolite and kyanite, a mineralogical signature that reflects extensive recycling of Kalahari Desert sand (Fig 6.11 and 6.12). The sedimentary succession of this vast rim basin, formed on the low-relief southern Africa plateau confined between the rejuvenated shoulders of the Indian and Atlantic rifted margins, is largely of fluvial origin with secondary eolian imprint (Moore and Dingle 1998). Kalahari dunes are generally best developed west of river channels, suggesting deflation of fluvial sediments by easterly winds during drier periods (Shaw and Goudie 2002). Conversely, rivers have inundated interdune areas and incised their course across dune ridges during wetter periods (Thomas et al. 2000). Between a fourth and a half of quartz grains are well rounded in both dune and river sediments, indicating that climate-controlled cycling of quartz-rich sand has taken place repeatedly from the fluvial to the eolian environment and back (Thomas and Shaw 2002).

6.6.2 The Upper Zambezi: Mixing with Detritus from Karoo Basalts

The Zambezi first meets Karoo basalt at Ngonye Falls in southwest Zambia and from there on the river flows along Karoo rift basins as far as the Mozambican lowlands. Pure quartzose sand recycled from the Kalahari mixes downstream with detritus derived locally from Lower Jurassic Karoo basalt in increasing proportions, determined accurately with forward-mixing models based on integrated petrographic and heavy-mineral data (Garzanti et al. 2012b; Resentini et al. 2017). Although the sand generation potential of basalt is notably less than that of sandstone or granite (Garzanti et al. 2019c, 2021b, 2021c; Le Pera and Morrone 2020; Morrone et al. 2020), mafic lava contains and sheds much more clinopyroxene than the few heavy minerals that quartzose sandstone contains and can thus

supply. Therefore, wherever basaltic detritus mixes with recycled quartz, as in the Upper Zambezi, quartz still dominates among main framework grains but the tHM suite rapidly becomes clinopyroxene dominated (figs. 6.11 and 6.12). From upstream of Victoria Falls to the Batoka Gorge, basaltic detritus accounts for <3% of total sediment only and Upper Zambezi sand remains pure quartzose, although clinopyroxene steadily increases from 14% to 86% of the very poor to poor tHM suite. Basaltic detritus increases to ~12% upstream of Lake Kariba, with composition changed to quartzose with 9% basaltic rock fragments in bedload sand and to litho-feldspatho-quartzose in levee silty sand.

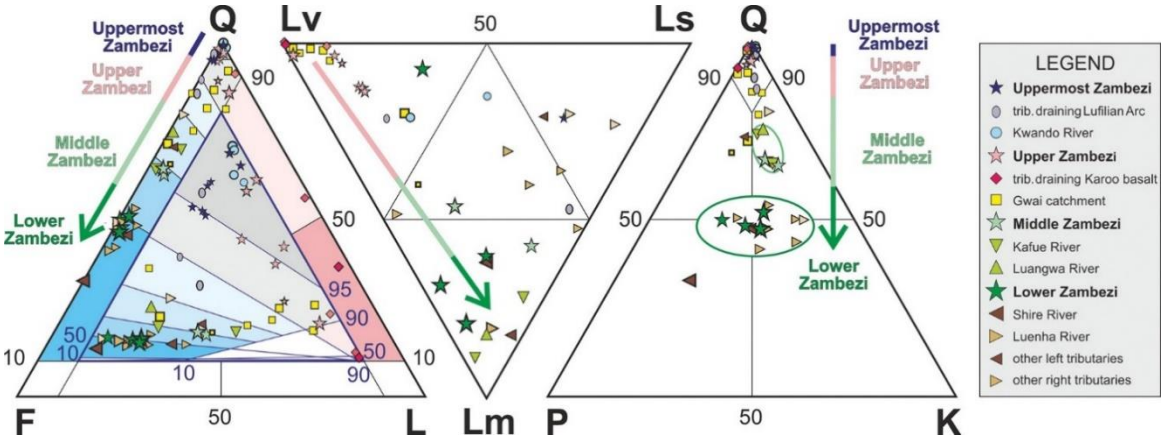

Figure 6.11 Downstream quartz decrease along segmented Zambezi sediment-routing system. Composition changes stepwise from pure quartzose (Uppermost Zambezi) to quartzose volcaniclastic (Upper Zambezi), feldspar-rich feldspatho-quartzose (Middle Zambezi), and finally quartzo-feldspathic metamorphiclastic (Lower Zambezi). Symbol size is roughly proportional to tributary (trib.) size and increases downstream along the main stem. Smaller symbols with thicker outline are Upper Zambezi and Gwai River levee samples representing deep suspended load. Q p quartz; F=feldspars (P=plagioclase; K=K-feldspar); L= lithics (Lm=metamorphic; Lv=volcanic; Ls=sedimentary). Fields in the QFL diagram after Garzanti (2019b); in the nested blue version of the same QFL plot, data are centered to allow better visualization of quartz-rich samples (von Eynatten et al. 2002).

Clinopyroxene represents 95% and 90% of the moderately rich and rich tHM suite, respectively. Among Upper Zambezi tributaries, basaltic detritus represents ~10% of Sinde sand in Zambia, and ~15% of Shangani sand, 50% of Masuie sand, and up to 70% of Matetsi sand in Zimbabwe, the rest being mostly represented by quartz recycled from Kalahari dunes. Clinopyroxene invariably represents 190% of the tHM suite in these rivers. Such estimates are corroborated by clay-mineral and geochemical data, displaying an increase in smectite and in the concentration of Fe, Mg, Ca, Na, Sr, Ti, Eu, V, Cr, Mn, Co,

Ni, Cu, and P along the Upper Zambezi, whereas the $^{87}Sr/^{86}Sr$ and weathering indices decrease, $\varepsilon_{Nd(0)}$ becomes only moderately negative, and T_{DM} model ages younger (Garzanti et al. 2014a). Forward-mixing calculations based on the integrated geochemical data set indicate that volcanic detritus increases from ~1% for sand and ~14% for cohesive (<32 μm) mud upstream of Victoria Falls up to 17%–18% for sand, 19%–20% for sandy silt, and ~41% for cohesive mud upstream of Lake Kariba. These estimates imply that up to ~27% of the sand and ~45% of the mud that the Upper Zambezi carries toward Lake Kariba is generated downstream of Victoria Falls, from basaltic rocks of the Batoka Gorge and supplied by tributaries draining Karoo lavas and overlying Kalahari dunes.

6.6.3 The Middle Zambezi: First-Cycle and Recycled Detritus from Zambia

The Middle Zambezi flows along Karoo extensional troughs (Fig 6.1). These formed on top of the Kuunga suture zone, marking the boundary between the Zimbabwe-Kalahari and Congo cratonic blocks and sealed during the final stages of the Neoproterozoic Pan-African orogeny (Goscombe et al. 2020). The first major tributary joining the Zambezi ~70 km downstream of Lake Kariba is the Kafue River, which largely drains mid-Neoproterozoic volcano-sedimentary rocks and upper Tonian granites of the Lufilian Arc in the upper course. In the lowermost course, the Kafue cuts across the West Zambezi Belt, including polymetamorphic basement of the Congo Craton deformed at upper amphibolite-facies conditions around 675 Ma (Goscombe et al. 2020). Because sand cannot pass Lake Kariba,

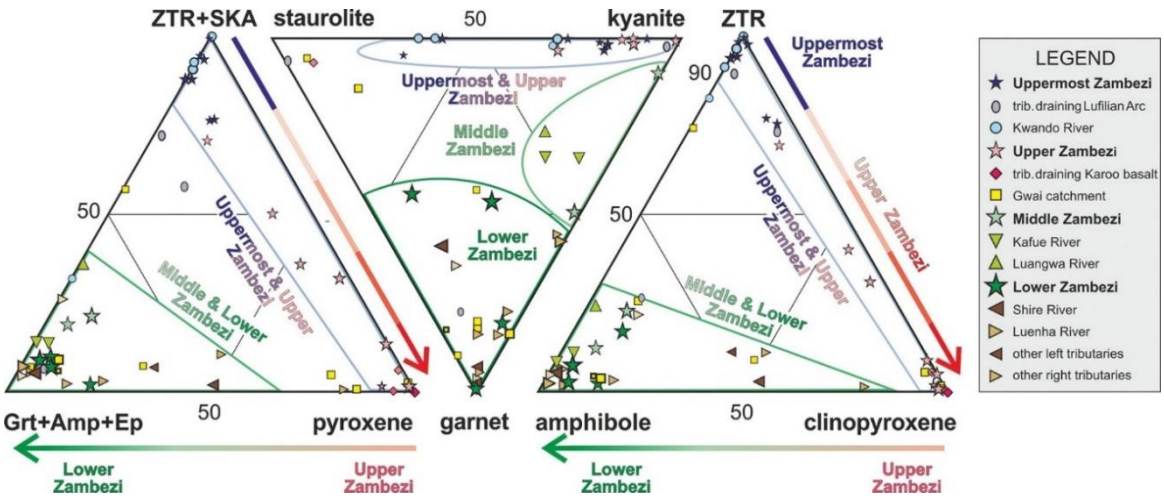

Figure 6.12. Changes in transparent heavy-mineral suites downstream on the segmented Zambezi sediment-routing system. Note (1) dominance of durable ZTR (zircon, tourmaline, and rutile) and SKA (staurolite, kyanite, sillimanite, and andalusite) minerals in the Uppermost Zambezi; (2) progressive increase in clinopyroxene along the Upper Zambezi; and (3) sharp increase in basement-derived garnet (Grt), amphibole (Amp), and epidote (Ep) in the Middle and Lower Zambezi. Scarcity

of garnet in Uppermost and Upper Zambezi sand is ascribed to high weatherability inherited from past hot-humid subequatorial climate. Symbol size is roughly proportional to tributary (trib.) size and increases downstream along the main stem. Smaller symbols with thicker outline are Upper Zambezi and Gwai River levee samples representing deep suspended load.

Middle Zambezi sand downstream of the Kafue confluence acquires the same feldspar-rich feldspatho-quartzose metamorphiclastic signature of Kafue sand, with a little more siltstone/sandstone rock fragments and clinopyroxene derived locally from the Karoo Supergroup, which is maintained as far as the confluence with the Luangwa River near the entry point into Lake Cahora Bassa (Fig 6.13). The Luangwa River, sourced in Paleoproterozoic gneisses of the Ubendian Belt, follows for most of its course another arm of the Karoo rift network. The Luangwa rift is bordered to the north by the external nappes of the Irumide Belt, including Paleoproterozoic granitoid gneiss overlain by quartzite and schist of the Muva Supergroup deformed at greenschist to amphibolite facies at 1.05–1.02 Ga (De Waele et al. 2009). Exposed to the south is the high-grade internal zone of the southern Irumide Province (Goscombe et al. 2020). Luangwa sand is thus a mixture of detritus derived from up to high-grade metamorphic rocks and recycled from Carboniferous to Jurassic siliciclastic strata, as indicated by relatively high quartz and ZTR minerals coexisting with blue-green to brown hornblende and mainly prismatic sillimanite.

6.6.4 The Lower Zambezi: Feldspar-Rich Sand from Precambrian Basements

As Upper Zambezi sand is dumped into Lake Kariba, Middle Zambezi sand is stored in Lake Cahora Bassa. Composition changes therefore again in the Lower Zambezi, where sand supplied by tributaries largely draining felsic to mafic igneous and up to high-grade metamorphic rocks acquires a quartzo-feldspathic signature unique among the Earth's big rivers (Potter 1978; Garzanti 2019a). Most Lower Zambezi tributaries carry sand with Q/F ratio ≤ 1 (Fig 6.11), reflecting mostly first-cycle provenance from midcrustal crystalline basements. Detritus recycled from the sedimentary fill of Karoo, Cretaceous, or Cenozoicextensional basins is widespread, although subordinate. This is revealed by sandstone and shale rock fragments in Chacangara sand and by a higher Q/F ratio and poor tHM suite in sand of the Zangue River draining the northern edge of the Urema Graben and of the Minjova River draining the Karoo Moatize-Minjova Basin (Fernandes et al. 2015). The Sangara, Chacangara, and Mufa west-bank tributaries and the Morrunguze and Minjova eastbank tributaries drain high-grade rocks of the internal zone of the southern Irumide Province, including the Tete gabbro-anorthosite complex (Goscombe et al. 2020).

This is reflected by the occurrence of gabbroic or metabasite rock fragments and by up to very rich tHM suites including hypersthene and clinopyroxene, brown hornblende, and rare olivine. The Luenha-Mazowe river system drains well into the Archean Zimbabwe Craton in the upper course and cuts downstream across the polymetamorphic Mudzi migmatitic gneisses remobilized during the Pan-African orogeny, and next across the Neoproterozoic Marginal Gneiss. The mostly firstcycle origin of their quartzo-feldspathic sand is reflected by the rich amphibole-dominated tHM suite, as in Mufa sand to the north (Fig 6.12). The lowest Q/F ratio is recorded in Shire sand, also including a very rich, amphibole-dominated tHM suite derived from granitic orthogneisses of the Blantyre domain (southern Malawi-Unango Complex), where Stenian-age crust underwent granulitefacies metamorphism during the Pan-African orogeny (Goscombe et al. 2020).

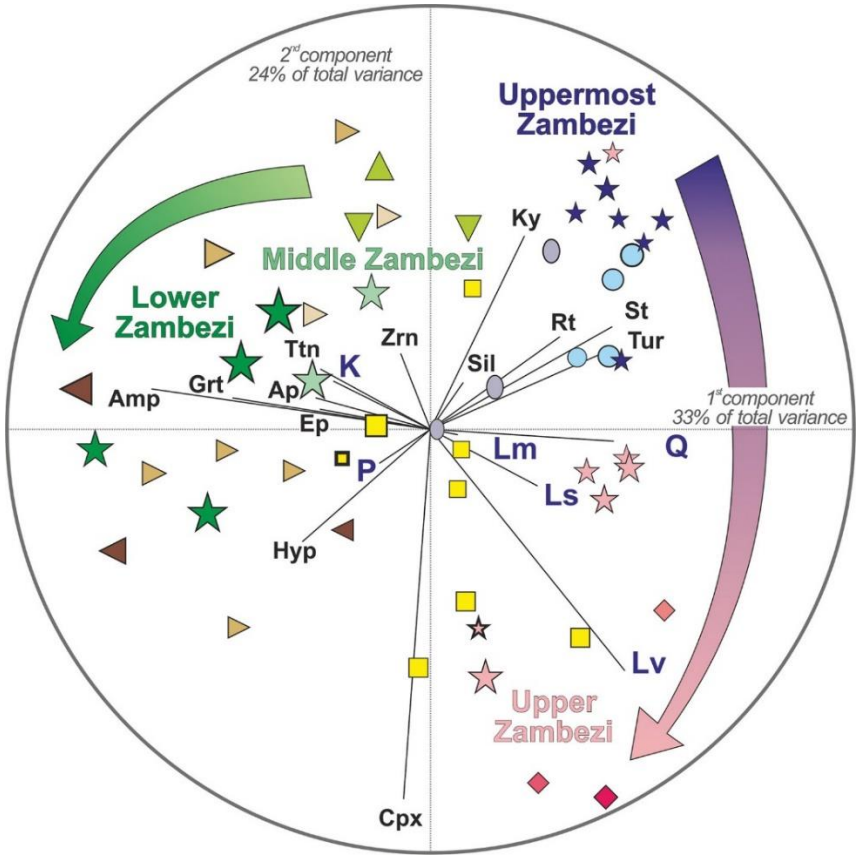

Figure 6.13. Stepwise changes in compositional signatures along segmented Zambezi sediment-routing system. Pure quartzose sand in the Uppermost Zambezi and Kwando Rivers is progressively enriched in clinopyroxene and basaltic rock fragments downstream in the Upper Zambezi. Middle Zambezi sand chiefly reflects contribution from the Kafue River. Lower Zambezi sand is markedly enriched in feldspars, amphibole, and garnet largely derived from Irumide Belts strongly affected by the Pan-African orogeny. The biplot (Gabriel 1971) displays multivariate observations (points) and variables (rays). Ap = apatite; Hyp = hypersthene; Ky = kyanite; Rt = rutile; Sil = sillimanite; St = staurolite; Ttn = titanite; Tur = tourmaline; Zrn = zircon. Other symbols as in figures 6.6 and 6.7.

The Sangadze and Zangue lowermost-course tributaries are sourced in the Pan-African Umkondo Belt, including greenschist facies to lower-amphibolitefacies schists thrust onto the margin of the Zimbabwe Craton and upper-amphibolite-facies migmatitic gneisses in the core, whereas the lower course cuts across the Cretaceous to Cenozoic sediment fill of the Lower Zambezi graben. Recycling is manifested in Zangue sand by the highest Q/F ratio of all Lower Zambezi tributaries. Poor to moderately poor, garnet-dominated (Sangadze) or garnetstaurolite (Zangue) tHM suites reflect both firstcycle provenance from lower-amphibolite-facies metasediments of the Umkondo Belt and recycling of Cretaceous sandstones derived from them (e.g., Sena Formation; Salman and Abdula 1995). The occurrence of brown amphibole and prismatic sillimanite, instead, reveals minor but significant contribution from upper-amphibolite-facies to granulite-facies gneisses of the orogen's core (e.g., Stenian Barue Complex; Goscombe et al. 2020). Forward-mixing models based on integrated petrographic and heavy-mineral data suggest that most Lower Zambezi sand (60%–80%) is generated in subequal proportions in the Luenha-Mazowe river system sourced in the Zimbabwe Craton and in the trunk-river catchment upstream of the Luenha confluence, including the Zambezi Belt and the southern Irumide Province. Additional contributions from the Umkondo Belt and recycled from the Karoo, Cretaceous, or Cenozoic extensional basins drained by the Minjova, Sangadze, and Zangue tributaries are significant (~20%), whereas supply from the Tete gabbro-anorthosite complex and Blantyre domain, drained respectively by the Morrunguze and Shire tributaries, appears to be subordinate (~10%).

6.6.5 The Zambezi Passive Margin

Detrital modes of Lower Zambezi sand match neither those of estuary and beach sands in the northern delta near Quelimane nor sediments cored offshore of both the Zambezi mouth and Quelimane area and deposited during either the Holocene highstand or the previous postglacial and glacial relative lowstands (Table 6.1). The Q/F ratio is 1.0 ± 0.1 in Lower Zambezi sand but 2.5 ± 0.5 in sand of the Quelimane area and 1.6 ± 0.3 in offshore samples. The homogeneous composition of offshore sediments generated before the mid-Holocene (older than 4 ka) suggests that this could represent the original, preAnthropocene signature of Zambezi sediment. Subsequent closure of the Kariba and Cahora Bassa dams, with consequent drastic reduction of the catchment area effectively contributing sediment to the Zambezi Delta, explains the peculiar mineralogical signatures characterizing Lower Zambezi sand today. Besides the abundance of feldspars, these include the high tHMC and

ACI indices, reflecting provenance dominantly from middle-crustal igneous and high-grade metamorphic rocks. The abundance of mica in offshore sediments, instead, is the effect of preferential winnowing of slow-settling platy phyllosilicates by waves, a phenomenon observed along continental shelves worldwide (Doyle et al. 1968; Garzanti et al. 2015b, 2019a). The mineralogy of estuary and beach sand in the Quelimane area is not the same as either Lower Zambezi or offshore sediment (Table 6.1). This is more difficult to explain, because predominantly northward littoral drift would be expected to entrain sand from the Zambezi delta, leading to homogeneous composition along the coast. Reasons for such discrepancy may include local reworking of floodplain sediments, whereas littoral drift from the north is unsupported by prevailing longshore-current patterns (Schulz et al. 2011; van der Lubbe et al. 2014).

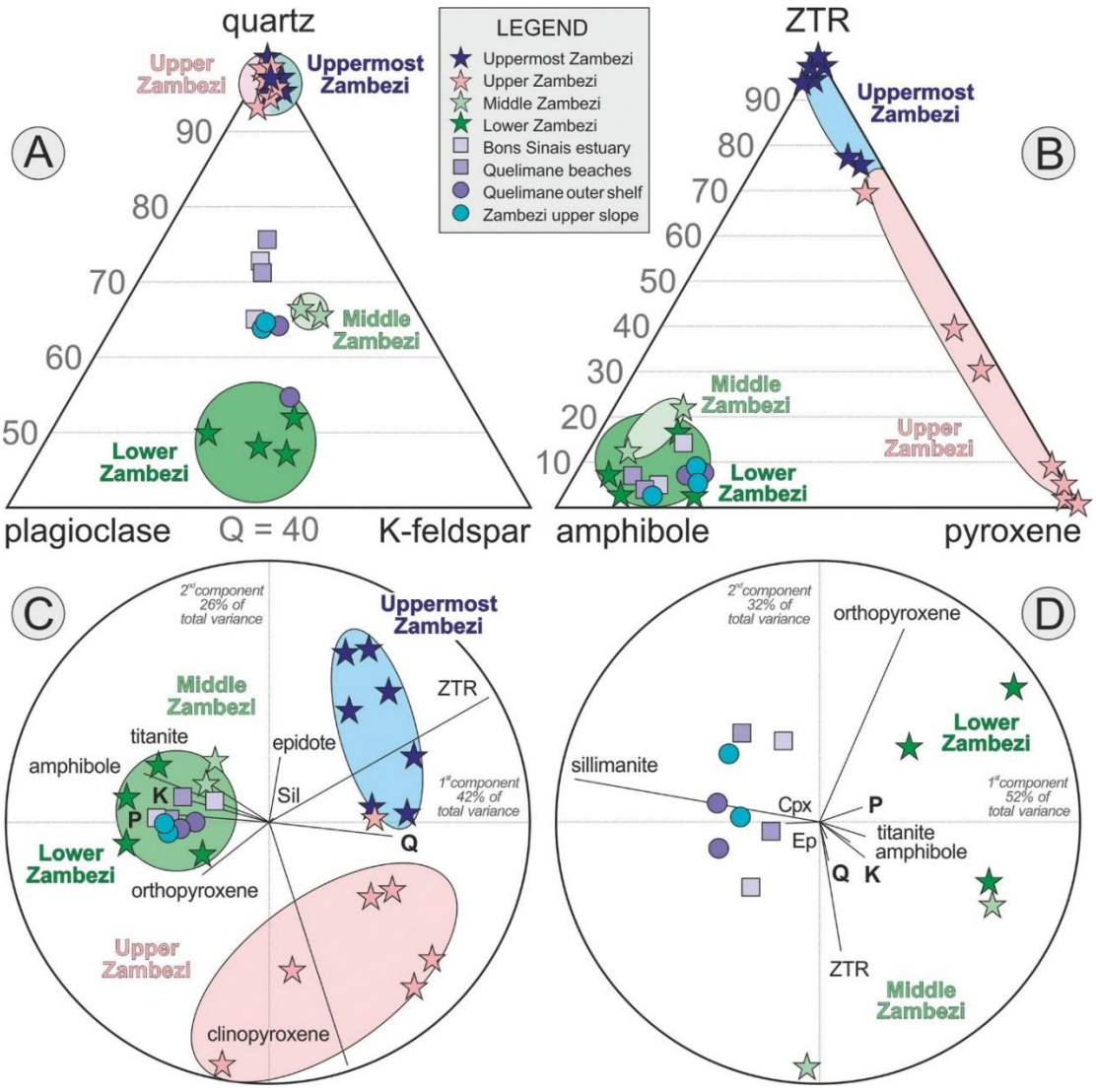

Figure 6.14. Zambezi River sands compared with coastal and offshore sediments. A–C, Uppermost and Upper Zambezi detritus is clearly distinct from any downstream sample. Sediment fed into the

Indian Ocean was thus mostly derived from the middle–lower catchment even before closure of the Kariba and Cahora Bassa dams. D, Passive-margin sediments, however, do not closely match either Middle or Lower Zambezi sand, suggesting significant additional contribution from both the upper catchment and Mozambican lowlands in pre-Anthropocene times. Biplots C and D (Gabriel 1971) were drawn with CoDaPack software by Comas-Cufí and Thió-Henestrosa (2011). Q = quartz; P = plagioclase; K = K-feldspar; ZTR = zircon + tourmaline + rutile; Cpx = clinopyroxene; Ep = epidote; Sil = sillimanite.

6.7 Provenance Insights from Clay Mineralogy, Sediment Geochemistry and Detrital Zircon Geochronology

The aim of this section is to complement previous considerations based only on sand with inferences derived independently from the mineralogy and geochemistry of mud.

6.7.1 Clay Minerals

The clay mineralogy of unconsolidated mud depends on weathering processes in soils but reflects provenance as well, especially in dry climates where illite and chlorite are largely derived from phyllosilicate-rich metamorphic bedrock, whereas smectite is shed by mafic lava (Chamley 1989). Among the studied samples, smectite is the dominant clay mineral (≥87%) in mud transported by the Sinde and Matetsi tributaries of the Upper Zambezi and by the Umguza tributary of the Gwai River, all partly draining Karoo basalt between southern Zambia and western Zimbabwe. Smectite, however, is also produced in abundance in regions lacking significant exposures of mafic rocks (e.g., the Kwando catchment) and represents the virtually exclusive clay mineral in mud of the Sangadze River flowing across Mozambican lowlands, indicating incomplete flushing of mobile ions in poorly drained low-relief regions (Wilson 1999). Illite is the most abundant clay mineral in mud of the Kafue and Shire Rivers, chiefly draining Proterozoic metamorphic basement, and in mud of the Tinde River, draining Neoproterozoic molasse (Fig 6.6).

6.7.2 Mud Geochemistry

The piece of provenance information most readily obtained from geochemical data is the supply from mafic rocks, revealed by high concentrations of ferromagnesian metals, including Mg, Sc, Ti, V, Cr, Mn, Fe, Co, and Ni (Fig 6.8; McLennan et al. 1993; von Eynatten et al. 2003). Among the analyzed samples, these elements reach the highest values in Masuie and Matetsi sands, draining Karoo basalts, and in Morrunguze sand, draining the Tete gabbro-anorthosite (Fig 6.8). Intermediate values for these elements are obtained for the Sinde and Umguza Rivers and for the Middle Zambezi upstream of Lake Kariba, all draining Karoo basalts more marginally (Table 6.2). Other samples in the Upper Zambezi

catchment have SiO_2 > 90%, revealing extensive recycling of pure quartzose Kalahari sand. The virtually identical chemical composition of Kafue and Middle Zambezi muds confirms that the Kafue is by far the most important source of sediment to the Middle Zambezi between Lake Kariba and the Luangwa confluence. Slightly above 80% in Kafue and Middle Zambezi sand, SiO_2 rises to nearly 90% in Luangwa sand, which contains a greater proportion of detritus recycled from Karoo siliciclastic strata. In sand of Lower Zambezi tributaries, SiO_2 mostly ranges between 70% and 80%. Composition is closest to the UCC for sand carried by the Lower Zambezi to the Indian Ocean, confirming its dominantly first-cycle provenance from midcrustal basement rocks. Chemical indices provide further clues. Because the addition of quartz grains profoundly affects the WIP, but not the CIA*, the CIA*=WIP ratio can be used to detangle the effects of weathering and recycling. This ratio reaches ≥100 in Uppermost Zambezi and Kwando sands consisting almost entirely of recycled Kalahari dune sand and decreases first to 30 ± 9 in Upper Zambezi sand above and below Victoria Falls and then drastically to 3.1 ± 0.7 in Upper Zambezi sand and silty sand upstream of Lake Kariba. The CIA*=WIP ratio decreases further to 1.7 ± 0.3 in sands of Middle Zambezi tributaries and main stem and is lowest (0.9±0.1) in sands of Lower Zambezi tributaries and main stem, further confirming their mostly first-cycle provenance.

6.7.3 Sand Geochemistry

The geochemical composition of mud samples is more homogeneous. SiO_2 varies between 42% and 54%, being notably higher (68%) only for Tinde mud, reflecting recycling of siliciclastic Pan-African molasse. Kwando mud is markedly enriched in Ca, Sr, Mg, and Ba (Fig 6.8B), revealing contributions from calcrete and dolocrete soils (Shaw 2009; McFarlane et al. 2010). Fe, Ti, Sc, V, Co, and Cu are highest in Sinde mud and Mg in Matetsi mud (Fig 6.8A, B), largely derived from Karoo basalt. Lower Zambezi mud upstream of the delta is richest in Cr and Ni (Fig 6.8H), suggesting significant supply from mafic Proterozoic rocks, including the Tete gabbro-anorthosite.

6.7.4 Nd Isotope Geochemistry

Although the $^{143}Nd/^{144}Nd$ composition of sediments is controlled by multiple factors, the provenance signal emerges clearly from data obtained from all analyzed size fractions, cohesive mud (<32 μm), very coarse silt (32–63 μm), and sand (63–2000 μm), allowing a sharp distinction between sediments derived from mafic igneous rocks and old granitoid basements (Fig 6.16).

The least negative ε_{Nd} values characterize Morrunguze sand, largely derived from the upper

Stenian Tete gabbro-anorthosite, and Sinde and Matetsi muds, partly derived from Lower Jurassic Karoo basalt (Fig 6.7). Mildly negative values were also obtained from Mufa sand, partly derived from Tete mafic rocks; from Shire sediments largely derived from mafic granulites of the Blantyre domain; and from Lower Zambezi silt collected at Tete and mostly derived from the southern Irumide Province (Table 6.4). At the other extreme, most negative ε_{Nd} values identify Gwai, Mazowe, and Luenha sands sourced from Archean gneiss of the Zimbabwe Craton. Markedly negative values also characterize mud in the upper catchments of the Zambezi and Gwai Rivers. The ε_{Nd} values becomes less negative as the Upper Zambezi rushes through the basaltic gorges downstream of Victoria Falls but much more negative as the lower Gwai cuts steeply across gneisses of the Dete-Kamativi Inlier. Strongly negative values also characterize Kafue and Luangwa sediments in the middle catchment, Sangadze sediment in the lowermost catchment, and Lower Zambezi sediment upstream of the delta.

6.7.5 Intrasample Variability

The grain size–controlled intrasample variability of ε_{Nd} values is limited (average standard deviation: 1.6 ± 0.9). The sand fraction (63–2000 μm) typically yields a more negative ε_{Nd} than the cohesive-mud fraction (<32 μm). The most negative ε_{Nd} values are obtained from the 32–63 μm size class of sand samples, representing the fine tail of the size distribution, where ultradense minerals, including LREE-rich monazite, concentrate because of the settling equivalence effect (Rubey, 1933). This is documented by La, Th, and Zr concentrations, respectively 7 ± 5, 9 ± 7, and 6 ± 3 times higher in the 32–63 μm size class than in the 63–2000 μm fraction of sand samples, with enrichment factors increasing sharply with sample grain size (correlation coefficient is 0.91). The opposite holds for the Lower Zambezi silt collected at Tete (Fig 6.7), where the 32–63 μm size class is part of the coarse tail of the size distribution, which is depleted in denser minerals and yields a less negative ε_{Nd} than both the <32 μm and 63–2000 μm fractions (Table 6.4).

6.7.6 Intersample Variability

Samples collected in nearby localities along the Kafue and Lower Zambezi Rivers confirm a tendency toward more negative ε_{Nd} values with increasing grain size. Strong grain-size control on ε_{Nd} has been recently documented in Congo Fan sediments, where it was ascribed to the more negative ε_{Nd} carried by multiply recycled quartz grains originally derived from older terrains on average (figs. 6.7 and 6.15). In recycled Congo Fan sediments, however, quartz and monazite account for similar amounts of Nd, quartz being 10^5 times more

abundant in weight but monazite containing 10^5 times more Nd. In first-cycle Lower Zambezi sediments, instead, heavy minerals (including monazite) are an order of magnitude more abundant than in Congo sediments and are thus expected to dominate the REE budget (Totten et al. 2000). Among minerals frequently found in sediments, only monazite and allanite display very high LREE content, monazite being about three times richer in LREEs. In the sample set, monazite is about five times more abundant than allanite, which implies an order of magnitude greater contribution to the LREE sedimentary budget by monazite than by allanite. The tendency of ε_{Nd} values to become more negative in sand, and more markedly in the 32–63 μm size class of Middle and Lower Zambezi sand samples, thus suggests that ultradense monazite, strongly concentrated in the fine tail of the size distribution because of the settling-equivalence effect, carries an older (more negative) ε_{Nd} signal than other less dense and less durable minerals (e.g., allanite, titanite, apatite, epidote, and amphibole).

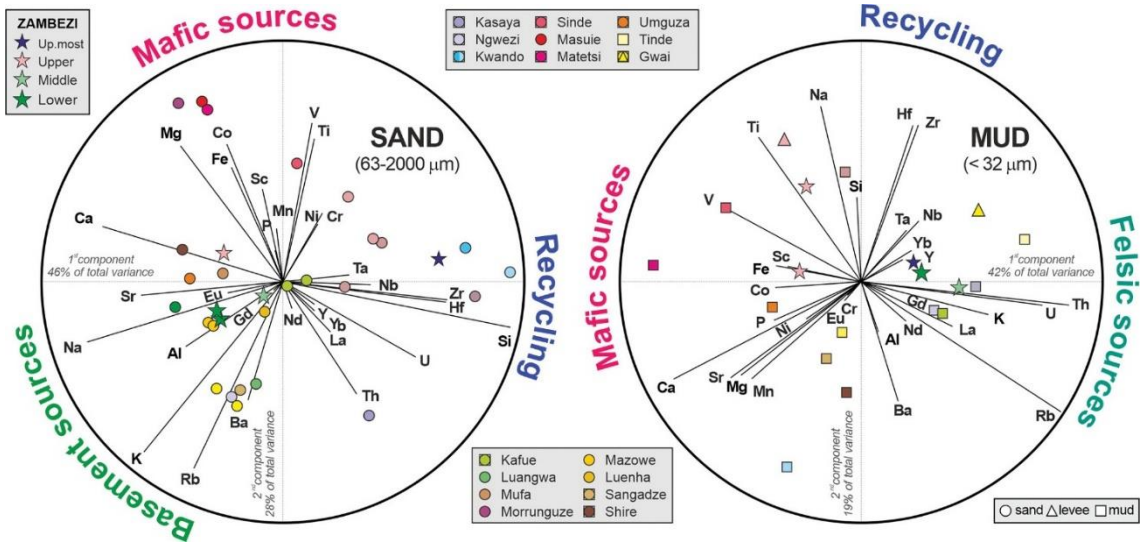

Figure 6.15. The biplots highlight the relationships among chemical elements in Zambezi sand and cohesive mud. Provenance control is most evident for sand. Ferromagnesian metals are enriched in basaltic or gabbroic detritus. Al, Na, Ca, K, Rb, Ba, and Eu hosted in feldspars are enriched in first-cycle detritus from midcrustal basements. Si, Zr, and Hf are enriched in sediment recycled from Kalahari dunes dominated by quartz and durable heavy minerals.

6.7.7 Model Ages

The $T_{Nd,DM}$ model ages for the Zambezi main stream and tributaries mainly range between 2.0 and 2.3 Ga (Fig 6.7). Mud partly derived from Karoo basalt yielded notably younger values (1.6 Ga for Sinde and 1.45 Ga for Matetsi), like all size fractions of Shire sediment largely derived from mafic granulites of the Blantyre domain (1.25– 1.45 Ga). Morrunguze sand, largely derived from gabbroic rocks of the Tete domain, yielded the youngest value

(1.16 Ga), whereas the oldest values (2.5–2.8 Ga) characterize the three rivers sourced in the Archean Zimbabwe Craton (Gwai, Mazowe, and Luenha; Fig 6.10). Sm-Nd model ages depend on REE fractionation, being lower in samples containing LREE-rich minerals such as monazite or allanite and higher in samples containing middle-REE-rich minerals such as xenotime, titanite, or apatite (Fig 6.16). Because of the settling-equivalence effect, ultra-dense monazite grains occur only in the fine tail of the size distribution, which explains why the 32–63 μm size class of the cohesive Zambezi silt collected at Tete has a higher Sm/Nd ratio and thus yielded a notably higher Sm-Nd model age than the <32 μm fraction, despite its slightly lower ε_{Nd} (Fig 6.7). In the two Zambezi samples upstream of the delta, the 63–2000 μm fraction has lower LREE fractionation (higher Sm/Nd) than both the 32–63 μm and <32-mm fractions and thus yielded older Sm-Nd model ages than the <32 μm fraction, despite similar ε_{Nd} values, and almost the same Sm-Nd model ages as the 32–63 μm size class, despite the latter yielding notably more negative ε_{Nd} (Fig 6.7).

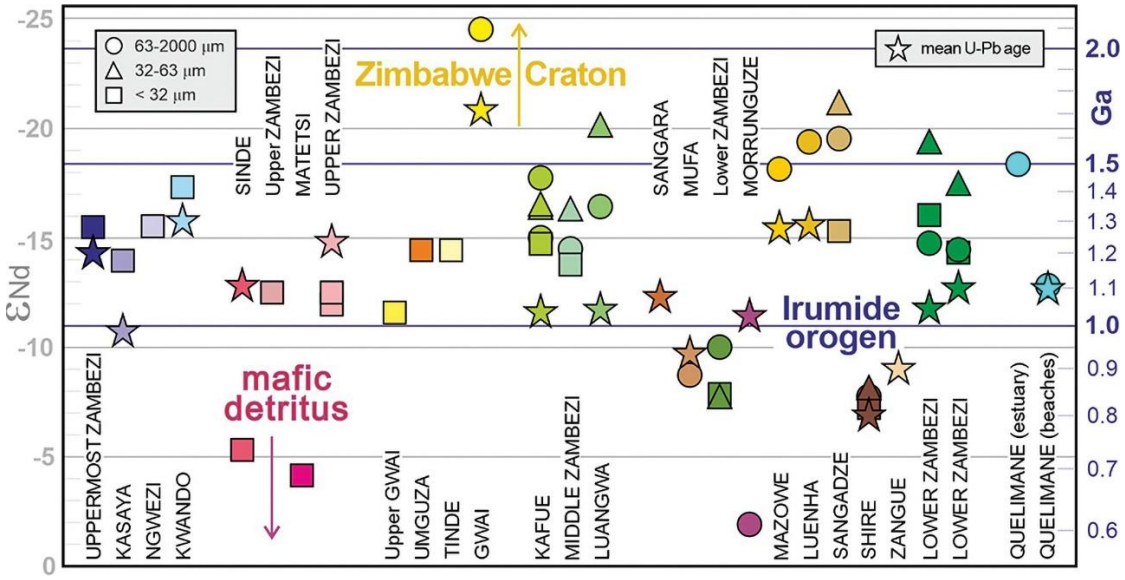

Figure 2.16. Multiple controls on Nd isotope values. Most prominent are the effects of lithology (mafic detritus being least negative) and average age of source rocks (as highlighted by generally good correlation with U-Pb age of detrital zircon). Grain size–controlled intrasample variability is limited.

6.7.8 Detrital Zircon Geochronology

Age spectra of detrital zircons enrich provenance information by providing insight into events of crustal growth in diverse source-rock domains (Fig 6.18). In the general case, however, these can be considered only "protosources" (Andersen et al. 2016, 2018). They represent the true sediment source only in the specific case of first-cycle detritus supplied directly from igneous or metamorphic basement (Dickinson et al. 2009). This introduces a further major uncertainty in zircon-based provenance analysis, because most sedimentary

basins are fed with a mixture of recycled and first-cycle sediments in a proportion that can be evaluated only roughly from independent compositional data. Petrographic, mineralogical, and geochemical data collectively concur to reveal that Uppermost Zambezi sand is dominantly recycled from Kalahari dune fields (Garzanti et al. 2014b). The Kwando River, in particular, drains entirely within the Kalahari Basin, whereas some first-cycle detritus is supplied by Zambian tributaries sourced in the Lufilian arc or the Choma-Kalomo Block. In sharp contrast, Lower Zambezi sand is mostly first cycle and derived from igneous and metamorphic Precambrian basements rejuvenated during Neogene southward propagation of the East African Rift. Geochronological analysis indicates the Irumide and Pan-African crustal domains as the main protosources of zircon grains in rivers draining the northern Kalahari Plateau (Fig 6.10). Neoarchean ages ultimately derived from the Kasai Shield are common only for Kwando sand in the west. Paleoproterozoic grains ultimately derived from the Angola Block are more common in Kwando and Uppermost Zambezi sand than in eastern Zambian tributaries. Among these, Paleoproterozoic zircons are more common in Sinde sand sourced in the Choma-Kalomo Block, whereas Neoproterozoic zircons are much more abundant in Kasaya sand largely derived from the Lufilian Arc. The Irumide peak is invariably prominent. Zircon grains yielding Permian to Triassic Karoo ages constitute a minor population in Sinde sand but are lacking in Upper Zambezi sand downstream of the basaltic gorges, indicating that zircon occurs in tuffs interlayered within Karoo siliciclastic strata but not in the overlying Lower Jurassic basalt. Despite extensive remobilization during the PanAfrican orogeny (Goscombe et al. 2020), the analyzed center of zircon grains in sand of northern (Kafue, Luangwa, Morrunguze) and western (Sangara, Mufa) tributaries to the Middle and upper Lower Zambezi yielded mostly or even exclusively Irumide ages (Table 6.5). The dominant Irumide zircon age peak displayed by Kafue sand suggests that zircons sourced from the Neoproterozoic Lufilian Arc are retained in the Itezhi-Tezhi Reservoir and/ or in the Kafue Flats and do not reach the lower gorge, where Irumide-aged zircons are derived largely from the Mpande Gneiss (~1.1. Ga; Hanson et al. 1994; Goscombe et al. 2020). Late Neoproterozoic ages are lacking in sand of the Morrunguze River, draining entirely within the southern Irumide Province, but are more abundant than Irumide ages in sand of the Shire and Zangue tributaries joining the Zambezi upstream of the delta (Fig 6.10). Archean zircons are common (24% ± 2%) in the Gwai, Mazowe, and Luenha Rivers, sourced in the Zimbabwe Craton. Gwai sand also carries ~30% of Paleoproterozoic zircons, largely derived from the Dete-Kamativi Inlier cut across in the lower course. The multimodal age spectrum of

Zambezi zircons eventually supplied to the delta and dragged by littoral currents to the northern Quelimane region indicates predominance of zircon grains derived directly or indirectly from the Irumide Belt, with subordinate late Neoproterozoic zircons mainly supplied by geological domains most severely remobilized during the Pan-African orogeny (Fig 6.10). Orosirian zircons are frequent, Neoarchean grains minor, and Permian–Triassic zircons rare (Table 6.5). A few Permian–Triassic zircons derived from Karoo volcanic or volcaniclastic layers are identified in Kasaya, Sinde, Gwai, Kafue, and Luangwa sands, but none were recorded from any Lower Zambezi tributary. Yet a few Permian–Triassic zircons occur in Lower Zambezi sand upstream of the delta, suggesting recycling of Karoo strata exposed in the Moatize-Minjova basin. Jurassic or Cretaceous ages are sporadically recorded. Among these, most significant are a couple of grains dated as ~120 Ma in the terminal tract of the Lower Zambezi, indicating provenance from igneous rocks emplaced during the incipient opening of the Mozambique Channel (König and Jokat 2010; Chanvry et al. 2018).

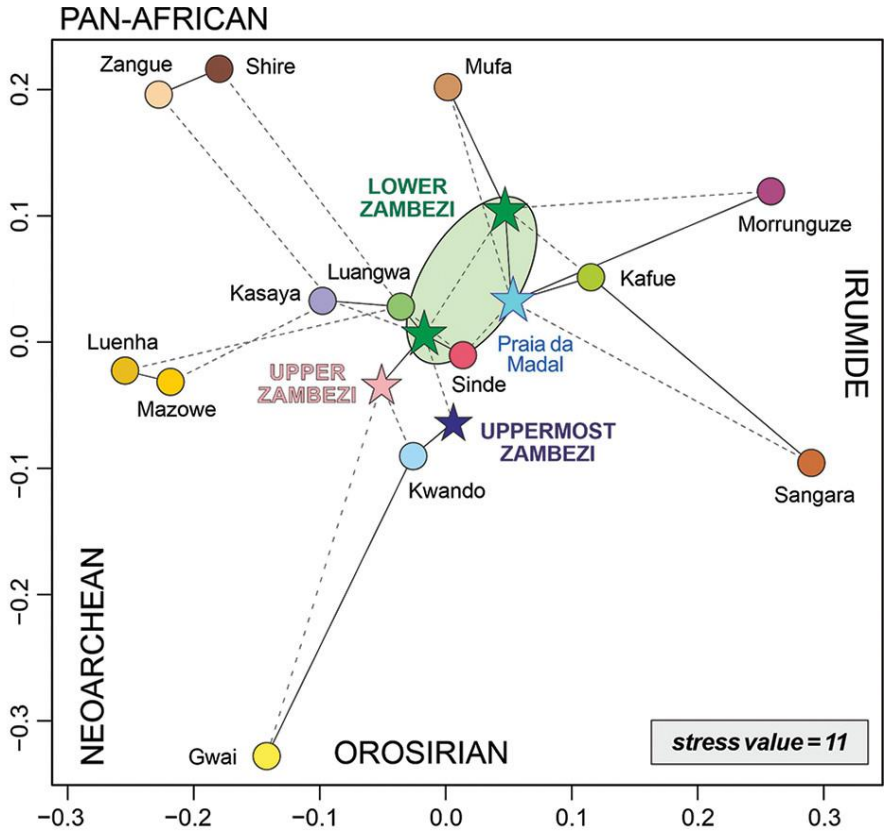

Figure 6.17 Multidimensional scaling map based on U-Pb zircon age spectra (green field defined by two Lower Zambezi samples upstream of the delta and Praia da Madal beach). Irumide ages are dominant in Sangara and Morrunguze sands. Pan-African ages prevail in Shire and Zangue sands. Neoarchean ages prevail in Gwai sand and are common in Luenha and Mazowe sands. Eburnean ages

are common in Upper Zambezi, Kwando, and Gwai sands but never prevalent. A few Karoo ages occur in Kasaya and Sinde sands. Closest and second-closest neighbors are linked by solid and dashed lines, respectively. PC = principal component.

	Karoo	*freq*	Pan-African I	*freq*	Pan-African II	*freq*	Irumide	*freq*	MesoProterozoic	*freq*	Paleoproterozoic	*freq*	NeoArchean	*freq*
Kwando			575 ± 11	*27%*			990 ± 17	*36%*			1891 ± 36	*25%*	2571 ± 78	*12%*
Uppermost Zambez	235 ± 14	*2%*	561 ± 10	*27%*			1009 ± 15	*39%*			1989 ± 31	*32%*		
Kasaya	281 ± 12	*8%*	558 ± 10	*34%*			1100 ± 16	*45%*			2064 ± 58	*13%*		
Sinde	255 ± 9	*7%*	570 ± 16	*15%*	816 ± 30	*15%*	1079 ± 21	*42%*			1968 ± 46	*21%*		
Gwai	243 ± 11	*4%*	589 ± 12	*19%*			1064 ± 23	*17%*			2028 ± 40	*29%*	2606 ± 52	*31%*
Upper Zambezi			593 ± 11	*33%*			987 ± 20	*34%*			1905 ± 46	*24%*	2578 ± 103	*9%*
Kafue	230 ± 13	*3%*	616 ± 22	*11%*			1035 ± 12	*79%*			1866 ± 87	*5%*	2579 ± 205	*2%*
Luangwa			550 ± 15	*20%*	717 ± 39	*8%*	1066 ± 17	*54%*	1530 ± 76	*8%*	1998 ± 82	*10%*		
Sangara							1061 ± 8	*100%*						
Mufa			559 ± 19	*13%*	754 ± 50	*12%*	1002 ± 14	*75%*						
Mazowe			555 ± 14	*14%*	844 ± 10	*57%*							2518 ± 41	*29%*
Luenha			529 ± 18	*12%*	831 ± 12	*58%*							2529 ± 49	*30%*
Morrunguze							1030 ± 18	*100%*						
Shire			564 ± 8	*46%*			1022 ± 13	*54%*						
Lower Zambezi			597 ± 15	*17%*			1013 ± 11	*72%*			1851 ± 82	*6%*	2522 ± 91	*5%*
Lower Zambezi			587 ± 11	*21%*			1039 ± 12	*49%*			1878 ± 35	*22%*	2545 ± 42	*8%*
Zangue			560 ± 18	*55%*			1036 ± 42	*33%*			1926 ± 197	*6%*	2676 ± 274	*6%*
Praia da Madal	272 ± 14	*4%*			686 ± 27	*21%*	1044 ± 15	*56%*			1998 ± 53	*17%*	2558 ± 72	*2%*

Table 6.5. U-Pb Age Peaks (Peak) of Detrital Zircons and Relative Frequencies (Freq.) in Modern Sands of the Zambezi Catchment. Ages and frequencies are calculated with Density Plotter (Vermeesch 2012). To treat all samples equally and avoid bias in intersample comparison, the laser spot was always placed blindly in the center of zircon grains.

6.7.9 Zircon Fertility

The joint consideration of petrographic, mineralogical, and geochemical data sets offers not only a panorama of compositional signatures but also useful information to evaluate the zircon fertility of sediment sources (e.g., diverse tributary catchments in the Zambezi drainage system), which is required for a correct use of zircon age data in the calculation of provenance budgets. Ultradense zircon is invariably segregated in the fine tail of the size distribution of each sample deposited by a tractive current and can be strongly concentrated locally by selective entrainment processes (Garzanti et al. 2008, 2009). These issues may hamper the accuracy of fertility determinations based on mineralogical or geochemical data (Malusà et al. 2016). In the presented sample set, sands from the upper part of the Zambezi catchment have a notably lower concentration of zirconium (Zr is 232 ppm in one trunk-river sample but otherwise invariably below the UCC standard and mostly in the 30–80-ppm range) than in the Middle and Lower Zambezi catchments (between 330 and 600 ppm in Kafue and Mufa samples, and also above the UCC standard for the Middle Zambezi, Luenha, and Shire samples). Zircon concentration, calculated by combining petrographic and heavy-mineral point-counting data, is markedly lower in the Uppermost to Upper

Zambezi catchment (median of bulk sand in volume is 0.02%, with a maximum of 0.2%) than in the Middle to Lower Zambezi catchment (median is 0.16% and maximum 0.6% for Shire sand). A most useful parameter to detect hydraulically controlled concentration of denser minerals is the weighted average density of terrigenous grains (in g/cm^3; the SRD [source-rock density] index of Garzanti and Andò 2007b), which for each sample should be equal to the weighted average density of source rocks in the ideal absence of environmental bias. The SRD index of most sands in rivers on the Kalahari Plateau ranges between 2.65 and 2.68 (just a little higher than quartz density), increasing to 2.79 and to 2.90 for Masuie and Matetsi sands containing, respectively, 50% and 70% detritus from dense basaltic rocks. In the Middle to Lower Zambezi catchment, SRD mostly ranges between 2.7 and 2.8, which matches the expected density range for upper to middle crustal basement rocks (Garzanti et al. 2006). The finer-grained Kafue (SRD: 2.79) and Luenha (SRD: 2.78) sands are richest in elements preferentially hosted in ultradense minerals (Fig 6.8). Luenha sand has high LREE and Th contents and negative LOI but only moderately high Zr, indicating concentration of ultradense monazite and magnetite but only moderately high zircon content (0.16% of bulk sand in volume). The higher SRD values observed for Shire (2.82) and Morrunguze (2.87) sands reflect contribution from high-grade and largely mafic basement rocks of the Blantyre and Tete domains (Goscombe et al. 2020). Ultradense garnet, zircon, monazite, and opaque Fe-Ti-Cr oxides have been markedly concentrated by selective entrainment processes only in Lower Zambezi sample S5778 (SRD 3.34), a fluvial garnet placer not analyzed for either geochemistry or zircon geochronology. Petrographic, heavy-mineral, and geochemical data converge to indicate that the zircon concentration in the samples provides a broadly reliable indication of zircon fertility in the corresponding catchments. Zircon fertilities are estimated to range from 0.02% for Kalahari dune sands to 0.2% for midcrustal basement rocks exposed in the Lower Zambezi catchment.

6.8 Provenance Budgets and Erosion Patterns

6.8.1 Provenance Budgets

In this section, independent calculations based on elemental geochemistry and Nd isotope and geochronological data are used to better constrain the rough provenance budget based on detrital modes. Integrated compositional data indicate that Upper Zambezi sand and silty sand delivered to Lake Kariba consist of ≥80% recycled quartz-rich Kalahari dunes and 16% ± 4% largely basaltic volcanic detritus, the remaining ≤5% being derived from Precambrian basements exposed in Zambia and Zimbabwe. The age spectrum of zircon

grains supplied by the Upper Zambezi to Lake Kariba is intermediate between those of Uppermost Zambezi and Kwando sands. These two river branches are thus revealed as the most prominent zircon sources, in a relative proportion that cannot be accurately determined because of the low and similar zircon concentration in their sands indicated by mineralogical and geochemical data (Table 6.2). Because sand generated in the Upper and Middle Zambezi catchments is trapped in Lakes Kariba and Cahora Bassa, all sand ultimately delivered to the delta (zircon grains included) is generated within the Lower Zambezi catchment. Petrographic and heavy-mineral data indicate contributions in similar proportions (ca. 30%–40% each) from the southern Irumide Province, drained upstream of the Luenha confluence, and the Mazowe-Luenha river system, sourced in the Zimbabwe Craton. The Umkondo Belt and the Karoo, Cretaceous, and Cenozoic extensional basins, drained by the Minjova, Sangadze, and Zangue tributaries, contribute much of the rest (~20%), whereas supply from the Tete and Blantyre domains, drained respectively by the Morrunguze and Shire tributaries, is subordinate (≤10% each). New complementary information obtained from elemental geochemistry suggests that as much as 70% of Lower Zambezi sand may be supplied by the Mazowe-Luenha river system, with subordinate contribution from the main stem upstream of the Zambezi-Luenha confluence (20%–25%) and minor supply from the Morrunguze and Shire Rivers (<5% each) and other lowermost-course tributaries (~5%). Calculations based on ε_{Nd} values of sand (63–2000-μm fraction) confirm that most Lower Zambezi sand is generated in the Mazowe-Luenha catchment (55%–65%), with subordinate contributions from the main stem upstream of the Luenha confluence and other sources. The ε_{Nd} values of cohesive mud (<32 μm fraction) in the Lower Zambezi upstream of the delta are similar to or more negative than those for sand (Table 6.4). This indicates that the contribution from the Mazowe-Luenha river system is certainly not lower, and is probably higher, for mud than for sand. Forward-mixing calculations based on zircon age data suggest that at least half of the zircon grains are derived from the Irumide domain, that a quarter, at most, are generated in the Mazowe-Luenha catchment, and that a fifth, at most, are generated in the final part of the Zambezi drainage basin, with a minor contribution from the Shire River. Because mineralogical and geochemical data indicate a relatively high zircon fertility for the Shire catchment, all compositional information converges to indicate that the Shire River supplies only a very small part (<5%) of the sediment to the Zambezi Delta. This holds true also for mud, because the smectite/kaolinite ratio increases sharply downstream of the Lower Zambezi, whereas Shire mud contains abundant kaolinite and minor smectite (Table 6.3). Minor

sediment supply from the Shire River is explained by sequestration in Lake Malawi of all sediment generated in the upper catchment and by further sediment trapping in wetlands and artificial reservoirs downstream (Mzuza et al. 2019). This inference contrasts with the findings of Just et al. (2014), who reckoned that the Shire River contributes ~28% of total Zambezi sediment load at present (~21% before construction of the Cahora Bassa Dam).

6.8.2 Weighing Up Informations

Provenance budgets based on independent data sets and on diverse size fractions are not entirely consistent. Age spectra of detrital zircons point at predominant zircon supply from the Irumide domain exposed in the upper part of the Lower Zambezi catchment, with minor zircon contribution from the Zimbabwe Craton, drained by the Mazowe and Luenha Rivers. Instead, elemental geochemistry and Nd isotope data suggest that most Lower Zambezi sediment is generated in the Mazowe-Luenha catchment. Although the robustness of diverse sets of calculations is not easily evaluated, it notably increases if end-member signatures are well distinct, precisely determined, and have little variability dependent on grain size, weathering, or hydraulic sorting. Conversely, estimates obtained on a narrow grainsize window or, worse, on a rare mineral within a narrow grain-size window, are least likely to be representative and accurately extrapolated to the entire sediment flux (Vezzoli et al. 2016). In the case of Lower Zambezi tributaries draining medium-/high-grade crystalline basements, sand petrography, heavy-mineral, and elemental geochemistry signatures show significant overlap and hydrodynamically controlled variability. Least robust are calculations based on zircon age spectra, because of the uncertainties involved in zircon fertility determinations. Nd isotope geochemistry suffers from a limited number of analyzed samples, but the end members are well distinct and precisely defined, all grain sizes have been considered, and grain size–dependent variability is limited (Fig 6.16). The change toward much more negative ε_{Nd} documented in all size fractions of Lower Zambezi sediments downstream of the Luenha confluence cannot be ascribed to Shire sediments, which yielded even less negative ε_{Nd} values for all size fractions (Fig 6.7), but clearly indicates major sediment supply from the Mazowe-Luenha River system. Weighing up all obtained information, we conclude that up to two-thirds of the sediment reaching the Zambezi Delta at present is generated in the Mazowe-Luenha catchment, between a quarter and a third between Lake Cahora Bassa and the Zambezi-Luenha confluence, and the rest downstream, with a very limited supply (≤5%) from the Shire River.

6.8.3 Erosion Patterns

Because of a general lack of gauged sediment loads, Zambezi sediment fluxes are evaluated with large uncertainties of a full order of magnitude. Erosion patterns across the catchment can thus be only grossly determined. On the basis of available sediment concentration data and sediment transport models, two end-member domains can be distinguished by their contrasting geomorphological conditions and sediment-generation modality: the low-relief Kalahari Plateau largely covered by eolian sand in headwater regions and the rugged igneous and metamorphic terranes extensively exposed between Victoria Falls and the Mozambican lowlands. On the plateau, rivers with low channel steepness sluggishly flow for large tracts through wetlands, where sediment is sequestered rather than produced, as in the Barotse floodplain and Chobe marshes on the main stem or the Machili and Kafue Flats traversed by the Kasaya, Ngwezi, and Kafue tributaries. Because data on Kwando sediment load are, to the best of our knowledge, unavailable, information from the Okavango River, similarly draining entirely within the Kalahari Basin in Angola (Shaw and Thomas 1992; McCarthy et al. 2012), allows us to broadly constrain the annual sediment yield and erosion rate in the Kalahari Basin as 2 ± 2 tons/km^2 and 0.001 ± 0.001 mm, respectively. This is notably lower than estimates based on cosmogenic nuclides for the Uppermost Zambezi catchment, including Precambrian terranes in the north (16 ± 2 tons/km^2 and 0.006 ± 0.001 mm; Wittmann et al. 2020). Sediment yield increases by an order of magnitude where channel steepness reaches very high values, as in basaltic gorges downstream of Victoria Falls (40–90 tons/km^2; Fig 6.3). A similar sediment-generation pattern characterizes other rivers flowing on the Kalahari Plateau in the headwaters and plunging into bedrock gorges downstream. For the Gwai River, a provenance budget based on petrographic, heavy-mineral, and geochemical data on both fluvial bar and levee silty sands indicates that sediment yield and erosion rate are between 20 and 50 times higher in the lower course cutting steeply across the Dete-Kamativi Inlier of the Magondi Belt than in the upper course sourced in the Zimbabwe Craton and draining the Kalahari Basin. The same may hold true for the Kafue River, where much of the sediment is, however, trapped in the Kafue Flats and behind the Itezhi-Tezhi and Kafue Gorge Dams. Annual yields of 150 ± 50 tons/km^2, corresponding to erosion rates of 0.06 ± 0.02 mm, were estimated for Middle and Lower Zambezi tributaries flowing steeply across basement rocks exposed in the Archean Zimbabwe Craton or the Proterozoic lrumide, Umkondo, and Zambezi Belts of southern Zambia, northeastern Zimbabwe, and western Mozambique, respectively (Bolton 1984; Ronco et al. 2010). Considering that the Lower Zambezi upstream of the

Luenha confluence and the Mazowe-Luenha river system have similar catchment areas, the provenance budget implies sediment yields and erosion rates between 1.5 and 2.5 times higher in the latter. Extensive sediment trapping in Lake Malawi upstream and across wetlands or behind dams downstream (Mzuza et al. 2019) prevents us from making considerations concerning erosion rates in the Shire catchment. Comparing these results with the long history of sediment fluxes needs to consider the exhumation rates of southern Africa and the evolution of the Zambezi catchment. Walford et al. (2005) identified three periods of high sediment flux in the Zambezi catchment area. The first occurred in the Late Cretaceous and coincided with a period of denudation in southwestern Africa, as indicated by apatite fission track data (Gallagher and Brown, 1999). The second increase in sediment flux occurred during the Oligocene, following a period of sediment starvation in the Paleocene and Eocene. The third increase took place during the Late Miocene to the present, due to the expansion of the catchment area. Sediment yield is calculated considering a broad increment of the Zambezi catchment (Cretaceous = 0.31×10^6 km^2; Paleocene–Pliocene= 0.70×10^6 km^2; Pleistocene =1.40×10^6 km^2) showing an increase in the Late Cretaceous of ~30 tons/km^2 (with a large uncertainty error), the Oligocene had a yield of ~15 tons/km^2, and the Late Miocene to the present had a yield of ~10 tons/km^2 (Walford et al., 2005). Apatite fission track data also indicate that during the Early Cretaceous, regional uplift led to increased erosion rates of around 0.095 mm, which later slowed to a rate of about 0.014 mm (Brown et al., 2002), similar to the present-day erosion rate in the Middle and Lower Zambezi region. Combining this information with the mineralogical segmented nature of the Zambezi route could grant us the possibility to observe which portion of the catchment was affected by each denudation pulse. The comprehensive characterization of the Zambezi routing system discloses peculiar "provenance fingerprints" that can be traced in space and time. A future extensive study on the sediment signal transferred and stored in the Zambezi Delta and Zambezi Fan may test if changes in erosion rates over longer time scales have affected different tectonic domains, or have been influenced by regional exhumation and climatic factors.

6.8.4 The Final Signature of Zambezi Sand

The Zambezi River carries to the Indian Ocean quartzo-feldspathic sand, a fingerprint that has hardly an equivalent among the world's big rivers (Potter 1978; Garzanti 2019a). Such a composition compares with that of granitoid-derived sand generated in dry southern California (Dickinson 1985) and represents a typical mark of dissected continental block

subprovenance. Shire sand is the richest in feldspars and thus a good example of "ideal arkose" (Dickinson 1985). Vast river catchments typically embrace a very wide range of rocks produced in different geodynamic settings at different times. Their sediments are thus mixtures of different provenances including a considerable fraction of recycled grains. Lower Zambezi sand, characterized by feldspar ≈ quartz, very few aphanite lithics, and a rich hornblende dominated tHM suite largely shed first-cycle from plutonic and high-grade metamorphic rocks, represents an anomaly in this respect. One main reason, discussed further below, is that quartz dominated sand recycled in the upper reaches is not transferred to the lower course. Detritus reaching the Indian Ocean is thus generated mostly in eastern Zimbabwe, central Mozambique, and southern Malawi, where the roots of Archean cratons and Proterozoic orogens have been uplifted and progressively eroded during the southward propagation of the East African rift (Fernandes et al. 2015). Consequently, sand composition is the same as detritus shed from midcrustal basement rocks exposed along actively uplifted and deeply dissected rift shoulders, such as those flanking the Red Sea (Garzanti et al. 2001, 2013a), rather than that expected for a mature passive margin.

6.8.5 Broken Transmission of Provenance Signals: The Anthropogenic Effect

One main reason why traditional petrological models apply so badly to the Zambezi is the pronounced segmentation of the fluvial system, which reflects its multistep Neogene evolution finally fixed by man's construction of Kariba and Cahora Bassa dams. Development of the Zambezi River is held to have started by headward erosion operated by a coastal river that captured first the Luangwa River and next the Kafue River after reincision of the Cahora Bassa and Gwembe troughs upstream. Only sometime around the early Pleistocene was the gentle-gradient Upper Zambezi captured as well, finally linking the Kalahari Plateau with the Indian Ocean via Victoria Falls (Moore et al. 2007). Rim basins such as the Mega-Kalahari represent huge reservoirs of quartz-rich polycyclic sand stored in continental interiors. Such reservoirs may be tapped by headward-eroding coastal rivers that progressively enhance their discharge as larger segments of endorheic drainage are captured, a process continuing today with incipient piracy of the Okavango (Moore and Larkin 2001). The undissected continental block (craton interior) subprovenance signal carried by the Upper Zambezi, however, fails to be transmitted beyond Lake Kariba. In the same way, the transitional continental block subprovenance signal carried by the Middle Zambezi fails to be transmitted downstream of Lake Cahora Bassa. The Lower Zambezi thus carries a pure dissected continental block (basement uplift) subprovenance signal to

the Indian Ocean, the same that the coastal proto-Zambezi would have had before starting its inland expansion, punctuated by the progressive capture of interior drainage. River segmentation was far less pronounced before man's intervention, as indicated by the poor compositional match between the present Lower Zambezi sand and upper Quaternary offshore sediments, which have notably higher Q/F ratio and a little more clinopyroxene. Such differences cannot be dismissed as a grain-size effect because the Q/F ratio typically increases with increasing grain size and the river samples are very fine to fine sands, whereas offshore samples are sandy silts. Rather than additional contribution by longshore-drifting sediment from outside the Zambezi delta, the plausible explanation is that a larger amount of detritus generated in the upper and middle catchment reached the ocean before closure of Kariba and Cahora Bassa dams. Forward-mixing calculations allow us to estimate that, before the Anthropocene, as much as 40% of detritus transferred to the coast was generated by erosion of Phanerozoic covers (~35% recycled from pure quartzose sand or sandstone and ~5% from basalt). Quartz-rich sand and sandstones and Karoo lavas are widespread in the Zambezi catchment, from Ngonye Falls in the Uppermost Zambezi to the lowermost course. The pre-Anthropocene contributions from the Upper or Middle Zambezi are therefore hard to accurately quantify, although the sharp mineralogical contrast between Upper Zambezi and offshore sediments indicates that most detritus was derived from the middle–lower reaches even in pre-Anthropocene times (figs. 6.14A, C).

6.9 Conclusions

Any compositional parameter is invariably controlled by multiple physical and chemical processes that must be carefully evaluated before provenance and environmental information can be correctly detangled and understood. Diverse data sets obtained by a range of independent methods were thus integrated to constrain the many unknowns, reduce the number of potential alternative solutions, and increase the plausibility of the suggested inferences. Following this rationale, this work of thesis applied a spectrum of mineralogical, geochemical, and geochronological techniques to shed light on sedimentary processes active in the complex Zambezi big-river system. In this study, such an approach allowed us to (1) characterize the composition of mud and sand generated in, and transported across, the Zambezi drainage basin; (2) monitor the evolution of compositional signals across a routing system rigidly segmented by both natural (tectonic depressions, lakes, wetlands) and anthropic (large reservoirs trapping all sediment generated upstream) factors; (3) make inferences on sediment yields and erosion rates even with a lack of gauged

sediment fluxes. To assess the intensity of weathering and the origin of weathering signatures (i.e., present vs. recycled) in diverse parts of the vast catchment we need to compare the results with the one of the Kalahari Desert and will be discussed in Chapter 7. Sand in the Uppermost Zambezi is pure quartzose and almost entirely recycled from desert dunes across the Kalahari Plateau, thus matching the theoretical sediment composition produced in cratonic interiors (undissected continental block subprovenance). At the opposite end of both the drainage basin and the petrologic spectrum of sediment shed from continental blocks, sand of the Lower Zambezi and many of its major tributaries is quartzo-feldspathic, even reaching an "ideal arkose" composition (dissected continental block subprovenance). Sand of the Middle Zambezi and its major tributaries has an intermediate feldspatho-quartzose composition (transitional continental block subprovenance).

The age spectra of detrital zircons reflect the major episodes of crustal growth in Precambrian southern Africa. Irumide ages are dominant in the Lower Zambezi and in most of its tributaries, excepting the Shire and the Zangue Rivers, where Pan-African ages prevail. Neoarchean ages characterize the Gwai, Mazowe, and Luenha Rivers, sourced in the Zimbabwe Craton. Eburnean ages are widely distributed but never prevail. Permian–Triassic (Karoo) ages are minor and Cretaceous ages rare. Smectite is the most widespread clay mineral, dominant in mud from Karoo basalts, as in the warm and poorly drained Mozambican lowlands characterized by equatorial/winter-dry climate. Illite is prevalent locally (e.g., Kafue mud), and kaolinite is ubiquitous, reaching maximum abundance in both the uppermost and lower parts of the Zambezi catchment. Elemental geochemistry reflects overwhelming quartz addition by recycling of Kalahari dune sand in the Uppermost Zambezi, local supply from Lower Jurassic Karoo basalt in the Upper Zambezi, and chiefly first-cycle provenance from Precambrian basements in the Lower Zambezi. The ε_{Nd} values range from mildly negative for sediment derived from Stenian gabbro, Tonian mafic granulite, and Jurassic basalt to strongly negative for sand derived from Neoarchean cratonic gneiss. The preferential concentration of ultradense monazite in the fine tail of the size distribution, owing to the settling-equivalence effect, controls the intrasample ε_{Nd} variability among cohesive-mud (<32 μm), very coarse silt (32–63 μm), and sand (63–2000 μm) fractions as well as deviations from the theoretical relationships between ε_{Nd} and $T_{Nd,DM}$ model ages, suggesting that durable monazite carries a more negative ε_{Nd} signal than other REE-bearing minerals (e.g., allanite, titanite, apatite, epidote, and amphibole). Elemental and isotope geochemistry reveals that 55%–65% of mud and sand reaching the Zambezi Delta today, after the construction of the Kariba and Cahora Bassa Dams, is

generated in the Mazowe-Luenha catchment. The contribution from Irumide terranes exposed upstream of the Luenha confluence is subordinate, and supply from the Shire River, the outlet of Lake Malawi, is minor. Although an accurate assessment of sediment yields and erosion rates is hampered by the lack of gauged sediment fluxes, annual estimates are lower by an order of magnitude on the Kalahari Plateau (10–20 tons/km^2 and ~0.005 mm) than in rugged terranes exposing Precambrian basements downstream (100–200 tons/km^2 and ~0.05 mm). In conclusion the thorough investigation of each part of the river catchment and the precise definition of the mineralogical correspondence between parent rocks and daughter sediments is indispensable to forge a key able to unlock the sedimentary archives represented by the thick stratigraphic successions accumulated throughout the late Mesozoic and Cenozoic in onshore and offshore basins and thus reconstruct with improved robustness the complex history of the Zambezi River.

The relative abundance of durable quartz and ZTR minerals thus decreases steadily along the sediment-routing system, a trend that denies the naive but still popular idea that sediment "matures" with transport distance. Although enhanced by the artificial segmentation of the river course after the closure of the Kariba and Cahora Bassa dams that prevented the continuity of sand transport across the reservoirs, such a downstream trend toward less durable mineralogical assemblages is primarily a natural phenomenon reflecting the dynamic uplift of the low-relief plateau of cratonic central southern Africa in the upper reaches and polyphase, ongoing rift-related rejuvenation of Precambrian mobile belts in the middle and lower reaches.

Chapter 7: Zambezi River interaction with the Kalahari Desert

The petrographic and mineralogical changes documented along the Zambezi sediment-routing system allow some considerations of consequence concerning his interaction with Kalahari Desert. In particular, it demonstrates that the interaction between a big river system with one of the largest reservoirs of recycled sediments on Earth may lead to wrong tectonic and climatic considerations based on sediment composition. The direct observations of mineralogical and provenance signature is of major importance to unveil the complexities of the present day routing system where recycled sediments from the Kalahari remains visible far downstream with their peculiar signature of weathering.

7.1 Do Minerals "Mature" during Fluvial Transport?

A widely held belief in sedimentary petrology, persistent although long demonstrated untrue (e.g., Russell 1937; Shukri 1950) , is that chemically and mechanically durable minerals must increase at the expense of unstable and less resistant minerals during long-distance fluvial transport. Uppermost Zambezi sand consists almost entirely of quartz associated with the most durable heavy minerals zircon, tourmaline, and rutile, thus representing a good example of "highly mature" sediment (Folk 1951; Hubert 1962). Downstream in the Upper Zambezi, however, mafic volcanic rock fragments increase and clinopyroxene becomes first a significant, then the main, and finally the nearly exclusive transparent heavy mineral. The progressive downstream increase of detritus derived from Karoo lavas, locally including unstable olivine, results in decreasing the degree of "maturation" downstream. Decreasing "maturity" with transport distance is not unusual in modern rivers wherever less durable detrital components are added downstream, as observed for instance along the Kagera River in equatorial Africa (Garzanti et al. 2013b). In the Middle Zambezi, sand is notably enriched in feldspars and diverse types of rock fragments supplied by the Kafue and other tributaries draining both Precambrian orogenic belts and Permo-Triassic rift-basin fills. Composition thus becomes progressively less "mature." In the Lower Zambezi, owing to prominent supply from local tributaries draining midcrustal Precambrian basements, quartz content decreases further, becoming equally or even less abundant than feldspar. The Zambezi is thus an exemplary case of a sediment-routing system along which the ratio between stable and unstable minerals (too often inappropriately portrayed as degree of "maturity"; Garzanti 2017) decreases steadily with

distance. Although enhanced by the artificial segmentation of the river course after the closure of the Kariba and Cahora Bassa dams, preventing the continuity of sand transport across the reservoirs, such a trend toward less durable mineralogical assemblages downstream is primarily a natural phenomenon reflecting the multistep evolution of the river and location of erosional foci (fig. 9). The Zambezi progressively connected stepwise the broad low-relief southern Africa plateau underlain by thick cratonic crust and sustained by dynamic uplift since mid-Cenozoic times (Lithgow-Bertelloni and Silver 1998; Moore et al. 2009a; Flügel et al. 2018) with the middle and lower reaches, entrenched in Karoo rifts and cutting across Precambrian mobile belts rejuvenated by the southward propagation of the East African rift in the late Neogene (Roberts et al. 2012; Hopper et al. 2020). If we just look at the compositional signature of Lower Zambezi sand and uncritically apply traditional ideas of "maturity," disregarding the character and history of the catchment, then we would falsely infer a scenario similar to Red Sea shoulders, involving short fluvial transport from locally uplifted rift highlands. The largest river sourced in the heart of cratonic southern Africa would be left unseen.

7.2 Weathering versus Recycling

7.2.1 Insights from Clay Minerals

Clay mineralogy is quite sensitive to weathering conditions. It has long been observed that kaolinite is abundant in hot humid regions where feldspar hydrolysis is intense, whereas smectite is common in warm regions with a dry season characterized by intense evaporation, and illite and chlorite dominate where chemical weathering is minor (Chamley 1989; Velde 1995). In modern sediments, the ratio between kaolinite and illite + chlorite (Kao/(Ill + Chl)) may thus be used as a proxy for weathering intensity (Liu et al. 2007; He et al. 2020). Within the Zambezi sample set, kaolinite is significant in all catchments and represents ~40% of the clay mineral assemblage in Uppermost Zambezi, Lower Zambezi (Tete sample), and Shire muds (Fig 6.6). The Kao/(Ill + Chl) ratio is >> in Uppermost Zambezi, Kwando, Ngwezi, and upper Gwai muds generated on the Kalahari Plateau but 1 in Middle and Lower Zambezi tributaries downstream (Table 6.3).

7.2.2 Insights from Mud and Sand Geochemistry

Geochemical indices have long been used as proxies for weathering intensity (Nesbitt and Young 1982; Price and Velbel 2003), although they may be even predominantly controlled by grain size (von Eynatten et al. 2012, 2016), provenance (Garzanti and Resentini 2016; Dinis et al. 2017), hydraulic sorting, or quartz addition by recycling (Fig 7.1). This is

especially true for sand, and weathering conditions are thus better reflected in the geochemistry of mud (Dinis et al. 2020a). A most reliable indicator of weathering intensity is α^{Al}Na, which chiefly measures the progressive leaching of Na from the plagioclase lattice. The α^{Al}Na value decreases quite regularly from the Uppermost Zambezi and Kwando Rivers (21–22 for mud, ≥4 for sand) to Victoria Falls (4.6 for mud, 2.1 ± 0.1 for sand) and the Middle and Lower Zambezi (4.6 ± 0.4 for mud, 1.2 ± 0.1 for sand). Other α^{Al} values, and consequently the CIA* and its several derivative indices, are more significantly affected by the mineralogy of sediment sources. Most evident is the anomaly of Kwando mud, which is notably enriched in Ca, Sr, Mg, and Ba derived from erosion of calcrete soils (Fig 7.1) and consequently, yields very low corresponding αAl indices (≤0.4). Masuie, Matetsi, and Morrunguze sediments largely derived from basaltic or gabbroic rocks have high Mg and Ca contents and consequently low α^{Al}Mg and α^{Al}Ca (0.4–0.6) (Table 6.2). Conversely, sediments derived from gneissic basements are enriched in K and Rb largely hosted in K-feldspar and mica, which explains why α^{Al}K and α^{Al}Rb are <1 in several tributaries (e.g., Kasaya, Ngwezi, Gwai, Kafue, Luangwa, Mazowe, Luenha, and Sangadze). Sangadze sediments have the lowest plagioclase/K-feldspar ratio of all analyzed sands from the Lower Zambezi catchment and consequently yielded the highest α^{Al}Na in both mud and sand, and the lowest α^{Al}K and α^{Al}Rb in sand.

7.2.3 Insights from Detrital Minerals

The differing chemical durability of heavy minerals is a reliably index of weathering intensity (Bateman and Catt 2007), whereas other mineralogical indexes may strongly be influenced by grainsize (Odom et al., 1976) or, as we have seen in the previous chapters, by recycling in deserts or hyperhumid environments (Garzanti et al., 2019). Particularly useful is the ratio between garnet (G) and other nesosilicates found in amphibole facies metapelites (SKAS =staurolite + kyanite + andalusite + sillimanite), which in sand of the Lower Zambezi catchment (G/(G+ SKAS) = 72% ± 21%) is the same as in modern first-cycle sand derived from metamorphic basements (G/(G+SKAS) = 70% ± 20%; Garzanti et al. 2010a). In contrast, the markedly anomalous low ratios (G/(G+SKAS) < 5%) that characterize sand in the Uppermost Zambezi catchment testify to an almost complete breakdown of garnet, a mineral that proves to be extremely vulnerable in equatorial soils (Garzanti et al. 2013c) but very durable in a dry tropical climate (Garzanti et al. 2015b). In recycled sand of the Kalahari Plateau, even zircon is selectively weathered out relative to quartz, as indicated by a zircon concentration lower by an order of magnitude than that of

first-cycle sand shed by Precambrian basement rocks in the Middle to Lower Zambezi catchment. Zircon depletion is chiefly ascribed to breakdown of preferentially weathered, strongly metamict old grains (Balan et al. 2001; Resentini et al. 2020).

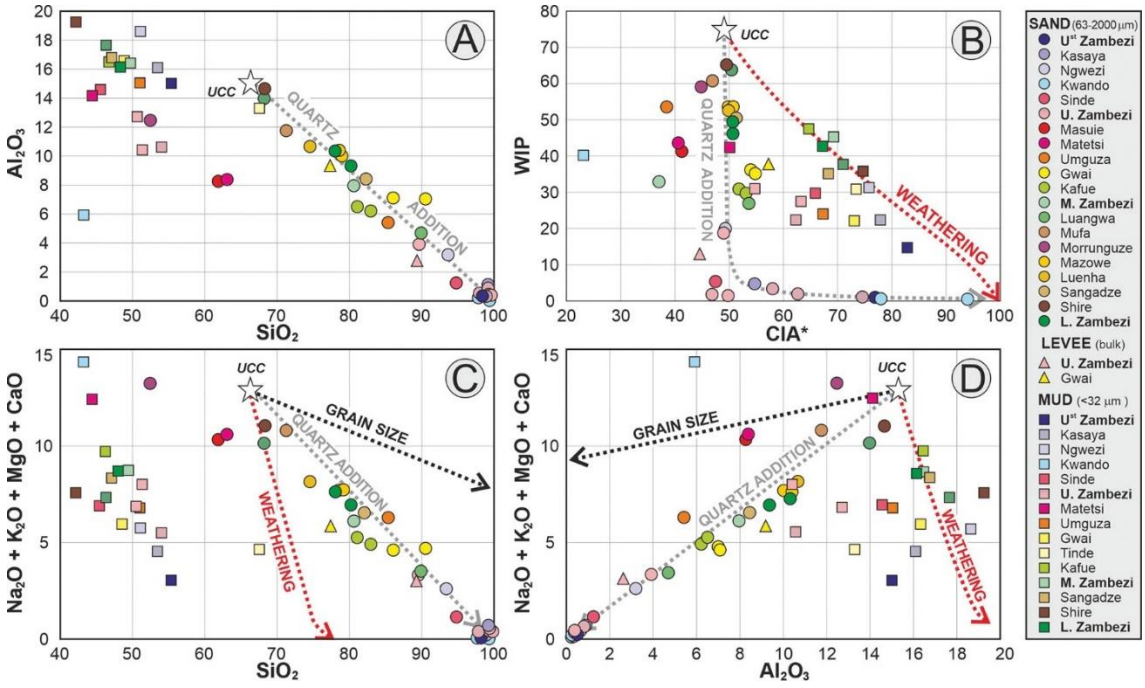

Figure 7.1 Discriminating the effects of weathering, recycling, and grain size from geochemical data. Theoretical trends are calculated starting from the UCC (upper continental crust) standard: the quartz-addition trend by progressively adding SiO_2, the weathering trend by progressively subtracting mobile metals relative to Si and Al. The grain-size trend is based on data from Alpine and Himalayan sediments (Garzanti et al. 2010a, 2011, 2012). In all four panels, sand follows the quartz-addition trend, reflecting recycling of Kalahari sands (Uppermost and Upper Zambezi catchments) or Karoo and older sandstones and metasandstones (Middle and Lower Zambezi catchments) to various degrees. Mud samples broadly follow the weathering trend. *A*, Samples plotting far below the regression line ($Al_2O_3=-0.45SiO_2+45Al_2O_3=-0.45SiO_2+45$) include Fe-rich Masuie and Matetsi sands from Karoo basalts and Kwando mud enriched in Ca, Sr, Mg, and Ba from calcrete soils. *B*, Uppermost (U^{st}) and Upper (U.) Zambezi muds plot below the weathering trend (low weathering index of Parker 1970 [WIP]), suggesting weathering signature inherited by recycling. CIA∗CIA* = chemical index of alteration. Middle (M.) and Lower (L.) Zambezi muds follow the theoretical trend, hinting at slightly increasing weathering intensity toward the coast. Calcrete erosion explains anomalously low CIA∗CIA* in Kwando mud. *C*, *D*, Cohesive muds collected upstream of Lake Kariba reflect quartz addition from Kalahari dunes (Uppermost Zambezi) or Neoproterozoic sandstones (Tinde).

7.2.4 Corrosion Features

Direct evidence of chemical weathering is provided by surficial dissolution textures on labile ferromagnesian minerals (Velbel, 2007). This approach, however, has drawbacks: (1) surficial features tell us the state of what is preserved but nothing about how much was

destroyed; (2) fresh and strongly weathered grains of the same detrital mineral commonly occur jointly (Van Loon and Mange 2007); and (3) slight degrees of corrosion might not be evaluated consistently by different operators. Only semiquantitative hints on the intensity of weathering can thus be obtained. With this aim, the percentage of surficially etched grains and the degree of corrosion were recorded for over 4000 identified transparent heavy minerals, following the classification of Andò et al. (2012). In the Uppermost Zambezi main stem and tributaries, pyroxene, amphibole, epidote, staurolite, kyanite, and andalusite are all mainly unweathered, a minority of grains are corroded, and only a few pyroxene grains are deeply etched. In the Upper Zambezi main stem and tributaries, most grains are unweathered, but the percentage of corroded grains increases, and both pyroxene and amphibole may be deeply etched. In the Middle Zambezi main stem and tributaries, the percentage of corroded heavy minerals increases further, a larger percentage of pyroxene and amphibole grains are deeply etched, and also epidote, garnet, or kyanite may show deep etching. Similar features characterize the Lower Zambezi main stem and tributary sands, where epidote and garnet are even more extesively corroded.

7.2.5 Recycled Weathering Signatures

In the Uppermost Zambezi and Kwando Rivers, sand consists of quartz and durable heavy minerals, with very low G=(G + SKAS) ratios and CIA* > 75; mud contains abundant kaolinite, CIA* is 180, and $a^{Al}Na$ is 120. Such compositional features, typical of sediment produced in a hot, humid equatorial climate, are at odds with the semiarid conditions of the Kalahari Plateau today. They testify to an intensity of chemical weathering that cannot occur in the present climatic regime but must have been inherited through multiple recycling from much wetter conditions of the past, most plausibly characterizing the subequatorial belt to the north (Chapter 4). Diagenesis during sedimentary cycles contributed too, but cannot account for all features (e.g. virtually complete selective breakdown of garnet). Weathered detritus from lower latitudes (~107S), for instance, was supplied to the Kalahari Basin by the onceconnected Chambeshi-Kafue river system, reaching the Uppermost Zambezi via the Machili Flats, as supported by fish lineages (Moore and Larkin 2001; Katongo et al. 2005).

Clay mineral assemblages in river muds across southern Africa are not kaolinite dominated, reflecting the limited efficiency of soil-forming processes and incomplete feldspar leaching under the present climatic conditions (Garzanti et al. 2014c). Kaolinite must thus be largely recycled from widespread relic lateritic paleosols and duricrusts (Partridge and Maud 1987;

Dill 2007; Moore et al. 2009b). Even in southern Malawi, where annual rainfall increases eastward from ~0.8 to 1.6 m at the foot of Mount Mulanje and 2.8 m at high elevation (3002 m above sea level), kaolinite is mostly recycled by fluvial incision of peneplains of Cretaceous–Cenonzoic age triggered by base-level lowering of the Shire River (Dill et al. 2005). This is corroborated by the great abundance of fresh feldspar in Shire sand (Fig. 6.5G), where inefficient plagioclase hydrolysis is testified to by undepleted Na and Ca ($\alpha^{Al}Na = \alpha^{Al}Ca = 1.0$). All mineralogical and geochemical parameters, including Kao/(Ill + Chl), CIA*, and $\alpha^{Al}Na$, would consistently indicate that the weathering intensity recorded in modern river sediments decreases downstream the Zambezi River. Even when depurated from the physical effect of recycling (i.e., quartz addition), mud generated in the Uppermost Zambezi catchment appears to be more affected by weathering than Middle and Lower Zambezi mud (Fig 7.1). Such evidence, however, by no means implies that weathering on the dry Kalahari Plateau is at present more intense than that in the wetter Middle to Lower Zambezi catchment. Rather, this trend reflects mixing of distilled polycyclic detritus originally generated during some wetter stages of the past to the north of the Kalahari dryland, with first-cycle detritus shed from Karoo basalts along the Upper Zambezi, followed by abrupt replacement, downstream of Lake Kariba first and of Lake Cahora Bassa next, by largely first-cycle detritus derived from Precambrian basements. Only in the Middle and Lower Zambezi, where detrital minerals are directly derived from basement rocks, do their surficial dissolution textures chiefly reflect present conditions of weathering. Together with trends displayed by cohesive mud (Fig 7.1B), these are the only features that document a slight increase in weathering intensity from the Middle to the Lower Zambezi catchment.

This effect of "recycled weathering" is enhanced by the segmentation of the Zambezi River, which allows to follow, along its course, the mixing of detritus, hereby proving that the remarkable storage of polycyclic sediment in desert environments can preserve fruitful climatic information. The erosion of dunes by major rivers enable later on the transport of huge amounts of sediment that can be transported to different and distal sedimentary systems, carrying along this inherited climatic data. The Kalahari-Zambezi interaction raises a warning in the study of sedimentary basins to carefully consider that the provenance signal of desert can induce wrong deduction of drainage source, but also climatic conditions.

Chapter 8: Conclusions

The presented thesis illustrates the provenance analysis on Sahara Desert, Kalahari Desert and Zambezi River with the aim of deciphering the relative interplay of wind and river transport in arid environment, of improving our knowledge on deserts formation and their climatic development and for the study of sediment mixing from different sources or long-term recycle. The presented datasets of petrographic, heavy mineral, detrital zircon U-Pb ages, geochemical and isotopic data represent a great complexity to be discussed, but also allows to balance and exclude provenance bias and the possibility to weight the overall framework of information.

The vast extension of Sahara Desert is contrasted by a remarkably homogeneous composition of dune sand, consisting almost everywhere of > 95% quartz and durable minerals such as zircon, tourmaline, and rutile. Zircon U-Pb dating does not allow to break this homogeneity, reflecting extensive recycling repeated through geological time after the end of the Neoproterozoic, indicated as the last major event of crustal growth in the region. This case study allows to emphasise that in provenance studies based on detrital-zircon ages alone, the assumption that observed age patterns reflect transport pathways existing at the time of deposition rather than inheritance from even multiple and remote landscapes of the past thus needs to be carefully investigated and convincingly demonstrated rather than implicitly assumed.

The compositional fingerprints of aeolian dune and river sands of Kalahari Desert allow to illustrate the key processes of fluvial-aeolian interactions across the sand seas. Composition of river and dune sediments are remarkably similar and reflect two active sedimentary processes. In Angola, Zambia, and over much of Botswana and parts of Zimbabwe and Namibia the sediment composition is homogeneously quartz-rich and ZTR-rich-heavy-mineral-poor; here the dominant process is dune erosion and transfer of the “desert signal” to the river system, as testified to by the amount of rounded quartz grains in river sediments, which allows the estimation of sediment contribution from dunes to bedload. In contrast, composition varies markedly only at the western and eastern edges of the erg, in the Damara Belt of central Namibia, in the Zimbabwe Craton or the Zambezi basaltic gorges near Victoria Falls, ranging from feldspar-rich feldspatho-quartzose and hornblende-rich to litho-quartzo-feldspathic and clinopyroxene-rich. This indicates partly first-cycle but largely polycyclic provenance from Mesoproterozoic crustal domains, Damara Belt, Nama and Karoo Groups close to the borders of Kalahari basin, with a more developed fluvial

network. In addition, in northern Kalahari dunefields adjacent to humid subequatorial regions, widespread monocrystalline quartz, commonly showing abraded overgrowths, combined with strongly depleted ZTR-rich heavy-mineral assemblages (lacking garnet but containing staurolite and kyanite), common kaolinite in river muds, and geochemical indices reveal that the sediments have undergone very extensive weathering in humid subequatorial climate before being stored into the erg. The composition of aeolian-dune sands thus reverberates the echo of paleo-weathering passed on to the present landscape through multiple recycling episodes.

The mineralogical composition of dunes and its variability across sand seas reflect the relative importance of fluvial and aeolian processes and reveal the type and degree of their interactions. Sand seas largely fed by fluvial sediments are typically characterized by partly first-cycle detritus including various amounts of diverse types of rock fragments, feldspars, and heavy minerals, generally allowing identification of a single dominant source. The opposite end member is represented by dunefields where sand is dominantly generated in situ from disaggregation of locally exposed rocks with high sand-generation potential (e.g., sandstones), and next reworked and homogenized by wind action during several sedimentary cycles driven by climate change. In these cases, sand typically bears a distilled homogenous composition consisting almost exclusively of mostly rounded monocrystalline quartz associated with an extremely poor tHM suite dominated by ZTR minerals.

The geographic distribution of such contrasting desert types is mainly controlled by precipitation in adjacent highlands fuelling fluvial discharge. In wind-dominated hyperarid deserts of the tropical belt, such as the Sahara or the Great Nafud in Arabia, river action may be weakened to the point that fluvial contribution to the dunes becomes insignificant. Conversely, dry river valleys are invaded by pure quartzose sand, thus erasing all local sources of mineralogical heterogeneity. Fluvial sources are instead readily identified in dunefields at the foot of high mountain areas, as in central Asia or Argentina. It can be inferred that the development and extension of river networks plays a crucial role in determining the mineralogy and provenance of desert regions around the world. The main factors that influence the presence of river routing systems in these areas are climate and tectonics. The Sahara Desert, for example, has a stable tectonic environment and extreme aridity, which promotes the recycling and stability of dune systems. On the other hand, the Kalahari Desert is located in a craton interior, but is affected more by variable climatic conditions. At the edges of the Kalahari, where recent geologic events have created tectonically active structures and stable river network, fresh sediment is more likely to be

transported to the dune system. This understanding of the roles of climate and tectonics in shaping desert environments can be useful for studying both present and past deserts.

The provenance study of Zambezi River system aims to investigate the composition of big rivers that flow across large dune fields to estimate the transport of sediment from large ergs to a passive margin. In this study, such an approach allowed us to characterize the composition of mud and sand generated in, and transported across, the Zambezi drainage basin; monitor the evolution of compositional signals across a routing system rigidly segmented by both natural (tectonic depressions, lakes, wetlands) and anthropic (large reservoirs trapping all sediment generated upstream) factors; make inferences on sediment yields and erosion rates even with a lack of gauged sediment fluxes; and to assess the intensity of weathering and the origin of weathering signatures (i.e., present vs. recycled).

All mineralogical and geochemical parameters consistently point to an intensity of chemical weathering on the Kalahari Plateau that cannot be related to modern dry-climate conditions. Chemical breakdown of virtually all minerals relative to quartz, including feldspars, garnet that is very labile in lateritic soils, and even zircon, if strongly metamict, cannot occur in the Kalahari dryland, where kaolinite is recycled. Kaolinite is mostly produced by fluvial incision of relic Cretaceous–Cenozoic paleosols even in the Shire catchment closer to the wetter Mozambican coast, where inefficient plagioclase hydrolysis is testified to by the dominance of fresh feldspars and undepleted Ca and Na. Indications of only slightly increasing weathering conditions in the Middle to Lower Zambezi catchment at present times are provided by mud geochemistry and surficial corrosion of pyroxene, amphibole, epidote, kyanite, and garnet. The relative abundance of durable quartz and ZTR minerals decreases steadily along the sediment-routing system, a trend that denies the naive but still popular idea that sediment “matures” with transport distance. Although enhanced by the artificial segmentation of the river course after the closure of the Kariba and Cahora Bassa dams that prevented the continuity of sand transport across the reservoirs, such a downstream trend toward less durable mineralogical assemblages is primarily a natural phenomenon reflecting the dynamic uplift of the low-relief plateau of cratonic central southern Africa in the upper reaches and polyphase, ongoing rift-related rejuvenation of Precambrian mobile belts in the middle and lower reaches. Based on all available information, it is believed that approximately 5-10 million tons (≤ 10%) of sediment are generated in the upper catchment and trapped in the Kariba reservoir, 50-60 million tons (60-65%) are generated in the middle catchment and trapped in the Cahora Bassa reservoir, and 20-25 million tons (25-30%) are generated in the lower catchment and

carried to the Zambezi Delta annually. These estimates suggest that less than a third of the original sediment flux is reaching the ocean today. This significant change can be further investigated by comparing the compositional signatures of modern Lower Zambezi fluvial sediments and pre-dam turbidites found in the deep sea, which will be the subject of future work.

Intracratonic sag basins such as the Kalahari, straddling the arid tropical belt, contain vast amounts of quartz-rich polycyclic sand. Whenever tectonic or climatic conditions favour the development of an integrated drainage system connecting the continental interiors with the coast, tapping into such a huge sediment reservoir may induce a sudden pulse of quartz-rich sand to the oceans and thus a significant mineralogical change in continental-embankment successions. Such an event, recorded in post-Tortonian sediments of the Zambezi Delta, may occur again in the future if development of the Okavango rift will lead to the incorporation of the entire Okavango River to the Zambezi drainage system.

8.1 Future work

This thesis demonstrates the importance of provenance studies in large deserts as a way to further understand the sedimentary processes in continental basins, which can either recycle and store sediment for extended periods of time, provide sediment to rejuvenated river network, or act as collectors of freshly-eroded sediment from exposed outcrops. One of the largest and least studied rivers in Africa, the Niger River, is of particular interest due to its interaction with the desert. The Niger River has its source in the wet region of Mali and flows through the Archean Core of the Man Shield before entering the Sahara near Timbuktu. It then turns south towards the Nigeria Basement before emptying into the Gulf of Guinea. Comparing the Niger River with the Zambezi dataset could provide insight into the erosion of dunes by rivers versus the supply of river bar sediments to the erg. Long-term sediment recycling sediments and zircon ages present a geological puzzle: how to deal with recycled ages? An area of increasing interest quantifying the time spend by sediment in a sedimentary basin. One possible approach could be to combine Zircon U-Pb ages with other mineral geochronometers, other could be disclosing information from the annealing stages of zircon lattice. As mentioned, future part of the work will also be focused on the Zambezi Fan turbiditic system to compare present-day river provenance signal, with Pleistocene sediments.

References

- Abdelhak, M., Ahmed, K., Abdelkader, B., Brahim, Z., Rachid, K., 2014. Algerian Sahara sand dunes characterization. Silicon 6, 149-154.
- Abdelkareem, M., El-Baz, F., 2015. Regional view of a trans-African drainage system. Journal of Advanced Research 6, 433-439.
- Abdelsalam, M.G., Liégeois, J.P., Stern, R.J., 2002. The Saharan Metacraton. Journal of African Earth Sciences 34, 119-136.
- Abdelsalam, M.G., 2018. The Nile's journey through space and time: A geological perspective. Earth-Science Reviews 177, 742-773.
- Abouchami, W., Boher, M., Michard, A., Albarede, F., 1990. A major 2.1 Ga event of mafic magmatism in West Africa: an early stage of crustal accretion. Journal of Geophysical Research: Solid Earth 95, 17605-17629.
- Aitchison, J., and Greenacre, M. 2002. Biplots of compositional data. J. R. Stat. Soc. C 51(4):375–392.
- Alessio, B. L.; Collins, A. S.; Clark, C.; Glorie, S.; Siegfried, P. R.; and Taylor, R. 2019. Age, origin and palaeogeography of the southern Irumide Belt, Zambia. J. Geol. Soc. Lond. 176(3):505–516.
- Al-Gamal, S.A., 2011. An assessment of recharge possibility to North-Western Sahara Aquifer System (NWSAS) using environmental isotopes. Journal of Hydrology, 398, 184-190.
- Al-Hafdh, N.M., El-Shaafi, A.E.S.S., 2015. Geochemistry and petrology of basic volcanic rocks of Jabal Al Haruj Al-Aswad, Libya. International Journal of Geosciences 6, 109-144.
- Al-Hajri, Y., White, N. and Fishwick, S., 2009. Scales of transient convective support beneath Africa. Geology, 37(10), 883-886.
- Allen, P. A. 2017. Sediment routing systems: the fate of sediment from source to sink. Cambridge, Cambridge University Press, 407 p.
- Altumi, M.M., Elicki, O., Linnemann, U., Hofmann, M., Sagawe, A., Gärtner, A., 2013. U–Pb LA-ICP-MS detrital zircon ages from the Cambrian of Al Qarqaf Arch, central-western Libya: Provenance of the West Gondwanan sand sea at the dawn of the early Palaeozoic. Journal of African Earth Sciences 79, 74-97.
- Andersen, T., Kristoffersen, M., Elburg, M.A., 2016. How far can we trust provenance and crustal evolution information from detrital zircons? A South African case study. Gondwana Research, 34, 129–148.
- Andersen, T.; Elburg, M. A.; van Niekerk, H. S.; and Ueckermann, H. 2018. Successive sedimentary recycling regimes in southwestern Gondwana: evidence from detrital zircons in Neoproterozoic to Cambrian sedimentary rocks in southern Africa. Earth-Sci. Rev. 181:43–60.
- Andò, S., 2020. Gravimetric separation of heavy-minerals in sediments. Minerals 10(3), 273, doi:10.3390/min10030273.
- Andò, S.; Garzanti, E.; Padoan, M.; and Limonta, M. 2012. Corrosion of heavy minerals during weathering and diagenesis: a catalog for optical analysis. Sediment. Geol. 280:165–178.
- Andò, S., Morton, A., Garzanti, E. 2014. Metamorphic grade of source rocks revealed by chemical fingerprints of detrital amphibole and garnet. In: Scott, R.A., Smyth. H.R., Morton, A.C., Richardson, N. (Eds.), Sediment provenance studies in hydrocarbon exploration and production. Geological Society London, Special Publication 386, 351-371.
- Arbuszewski, J.A., deMenocal, P. B., Cléroux, C., Bradtmiller, L., Mix, A., 2013. Meridional shifts of the Atlantic intertropical convergence zone since the Last Glacial Maximum. Nature Geoscience 6, 959-962.
- Avigad, D., Sandler, A., Kolodner, K., Stern, R. J., McWilliams, M., Miller, N., Beyth, M., 2005. Mass-production of Cambro–Ordovician quartz-rich sandstone as a consequence of chemical weathering of Pan-

African terranes: environmental implications. Earth and Planetary Science Letters 240, 818-826.

- Avigad, D., Gerdes, A., Morag, N., Bechstädt, T., 2012. Coupled U–Pb–Hf of detrital zircons of Cambrian sandstones from Morocco and Sardinia: implications for provenance and Precambrian crustal evolution of North Africa. Gondwana Research 21, 690-703.
- Bagnold, R.A., 1942. The physics of blown sand and desert dunes. Methuen & Co., Ltd., London, 265 p.
- Baillieul, T.A. 1975. A reconnaissance survey of the cover sands in the Republic of Botswana. J. Sediment. Petrol. 45:494-503.
- Baird, T., Bristow, C. S., Vermeesch, P., 2019. Measuring Sand Dune Migration Rates with COSI-Corr and Landsat: Opportunities and Challenges. Remote Sensing 11, 2423.
- Bakker, N.L., Drake, N.A., Bristow, C.S., 2019. Evaluating the relative importance of northern African mineral dust sources using remote sensing. Atmospheric Chemistry and Physics 19(16), 10525–10535.
- Balan, E.; Neuville, D. R.; Trocellier, P.; Fritsch, E.; Muller, J.-P.; and Calas, G. 2001. Metamictization and chemical durability of detrital zircon. Am. Mineral. 86:1025–1033.
- Banks, N. L.; Bardwell, K. A.; and Musiwa, S. 1995. Karoo Rift basins of the Luangwa Valley, Zambia. In Lambiase, J. J., ed. Hydrocarbon habitat in rift basins. Geol. Soc. Lond. Spec. Publ. 80:285–295.
- Barrat, J. A.; Keller, F.; Amossé, J.; Taylor, R. N.; Nesbitt, R. W.; and Hirata, T. 1996. Determination of rare earth elements in sixteen silicate reference samples by ICP-MS after Tm addition and ion exchange separation. Geostand. Newsl. 20(1):133–139.
- Barrat, J. A.; Zanda, B.; Moynier, F.; Bollinger, C.; Liorzou, C.; and Bayon, G. 2012. Geochemistry of CI chondrites: major and trace elements, and Cu and Zn isotopes: Geochim. Cosmochim. Acta 83:79–92.
- Basu, A., 2020. Chemical weathering, first cycle quartz sand, and its bearing on quartz arenite. Journal Indian Association of Sedimentologists 37(2), 3-14.
- Bateman, M.D., Thomas, D.S.G., Singhvi, A.K., 2003. Extending the aridity record of the Southwest Kalahari: current problems and future perspectives. Quaternary International 111, 37-49.
- Bateman, R. M., and Catt, J. A. 2007. Provenance and palaeoenvironmental interpretation of superficial deposits, with particular reference to post-depositional modification of heavy mineral assemblages. In Mange, M. A., and Wright, D. T., eds. Heavy minerals in use (Dev. Sedimentol., vol. 58). Amsterdam, Elsevier, p. 151–188.
- Bayon, G.; German, C. R.; Boella, R. M.; Milton, J. A.; Taylor, R. N.; and Nesbitt, R. W. 2002. An improved method for extracting marine sediment fractions and its application to Sr and Nd isotopic analysis. Chem. Geol. 187:179–199.
- Becker, T., Schreiber, U., Kampunzu, A.B., Armstrong, R., 2006. Mesoproterozoic rocks of Namibia and their plate tectonic setting. Journal of African Earth Sciences, 46, 112-140.
- Beiersdorf, H.; Kudrass, H. R.; and von Stackelberg, U. 1980. Placer deposits of ilmenite and zircon on the Zambezi Shelf. Geol. Jahrb. D36:5–85.
- Beilfuss, R., and dos Santos, D. 2001. Patterns of hydrological change in the Zambezi delta, Mozambique. Program for the Sustainable Management of the Cahora Bassa Dam and the Lower Zambezi Valley Working Paper no. 2. Baraboo, WI, Int. Crane Found., 159 p.
- Bertolini, G., Marques, J.C., Hartley, A.J., Da-Rosa, A.A., Scherer, C.M., Basei, M.A., Frantz, J.C., 2020, Controls on Early Cretaceous desert sediment provenance in south-west Gondwana, Botucatu Formation (Brazil and Uruguay). Sedimentology 67(5), 2672-2690.
- Bertrand, J.M.L., Caby, R., 1978. Geodynamic evolution of the Pan-African orogenic belt: a new interpretation of the Hoggar shield (Algerian Sahara). Geologische Rundschau 67, 357-388.
- Bhattachan, A., D'Odorico, P., Okin, G.S. and Dintwe, K., 2013. Potential dust emissions from the southern

Kalahari's dunelands. Journal of Geophysical Research: Earth Surface, 118(1), 307-314.

- Bicca, M. M.; Philipp, R. P.; Jelinek, A. R.; Ketzer, J. M. M.; dos Santos Scherer, C. M.; Jamal, D. L.; and dos Reis, A. D. 2017. Permian–Early Triassic tectonics and stratigraphy of the Karoo Supergroup in northwestern Mozambique. J. Afr. Earth Sci. 130:8–27.
- Bird, P., 1979. Continental delamination and the Colorado Plateau. Journal of Geophysical Research 84, 7561-7571.
- Birkett, C. M., 2000. Synergistic remote sensing of Lake Chad: Variability of basin inundation. Remote sensing of Environment 72, 218-236.
- Black, R., 1965. Sur la signification pétrogénétique de la découverte d'anorthosites associées aux complexes subvolcaniques du Niger. Comptes rendus de l'Académie des Sciences 260, 5829-5832.
- Black, R., Caby, R., Moussine-Pouchkine, A., Bayer, R., Bertrand, J.M., Boullier, A.M., Fabre, J., Lesquer, A., 1979. Evidence for late Precambrian plate tectonics in West Africa. Nature 278, 223-227.
- Blanchet, C. L., Osborne, A. H., Tjallingii, R., Ehrmann, W., Friedrich, T., Timmermann, A., Bruckmann, W., and Frank, M. 2021. Drivers of river reactivation in North Africa during the last glacial cycle. Nature Geoscience, 14(2), 97-103.
- Blanco, G.; Germs, G.J.B; Rajesh, H.M; Chemale, F.; Dussin, I.A.; and Justino, D. 2011. Provenance and paleogeography of the Nama Group (Ediacaran to early Palaeozoic, Namibia): petrography, geochemistry and U–Pb detrital zircon geochronology. Precambrian Res. 187:15-32.
- Blatt, H., 1967. Provenance determinations and recycling of sediments. Journal of Sedimentary Petrology 37, 1031-1044.
- Blenkinsop, T., and Moore, A., 2013. Tectonic geomorphology of passive margins and continental hinterlands, in Shroder, J.F. (ed.), Treatise on Geomorphology. Academic Press, San Diego, Vol. 5, pp. 71-92.
- Bolton, P. 1984. Sediment deposition in major reservoirs in the Zambezi Basin. In Walling, D. E.; Foster, S. S. D.; and Wurzel, P., eds. Challenges in African hydrology and water resources: proceedings of the Harare Symposium, July 1984. Int. Assoc. Hydrol. Sci. Publ. 144:559–567.
- Boniface, N., and Appel, P. 2018. Neoproterozoic reworking of the Ubendian Belt crust: implication for an orogenic cycle between the Tanzania Craton and Bangweulu Block during the assembly of Gondwana. Precambrian Res. 305:358–385.
- Boullier, A.M., Rocci, G., Cosso, N.Y., 1991. La chaîne pan-africaine d'Aouzegeur en Aïr (Niger): un trait majeur du bouclier Touareg. Comptes rendus Académie des Sciences de Paris 313, 63-68.
- Bouvier, A.; Vervoort, J. D.; and Patchett, P. J. 2008. The Lu-Hf and Sm-Nd isotopic composition of CHUR: constraints from unequilibrated chondrites and implications for the bulk composition of terrestrial planets. Earth Planet. Sci. Lett. 273:48–57.
- Breed, C.S., Fryberger, S.G., Andrews, S., McCauley, C., Lennartz, F., Gebel, D., Horstman, K., 1979. Regional studies of sand seas using Landsat (ERTS) imagery. A study of global sand seas. US Geological Survey, Professional Paper 1052, 305-397.
- Brenchley, P.J., Marshall, J.D., Carden, G.A.F., Robertson, D.B.R., Long, D.G.F., Meidla, T., Hints, L., Anderson, T.F., 1994. Bathymetric and isotopic evidence for a short-lived Late Ordovician glaciation in a greenhouse period. Geology 22, 295-298.
- Bristow, C.S., and Armitage, S.J., 2016. Dune ages in the sand deserts of the southern Sahara and Sahel. Quaternary International 410, 46-57.
- Bristow, C.S., Drake, N., Armitage, S., 2009. Deflation in the dustiest place on Earth: the Bodélé Depression, Chad. Geomorphology 105, 50-58.

- Brook, G.A., Cowart, J.B., Brandt, S.A., 1998. Comparison of Quaternary environmental change in eastern and southern Africa using cave speleothem, tufa and rock shelter sediment data. In: Alsharhan, G., Whittle, Kendall (Eds.), Quaternary Deserts and Climate Change. Balkema, Rotterdam, pp. 239–250.
- Brook, G.A., Scott, L. Railsback, L.B., Goddard, E.A., 2010. A 35ka pollen and isotope record of environmental change along the southern margin of the Kalahari from a stalagmite and animal dung deposits in Wonderwerk Cave, South Africa. Journal of Arid Environments 74, 870-884.
- Brown, R. W., Summerfield, M. A., & Gleadow, A. J., 2002. Denudational history along a transect across the Drakensberg Escarpment of southern Africa derived from apatite fission track thermochronology. Journal of Geophysical Research: Solid Earth, 107(B12), ETG-10.
- Bulambo, M.; De Waele, B.; Kokonyangi, J.; Johnson, S. P.; Kampunzu, A. B.; and Tembo, F. 2006. SHRIMP zircon U-Pb geochronology and geochemistry of the Choma-Kalomo Block granitoids (Zambia): geological implications. In Colloquium of African Geology, 21st (Maputo, Mozambique), Abstr., p. 26–27.
- Bullard, J.E., and Nash, D.J., 1998. Linear dune pattern variability in the vicinity of dry valleys in the south-west Kalahari. Geomorphology 23: 35-54. https://doi.org/10.1016/S0169-555X(97)00090-1
- Bullard, J.E., and Nash, D.J., 2000. Valley-marginal sand dunes in the south-west Kalahari: their nature, classification and possible origins. J Arid Environ 45: 369-383. https://doi.org/10.1006/jare.2000.0646
- Bullard, J.E., Thomas, D.S.G., Livingstone, I., Wiggs, G.F.S., 1995. Analysis of linear sand dune morphological variability, southwestern Kalahari dunefield Geomorphology 11, 189-203.
- Bultot, F., and Griffiths, J.W., 1972. The equatorial wet zone. In: Griffiths, J.W. (ed.), Climates of Africa. Elsevier, Amsterdam, World Survey of Climatology, vol. 10, pp. 259–311.
- Bumby, A.J., Guiraud, R., 2005. The geodynamic setting of the Phanerozoic basins of Africa. Journal of African Earth Sciences 43, 1-12.
- Burke, K., 1999. Tectonic significance of the accumulation of the voluminous early Paleozoic reservoir containing quartz-rich sandstones of North Africa and Arabia. Bulletin of the Geological Society Houston, 11-13.
- Burrough, S.L., and Thomas, D.S.G., 2008. Late Quaternary lake-level fluctuations in the Mababe Depression: Middle Kalahari palaeolakes and the role of Zambezi inflows. Quaternary Research, 69, 388–403.
- Burrough, S.L., Thomas, D.S. and Bailey, R.M., 2009a. Mega-Lake in the Kalahari: a Late Pleistocene record of the Palaeolake Makgadikgadi system. Quaternary Science Reviews, 28(15-16), 1392-1411.
- Burrough, S.L., Thomas, D.S. and Singarayer, J.S., 2009b. Late Quaternary hydrological dynamics in the Middle Kalahari: forcing and feedbacks. Earth-Science Reviews, 96(4), pp.313-326.
- Burrough, S.L., Thomas, D.S., Bailey, R.M. and Davies, L., 2012. From landform to process: Morphology and formation of lake-bed barchan dunes, Makgadikgadi, Botswana. Geomorphology, 161, 1-14.
- Burrough, S.L., Thomas, D.S.G. and Barham, L.S., 2019. Implications of a new chronology for the interpretation of the Middle and Later Stone Age of the upper Zambezi Valley. Journal of Archaeological Science: Reports, 23, 376-389.
- Butt, A. J., and Gould, K. 2018. 3D source-rock modelling in frontier basins: a case study from the Zambezi Delta Depression. Pet. Geosci. 24(3):277–286.
- Caby, R., Bertrand, J.M.L., Black, R., 1981. Pan-African ocean closure and continental collision in the Hoggar-Iforas segment, central Sahara. Precambrian Plate Tectonics 16, 407-434.
- Caby, R., Andreopoulos-Renaud, U., Pin, C., 1989. Late Proterozoic arc–continent and continent–continent collision in the Pan-African Trans-Saharan Belt of Mali. Canadian Journal of Earth Sciences 26, 1136-1146.
- Calamita, E.; Schmid, M.; Kunz, M.; Ndebele-Murisa, M. R.; Magadza, C. H.; Nyambe, I.; and Wehrli, B.

2019. Sixty years since the creation of Lake Kariba: thermal and oxygen dynamics in the riverine and lacustrine sub-basins. PloS ONE 14(11):e0224679. https://doi.org/10.1371/journal.pone.0224679.

- Capot-Rey, R., 1945. Dry and humid morphology in the Western Erg. Geographical Review 35, 391-407.
- Caracciolo, L., 2020. Sediment generation and sediment routing systems from a quantitative provenance analysis perspective: Review, application and future development. Earth-Science Reviews, 209, 103226.
- Carr, I.D., 2003. A sequence stratigraphic synthesis of the North African Mesozoic. Journal of Petroleum Geology 26, 133-152.
- Carroll, J.D., Chang, J.J., 1970. Analysis of individual differences in multidimensional scaling via an N-way generalization of Eckart–Young decomposition. Psychometrika 35, 283–319.
- Catuneanu, O.; Wopfner, H.; Eriksson, P. G.; Cairncross, B.; Rubidge, B. S.; Smith, R. M. H.; and Hancox, P. J. 2005. The Karoo basins of south-central Africa. J. Afr. Earth Sci. 43(1–3):211–253.
- CGMW-BRGM, 2016.Geological Map of Africa, 1:10 million scale. Thiéblemont, D. et al. (eds.), www.brgm.fr.
- Chamley, H. 1989. Clay mineralogy. Berlin, Springer, 623 p.
- Chanvry, E., Ando, S., Garzanti, E., Guillocheau, F., Dall'Asta, M., Beaufort, D. and Patrier, P., 2018. Impact of hinterland evolution in mineralogy of clastics sediments: first results from mineralogical analysis focus on the Zambezi system during Meso-Cenozoic times. EGU General Assembly Conference Abstracts, p. 18077.
- Chikhaoui, M., Dupuy, C., Dostal, J., 1978. Geochemistry of late Proterozoic volcanic rocks from Tassendjanet area (N.W. Hoggar, Algeria). Contributions to Mineralogy and Petrology 66, 157-164.
- Coe, M.T., Foley, J.A., 2001. Human and natural impacts on the water resources of the Lake Chad basin. Journal of Geophysical Research: Atmospheres 106, 3349-3356.
- Collins, A. S.; Reddy, S. M.; Buchan, C.; and Mruma, A. 2004. Temporal constraints on Palaeoproterozoic eclogite formation and exhumation (Usagaran Orogen, Tanzania). Earth Planet. Sci. Lett. 224(1– 2):175–192.
- Comas, M., and Thió-Henestrosa, S. 2011. CoDaPack 2.0: a stand-alone, multi-platform compositional software. In Egozcue, J. J.; Tolosana-Delgado, R.; and Ortego, M. I. eds. International Workshop on Compositional Data Analysis, 4th (Girona, Spain), Proc., 10 p. Cox, K. G. 1989. The role of mantle plumes in the development of continental drainage patterns. Nature 342(6252):873–877.
- Cook, K., 2000. The South Indian convergence zone and interrannual rainfall variability over southern Africa. Journal of Climate 13, 3789–3804.
- Coward, M. P., Ries, A. C., 2003. Tectonic development of North African basins. Geological Society, London, Special Publications 207, 61-83.
- Cox, K. G. 1989. The role of mantle plumes in the development of continental drainage patterns. Nature 342:873–877.
- Crouvi, O., Schepanski, K., Amit, R., Gillespie, A.R., Enzel, Y., 2012. Multiple dust sources in the Sahara Desert: The importance of sand dunes. Geophysical Research Letters 39, L13401, doi:10.1029/2012GL052145.
- Cvetković, V., Toljić, M., Ammar, N.A., Rundić, L., Trish, K. B., 2010. Petrogenesis of the eastern part of the Al Haruj basalts (Libya). Journal of African Earth Sciences 58, 37-50.
- Daly, M. C.; Green, P.; Watts, A. B.; Davies, O.; Chibesakunda, F.; and Walker, R. 2020. Tectonics and landscape of the Central African Plateau and their implications for a propagating Southwestern Rift in Africa. Geochem. Geophys. Geosyst. 21(6):e2019GC008746. https://doi.org/10.1029/2019GC008746.
- Davies, B. R.; Beilfuss, R. D.; and Thoms, M. C. 2000. Cahora Bassa retrospective, 1974–1997: effects of flow regulation on the Lower Zambezi River. Int. Ver. Theor. Angew. Limnol. Verh. 27(4):2149–2157.

- De Carvalho, H.; Tassinari, C.; Alves, P. H.; Guimarães, F.; and Simões, M. C. 2000. Geochronological review of the Precambrian in western Angola: links with Brazil. J. Afr. Earth Sci. 31(2):383–402.
- De Paolo, D. J. 1981. Neodymium isotopes in the Colorado Front Range and crust-mantle evolution in the Proterozoic. Nature 291(5812):193–196.
- De Waele, B.; Wingate, M. T.; Fitzsimons, I. C.; and Mapani, B. S. 2003. Untying the Kibaran knot: a reassessment of Mesoproterozoic correlations in southern Africa based on SHRIMP U-Pb data from the Irumide Belt. Geology 31(6):509–512.
- De Waele, B.; Kampunzu, A. B.; Mapani, B. S. E.; and Tembo, F. 2006. The Mesoproterozoic Irumide Belt of Zambia. J. Afr. Earth Sci. 46(1–2):36–70.
- De Waele, B.; Fitzsimons, I. C. W.; Wingate, M. T. D.; Tembo, F.; Mapani, B.; and Belousova, E. A. 2009. The geochronological framework of the Irumide Belt: a prolonged crustal history along the margin of the Bangweulu Craton. Am. J. Sci. 309(2):132–187.
- De Wit, M., 2007. The Kalahari Epeirogeny and climate change: differentiating cause and effect from core to space. South African Journal of Geology, 110(2-3), 367-392.
- Debruyne, D.; Hulsbosch, N.; Van Wilderode, J.; Balcaen, L.; Vanhaecke, F.; and Muchez, P. 2015. Regional geodynamic context for the Mesoproterozoic Kibara Belt (KIB) and the Karagwe-Ankole Belt: evidence from geochemistry and isotopes in the KIB. Precambrian Res. 264:82–97.
- deMenocal, P., Ortiz, J., Guilderson, T., Adkins, J., Sarnthein, M., Baker, L., Yarusinsky, M., 2000. Abrupt onset and termination of the African Humid Period: Rapid climate responses to gradual insolation forcing. Quaternary Science Reviews 19, 347-361.
- Denkler, T., Franz, G., Schandelmeier, H., 1994. Tectonometamorphic evolution of the Neoproterozoic Delgo suture zone, northern Sudan. Geologische Rundschau 83, 578-590.
- Derricourt, R. M. 1976. Regression rate of the Victoria Falls and the Batoka Gorge. Nature 264:23–25.
- Dickinson, W. R. 1985. Interpreting provenance relations from detrital modes of sandstones. In Zuffa, G. G., ed. Provenance of arenites. Dordrecht, Reidel, NATO ASI Series 148:333–361.
- Dickinson, W. R.; Lawton, T. F.; and Gehrels, G. E. 2009. Recycling detrital zircons: a case study from the Cretaceous Bisbee Group of southern Arizona. Geology 37(6):503–506.
- Dill, H. G.; Ludwig, R. R.; Kathewera, A.; and Mwenelupembe, J. 2005. A lithofacies terrain model for the Blantyre region: implications for the interpretation of palaeosavanna depositional systems and for environmental geology and economic geology in southern Malawi. J. Afr. Earth Sci. 41(5):341–393.
- Dill, H. G. 2007. A review of mineral resources in Malawi: with special reference to aluminium variation in mineral deposits. J. Afr. Earth Sci. 47(3):153–173.
- Dinis, P.; Garzanti, E.; Vermeesch, P.; and Huvi, J. 2017. Climatic zonation and weathering control on sediment composition (Angola). Chem. Geol. 467:110–121.
- Dinis, P.; Garzanti, E.; Hahn, A.; Vermeesch, P.; and Cabral-Pinto, M. 2020a. Weathering indices as climate proxies. A step forward based on Congo and SW African river muds. Earth-Sci. Rev. 201:103039.
- Dinis, P.; Sequeira, M.; Tavares, A. O.; Carvalho, J.; Castilho, A.; and Cabral-Pinto, M. 2020b. Post-wildfire denudation assessed from compositional features of river sediments (central Portugal). Appl. Clay Sci. 193:105675.
- Dirks, P.H.G.M., Blenkinsop, T.G., Jelsma, H.A., 2009. The Geological Evolution of Africa. In: De Vito, B., Grasemann, B., Stuwe, K. (Eds.), Geology. Encylopedia of Life Support Systems. Vol. IV., EOLSS Publishers, Paris, 978-1-84826-457-1, pp. 230-251.
- Dott, R.H., 2003. The importance of eolian abrasion in supermature quartz sandstones and the paradox of weathering on vegetation-free landscapes. The Journal of Geology 111, 387-405.

- Dott, R.H., Byers, C.W., Fielder, G.W., Stenzel, S.R., Winfree, K.E., 1986. Aeolian to marine transition in Cambro-Ordovician cratonic sheet sandstones of the northern Mississippi Valley, U.S.A. Sedimentology 33, 345–367.
- Doyle, L. J.; Cleary, W. J.; and Pilkey, O. H. 1968. Mica: its use in determining shelf-depositional regimes. Mar. Geol. 6:381–389.
- Doucouré, C. M., & de Wit, M. J. ,2003. Old inherited origin for the present near-bimodal topography of Africa. Journal of African Earth Sciences, 36(4), 371-388.
- Drake, N. A., Blench, R. M., Armitage, S. J., Bristow, C. S., White, K. H., 2011. Ancient watercourses and biogeography of the Sahara explain the peopling of the desert. Proceedings of the National Academy of Sciences 108, 458-462.
- Droz, L., and Mougenot, D. 1987. Mozambique upper fan: origin of depositional units. Am. Assoc. Pet. Geol. Bull. 71(11):1355–1365.
- Dutta, P.K., Zhou, Z., dos Santos, P.R., 1993. A theoretical study of mineralogical maturation of eolian sand. In: Basu, A., Johnsson, M. (eds.), Processes Controlling the Composition of Clastic Sediments. Geological Society of America, Special Paper 284, 203-209.
- East, A.E., Clift, P.D., Carter, A., Alizai, A., Van Laningham, S., 2015. Fluvial–eolian interactions in sediment routing and sedimentary signal buffering: an example from the Indus Basin and Thar Desert. Journal of Sedimentary Research 85(6), 715-728.
- Ebinger, C. E., and Scholz, C. A. 2012. Continental rift basins: the East African perspective. In Busby, C., and Azor, A., eds. Tectonics of sedimentary basins: recent advances. Oxford, Wiley-Blackwell, p. 185– 208.
- Eglinger, A., Vanderhaeghe, O., André-Mayer, A.S., Goncalves, P., Zeh, A., Durand, C. and Deloule, E., 2016. Tectono-metamorphic evolution of the internal zone of the Pan-African Lufilian orogenic belt (Zambia): Implications for crustal reworking and syn-orogenic uranium mineralizations. Lithos, 240, pp.167-188.
- Eglington, B.M. 2006. Evolution of the Namaqua–Natal Belt, southern Africa—a geochronological and isotope geochemical review. J. Afr. Earth Sci. 46:93-111.
- Eglington, B.M., and Armstrong, R.A. 2004. The Kaapvaal Craton and adjacent orogens, Southern Africa: a geochronological database and overview of the geological development of the craton. S. Afr. J. Geol. 107:13-32.
- El-Baz, F., 1983: A geological perspective of the desert. In Origin and Evolution of Deserts. S. G. Wells and D. R. Haragan (Eds.), University of New Mexico Press,Albuquerque, pp. 163–83.
- El-Baz, F., 1998. Sand accumulation and groundwater in the eastern Sahara. Episodes 21, 147-151.
- El-Baz, F., 2000. Satellite observations of the interplay between wind and water processes in the Great Sahara. Photogrammetric Engineering and Remote Sensing 66(6), 777-782.
- Elbelrhiti, H., 2012. Initiation and early development of barchan dunes: A case study of the Moroccan Atlantic Sahara Desert. Geomorphology 138, 181-188.
- Elshaafi, A., Gudmundsson, A., 2016. Volcano-tectonics of the Al haruj volcanic province, Central Libya. Journal of Volcanology and Geothermal Research 325, 189-202.
- Ennih, N. and Liegeois, J. P., 2001. The Moroccan Anti-Atlas: the West African craton passive margin with limited Pan-African activity. Implications for the northern limit of the craton. Precambrian Research 112, 291-304.
- Ennih, N., and Liégeois, J.P., 2008. The boundaries of the West African craton, with special reference to the basement of the Moroccan metacratonic Anti-Atlas belt. Geological Society, London, Special Publications 297, 1-17.

- ERM (Environmental Resources Management). 2011. Riversdale's Zambezi River Barging Project, Zambezi River, Mozambique: final environmental and social impact assessment report. Johannesburg, ERM, 335 p.
- Fabre, J., Ba, H., Black, R., Caby, R., Leblanc, M., Lesquer, A., 1982. La chaîne Pan-Africaine, son avant-pays et la zone de suture au Mali. Carte géologique et gravimétrique de l'Adrar des Iforas au 1/500 000, notice and map. Direction nationale de la Géologie et des Mines, Bamako, 85.
- Feder, A., Zimmermann, R., Stollhofen, H., Caracciolo, L., Garzanti, E., Andreani, L., 2018. Fluvial-aeolian sedimentary facies, Sossusvlei, Namib Desert. Journal of Maps 14(2), 630-643.
- Fedo, C. M.; Nesbitt, H. W.; and Young, G. M. 1995. Unraveling the effects of potassium metasomatism in sedimentary rocks and paleosols, with implications for paleoweathering conditions and provenance. Geology 23:921–924.
- Fekirine, B., and Abdallah, H., 1998. Palaeozoic lithofacies correlatives and sequence stratigraphy of the Saharan Platform, Algeria. Geological Society, London, Special Publications 132, 97-108.
- Feller, W., 1948. On the Kolmogorov-Smirnov limit theorems for empirical distributions. Annals of Mathematical Statistics 19, 177-189.
- Fernandes, P.; Cogné, N.; Chew, D. M.; Rodrigues, B.; Jorge, R. C. G. S.; Marques, J.; Jamal, D.; and Vasconcelos, L. 2015. The thermal history of the Karoo Moatize-Minjova Basin, Tete Province, Mozambique: an integrated vitrinite reflectance and apatite fission track thermochronology study. J. Afr. Earth Sci. 112:55–72.
- Feybesse, J.L., Milési, J.P., 1994. The Archaean/Proterozoic contact zone in West Africa: A mountain belt of décollement thrusting and folding on a continental margin related to 2.1 Ga convergence of Archaean cratons? Precambrian Research 69, 199-227.
- Fezaa, N., Liégeois, J.P., Abdallah, N., Bruguier, O., De Waele, B., Ouabadi, A., 2019. The 600 Ma-old Pan-African magmatism in the In Ouzzal terrane (Tuareg Shield, Algeria): Witness of the metacratonisation of a rigid block. The Geology of the Arab World - An Overview. Springer, Cham., 109-148.
- FFEM (Fonds Français pour l'Environnement Mondial). 2005. Pollution monitoring and management on the Zambezi River: final report. Lusaka, Zambia, FFEM.
- Fierens, R.; Droz, L.; Toucanne, S.; Raisson, F.; Jouet, G.; and Babonneau, N. 2019. Late Quaternary geomorphology and sedimentary processes in the Zambezi turbidite system (Mozambique Channel). Geomorphology 334:1–28.
- Fierens, R.; Toucanne, T.; Droz, L.; Jouet, G.; Raisson, F.; Jorissen, E. L.; Bayon, G.; Giraudeau, J.; and Jorry,S. J. 2020. Quaternary sediment dispersal in the Zambezi turbidite system (SW Indian Ocean). Mar. Geol. 428:106276. https://doi.org/10.1016/j.margeo.2020.106276
- Flint, J. J. 1974. Stream gradient as a function of order, magnitude, and discharge. Water Resour. Res. 10:969–973.
- Flügel, T. J.; Eckardt, F. D.; and Cotterill, W. P. D. 2018. The geomorphology and river longitudinal profiles of the Congo-Kalahari Watershed. In Runge, J., ed. The African Neogene—climate, environments and people (Palaeoecol. Afr. 34). Leiden, CRC, p. 31–52.
- Folk, R. L. 1951. Stages of textural maturity in sedimentary rocks. J. Sediment. Petrol. 21:127–130.
- Folk, R. L. 1980. Petrology of sedimentary rocks. Austin, TX, Hemphill, 184 p.
- Frimmel, H. E.; Basei, M. S.; and Gaucher, C. 2011. Neoproterozoic geodynamic evolution of SW-Gondwana: a southern African perspective. Int. J. Earth Sci. 100:323– 354.
- Fritz, H.; Abdelsalam, M.; Ali, K. A.; Bingen, B.; Collins, A. S.; Fowler, A. R.; Ghebreab, W.; et al. 2013. Orogen styles in the East African orogen: a review of the Neoproterozoic to Cambrian tectonic evolution. J. Afr. Earth Sci. 86:65–106.

- Gabriel, K. R. 1971. The biplot graphic display of matrices with application to principal component analysis. Biometrika 58:453–467.
- Gaillardet, J.; Dupré, B.; and Allègre, C. J. 1999. Geochemistry of large river suspended sediments: silicate weathering or recycling tracer? Geochim. Cosmochim. Acta 63:4037–4051.
- Galehouse, J.S., 1971. Point counting. In: Carver, R.E. (Ed.), Procedures in sedimentary petrology. Wiley, New York, pp. 385-407.
- Gallagher, K., & Brown, R., 1999. The Mesozoic denudation history of the Atlantic margins of southern Africa and southeast Brazil and the relationship to offshore sedimentation. Geological Society, London, Special Publications, 153(1), 41-53.
- Gao, H., Bohn, T. J., Podest, E., McDonald, K.C., Lettenmaier, D.P., 2011. On the causes of the shrinking of Lake Chad. Environmental Research Letters 6, 034021.
- Gärtner, A., Linnemann, U. and Hofmann, M., 2014. The provenance of northern Kalahari Basin sediments and growth history of the southern Congo Craton reconstructed by U–Pb ages of zircons from recent river sands. International Journal of Earth Sciences, 103(2), pp.579-595.
- Garzanti, E., 1991. Non-carbonate intrabasinal grains in arenites: Their recognition, significance and relationship to eustatic cycles and tectonic setting. Journal of Sedimentary Petrology 61, 959-975.
- Garzanti, E., 2016. From static to dynamic provenance analysis – Sedimentary petrology upgraded. In: Caracciolo, L., Garzanti, E., von Eynatten, H., Weltje, G.J. (Eds.), Sediment generation and provenance: processes and pathways. Sedimentary Geology, 336, 3-13.
- Garzanti, E., 2017. The maturity myth in sedimentology and provenance analysis. Journal of Sedimentary Research 87, 353-365.
- Garzanti, E., 2019. Petrographic classification of sand and sandstone. Earth-Science Reviews 192, 545-563.
- Garzanti, E., Andò, S., 2007a. Plate tectonics and heavy-mineral suites of modern sands. In: Mange, M.A., Wright, D.T. (eds.), Heavy minerals in use. Elsevier, Amstrerdam, Developments in Sedimentology 58, 741-763.
- Garzanti, E., and Andò, S., 2007b. Heavy-mineral concentration in modern sands: implications for provenance interpretation. In: Mange, M.A., Wright, D.T. (Eds.), Heavy minerals in use. Elsevier, Amsterdam, Developments in Sedimentology Series, 58, 517-545.
- Garzanti, E., and Vezzoli, G., 2003. A classification of metamorphic grains in sands based on their composition and grade. Journal of Sedimentary Research, 73, 830-837.
- Garzanti, E., and Resentini, A. 2016. Provenance control on chemical indices of weathering (Taiwan river sands). Sediment. Geol. 336:81–95.
- Garzanti, E., and Sternai, P. 2020. Against steady state: a quixotic plea for science. Earth ArXiv. https://eartharxiv.org/p9xq7/; https://doi.org/10.31223/osf.io/p9xq7.
- Garzanti E., Vezzoli G., Andò S., Castiglioni G., 2001. Petrology of rifted-margin sand (Red Sea and Gulf of Aden, Yemen). The Journal of Geology 109, 277-297.
- Garzanti, E., Ando, S., Vezzoli, G. and Dell'Era, D., 2003. From rifted margins to foreland basins: investigating provenance and sediment dispersal across desert Arabia (Oman, UAE). Journal of Sedimentary Research, 73(4), 572-588.
- Garzanti, E.; Vezzoli, G.; Andò, S.; Paparella, P.; and Clift, P. D. 2005. Petrology of Indus River sands: a key to interpret erosion history of the Western Himalayan Syntaxis. Earth Planet. Sci. Lett. 229(3–4):287– 302.
- Garzanti, E., Ando, S. and Vezzoli, G., 2006. The continental crust as a source of sand (southern Alps cross section, northern Italy). The Journal of Geology, 114(5), 533-554.
- Garzanti E., Doglioni C., Vezzoli G., Andò S., 2007a. Orogenic belts and orogenic sediment provenances.

The Journal of Geology 115, 315-334.

- Garzanti, E.; Vezzoli, G.; Andò, S.; Lavé, J.; Attal, M.; France-Lanord, C.; and DeCelles, P. 2007b. Quantifying sand provenance and erosion (Marsyandi River,Nepal Himalaya). Earth Planet. Sci. Lett. 258(3–4):500–515.
- Garzanti, E.; Andò, S.; and Vezzoli, G. 2008. Settling equivalence of detrital minerals and grain-size dependence of sediment composition. Earth Planet. Sci. Lett. 273(1–2):138–151.
- Garzanti, E.; Andò, S.; and Vezzoli, G. 2009. Grain-size dependence of sediment composition and environmental bias in provenance studies. Earth Planet. Sci. Lett. 277:422–432.
- Garzanti, E., Resentini, A., Vezzoli, G., Ando, S., Malusa, M.G., Padoan, M. and Paparella, P., 2010a. Detrital fingerprints of fossil continental-subduction zones (Axial Belt Provenance, European Alps). The Journal of Geology, 118(4), 341-362.
- Garzanti, E.; Andò, S.; France-Lanord, C.; Vezzoli, G.; Censi, P.; Galy, V.; and Najman, Y. 2010b. Mineralogical and chemical variability of fluvial sediments: 1. Bedload sand (Ganga-Brahmaputra, Bangladesh). Earth Planet. Sci. Lett. 299(3–4):368–381.
- Garzanti, E., Andò, S., Vezzoli, G., Lustrino, M., Boni, M., Vermeesch, P., 2012a. Petrology of the Namib sand sea: long-distance transport and compositional variability in the wind-displaced Orange Delta. Earth-Science Reviews, 11, 173-189.
- Garzanti, E.; Resentini, A.; Vezzoli, G.; Andò, S.; Malusà, M.; and Padoan, M. 2012b. Forward compositional modelling of Alpine orogenic sediments. Sediment. Geol. 280:149–164.
- Garzanti, E., Vermeesch, P., Andò, S., Vezzoli, G., Valagussa, M., Allen, K., Kadi, K.A. and Al-Juboury, A.I., 2013a. Provenance and recycling of Arabian desert sand. Earth-Science Reviews, 120, pp.1-19.
- Garzanti, E.; Padoan, M.; Andò, S.; Resentini, A.; Vezzoli, G.; and Lustrino, M. 2013b. Weathering and relative durability of detrital minerals in equatorial climate: sand petrology and geochemistry in the East African Rift. J. Geol. 121:547–580.
- Garzanti, E.; Padoan, M.; Setti, M.; Peruta, L.; Najman, Y.; and Villa, I. M. 2013c. Weathering geochemistry and Sr-Nd fingerprints of equatorial upper Nile and Congo muds. Geochem. Geophys. Geosyst. 14:292–316.
- Garzanti. E., Vermeesch, P., Andò, S., Lustrino, M., Padoan, M., Vezzoli, G., 2014a. Ultra-long distance littoral transport of Orange sand and provenance of the Skeleton Coast Erg (Namibia). Marine Geology 357, 25-36.
- Garzanti, E.; Vermeesch, P.; Padoan, M.; Resentini, A.; Vezzoli, G.; and Andò, S. 2014b. Provenance of passive margin sand (southern Africa). J. Geol. 122:17–42.
- Garzanti, E., Padoan, M., Setti, M., López-Galindo, A., Villa, I.M., 2014c. Provenance versus weathering control on the composition of tropical river mud (southern Africa). Chemical Geology, 366, 61-74.
- Garzanti, E., Andò, S., Padoan, M., Vezzoli, G. and El Kammar, A., 2015a. The modern Nile sediment system: Processes and products. Quaternary Science Reviews, 130, 9-56.
- Garzanti, E., Resentini, A., Andò, S., Vezzoli, G., Vermeesch, P., 2015b. Physical controls on sand composition and relative durability of detrital minerals during long-distance littoral and eolian transport (coastal Namibia). Sedimentology, 62, 971-996.
- Garzanti, E., Al-Juboury, A.I., Zoleikhaei, Y., Vermeesch, P., Jotheri, J., Akkoca, D.B., Allen, M., Andò, S., Limonta, M., Padoan, M., Resentini, A., Rittner, M., Vezzoli, G., 2016. The Euphrates-Tigris-Karun river system: Provenance, recycling and dispersal of quartz-poor foreland-basin sediments in arid climate. Earth-Science Reviews 162, 107-128.
- Garzanti, E., Vermeesch, P., Al-Ramadan, K.A., Andò, S., Limonta, M., Rittner, M. and Vezzoli, G., 2017. Tracing transcontinental sand transport: from Anatolia–Zagros to the Rub'Al Khali Sand Sea. Journal of Sedimentary Research, 87(11), 1196-1213.

- Garzanti, E., Dinis, P., Vermeesch, P., Andò, S., Hahn, A., Huvi, J., Limonta, M., Padoan, M., Resentini, A., Rittner, M., Vezzoli, G., 2018a. Dynamic uplift, recycling, and climate control on the petrology of passive-margin sand (Angola). Sedimentary Geology 375, 86-104.
- Garzanti, E., Vermeesch, P., Rittner, M., Simmons, M., 2018b. The zircon story of the Nile: Time-structure maps of source rocks and discontinuous propagation of detrital signals. Basin Research 30, 1098-1117.
- Garzanti, E., Dinis, P., Vermeesch, P., Andò, S., Hahn, A., Huvi, J., Limonta, M., Padoan, M., Resentini, A., Rittner, M., Vezzoli, G., 2018c. Sedimentary processes controlling ultralong cells of littoral transport: Placer formation and termination of the Orange sand highway in southern Angola, Sedimentology 65, 431-460.
- Garzanti, E.; Andò, S.; Limonta, M.; Fielding, L.; and Najman, Y. 2018d. Diagenetic control on mineralogical suites in sand, silt, and mud (Cenozoic Nile Delta): implications for provenance reconstructions. Earth Sci. Rev. 185:122–139.
- Garzanti, E., Vermeesch, P., Vezzoli, G., Andò, S., Botti, E., Limonta, M., Dinis, P., Hahn, A., Baudet, D., De Grave, J., Yaya, N.K., 2019a. Congo River sand and the equatorial quartz factory. Earth-Science Reviews 197, 102918.
- Garzanti, E., Ghassemi, M.R., Limonta, M., Resentini, A., 2019b. Provenance of Karakum Desert sand (Turkmenistan): Lithic-rich orogenic signature of central Asian dune fields. Rivista Italiana di Paleontologia e Stratigrafia 125(1), 77-89.
- Garzanti, E.; Limonta, M.; Vezzoli, G.; An, W.; Wang, J.; and Hu, X. 2019c. Petrology and multimineral fingerprinting of modern sand generated from a dissected magmatic arc (Lhasa River, Tibet). In Ingersoll, R. V.; Lawton, T. F.; and Graham, S. A., eds. Tectonics, sedimentary basins, and provenance: a celebration of William R. Dickinson's career. Geol. Soc. Am. Spec. Pap. 540:197–221. https://doi.org/10.1130/2018.2540(09).
- Garzanti, E., Liang, W., Andò, S., Clift, P.D, Resentini, A., Vermeesch, P., Vezzoli, G., 2020. Provenance of Thal Desert sand: Focused erosion in the western Himalayan syntaxis and foreland-basin deposition driven by latest Quaternary climate change. Earth-Science Reviews, 207, 103220.
- Garzanti, E.; Bayon, G.; Dennielou, B.; Barbarano, M.; Limonta, M.; and Vezzoli, G. 2021a. The Congo deepsea fan: mineralogical, REE, and Nd-isotope variability in quartzose passive-margin sand. J. Sediment. Res. 91(5):433–450.
- Garzanti, E.; Dinis, P.; Vezzoli, G.; and Borromeo, L. 2021b. Sand and mud generation from Paraná Etendeka continental flood basalts in contrasting climatic conditions (Uruguay vs. Namibia). Sedimentology. https://doi.org/10.1111/sed.12902.
- Garzanti, E.; He, J.; Barbarano, M.; Resentini, A.; Li, C.; Yang, L.; Yang, S.; and Wang, H. 2021c. Provenance versus weathering control on sediment composition in tropical monsoonal climate (South China)2. Sand petrology and heavy minerals. Chem. Geol. 564:119997.119997. https://doi.org/10.1016/j.chemgeo.2020
- Garzanti, E., Capaldi, T., Tripaldi, A., Zárate, M., Limonta, M. and Vezzoli, G., 2022. Andean retroarc-basin dune fields and Pampean Sand Sea (Argentina): Provenance and drainage changes driven by tectonics and climate. Earth-Science Reviews, p.104077.
- Gasse, F., 2000. Hydrological changes in the African tropics since the Last Glacial Maximum. Quaternary Science Reviews 19, 189-211.
- Gbélé, C.; Tchaméni, R.; and Fernandez-Alonso, M. 2016. Geological map of Africa at 1:10 million scale. Orléans, CGMW-BRGM (Commission for the Geological Map of the World–Bureau de Recherches Géologiques et Minières).
- Geyh, M.A., Thiedig, F., 2008. The Middle Pleistocene Al Mahrúqah Formation in the Murzuq Basin, northern Sahara, Libya: evidence for orbitally-forced humid episodes during the last 500,000 years. Palaeogeography, Palaeoclimatology, Palaeoecology 257, 1-21.

- Ghienne, J.F., Desrochers, A., Vandenbroucke, T.R., Achab, A., Asselin, E., Dabard, M.P., Farley, C., Loi, A., Paris, F., Wickson, S., Veizer, J., 2014. A Cenozoic-style scenario for the end-Ordovician glaciation. Nature Communications 5, 1-9.
- Ghoneim, E., Robinson, C., El-Baz, F., 2007. Radar topography data reveal drainage relics in the eastern Sahara. International Journal of Remote Sensing 28, 1759-1772.
- Ghuma, M.A., Rogers, J.J.W., 1978. Geology, geochemistry, and tectonic setting of the Ben Ghnema batholith, Tebisti Massif, southern Libya. Geological Society America Bulletin 89, 1315–1358.
- Gischler, C.E., 1976. Hydrology of the Sahara. Ecological Bulletins, 83-101.
- Glynn, S. M.; Master, S.; Frei, D.; and Wiedenbeck, M. 2020. U-Pb zircon geochronology of the Dete Kamativi Inlier, NW Zimbabwe, with implications for the western margin of the Archaean Zimbabwe Craton. Precambrian Res. 346:105824.
- Glynn, S. M.; Master, S.; Wiedenbeck, M.; Davis, D. W.; Kramers, J. D.; Belyanin, G. A.; Frei, D.; and Oberthür, T. 2017. The Proterozoic Choma-Kalomo Block, SE Zambia: exotic terrane or a reworked segment of the Zimbabwe Craton? Precambrian Res. 298:421–438.
- Goscombe, B., Foster, D.A., Gray, D. and Wade, B., 2020. Assembly of central Gondwana along the Zambezi Belt: Metamorphic response and basement reactivation during the Kuunga Orogeny. Gondwana Research, 80, pp.410-465.
- Gossel, W., Ebraheem, A.M., Wycisk, P., 2004. A very large scale GIS-based groundwater flow model for the Nubian sandstone aquifer in Eastern Sahara (Egypt, northern Sudan and eastern Libya). Hydrogeology Journal 12, 698-713.
- Goudie, A.S., 2005. The drainage of Africa since the Cretaceous. Geomorphology 67, 437-456.
- Goudie, A.S., and Middleton, N.J., 2006. Desert dust in the global system. Springer Science & Business Media. Berlin, 286 p.
- Goudie A.S., and Thomas, D.S.G., 1985. Pans in southern Africa with particular reference to South Africa and Zimbabwe. Zeitschrift für Geomorphologie N.F. 29(1): 1-19.
- Goudie, A.S., and Viles, H., 2015. Landscapes and Landforms of Namibia. Springer Netherlands, 173 p.
- Gower, J.C., 1975. Generalized procrustes analysis. Psychometrika 40, 33-51.
- Grantham, G. H.; Marques, J.; Wilson, M.; Manhiça, V.; and Hartzer, F. 2011. Explanation of the geological map of Mozambique, 1:1 000 000. Maputo, Direcção Nacional de Geologia, 383 p.
- Greber, N. D.; Davies, J. H.; Gaynor, S. P.; Jourdan, F.; Bertrand, H.; and Schaltegger, U. 2020. New high precision U-Pb ages and Hf isotope data from the Karoo large igneous province; implications for pulsed magmatism and early Toarcian environmental perturbations. Results Geochem. 1:100005.
- Greenacre, M., 2017. Correspondence analysis in practice. CRC press, Boca Raton (FL), 327 p.
- Griffin, W. L.; Powell, W. J.; Pearson, N. J.; and O'Reilly, S. Y. 2008. GLITTER: data reduction software for laser ablation ICP-MS. In Sylvester, P., ed. Laser ablationICP-MS in the earth sciences: current practices and outstanding issues. Mineral. Assoc. Can. Short Course 40:204–207.
- Grove, A.T., 1969. Landforms and climatic change in the Kalahari and Ngamiland. Geogr J 135:191–212.
- Grove, A.T., and Warren, A., 1968. Quaternary landforms and climate on the south side of the Sahara. The Geographical Journal 134, 194-208.
- Guillocheau, F.; Chelalou, R.; Linol, B.; Dauteuil, O.; Robin, C.; Mvondo, F.; Callec, Y.; and Colin, J. P. 2015. Cenozoic landscape evolution in and around the Congo Basin: constraints from sediments and planation surfaces. In de Wit, M. J.; Guillocheau, F.; and de Wit, M. J. C., eds. Geology and resource potential of the Congo Basin (Reg. Geol. Rev.). Berlin, Springer, p. 271–313.

- Guillocheau, F.; Simon, B.; Baby, G.; Bessin, P.; Robin, C.; and Dauteuil, O. 2018. Planation surfaces as a record of mantle dynamics: the case example of Africa. Gondwana Res. 53:82–98.
- Gumbricht, T., McCarthy, T.S. and Merry, C.L., 2001. The topography of the Okavango Delta, Botswana, and its tectonic and sedimentological implications. South African Journal of Geology, 104(3), 243-264.
- Haddon, I.G., 2005. The sub-Kalahari geology and tectonic evolution of the Kalahari Basin, southern Africa. Unpublished Ph. D. thesis, University of the Witwatersrand, Johannesburg, 346 p.
- Haddon, I. G., and McCarthy, T. S. 2005. The Mesozoic– Cenozoic interior sag basins of Central Africa: the Late-Cretaceous–Cenozoic Kalahari and Okavango basins. J. Afr. Earth Sci. 43:316–333.
- Haddoum, H., Guiraud, R., Moussine-Pouchkine, A., 2001. Hercynian compressional deformations of the Ahnet-Mouydir Basin, Algerian Saharan Platform: Far-field stress effects of the Late Paleozoic orogeny. Terra Nova 13, 220-226.
- Haley, B. A.; Klinkhammer, G. P.; and McManus, J. 2004. Rare earth elements in pore waters of marine sediments. Geochim. Cosmochim. Acta 68:1265–1279.
- Hall, W.S., Hitzman, M.W., Kuiper, Y.D., Kylander-Clark, A.R., Holm-Denoma, C.S., Moscati, R.J., Plink-Björklund, P. and Enders, M.S., 2018. Igneous and detrital zircon U-Pb and Lu-Hf geochronology of the late Meso-to Neoproterozoic northwest Botswana rift: Maximum depositional age and provenance of the Ghanzi Group, Kalahari Copperbelt, Botswana and Namibia. Precambrian Research, 318, 133-155.
- Hanson, R. E.; Wilson, T. J.; and Munyanyiwa, H. 1994. Geologic evolution of the Neoproterozoic Zambezi orogenic belt in Zambia. J. Afr. Earth Sci. 18(2):135– 150.
- Hanson, R. E. 2003. Proterozoic geochronology and tectonic evolution of southern Africa. In Yoshida, M.; Windley, B. F.; and Dasgupta, S., eds. Proterozoic East Gondwana: supercontinent assembly and breakup. Geol. Soc. Lond. Spec. Publ. 206:427–463.
- Hanson, R.E.; Harmer, R.E.; Blenkinsop, T.G.; Bullen, D.S.; Dalziel, I.W.D.; Gose,W.A.; Hall, R.P.; Kampunzu, A.B.; Key, R.M.; Mukwakwami, J.; Munyanyiwa, H.; Pancake, J.A.; Seidel, E.K.; and Ward, S.E. 2006. Mesoproterozoic intraplate magmatism in the Kalahari Craton: a review. J. Afr. Earth Sci. 46: 141-167.
- Hargrove, U.S., Hanson, R.E., Martin, M.W., Blenkinsop, T.G., Bowring, S.A., Walker, N. and Munyanyiwa, H., 2003. Tectonic evolution of the Zambezi orogenic belt: geochronological, structural, and petrological constraints from northern Zimbabwe. Precambrian Research, 123(2-4), pp.159-186.
- Harnois, L. 1988. The CIW index: a new chemical index of weathering. Sediment. Geol. 55:319–322.
- Hartmann, D., and Christiansen, C. 1988. Settling-velocity distributions and sorting processes on a longitudinal dune: A case study. Earth Surface Processes and Landforms, 13(7), 649-656.
- Haug, G.H., Hughen, K.A., Sigman, D.M., Peterson, L.C., Röhl, U., 2001. Southward migration of the intertropical convergence zone through the Holocene. Science 293, 1304-1308.
- Hay, W.W., 1998. Detrital sediment fluxes from continents to oceans. Chemical geology, 145(3-4), 287-323.
- He, J.; Garzanti, E.; Dinis, P.; Yang, S.; and Wang, H. 2020. Provenance versus weathering control on sediment composition in tropical monsoonal climate (South China) 1. Geochemistry and clay mineralogy. Chem. Geol. 558:119860.
- Hinderer, M. 2012. From gullies to mountain belts: a review of sediment budgets at various scales. Sediment. Geol. 280:21–59.
- Holisticos, 2012. Environmental Impact Study for the Rehabilitation and Expansion of the Cambambe Hydroelectric Power Plant. https://www.miga.org/documents/Angola_ Cambambe_HPP_EIS.pdf.
- Holmgren, K., Karlén, W., Shaw, P. A., 1995. Paleoclimatic significance of the stable isotopic composition and petrology of a Late Pleistocene stalagmite from Botswana. Quaternary Research 32, 320-328.

- Holmgren, K., Lee-Thorp, J.A., Cooper, G.R., Lundblad, K., Partridge, T.C., Scott, L., Sithaldeen, R., Talma, A.S. and Tyson, P.D., 2003. Persistent millennial-scale climatic variability over the past 25,000 years in Southern Africa. Quaternary Science Reviews, 22(21-22), pp.2311-2326.
- Holzkämper, S., Holmgren, K., Lee-Thorp, J. L., Talma, S., Mangini, A., Partridge, T., 2009. Late Pleistocene stalagmite growth in Wolkberg Cave, South Africa. Earth and Planetary Science Letters 282, 212-221.
- Hopper, E.; Gaherty, J. B.; Shillington, D. J.; Accardo,N. J.; Nyblade, A. A.; Holtzman, B. K.; Havlin, C.; et al. 2020. Preferential localized thinning of lithospheric mantle in the melt-poor Malawi Rift. Nat. Geosci. 13(8):584–589.
- Howard, E., and Washington, R. 2019. Drylines in southern Africa: rediscovering the Congo Air Boundary. J. Climate 32:8223–8242.
- Hubert, J.F., 1962. A zircon–tourmaline–rutile maturity index and the interdependence of the composition of heavy mineral assemblages with the gross composition and texture of sandstones. Journal of Sedimentary Petrology, 32, 440-450.
- Hürkamp, K., Völkel, J., Heine, K., Bens, O., Leopold, M., Winkelbauer, J., 2011. Late Quaternary environmental changes from aeolian and fluvial geoarchives in the southwestern Kalahari, South Africa: implications for past African climate dynamics. South African Journal of Geology 114 (3–4), 459–474.
- Ingersoll, R. V.; Bullard, T. F.; Ford, R. L.; Grimm, J. P.; Pickle, J. D.; Sares, S. W. 1984. The effect of grain size on detrital modes: a test of the Gazzi-Dickinson point-counting method. J. Sediment. Petrol. 54:103–116.
- Inman, D.L. and Jenkins, S.A., 1984. The Nile littoral cell and man's impact on the coastal zone of the southeastern Mediterranean. Coastal Engineering, ch. 109, 1600-1617.
- J. L.; Higginson, M.; and Malifa, M. 1998. Punctuated aridity in southern Africa during the last glacial cycle: the chronology of linear dune construction in the northeastern Kalahari. Palaeogeogr. Palaeoclimatol. Palaeoecol. 137:305–322.
- Jackson, S.E., Pearson, N.J., Griffin, W.L., Belousova, E.A., 2004. The application of laser ablation-inductively coupled plasma-mass spectrometry to in situ U–Pb zircon geochronology. Chemical Geology 211, 47-69.
- Jacobs, J.; Pisarevsky, S.; Thomas, R.J.; and Becker, T. 2008. The Kalahari Craton during the assembly and dispersal of Rodinia. Precambrian Res. 160:142-158.
- Jelsma, H. A., and Dirks, P. H. G. M. 2002. Neoarchaean tectonic evolution of the Zimbabwe Craton. In: Fowler, C. M. R.; Ebinger, C. J.: and Hawkesworth, C., J. eds. The early Earth: physical, chemical and biological development. Geol. Soc. London Spec. Publ. 199, 183-211.
- Jelsma, H. A.; McCourt, S.; Perritt, S. H.; and Armstrong, R. A. 2018. The geology and evolution of the Angolan Shield, Congo Craton. In Siegesmund, S.; Basei, M.; Oyhantçabal, P.; and Oriolo, S., eds. Geology of Southwest Gondwana (Regional Geol. Rev.). Cham, Springer, p. 217–239. https://doi.org/10.1007/978-3-319-68920-3_9.
- Jewell, A.M., Drake, N., Crocker, A.J., Bakker, N.L., Kunkelova, T., Bristow, C.S., Cooper, M.J., Milton, J.A., Breeze, P.S., Wilson, P.A., 2020. Three North African dust source areas and their geochemical fingerprint. Earth and Planetary Science Letters 554, 116645, doi.org/10.1016/j.epsl.2020.116645.
- John, T.; Schenk, V.; Haase, K.; Scherer, E.; and Tembo, F. 2003. Evidence for a Neoproterozoic ocean in southcentral Africa from mid-ocean-ridge-type geochemical signatures and pressure-temperature estimates of Zambian eclogites. Geology 31:243–246.
- John, T., Schenk, V., Mezger, K. and Tembo, F., 2004. Timing and PT evolution of whiteschist metamorphism in the Lufilian Arc–Zambezi Belt orogen (Zambia): implications for the assembly of Gondwana. The Journal of geology, 112(1), pp.71-90.

- Johnson, M. R. 1991. Sandstone petrography, provenance, and plate tectonic setting in Gondwana context of the southeastern Cape-Karoo Basin. S. Afr. J. Geol. 94:137–154.
- Johnsson, M.J., 1993. The system controlling the composition of clastic sediments. In: Johnsson, M.J., Basu, A. (eds.), Processes controlling the composition of clastic sediments. Geological Society of America, Special Paper 284, pp. 1–19.
- Johnson, M.R.; van Vuuren, C.J.; Hegenberger, W.F.; Key, R.; and Shoko, U. 1996. Stratigraphy in the Karoo Supergroup in southern Africa: an overview. J. Afr. Earth Sci. 23:3-15.
- Jouet, G., and Deville, E. 2015. PAMELA-MOZ04 cruise, RV Pourquoi pas? https://doi.org/10.17600/15000700.
- Jourdan, F., Féraud, G., Bertrand, H., Kampunzu, A. B., Tshoso, G., Watkeys, M. K., and Le Gall, B., 2005. Karoo large igneous province: Brevity, origin, and relation to mass extinction questioned by new 40Ar/39Ar age data. Geology, 33(9), 745-748.
- Jourdan, F., Féraud, G., Bertrand, H. and Watkeys, M.K., 2007. From flood basalts to the inception of oceanization: Example from the 40Ar/39Ar high-resolution picture of the Karoo large igneous province. Geochemistry, Geophysics, Geosystems, 8(2), Q02002, doi:10.1029/2006GC001392.
- Jung, S., Hoffer, E., Hoernes, S., 2007. Neo-Proterozoic rift-related syenites (Northern Damara Belt, Namibia): Geochemical and Nd–Sr–Pb–O isotope constraints for mantle sources and petrogenesis. Lithos, 96, 415-435.
- Jury, M. 2010. Climate and weather factors modulating river flows in southern Angola. Int. J. Climatol. 30:901–908.
- Just, J.; Schefuß, E.; Kuhlmann, H.; Stuut, J.-B. W.; and Pätzold, J. 2014. Climate induced sub-basin source-area shifts of Zambezi River sediments over the past 17 ka. Palaeogeogr. Palaeoclimatol. Palaeoecol. 410:190– 199.
- Kahle, M.; Kleber, M.; and Jahn, R. 2002. Review of XRDbased quantitative analyses of clay minerals in soils: the suitability of mineral intensity factors. Geoderma 109:191–205.
- Kampunzu, A. B., and Cailteux, J. 1999. Tectonic evolution of the Lufilian Arc (Central Africa Copper Belt) during Neoproterozoic Pan African orogenesis. Gondwana Res. 2(3):401–421.
- Katongo, C.; Koblmüller, S.; Duftner, N.; Makasa, L.; and Sturmbauer, C. 2005. Phylogeography and speciation in the Pseudocrenilabrus philander species complex in Zambian rivers. In Segers, H., and Martens, K. eds. Aquatic biodiversity II (Dev. Hydrobiol., vol. 180). Dordrecht, Springer, p. 221–233.
- Key, R. M.; Cotterill, F. P. D.; and Moore, A. E. 2015. The Zambezi River: an archive of tectonic events linked to the amalgamation and disruption of Gondwana and subsequent evolution of the African Plate. S. Afr. J. Geol. 118(4):425–438.
- Kinabo, B. D.; Atakwana, E. A.; Hogan, J. P.; Modisi, M. P.; Wheaton, D. D.; and Kampunzu, A. B. 2007. Early structural development of the Okavango rift zone, NW Botswana. J. Afr. Earth Sci. 48:125–136.
- Kiss, T., Sipos, G., Kovács, F., 2009. Human impact on fixed sand dunes revealed by morphometric analysis. Earth Surface Processes and Landforms. 34(5), 700-711.
- Klimke, J.; Franke, D.; Gaedicke, C.; Schreckenberger, B.; Schnabel, M.; Stollhofen, H.; Rose, J.; and Chaheire, M. 2016. How to identify oceanic crust— evidence for a complex break-up in the Mozambique Channel, off East Africa. Tectonophysics 693:436–452.
- Klöcking M., Hoggard, M.J., Tribaldos, V.R., Richards, F.D., Guimarães, A.R., Maclennan, J. and White, N.J., 2020. A tale of two domes: Neogene to recent volcanism and dynamic uplift of northeast Brazil and southwest Africa. Earth and Planetary Science Letters, 547, 116464.
- Knight, J., and Grab, S. W. 2018. The geomorphic evolution of southern Africa during the Cenozoic. In Holmes, P. J., and Boardman, J., eds. Southern African landscapes and environmental change. New York,

Routledge, p. 6–28.

- Kokonyangi, J. W.; Kampunzu, A. B.; Armstrong, R.; Yoshida, M.; Okudaira, T.; Arima, M.; and Ngulube, D. A. 2006. The Mesoproterozoic Kibaride belt (Katanga, SE DR Congo). J. Afr. Earth Sci. 46(1–2):1–35.
- Kolla, V.; Kostecki, J. A.; Henderson, L.; and Hess, L. 1980. Morphology and Quaternary sedimentation of the Mozambique Fan and environs, southwestern Indian Oceans. Sedimentology 27:357–378.
- König, M., and Jokat, W. 2010. Advanced insights into magmatism and volcanism of the Mozambique Ridge and Mozambique Basin in the view of new potential field data. Geophys. J. Int. 180(1):158–180.
- Koren, I., Kaufman, Y.J., Washington, R., Todd, M.C., Rudich, Y., Martins, J.V., Rosenfeld, D., 2006. The Bodélé depression: A single spot in the Sahara that provides most of the mineral dust to the Amazon forest. Environmental Research Letters 1, 01400.
- Kottek, M., Grieser, J., Beck, C., Rudolf, B., Rubel, F., 2006.World map of the Köppen–Geiger climate classification updated. Meteorologische Zeitschrift, 15, 259–263.
- Krumbein, W. C., 1940, Flood gravels of San Gabriel Canyon, California: Geological Society of America Bulletin, 51:639-676.
- Kruskal, J. B., and Wish, M. 1978. Multidimensional scaling. Sage Univ. Paper no. 07-011. Newbury Park, CA, Sage, 92 p.
- Krynine, P. D. 1948. The megascopic study and field classification of sedimentary rocks. J. Geol. 56:130–165.
- Krynine, P.D., 1941. Paleogeographic and tectonic significance of sedimentary quartzites. Geological Society of America Bulletin 52, 1915–1916.
- Kulongoski, J.T., Hilton, D.R., Selaolo, E.T., 2004. Climate variability in the Botswana Kalahari from the late Pleistocene to the present day. Geophysical Research Letters 31, L10204.
- Kunz, M. J.; Anselmetti, F. S.; Wüest, A.; Wehrli, B.; Vollenweider, A.; Thüring, S.; and Senn, D. B. 2011. Sediment accumulation and carbon, nitrogen, and phosphorus deposition in the large tropical reservoir Lake Kariba (Zambia/Zimbabwe). J. Geophys. Res. Biogeosci. 116(G3):G03003. https://doi.org/10.1029/2010JG001538.
- Kuper, R., Kröpelin, S., 2006. Climate-controlled Holocene occupation in the Sahara: Motor of Africa's evolution. Science 313, 803-807.
- Kusky, T. M. 1998. Tectonic setting and terrane accretion of the Archean Zimbabwe craton. Geology 26:163–166.
- Kuster, D., Liégeois, J.-P., 2001. Sr, Nd isotopes and geochemistry of the Bayuda Desert high-grade metamorphic basement (Sudan): An early Pan-African oceanic convergent margin, not the edge of the East Saharan ghost craton. Precambrian Research 109, 1–23.
- Lancaster, N., 1978. The Pans of the southern Kalahari, Botswana. Geog J 144: 81-98. DOI: 10.2307/634651 https://www.jstor.org/stable/634651
- Lancaster, N., 1979. Quaternary environments in the arid zone of southern Africa, Dept. Geogr. and Envir. Studies, Occ. Pap. 22, pp. 73, Univ. Witswatersrand, Johannesburg
- Lancaster, N. 1981. Paleoenvironmental implications of fixed dune systems in southern Africa. Palaeogeography, Palaeoclimatology, Palaeoecology, 33(4), 327-346.
- Lancaster, N. 1986. Grain-size characteristics of linear dunes in the southwestern Kalahari. Journal of Sedimentary Research, 56(3), 395-400.
- Lancaster, N., 1986. Pans in the southwestern Kalahari: a preliminary report. Palaeoeco A 17: 59-67.
- Lancaster, N., 1989. The Namib Sand Sea: dune forms, processes and sediments. Balkema.

- Lancaster, N., 1995. Geomorphology of desert dunes. Psychology Press.
- Lancaster, N., 2020. On the formation of desert loess. Quaternary Research 96, 105-122. 247.
- Lanci, L., Tohver, E., Wilson, A. and Flint, S., 2013. Upper Permian magnetic stratigraphy of the lower Beaufort group, Karoo basin. Earth and Planetary Science Letters, 375, pp.123-134.
- Le Pera, E., and Morrone, C. 2020. The use of mineral interfaces in sand-sized volcanic rock fragments to infer mechanical durability. J. Palaeogeogr. 9(1):1–26.
- Lehmann, J., Saalmann, K., Naydenov, K.V., Milani, L., Belyanin, G.A., Zwingmann, H., Charlesworth, G. and Kinnaird, J.A., 2016. Structural and geochronological constraints on the Pan-African tectonic evolution of the northern Damara Belt, Namibia. Tectonics, 35(1), pp.103-135.
- Leistner, O.A., 1967. The plant ecology of the southern Kalahari. Botanical Research Institute Botanical. Republic of South Africa Department of Agricultural Technical Services, Pretoria, Memoir 38.
- Leopold, L. B.; Wolman, M. G.; and Miller, J. P. 1995. Fluvial processes in sedimentology. New York, Dover, 522 p.
- Liang, A., Dong, Z., Qu, J., Su, Z., Wu, B., Zhang, Z., Qian, G., Gao, J., Pang, Y., Yang, Z., 2020. Using spatial variations of grain size to reveal sediment transport in the Kumtagh Sand Sea, Northwest China. Aeolian Res. 46, 100599. https://doi.org/10.1016/j.aeolia.2020.100599
- Liang, W., Garzanti, E., Andò, S., Gentile, P., Resentini, A., 2019. Multimineral fingerprinting of Transhimalayan and Himalayan sources to Indus-derived Thal Desert sand (central Pakistan). Minerals, 9, 457; doi:10.3390/min9080457.
- Liégeois, J.P., 2019. A new synthetic geological map of the Tuareg Shield: An overview of its global structure and geological evolution. In The Geology of the Arab World - An Overview. Springer, Cham, 83-107.
- Liégeois, J.P., and Black, R., 1987. Alkaline magmatism subsequent to collision in the Pan-African belt of the Adrar des Iforas (Mali). Alkaline Igneous Rocks 30, 381-401.
- Liégeois, J.P., Black, R., Navez, J., Latouche, L., 1994. Early and late Pan-African orogenies in the Aïr assembly of terranes (Tuareg Shield, Niger). Precambrian Research 67, 59-88.
- Liégeois, J.P., Latouche, L., Navez, J., Black, R., 2000. Pan-African collision, collapse and escape tectonics in the Tuareg shield: Relations with the East Saharan Ghost craton and the West African craton. Journal of African Earth Sciences 30, 53-53.
- Linnemann, U., Ouzegane, K., Drareni, A., Hofmann, M., Becker, S., Gärtner, A., Sagawe, A., 2011. Sands of West Gondwana: An archive of secular magmatism and plate interactions—a case study from the Cambro-Ordovician section of the Tassili Ouan Ahaggar (Algerian Sahara) using U–Pb–LA-ICP-MS detrital zircon ages. Lithos 123, 188-203.
- Lithgow-Bertelloni, C., and Silver, P. G. 1998. Dynamic topography, plate driving forces and the African superswell. Nature 395(6699):269–272.
- Liu, Z.; Zhao, Y.; Li, J.; and Colin, C. 2007. Late Quaternary clay minerals off Middle Vietnam in the western South China Sea: implications for source analysis and East Asian monsoon evolution. Sci. China Ser. D Earth Sci. 50(11):1674–1684.
- Ludwig, K. R. 1998. On the treatment of concordant uranium-lead ages. Geochim. Cosmochim. Acta 62 (4):665–676.
- Lutjeharms, J.R.E., and Van Ballegooyen, R.C., 1988. The retroflection of the Agulhas Current. Journal of Physical Oceanography 18(11), 1570-1583.
- Macgregor, D. 2018. History of the development of Permian–Cretaceous rifts in East Africa: a series of interpreted maps through time. Thematic set: tectonics and petroleum systems of East Africa. Pet. Geosci. 24:8–20. https://doi.org/10.1144/petgeo2016-155.

- Mackintosh, V., Kohn, B., Gleadow, A., & Tian, Y., 2017. Phanerozoic morphotectonic evolution of the Zimbabwe Craton: Unexpected outcomes from a multiple low-temperature thermochronology study. Tectonics, 36(10), 2044-2067.
- Main, M. 1990. Zambezi: journey of a river. Halfway House, South Africa, Southern, 313 p.
- Mainguet, M., 1978. The influence of trade winds, local air-masses and topographic obstacles on the aeolian movement of sand particles and the origin and distribution of dunes and ergs in the Sahara and Australia. Geoforum 9, 17-28.
- Mainguet, M., Callot, Y., 1978. L'erg de Fachi-Bilma, Tchad-Niger: contribution à la connaissance de la dynamique des ergs et des dunes des zones arides chaudes. Éditions du Centre national de la recherche scientique.
- Mainguet, M., Chemin, M.C., 1983. Sand seas of the Sahara and Sahel: An explanation of their thickness and sand dune type by the sand budget principle. Elsevier, Amsterdam, Developments in sedimentology 38, 353-363.
- Majaule, T.; Hanson, R. E.; Key, R. M.; Singletary, S. J.; Martin, M. W.; and Bowring, S. A. 2001. The Magondi Belt in northeast Botswana: regional relations and new geochronological data from the Sua Pan area. J. Afr. Earth Sci. 32:257–267.
- Malusà, M. G.; Resentini, A.; and Garzanti, E. 2016. Hydraulic sorting and mineral fertility bias in detrital geochronology. Gondwana Res. 31:1–19.
- Manninen, T.; Eerola, T.; Makitie, H.; Vuori, S.; Luttinen, A.; Sénvano, A.; and Manhiça, V. 2008. The Karoo volcanic rocks and related intrusions in southern and central Mozambique. Geol. Surv. Finl. Spec. Pap. 48:211–250.
- Maselli, V.; Kroon, D.; Iacopini, D.; Wade, B. S.; Pearson,P. N.; and de Haas, H. 2019. Impact of the East African Rift System on the routing of the deep-water drainage network offshore Tanzania, western Indian Ocean. Basin Res. https://doi.org/10.1111/bre.12398.
- Master, S.; Bekker, A.; and Hofmann, A. 2010. A review of the stratigraphy and geological setting of the Palaeoproterozoic Magondi Supergroup, Zimbabwe—type locality for the Lomagundi carbon isotope excursion. Precambrian Res. 182(4):254–273.
- Matmon, A., Enzel, Y., Vainer, S., Grodek, T., Mushkin, A. and ASTER Team, 2018. The near steady state landscape of western Namibia. Geomorphology, 313, pp.72-87.
- Mattauer, M., Tapponier, P., Proust, F., 1977. Sur les mécanismes de formation des chaines intracontinentales: L'exemple des chaines atlasiques du Maroc, Bulletin de la Societé Géologique de France 77, 521-526.
- Mayaud, J.R., Bailey, R.M. and Wiggs, G.F., 2017. Modelled responses of the Kalahari Desert to 21 st century climate and land use change. Scientific reports, 7(1), 3887, doi:10.1038/s41598-017-04341-0.
- McCarthy, T.S. and Ellery, W.N., 1998. The Okavango delta. Transactions of the Royal Society of South Africa, 53(2), pp.157-182.
- McCarthy, T.S., and Metcalfe, J., 1990. Chemical sedimentation in the semi-arid environment of the Okavango Delta, Botswana. Chem. Geol. 89, 157–178.
- McCarthy, T. S.; Smith, N. D.; Ellery, W. N.; and Gumbricht, T. 2002. The Okavango Delta—semiarid alluvialfan sedimentation related to incipient rifting. In Renaut, R. E., and Ashley, G. M., eds. Sedimentation in continental rifts. SEPM Spec. Publ. 73:179–194.
- McCarthy, T. S.; Humphries, M. S.; Mahomed, I.; Le Roux, P.; and Verhagen, B. T. 2012. Island forming processes in the Okavango Delta, Botswana. Geomorphology 179:249–257.
- McCourt, S., Armstrong, R.A., Jelsma, H., Mapeo, R.B.M., 2013. New U–Pb SHRIMP ages from the Lubango region, SW Angola: insights into the Palaeoproterozoic evolution of the Angolan Shield, southern

Congo Craton, Africa. Journal of the Geological Society of London 170, 353–363.

- McFarlane, M. J.; Eckardt, F. D.; Coetzee, S. H.; and Ringrose, S. 2010. An African surface weathering profile in the Kalahari of North West Ngamiland, Botswana: processes and products. Z. Geomorphol. 54(3):273–303.
- McKay, M. P.; Coble, M. A.; Hessler, A. M.; Weislogel, A. L.; and Fildani, A. 2016. Petrogenesis and provenance of distal volcanic tuffs from the Permian–Triassic Karoo Basin, South Africa: a window into a dissected magmatic province. Geosphere 12(1):1–14.
- McKee, E. D. 1979. A study of global sand seas (Vol. 1052). US Government Printing Office.
- McLennan, S. M.; Hemming, S.; McDaniel, D. K.; and Hanson, G. N. 1993. Geochemical approaches to sedimentation, provenance, and tectonics. In Johnsson, M. J., and Basu, A. eds. Processes controlling the composition of clastic sediments. Geol. Soc. Am. Spec. Pap. 284:21–40.
- Meftah, N., Mahboub, M.S., 2020. Spectroscopic characterizations of sand dunes minerals of El-Oued (Northeast Algerian Sahara) by FTIR, XRF and XRD analyses. Silicon 12, 147-153.
- Meinhold, G., Morton, A.C., Fanning, C.M., Frei, D., Howard, J.P., Phillips, R.J., Strogen, D., Whitham, A.G., 2011. Evidence from detrital zircons for recycling of Mesoproterozoic and Neoproterozoic crust recorded in Paleozoic and Mesozoic sandstones of southern Libya. Earth and Planetary Science Letters 312, 164-175.
- Meinhold, G., Morton, A.C., Avigad, D., 2013. New insights into peri-Gondwana paleogeography and the Gondwana super-fan system from detrital zircon U–Pb ages. Gondwana Research 23, 661-665.
- Middleton, N.J., Goudie, A.S., 2001. Saharan dust storms: nature and consequences. Earth-Science Reviews 56, 179–204.
- Miller, R.M. 2008, The geology of Namibia. Ministry of Mines and Energy, Windhoek (3 vol.).
- Miller, R.M., Pickford, M. and Senut, B., 2010. The geology, palaeontology and evolution of the Etosha Pan, Namibia: Implications for terminal Kalahari deposition. South African Journal of Geology, 113(3), 307-334.
- Miller, R. McG, 2014. Evidence for the evolution of the Kalahari dunes from the Auob River, southeastern Namibia. T Roy Soc S AFr 69(3): 195-204. https://doi.org/10.1080/0035919X.2014.955555
- Milliken, K. L. 2007. Provenance and diagenesis of heavy minerals, Cenozoic units of the northwestern Gulf of Mexico sedimentary basin. In Mange, M. A., and Wright, D. T., eds. Heavy minerals in use (Dev. Sedimentol. 58). Amsterdam, Elsevier, p. 247–261.
- Milliman, J. D., and Farnsworth, K. L. 2011. River discharge to the coastal ocean: a global synthesis. Cambridge, Cambridge University Press, 384 p.
- Milliman, J. D., and Meade, R. H. 1983. World-wide delivery of river sediment to the oceans. J. Geol. 91(1):1–21. Moore, A., and Blenkinsop, T. 2002. The role of mantle plumes in the development of continental-scale drainage patterns: the southern African example revisited. S. Afr. J. Geol. 105(4):353–360.
- Miramontes, E.; Jouet, G.; Thereau, E.; Bruno, M.; Penven, P.; Guerin, C.; Le Roy, P.; et al. 2020. The impact of internal waves on upper continental slopes: insights from the Mozambican margin (southwest Indian Ocean). Earth Surf. Process. Landf. 45(6):1469–1482.
- Modisi, M. P.; Atekwana, E. A.; Kampunzu, A. B.; and Ngwisanyi, T. H. 2000. Rift kinematics during the incipient stages of continental extension: evidence from the nascent Okavango rift basin, northwest Botswana. Geology 28:939–942.
- Moore, A. E., and Blenkinsop, T. 2002. The role of mantle plumes in the development of continentalscale drainage patterns: the southern African example revisited. S. Afr. J. Geol. 105:353–360.
- Moore, A. E., and Dingle, R. V. 1998. Evidence for fluvial sediment transport of Kalahari sands in central Botswana. S. Afr. J. Geol. 101:143–153.

- Moore, A. E., and Larkin, P. A., 2001. Drainage evolution in south-central Africa since the breakup of Gondwana. S. Afr. J. Geol. 104(1):47–68.
- Moore, A. E.; Cotterill, F. P. D.; Main, M. P. L.; and Williams, H. B. 2007. The Zambezi River. In Gupta, A., ed. Large rivers: geomorphology and management. Chichester, Wiley, p. 311–332.
- Moore, A., Blenkinsop, T., Cotterill, F., 2008. Controls on post-Gondwana alkaline volcanism in Southern Africa. Earth and Planetary Science Letters, 268(1-2), pp.151-164.
- Moore, A. E.; Blenkinsop, T.; and Cotterill, F. P. D. 2009a. Southern African topography and erosion history: plumes or plate tectonics? Terra Nova 21:310–315.
- Moore, A. E.; Cotterill, F. P. D.; Broderick, T. G.; and Plowes, D. 2009b. Landscape evolution in Zimbabwe from the Permian to present, with implications for kimberlite prospecting. S. Afr. J. Geol. 112:65–86.
- Moore, A. E.; Cotterill, F. P. D.; and Eckardt, F. D. 2012. The evolution and ages of Makgadikgadi palaeo-lakes: consilient evidence from Kalahari drainage evolution south-central Africa. S. Afr. J. Geol. 115(3):385–413.
- Moore, D. M., and Reynolds, R. C. 1989. X-ray diffraction and the identification and analysis of clay minerals. Oxford, Oxford University Press.
- Moore, D. M., and Reynolds, R. C. 1997. X-ray diffraction and the identification and analysis of clay minerals (2nd ed.). Oxford, Oxford University Press.
- Moreau, C., Demaiffe, D., Bellion, Y., Boullier, A.M., 1994. A tectonic model for the location of Palaeozoic ring complexes in Air (Niger, West Africa). Tectonophysics 234, 129-146.
- Morrone, C.; Le Pera, E.; Marsaglia, K. M.; and De Rosa, R. 2020. Compositional and textural study of modern beach sands in the active volcanic area of the Campania region (southern Italy). Sediment. Geol. 396:105567.
- Morton, A. C., and Hallsworth, C. 2007. Stability of detrital heavy minerals during burial diagenesis. In Mange, M. A., and Wright, D. T., eds. Heavy minerals in use (Dev. Sedimentol. 58). Amsterdam, Elsevier,p. 215–245.
- Morton, A.C., Meinhold, G., Howard, J.P., Phillips, R.J., Strogen, D., Abutarruma, Y., Elgadry, M., Thusu, B., Whitham, A.G., 2011. A heavy mineral study of sandstones from the eastern Murzuq Basin, Libya: Constraints on provenance and stratigraphic correlation. Journal of African Earth Sciences 61, 308-330.
- Moucha, R., and Forte, A.M. 2011. Changes in African topography driven by mantle convection. Nature Geosci. 4:707-712.
- Muhs, D.R., 2004. Mineralogical maturity in dunefields of North America, Africa and Australia. Geomorphology 59, 247-269.
- Muhs, D.R., Bush, C.A., Stewart, K.C., Rowland, T.R., Crittenden, R.C., 1990. Geochemical evidence of Saharan dust parent material for soils developed on Quaternary limestones of Caribbean and western Atlantic islands. Quaternary Research 33, 157-177.
- Muhs, D.R., Roskin, J., Tsoar, H., Skipp, G., Budahn, J.R., Sneh, A., Porat, N., Stanley, J.D., Katra, I., Blumberg, D.G., 2013. Origin of the Sinai–Negev erg, Egypt and Israel: Mineralogical and geochemical evidence for the importance of the Nile and sea level history. Quaternary Science Reviews 69, 28-48.
- Muhs, D.R., Meco, J., Budahn, J.R., Skipp, G.L., Betancort, J.F., Lomoschitz, A., 2019. The antiquity of the Sahara Desert: New evidence from the mineralogy and geochemistry of Pliocene paleosols on the Canary Islands, Spain. Palaeogeography, Palaeoclimatology, Palaeoecology 533, 109245.
- Mzuza, M. K.; Zhang, W.; Kapute, F.; and Wei, X. 2019. The impact of land use and land cover changes on the Nkula Dam in the Middle Shire River catchment, Malawi. In Pepe, A., and Zhao, Q., eds. Geospatial analyses of earth observation (EO) data. London, IntechOpen, p. 37–66.

- Nance, R.D., Murphy, J.B., Strachan, R.A., Keppie, J.D., Gutiérrez-Alonso, G., Fernández-Suárez, J., Quesada, C., Linnemann, U., D'lemos, R., Pisarevsky, S.A., 2008. Neoproterozoic-early Palaeozoic tectonostratigraphy and palaeogeography of the peri-Gondwanan terranes: Amazonian v. West African connections. Geological Society, London, Special Publications 297, 345-383.
- Nash, D.J., 1992. The development and environmental significance of dry valley systems (mekgacha) in the Kalahari, central southern Africa. PhD theses, Department of Geography, University of Sheffield.
- Nash, D.J., 2015. Of dunes, depressions and dry valleys: the arid landscapes of the Kalahari desert. In Grab, S., Knight, J. (Eds) Landscapes and Landforms of South Africa. Springer, 129-137.
- Nash, D.J., and Endfield, G.H., 2002. Historical flows in the dry valleys of the Kalahari identified from missionary correspondence. South African Journal of Science 98, 244–248.
- Nash, D.J., Thomas, D.S.G., Shaw, P.A., 1994a. Timescales, environmental change and dryland valley development. In: Millington AC, Pye K (eds.) Environmental Change in Drylands. John Wiley, Chichester, p. 25–41.
- Nash, D.J., Shaw, P.A., Thomas, D.S.G., 1994b. Duricrust development and valley evolution: process-landform links in the Kalahari. Earth Surf Proc Land 19: 299-317. https://doi.org/10.1002/esp.3290190403
- Nechaev, V. P., and Isphording, W. C. 1993. Heavy mineral assemblages of continental margins as indicators of plate-tectonic environments. J. Sediment. Petrol. 63:1110–1117.
- Nesbitt, H. W., and Young, G. M. 1982. Early Proterozoic climates and plate motions inferred from major element chemistry of lutites. Nature 299:715–717.
- Nicholson, S.E., 1996. A review of climate dynamics and climate variability in eastern Africa. In: Johnson, T.C., Odada, E.O. (Eds.), The Limnology, Climatology and Palaeoclimatology of the East African Lakes. Gordon and Breach, Amsterdam, pp. 25–56.
- Nicholson, S.E., Flohn, H., 1980. African environmental and climatic changes and the general atmospheric circulation in late Pleistocene and Holocene. Climatic change 2, 313-348.
- Nie, J., Stevens, T., Rittner, M., Stockli, D., Garzanti, E., Limonta, M., Bird, A., Andò, S., Vermeesch, P., Saylor, J., Lu, H., Breecker, D., Hu, X., Liu, S., Resentini, A., Vezzoli, G., Peng, W., Carter, A., Ji, S., Pan, B., 2015. Loess Plateau storage of Northeastern Tibetan Plateau-derived Yellow River sediment. Nature Communications, 6, DOI: 10.1038/ncomms9511.
- Nugent, C. 1990. The Zambezi River: tectonism, climatic change, and drainage evolution. Palaeogeogr. Palaeoclimatol. Palaeoecol. 78:55–69.
- Nyambe, I. A. 1999. Tectonic and climatic controls on sedimentation during deposition of the Sinakumbe Group and Karoo Supergroup, in the mid-Zambezi Valley Basin, southern Zambia. J. Afr. Earth Sci. 28(2):443–463.
- Nyambe, I. A., and Utting, J. 1997. Stratigraphy and palynostratigraphy, Karoo Supergroup (Permian and Triassic), Mid-Zambezi Valley, southern Zambia. S. Afr. J. Geol. 24:563–583.
- O'Connor, P. W., and Thomas, D. S. G. 1999. The timing and environmental significance of late Quaternary linear dune development in western Zambia. Quat. Res. 52:44–55.
- Odom, I. E.; Doe, T. W.; and Dott, R. H. 1976. Nature of feldspar-grain size relations in some quartz-rich sandstones. J. Sediment. Petrol. 46(4):862–870.
- Pachur, H.J., Kröpelin, S., 1987. Wadi Howar: Paleoclimatic evidence from an extinct river system in the southeastern Sahara. Science 237, 298-300.
- Pang, H., Pan, B., Garzanti, E., Gao, H., Zhao, X., Chen, D., 2018. Mineralogy and geochemistry of modern Yellow River sediments: Implications for weathering and provenance. Chemical Geology, 488, 76-86.
- Parker, A. 1970. An index of weathering for silicate rocks. Geol. Mag. 107:501–504.

- Partridge, T. C., and Maud, R. R. 1987. Geomorphic evolution of southern Africa since the Mesozoic. S. Afr. J. Geol. 90(2):179–208.
- Pastore, G., Baird, T., Vermeesch, P., Resentini, A. and Garzanti, E., 2021. Provenance and recycling of Sahara Desert sand. Earth-Science Reviews, 216, 103606.
- Pickering, R., Hanock, P. J., Lee-Thopr, J.A., Grün, R., Mortimer, G.E., McCulloch, M., Berger, L.R., 2007. Stratigraphy, U-Th chronology, and paleoenvironments at Gladysvale Cave: insights into the climatic control of South African hominin-bearing cave deposits. Journal of Human Evolution 53, 602-619.
- Pinna, P., Calvez, J.Y., Abessolo, A., Angel, J.M., Mekoulou- Mekoulou, T., Mananga, G., Vernhet, Y., 1994. Neoproterozoic events in Tchollire area: Pan-African crustal growth and geodynamics in central-northern Cameroon (Adamawa and North Provinces). Journal African Earth Sciences 18, 347-353.
- Ponte, J. P.; Robin, C.; Guillocheau, F.; Popescu, S.; Suc, J. P.; Dall'Asta, M.; Melinte-Dobrinescu, M. C.; Bubik, M.; Dupont, G.; and Gaillot, J. 2019. The Zambezi delta (Mozambique Channel, East Africa): high resolution dating combining bio-orbital and seismic stratigraphies to determine climate (palaeoprecipitation) and tectonic controls on a passive margin. Mar. Pet. Geol. 105:293–312.
- Potter, P. E. 1978. Petrology and chemistry of modern big river sands. J. Geol. 86:423–449.
- Price, J. R., and Velbel, M. A. 2003. Chemical weathering indices applied to weathering profiles developed on heterogeneous felsic metamorphic parent rocks. Chem. Geol. 202(3–4):397–416.
- Prospero, J.M., 1996. Saharan dust transport over the North Atlantic Ocean and Mediterranean: An overview. In: Guerzoni, S., Chester, R. (eds.), The impact of desert dust across the Mediterranean. Springer, Dordrecht, 133-151.
- Pye, K., Tsoar, H., 2008. Aeolian sand and sand dunes. Springer Science & Business Media.
- Range, P., 1912. Topography and geology of the German South Kalahari. Trans Geol Soc South Africa 15, 63–73.
- Reason, C. J. C.; Landman, W.; and Tennant, W. 2006. Seasonal to decadal prediction of southern African climate and its links with variability of the Atlantic Ocean. Bull. Am. Meteorol. Soc. 87(7):941–955.
- Reason, C.J.C., 2001. Evidence for the influence of the Agulhas current on regional atmospheric circulation patterns. Journal of Climate 14, 2769–2778.
- Resentini, A.; Goren, L.; Castelltort, S.; and Garzanti, E. 2017. Partitioning sediment flux by provenance and tracing erosion patterns in Taiwan. J. Geophys. Res. Earth Surf. 122(7):1430–1454.
- Resentini, A., Andò, S., and Garzanti, E., 2018. Quantifying roundness of detrital minerals by image analysis: Sediment transport, shape effects, and provenance implications. Journal of Sedimentary Research, 88(2), 276-289.
- Resentini, A.; Andò, S.; Garzanti, E.; Malusà, M. G.; Pastore, G.; Vermeesch, P.; Chanvry, E.; and Dall'Asta, M. 2020. Zircon as a provenance tracer: coupling Raman spectroscopy and U-Pb geochronology in source-to-sink studies. Chem. Geol. 555:119828.
- Rittenhouse, G. 1943. Transportation and deposition of heavy mineral. Bulletin of the Geological Society of America, 54(12), 1725-1780.
- Rittner, M., Vermeesch, P., Carter, A., Bird, A., Stevens, T., Garzanti, E., Andò, S., Vezzoli, G., Dutt, R., Xu, Z., Lu, H., 2016. The provenance of Taklamakan desert sand. Earth and Planetary Science Letters 437, 127-137.
- Roberts, E. M.; Stevens, N. J.; O'Connor, P. M.; Dirks, P. H. G. M.; Gottfried, M. D.; Clyde, W. C.; Armstrong, R. A.; Kemp, A. I. S.; and Hemming, S. 2012. Initiation of the western branch of the East African Rift coeval with the eastern branch. Nat. Geosci. 5(4):289–294.
- Rogers, J., Bremner, J.M., 1991. The Benguela Ecosystem. Part VII. Marine-geological aspects. In: Barnes,

M. (Ed.), Oceanography and marine biology, an annual review, vol. 29. Aberdeen University Press, pp. 1–86.

- Rogers, J.W., Ghuma, M.A., Nagy, R.M., Greenburg, J.K., Fullagar, P.D., 1978. Plutonism in Pan-African belts and the geologic evolution of northeastern Africa. Earth Planetary Science Letters 39, 109–117.
- Romans, B.W., Castelltort, S., Covault, J.A., Fildani, A. and Walsh, J.P., 2016. Environmental signal propagation in sedimentary systems across timescales. Earth-Science Reviews, 153, 7-29.
- Ronco, P.; Fasolato, G.; Nones, M.; and Di Silvio, G. 2010. Morphological effects of damming on lower Zambezi River. Geomorphology 115(1–2):43–55.
- Rubey, W. W. 1933. The size distribution of heavy minerals within a water-laid sandstone. J. Sediment. Petrol. 3(1):3–29.
- Rudnick, R. L., and Gao, S. 2003. Composition of the continental crust. In Rudnick, R. L., ed. The crust. Vol. 3 of Treatise on geochemistry. Amsterdam, Elsevier, p. 1–64.
- Russell, R. D. 1937. Mineral composition of Mississippi River sands. Geol. Soc. Am. Bull. 48:1307–1348.
- Salman, G., and Abdula, I. 1995. Development of the Mozambique and Ruvuma sedimentary basins, offshore Mozambique. Sediment. Geol. 96:7–41.
- Salze, D., Belcourt, O., Harouna, M., 2018. The first stage in the formation of the uranium deposit of Arlit, Niger: Role of a new non-continental organic matter. Ore Geology Reviews 102, 604-617.
- Sarnthein, M., 1978. Sand deserts during glacial maximum and climatic optimum. Nature 272, 43-46.
- Schandelmeier, H., Darbyshire, D.P.F., Harms, U., Richter, A., 1988. The E Saharan craton: Evidence for pre-Pan-African crust in NE Africa W of the Nile. In: El-Gaby, S., Greiling, R.O. (eds.), The Pan-African belts of NE Africa and Adjacent areas. Friedrich Vieweg and Sohn, 69-94.
- Schlegel, G.C.J.; von Harmse, H.J.; and Brunke, O. 1989. Granulometric and mineralogical characteristics of the Kalahari sands of southern Africa. S. Afr. J. Geol. 92:207-222.
- Schlüter, T. 2008. Geological Atlas of Africa. Springer, Heidelberg, 307 p.
- Schüller, I., Blez, L., Wilkes, H., Wehrmann, A., 2018. Late Quaternary shift in southern African rainfall zones: sedimentary and geochemical data from Kalahari pans. Zeitschrift für Geomorphologie 61(4), 339-362.
- Schulz, H.; Lückge, A.; Emeis, K. C.; and Mackensen, A. 2011. Variability of Holocene to late Pleistocene Zambezi riverine sedimentation at the upper continental slope off Mozambique, 157–217S. Mar. Geol. 286:21–34.
- Schulze, B. 1972. South Africa. In: Griffiths, J.W. (ed.), Climates of Africa. Elsevier, Amsterdam, World Survey of Climatology, vol. 10, pp. 501–586.
- Schwanghart, W., and Scherler, D. 2014. TopoToolbox 2—MATLAB-based software for topographic analysis and modeling in Earth surface sciences. Earth Surf. Dyn. 2:1–7. https://doi.org/10.5194/esurf-2-1-2014.
- Selley, R.C., 1997. The sedimentary basins of northwest Africa: Stratigraphy and sedimentation. In: Selley, R.C. (ed.), Sedimentary Basins of the World 3, African Basins. Elsevier, Amsterdam, 3-16.
- Setti, M.; López-Galindo, A.; Padoan, M.; and Garzanti, E. 2014. Clay mineralogy in southern Africa river muds. Clay Miner. 49:717–733.
- Shaw, A. I. 2009. The characterisation of calcrete based on its environmental settings within selected regions of the Kalahari, southern Africa. PhD thesis, University of Oxford, 606 p.
- Shaw, A., and Goudie, A. S. 2002. Geomorphological evidence for the extension of the Mega-Kalahari into south-central Angola. S. Afr. Geogr. J. 84:182–194.

- Shaw, P., and Thomas, D. S. G. 1988. Lake Caprivi: a late Quaternary link between the Zambezi and middle Kalahari drainage. Z. Geomorphol. 32:329–337.
- Shaw, P.A., and de Vries, J.J., 1988. Duricrust, groundwater and valley development in the Kalahari of south-east Botswana. J Arid Environ 14: 245-254.
- Shaw, P.A., Thomas, D.S., and Nash, D.J., 1992. Late Quaternary fluvial activity in the dry valleys (mekgacha) of the Middle and Southern Kalahari, southern Africa. Journal of Quaternary Science, 7(4), 273-281.
- Shukri, N. M. 1950. The mineralogy of some Nile sediments. Q. J. Geol. Soc. Lond. 105:511–534.
- Shvetsov, M. S. 1934. Petrografiya osadochnykh porod [Petrography of sedimentary rocks]. Moscow-Leningrad, Gostoptekhizdat (1948), 387 p.
- Siwedza, S.; Mukonzo, S.; Ngambi, C.; and Shava, S. 2021. Impacts of cyclones Idai and Kenneth and the 2019 floods on the insurance sector in South Africa and Mozambique. In Nhamo, G., and Chapungu, L., eds. The increasing risk of floods and tornadoes in southern Africa (Sustainable Development Goals Ser.). Cham, Springer, p. 157–171. https://doi.org/10.1007/978-3-030-74192-1_9.
- Sláma, J., Košler, J., Condon, D.J., Crowley, J.L., Gerdes, A., Hanchar, J.M., Horstwood, M.S., Morris, G.A., Nasdala, L., Norberg, N., Schaltegger, U., 2008. Plešovice zircon—a new natural reference material for U–Pb and Hf isotopic microanalysis. Chemical Geology 249, 1-35.
- Slingerland, R. (1984). Role of hydraulic sorting in the origin of fluvial placers. Journal of Sedimentary Research, 54(1), 137-150.
- Smith, B.J., Wright, J.S., Whalley, W.B., 2002. Sources of non-glacial, loess-size quartz silt and the origins of "desert loess". Earth-Science Reviews 59, 1-26.
- Söderlund, U.; Hofmann, A.; Klausen, M. B.; Olsson, J. R.; Ernst, R. E.; and Persson, P. O. 2010. Towards a complete magmatic barcode for the Zimbabwe craton: baddeleyite U-Pb dating of regional dolerite dyke swarms and sill complexes. Precambrian Res. 183(3):388–398. Stokes, S.; Haynes, G.; Thomas, D. S. G.; Horrocks,
- Söderlund, U.; Hofmann, A.; Klausen, M. B.; Olsson, J. R.; Ernst, R. E.; and Persson, P. O. 2010. Towards a complete magmatic barcode for the Zimbabwe craton: baddeleyite U-Pb dating of regional dolerite dyke swarms and sill complexes. Precambrian Res. 183 (3):388–398.
- Stanistreet, I.G., Stollhofen, H., 2002. Hoanib River flood deposits of Namib Desert interdunes as analogues for thin permeability barrier mudstone layers in aeolianite reservoirs. Sedimentology 49, 719–736.
- Stern, R.J., 1985. The Najd fault system, Saudi Arabia and Egypt: A late Precambrian rift-related transform system? Tectonics 4, 497-511.
- Stern, R.J., Kröner, A., Reischmann, T., Bender, R., Dawoud, A.S., 1994. Precambrian basement around Wadi Halfa: A new perspective on the evolution of the Central Saharan Ghost craton. Geologische Rundschau 83, 564-577.
- Stevens, T., Carter, A., Watson, T.P., Vermeesch, P., Andò, S., Bird, A.F., Lu, H., Garzanti, E., Cottam, M.A., Sevastjanova, I., 2013. Genetic linkage between the Yellow River, the Mu Us desert and the Chinese Loess Plateau. Quaternary Science Reviews 78, 355-368.
- Stokes, S.; Haynes, G.; Thomas, D.S.G.; Horrocks, J.L.; Higginson, M.; and Malifa, M. 1998. Punctuated aridity in southern Africa during the last glacial cycle: the chronology of linear dune construction in the northeastern Kalahari. Palaeogeogr. Palaeoclim. Palaeoecol. 137:305-322.
- Stone, A., 2021. Dryland dunes and other dryland environmental archives as proxies for Late Quaternary stratigraphy and environmental and climate change in southern Africa. South African Journal of Geology 2021, 124, pp.927-962.
- Stone, A., 2022. Landscape Evolution of the Stampriet Transboundary Basin and Relation to the Groundwater

System: The Land of Duricrusts, Pans, Dry Valleys and Dunes, and the Relation to the Groundwater System. In Landscapes and Landforms of Botswana pp. 201-221.

- Stone, A, and Larsen, J., 2011. The peaks and troughs of dune records: (how much) should we worry about sampling resolution? Quaternary International 279-280 (XVII INQUA Congress 2011), 470.
- Stone, A. and Thomas, D.S.G., 2008. Linear dune accumulation chronologies from the southwest Kalahari, Namibia: challenges of reconstructing late Quaternary palaeoenvironments from aeolian landforms. Quaternary Science Reviews, 27(17-18), 667-1681.
- Stone, A., Bateman, M.D., Burrough, S.L., Garzanti, E., Limonta, M., Radeff, G. and Telfer, M.W., 2019. Using a portable luminescence reader for rapid age assessment of aeolian sediments for reconstructing dunefield landscape evolution in southern Africa. Quaternary Geochronology, 49, pp.57-64.
- Stute, M., and Talma, A.S., 1998. Glacial temperatures and moisture transport regimes reconstructed from noble gases and δ18O, Stampriet aquifer, Namibia. Isotope techniques in the study of environmental change. In: Proceedings of a Symposium, Vienna, April 1997, pp. 307-318.
- Stuut, J.B., Smalley, I. and O'Hara-Dhand, K., 2009. Aeolian dust in Europe: African sources and European deposits. Quaternary International, 198(1-2), 234-245.
- Sutcliffe, J.V., Parks, Y.P., 1999. The Hydrology of the Nile. International Association of Hydrological Sciences, Special Publication 5, 179 p.
- Suttner, L.J., Basu, A., Mack, G.H., 1981. Climate and the origin of quartz arenites. Journal of Sedimentary Petrology 51, 1235–1246.
- Svendsen, J., Stollhofen, H., Krapf, C.B.E., Stanistreet, I.G., 2003. Mass and hyperconcentrated flowdeposits record dune damming and catastrophic breakthrough of ephemeral rivers, Skeleton Coast Erg, Namibia. Sedimentary Geology 160, 7–31.
- Svensen, H.; Corfu, F.; Polteau, S.; Hammer, Ø.; and Planke, S. 2012. Rapid magma emplacement in the Karoo Large Igneous Province. Earth Planet. Sci. Lett. 325/326:1-9.
- Swap, R., Garstang, M., Greco, S., Talbot, R., Kållberg, P., 1992. Saharan dust in the Amazon Basin. Tellus B, 44(2), 133-149.
- Swezey, C., 2001. Eolian sediment responses to late Quaternary climate changes: Temporal and spatial patterns in the Sahara. Palaeogeography, Palaeoclimatology, Palaeoecology 167, 119-155.
- Swezey, C.S., 2009. Cenozoic stratigraphy of the Sahara, northern Africa. Journal of African Earth Sciences, 53, 89-121.
- Tanaka, T.; Togashi, S.; Kamioka, H.; Amakawa, H.; Kagami, H.; Hamamoto, T.; Yuhara, M.; et al. 2000. JNdi-1: a neodymium isotopic reference in consistency with La Jolla neodymium. Chem. Geol. 168(3–4):279–281.
- Taylor, S. R., and McLennan, S. M. 1995. The geochemical evolution of the continental crust. Rev. Geophys. 33:241–265.
- Taylor, S.R., McLennan, S.M., 1995. The geochemical evolution of the continental crust. Rev. Geophys. 33, 241–265.
- Tegen, I., Schepanski, K., Heinold, B., 2013. Comparing two years of Saharan dust source activation obtained by regional modelling and satellite observations. Atmospheric Chemistry and Physics 13(5), 2381–2390.
- Telbisz, T., Keszler, O., 2018. DEM-based morphometry of large-scale sand dune patterns in the Grand Erg Oriental (Northern Sahara Desert, Africa). Arabian Journal of Geosciences 11, 382.
- Telfer, MW., and Thomas, D.S.G., 2006. Complex Holocene lunette dune development, South Africa: Implications for palaeoclimate and models of pan development in arid regions. Geology 34(10), 853-856
- Telfer, M.W., Thomas, D.S.G., Parker, A.G., Walkington, H., Finch, A.A., 2009. Optically Stimulated

Luminescence (OSL) dating and palaeoenvironmental studies of pan (playa) sediment from Witpan, South Africa. Palaeogeography, Palaeoclimatology, Palaeoecology 273, 50–60.

- Thiéblemont, D.; Liégeois, J. P.; Fernandez-Alonso, M.; Ouabadi, A.; Le Gall, B.; Maury, R.; Jalludin, M.; et al. 2016. Geological map of Africa at 1:10M scale. Paris, CGMW-BRGM (Commission for the Geological Map of the World–Bureau de Recherches Géologiques et Minières).
- Thomas, D.S., 1984. Ancient ergs of the former arid zones of Zimbabwe, Zambia, and Angola. Transactions of the Institute of British Geographers, 75-88.
- Thomas, D.S.G., and Burrough, S.L., 2016. Luminescence-based chronologies in southern Africa: Analysis and interpretation of dune database records across the subcontinent. Quaternary International 410(B): 30-45. https://doi.org/10.1016/j.quaint.2013.09.008
- Thomas, D.S.G., and Shaw, P. A. 1988. Late Cainozoic drainage evolution in the Zambezi basin: evidence from the Kalahari rim. J. Afr. Earth Sci. 7:611– 618.
- Thomas, D.S.G. and Shaw, P.A., 1990. The deposition and development of the Kalahari Group sediments, Central Southern Africa. Journal of African Earth Sciences (and the Middle East), 10(1-2), pp.187-197.
- Thomas, D.S.G., and Shaw, P. A. 1991. The Kalahari environment. Cambridge, Cambridge University Press, 284 p.
- Thomas, D.S.G., and Shaw, P. A. 2002. Late Quaternary environmental change in central southern Africa: new data, synthesis, issues and prospects. Quat. Sci. Rev. 21:783–797.
- Thomas, D.S.G.; O'Connor, P. W.; Bateman, M. D.; Shaw, P. A.; Stokes, S.; and Nash, D. J. 2000. Dune activity as a record of late Quaternary aridity in the northern Kalahari: new evidence from northern Namibia interpreted in the context of regional arid and humid chronologies. Palaeogeogr. Palaeoclimatol. Palaeoecol. 156:243–259.
- Thomas, D.S.G., Brook, G., Shaw, P., Bateman, M., Haberyan, K., Appleton, C., Nash, D., McLaren, S., Davies, F., 2003. Late Pleistocene wetting and drying in the NW Kalahari: an integrated study from the Tsodilo Hills, Botswana. Quaternary International 104, 53–67.
- Thomas, D.S.G., Knight, M. and Wiggs, G.F., 2005. Remobilization of southern African desert dune systems by twenty-first century global warming. Nature, 435(7046), 1218-1221.
- Thomas, R.J., Chevallier, L.P., Gresse, P.G., Harmer, R.E., Eglington, B.M., Armstrong, R.A., De Beer, C.H., Martini, J.E.J., De Kock, G.S., Macey, P.H., Ingram, B.A., 2002. Precambrian evolution of the Sirwa window, Anti-Atlas orogen, Morocco. Precambrian Research 118, 1-57.
- Thusu, B., Mansouri, A., 1995. Reassignment of the Upper Amal Formation to Triassic and its implications for exploration in southeast Sirte, Libya. First Symposium on Hydrocarbon Geology of North Africa, London, 28–30 November, Abstracts 48.
- Todd, M.C., Washington, R., Palmer, P.I. 2002. Water vapour transport associated with tropical-temperate trough systems over southern Africa and the Southwest Indian Ocean. Journal of Climate 24,555–568.
- Totten, M. W.; Hanan, M. A.; and Weaver, B. L. 2000. Beyond whole-rock geochemistry of shales: the importance of assessing mineralogic controls for revealing tectonic discriminants of multiple sediment sources for the Ouachita Mountain flysch deposits. Geol. Soc. Am. Bull. 112(7):1012–1022.
- Trumbull, R.B., Harris, C., Frindt, S., Wigand, M., 2004. Oxygen and neodymium isotope evidence for source diversity in Cretaceous anorogenic granites from Namibia and implications for A-type granite genesis. Lithos, 73, 21– 40.
- Tyson, P.D., and Preston-Whyte, R.A., 2000. The Weather and Climate of Southern Africa, 2nd edition. Oxford University Press, Cape Town.
- Tyson, S.J. 1999 Sand ramps or climbing dunes? Identification and palaeoenvironmental significance of aeolian deposits in the southern Kalahari and Breede River Valley, South Africa. MSc Dissertation,

University of Cape Town, 136 p.

- Vainer, S., Dor, Y.B. and Matmon, A., 2018a. Coupling cosmogenic nuclides and luminescence dating into a unified accumulation model of aeolian landforms age and dynamics: The case study of the Kalahari Erg. Quaternary Geochronology, 48,133-144.
- Vainer, S., Erel, Y. and Matmon, A., 2018b. Provenance and depositional environments of Quaternary sediments in the southern Kalahari Basin. Chemical Geology, 476, 352-369.
- Vainer, S., Matmon, A., Erel, Y., Hidy, A.J., Crouvi, O., De Wit, M., Geller, Y. and ASTER Team, 2021. Landscape responses to intraplate deformation in the Kalahari constrained by sediment provenance and chronology in the Okavango Basin. Basin Research, 33(2), pp.1170-1193.
- Vallier, T. L. 1974. Volcanogenic sediments and their relation to landmass volcanism and sea floor-continent movements, western Indian Ocean, Leg 25, Deep Sea Drilling Project. Initial Rep. Deep Sea Drilling Project 25:515–542.
- van der Lubbe, J. (H.) J. L.; Tjallingii, R.; Prins, M. A.; Brummer, G.-J. A.; Jung, S. J. A.; Kroon, D.; and Schneider, R. R. 2014. Sedimentation patterns off the Zambezi River over the last 20,000 years. Mar. Geol. 355:189–201.
- van der Lubbe, J. J. L.; Tjallingii, R.; Prins, M. A.; Brummer, G. J. A.; Jung, S. J. A.; Kroon, D.; and Schneider, R. R. 2014. Sedimentation patterns off the Zambezi River over the last 20,000 years. Mar. Geol. 355:189–201.
- van der Lubbe, H. J. L.; Frank, M.; Tjallingii, R.; and Schneider, R. R. 2016. Neodymium isotope constraints on provenance, dispersal, and climate-driven supply of Zambezi sediments along the Mozambique Margin during the past ~45,000 years. Geochem. Geophys. Geosyst. 17(1):181–198.
- Van Loon, A. T., and Mange, M. A. 2007. "In situ" dissolution of heavy minerals through extreme weathering, and the application of the surviving assemblages and their dissolution characteristics to correlation of Dutch and German silver sands. In Mange, M. A., and Wright, D. T., eds. Heavy minerals in use (Dev. Sedimentol., vol. 58). Amsterdam, Elsevier, p. 189–213.
- Van Rensburg, H.J., 1971. Range ecology in Botswana. Vegetation studies in connection with vegetation/soil correlation and bush encroachment investigations. FAO Technical Document No. 2 UNDP/SF/359/(BOT.1), Rome.
- Van Veelen, M., Baker, T., Mulale, K., Bron, A., Fanta, A., Jonker, V., Mullins, W., Shoeman, H., 2009. Feasibility Study of the Potential for Sustainable Water Resources Development in the Molopo-Nossob Watercourse. ILISO Consulting LTD Project no 700192, 106 p.
- Velbel, M. A. 2007. Surface textures and dissolution processes of heavy minerals in the sedimentary cycle: examples from pyroxenes and amphiboles. In Mange, M. A., and Wright, D. T., eds. Heavy minerals in use (Dev. Sedimentol., vol. 58). Amsterdam, Elsevier, p. 113– 150.
- Velde, B. 1995. Origin and mineralogy of clays. Berlin, Springer.
- Velde, B., and Meunier, A. 2008. The origin of clay minerals in soils and weathered rocks. Berlin, Springer, 405 p.
- Vermeesch, P. 2012. On the visualisation of detrital age distributions. Chem. Geol. 312–313:190–194.
- Vermeesch, P., 2013. Multi-sample comparison of detrital age distributions. Chemical Geology 341, 140-146.
- Vermeesch, P., 2018a. IsoplotR: A free and open toolbox for geochronology. Geoscience Frontiers 9, 1479-1493.
- Vermeesch, P., 2018b. Dissimilarity measures in detrital geochronology. Earth-Science Reviews, 178, 310-321.Statistical models for point-counting data. Earth and Planetary Science Letters 501, 112-118.

- Vermeesch, P., 2021. On the treatment of discordant detrital zircon U–Pb data. Geochronology Discussions, 1-19. doi.org/10.5194/gchron-2020-38.
- Vermeesch, P., and Garzanti, E., 2015. Making geological sense of 'Big Data' in sedimentary provenance analysis. Chem. Geol. 409:20–27.
- Vermeesch, P., Resentini, A., Garzanti, E., 2016. An R package for statistical provenance analysis. Sedimentary Geology, 336, 14-25.
- Vermeesch, P., Rittner, M., Petrou, E., Omma, J., Mattinson, C., Garzanti, E., 2017. High throughput petrochronology and sedimentary provenance analysis by automated phase mapping and LAICPMS. Geochemistry, Geophysics, Geosystems 18, doi.org/10.1002/2017GC007109.
- Vezzoli, G.; Garzanti, E.; Limonta, M.; Andò, S.; and Yang, S. 2016. Erosion patterns in the Changjiang (Yangtze River) catchment revealed by bulk-sample versus single-mineral provenance budgets. Geomorphology 261:177–192.
- Vigaud, N., Richard, Y., Rouault, M., Fauchereau, N., 2009. Moisture transport between the South Atlantic Ocean and southern Africa: relationships with summer rainfall and associated dynamics. Climate Dynamics 32, 113-123.
- Villeneuve, M., 2008. Review of the orogenic belts on the western side of the West African craton: Tthe Bassarides, Rokelides and Mauritanides. Geological Society, London, Special Publications 297, 169-201.
- von Eynatten, H.; Pawlowsky-Glahn, V.; and Egozcue, J. J. 2002. Understanding perturbation on the simplex: a simple method to better visualise and interpret compositional data in ternary diagrams. Math. Geol. 34:249–257.
- von Eynatten, H.; Barcelò-Vidal, C.; and PawlowskyGlahn, V. 2003. Composition and discrimination of sandstones: a statistical evaluation of different analytical methods. J. Sediment. Res. 73(1):47–57.
- von Eynatten, H.; Tolosana-Delgado, R.; and Karius, V. 2012. Sediment generation in modern glacial settings: grain-size and source-rock control on sediment composition. Sediment. Geol. 280:80–92.
- von Eynatten, H.; Tolosana-Delgado, R.; Karius, V.; Bachmann, K.; and Caracciolo, L. 2016. Sediment generation in humid Mediterranean setting: grainsize and source-rock control on sediment geochemistry and mineralogy (Sila Massif, Calabria). Sediment. Geol. 336:68–80.
- Vörösmarty, C. J., and Moore, B. M., III. 1991. Modeling basin-scale hydrology in support of physical climate and global biogeochemical studies: an example using the Zambezi River. Surv. Geophys. 12(1–3):271–311.
- Walford, H. L.; White, N. J.; and Sydow, J. C. 2005. Solid sediment load history of the Zambezi Delta. Earth Planet. Sci. Lett. 238(1–2):49–63.
- Walker, N., 1990. Links between South African summer rainfall and temperature variability of the Agulhas and Benguela current systems. Journal of Geophysical Research 95, 3297–3319.
- Wang, Q., Spencer, C.J., Hamdidouche, R., Zhao, G., Evans, N.J., McDonald, B.J., 2020. Detrital zircon U–Pb–Hf data from Cambrian sandstones of the Ougarta Mountains Algeria: Implication for palaeoenvironment. Geological Journal 55(12), 7760-7774.
- Warner, T.T., 2009. Desert Meteorology. Cambridge University Press, 620 p.
- Washington, R., and Preston, A., 2006. Extreme wet years over southern Africa: role of Indian Ocean sea surface temperatures. Journal of Geophysical Research 111 doi:10.1029/2005JD006724
- Wellington, J. 1955. Southern Africa: a geographical study. Vol. 1. Physical geography, climate, vegetation and soils: hydrography. Cambridge, Cambridge University Press, 528 p.
- Weltje, G. J. 1997. End-member modeling of compositional data: numerical-statistical algorithms for solving the explicit mixing problem. Math. Geol. 29(4):503–549.
- Westerhof, A. P.; Lehtonen, M. I.; Mäkitie, H.; Manninen, T.; Pekkala, Y.; Gustafsson, B.; and Tahon, A.

2008. The Tete-Chipata Belt: a new multiple terrane element from western Mozambique and southern Zambia. In Pekkala, Y.; Lehto, T.; and Mäkitie, H., eds. GTK Consortium geological surveys in Mozambique 2002–2007. Geol. Surv. Finl. Spec. Pap. 48:145–166. Wilson, M. J. 1999. The origin and formation of clay minerals in soils: past, present and future perspectives. Clay Miner. 34(1):7–25.

- Whipple, K. X. 2004. Bedrock rivers and the geomorphology of active orogens. Annu. Rev. Earth Planet. Sci. 32:151–185.
- White, K., Bullard, J., Livingstone, I., Moran, L., 2015. A morphometric comparison of the Namib and southwest Kalahari dunefields using ASTER GDEM data. Aeolian Reserch 19, part A, 87-95.
- Wiggs, G.F., Livingstone, I., Thomas, D.S. and Bullard, J.E., 1996. Airflow and roughness characteristics over partially vegetated linear dunes in the southwest Kalahari Desert. Earth Surface Processes and Landforms, 21(1), pp.19-34.
- Wildman, M., Gallagher, K., Chew, D., & Carter, A., 2021. From sink to source: Using offshore thermochronometric data to extract onshore erosion signals in Namibia. Basin Research, 33(2), 1580-1602.
- Wilson, I.G., 1971. Desert sandflow basins and a model for the development of ergs. Geographical Journal 137(2), 180-199.
- Wittmann, H., Oelze, M., Gaillardet, J., Garzanti, E., von Blanckenburg, F., 2020. A global rate of denudation from cosmogenic nuclides in the Earth's largest rivers. Earth-Science Reviews, 204, 103147.
- Zeh, A.; Gerdes, A.; Klemd, R.; and Barton, J.M. 2007. Archaean to Proterozoic crustal evolution in the Central Zone of the Limpopo Belt (South Africa-Botswana): constraints from combined U-Pb and Lu-Hf Isotope analyses of zircon. J. Petrol. 48:1605-1639.
- Zhang, D., Narteau, C., Rozier, O., Du Pont, S.C., 2012. Morphology and dynamics of star dunes from numerical modelling. Nature Geoscience, 5(7), 463-467.
- Zindorf, M.; Rooze, J.; Meille, C.; März, C.; Jouet, G.; Newton, R.; Brandily, C.; and Pastor, L. 2021. The evolution of early diagenetic processes at the Mozambique margin during the last glacial-interglacial transition. Geochim. Cosmochim. Acta 300:9–94.
- Zuffa, G.G., 1985. Optical analyses of arenites: influence of methodology on compositional results In: Zuffa, G.G. (ed.), Provenance of Arenites. Reidel, Dordrecht, NATO ASI Series 148, 165-189.

Appendix

For this work of thesis, a large number of datasets have been produced, each containing a large number of data. For this purpose, all the datasets are stored in a Google Drive folder, together with all the file of the Figures in high resolution and the excel file of the Tables:

https://drive.google.com/drive/folders/1aOyU9DB1ZBpWYN2w4E3d3iwb6jfD_BRx?usp=sharing

List of files in the folder:

Chapter 3: Location of the samples, framework petrography and heavy minerals data, Detrital zircon measures.

Chapter 4: Location of the samples, framework petrography, heavy minerals data and geochemistry data, Detrital zircon measures.

Chapter 6: Location of the samples, framework petrography, heavy minerals data, geochemistry data, clay mineralogy and Nd isotopic data. Detrital zircon measures.

Forward Mixing Calculations

Terrigenous sediments are complex mixtures of single detrital minerals and rock fragments supplied in various proportions by numerous different end-member sources (e.g., rivers or source-rock domains). If the compositional signatures of detritus in each end-member source are known accurately, then the relative contribution of each source (provenance budget) can be quantified mathematically with forward mixing models (Draper and Smith 1981; Weltje, 1997). The forward mixing model calculates a row vector of compositional data (with columns representing variables) as a non-negative linear combination between a matrix of fixed end-member compositions (with rows representing observations and columns representing variables) and a row vector of coefficients representing the proportional contribution of each end member to the observation.

Several assumptions are made to derive a forward model from a series of compositions (Weltje and Prins 2003): 1) the order of the compositional variables or categories is irrelevant (permutation invariance); 2) the observed compositional variation reflects linear mixing or an analogous process with a superposed measurement error; 3) end-member compositions are fixed; 4) end-member compositions are as close as possible to observed compositions. The accuracy of forward-modelling calculations based on integrated

petrographic and heavy-mineral modes depends on how distinct and precisely assessed the end-member signatures of each potential source are. For a detailed illustration of several different practical applications the specifically interested reader is referred to Garzanti et al. (2005, 2007, 2012) and Resentini et al. (2017).

Geological data are often presented in percentages that represent relative contributions of the single variables to a whole (i.e., closed data; Chayes, 1971). This means that the relevant information is contained only in the ratios between variables of the data (i.e., compositions; Pawlowsky-Glahn and Egozcue, 2006). Compositional data are by definition vectors in which each variable (component) is positive, and all components sum to a constant *c*, which is usually chosen as 1 or 100.

The sample space for compositional data with *D* variables is not the real space R^D, but the simplex

S^D (Aitchison, 1986):

$$(1) \qquad S^D = \left\{ x = [x_1, x_2, \ldots\ldots, x_D]; \qquad x_i > 0; \qquad i = 1, 2, \ldots\ldots, D; \qquad \sum_{i=1}^{D} x_i = c \right\}.$$

Karl Pearson (1897) first highlighted problems that arise with the analysis of such compositional datasets. The obvious and natural properties of compositional data are in fact in contradiction with most methods of standard multivariate statistics. Principal-component analysis, for instance, may lead to questionable results if directly applied to compositional data. In order to perform standard statistics, a family of logratio transformations from the simplex to the standard Euclidean space were introduced (Aitchison, 1986; Egozcue et al., 2003; Buccianti et al., 2006).

The forward mixing model (regression model) stipulates a linear relationship between a dependent variable (also called a response variable) and a set of explanatory variables (also called independent variables, or covariates). The relationship is stochastic, in the sense that the model is not exact, but subject to random variation, as expressed in an error term (also called disturbance term).

Let *y* be the row vector of compositional data with *D* columns representing variables, *X* a matrix of end-member compositions with *n* rows representing observations and *D* columns representing variables, and β a row vector of coefficients with $q = n$ columns representing

the proportional contribution of the end members to the observation. In matrix notation, a forward mixing model can be expressed as

(2) $y = \beta X + e.$

The row vector y consists of a non-negative linear combination β of q end-member compositions, and

e is the row vector of errors with D columns representing variables.

In order to solve the linear-regression problem, we must determine an estimation of the row vector β describing a functional linear relation b between a matrix of end-member compositions X and an output row vector y. The solution of equation (2) consists in the calculation of the row vector of coefficients b such that

(3) $\hat{y} = bX,$

where is a row vector of calculated compositional data with D columns representing variables. This equation represents a forward mixing model (or "perfect mixing"). The model parameters are subject to the following non-negativity and constant-sum constraintsDigitare l'equazione qui.

(4) $\sum_{k=1}^{q} b_k = 1, \quad b_k \geq 0,$

(5) $\sum_{j=1}^{D} x_{kj} = 1, \quad x_{kj} \geq 0,$

It follows from equations (4) and (5) that:

(6) $\sum_{j=1}^{D} \hat{y}_j = c, \quad y_j \geq 0,$

And thus:

(7) $\sum_{j=1}^{D} e_j = 0,$

The goodness of fit of the forward mixing model can be assessed by the coefficient of multiple correlation R

(8) $R = \sqrt{1 - (\frac{RSS}{TSS})}$

Where RSS is the residual sum of squares

(9) $RSS = \sum(\hat{y}i - y)^2$

And TSS is the total sum of squares

(10) $TSS = \sum(\hat{y}i - ym)^2$

The coefficient *R* departs from a decomposition of the total sum of squares into the "explained" sum of squares (the sum of squares of predicted values, in deviations from the mean) and the residual sum of squares. *R* is a measure of the extent to which the total variation of the dependent variable is explained by the forward model. The *R* statistic takes on a value between 0 and 1. A value of *R* close to 1, suggesting that the model explains well the variation in the dependent variable, is obviously important if one wishes to use the model for predictive or forecasting purposes.

Reference cited in the Appendix

- Aitchison, J., 1986. The statistical analysis of compositional data. Chapman and Hall, London.
- Buccianti, A., Mateu-Figueras, G., Pawlowsky-Glahn, V. (Eds.), 2006. Compositional Data Analysis in the Geosciences: From Theory to Practice. Geological Society, Special Publications 264, London.
- Chayes, F. (1971). Ratio correlation: A manual for students of petrology and geochemistry. Univ.Chicago Press, Chicago (USA), 99 p.
- Draper, N., Smith, H. 1981. Applied regression analysis (2nd ed.). New York, Wiley, 709 p.
- Egozcue, J. J., Pawlowsky-Glahn, V., Mateu-Figueraz, G., Barceló-Vidal, C., 2003. Isometric logratio transformations for compositional data analysis. Math. Geol. 35, 279-300.
- Garzanti, E., Resentini, A., Vezzoli, G., Andò, S., Malusà, M., Padoan, M., 2012. Forward compositional modelling of Alpine orogenic sediments. Sedimentary Geology 280, 149-164.
- Garzanti, E., Vezzoli, G., Andò, S., Lavé, J., Attal, M., France-Lanord, C., DeCelles, P., 2007. Quantifying sand provenance and erosion (Marsyandi River, Nepal Himalaya). Earth and Planetary Science Letters 258(3-4), 500-515.
- Garzanti, E., Vezzoli, G., Andò, S., Paparella, P., Clift, P.D., 2005. Petrology of Indus River sands: a key to interpret erosion history of the Western Himalayan Syntaxis. Earth and Planetary Science Letters 229(3-4), 287-302.
- Pawlowsky-Glahn, V., Egozcue, J.J., 2006. Compositional data and their analysis: an introduction. In: Buccianti, A., Mateu-Figueras, G., Pawlowsky- Glahn, V. (Eds.), Compositional data analysis in the geosciences: From theory to practice. Geological Society of London Special Publications 264, 1–10.
- Pearson, K., 1897. Mathematical contributions to the theory of evolution. On a form of spurious correlation which may arise when indices are used in the measurement of organs. Proceedings of the Royal Society of London LX, 489–502.

- Resentini, A., Goren, L., Castelltort, S., Garzanti, E., 2017. Partitioning the sediment flux by provenance and tracing erosion patterns in Taiwan. Journal Geophysical Research - Earth Surface 122(7), 1430- 1454.
- Weltje, G.J., 1997. End-member modeling of compositional data: Numerical-statistical algorithms for solving the explicit mixing problem. Mathematical Geology 29(4), 503-549.
- Weltje, G.J., Prins, M.A., 2003. Muddled or mixed? Inferring palaeoclimate from size distributions of deep-sea clastics. Sedimentary Geology 162, 39–62.De Paolo, D.J., 1981. Neodymium isotopes in the Colorado Front Range and crust–mantle evolution in the Proterozoic. Nature 291(5812), 193-196.

Acknowledgments

A large number of people have to be thanked for scientific and personal support in the achievement of this thesis and fulfillment of research years.

Prof. Alberto Resentini, for his relentless and kind supervision of my PhD. Ideas, help, discussions, and support have always been granted to me, and I am very grateful for that.

Prof. Eduardo Garzanti exhorted me to embrace this journey and guided me through the dunes of this "desert tour".

Prof. Pieter Vermeesch, welcoming me in the London geochronology center when I was just a student and revealing to me the exciting science of U-Pb geochronology. Your gentle teaching truly inspired me.

Prof. Sergio Andò, Prof. Giovanni Vezzoli, Prof. Marco Malusà, PhD Mara Limonta, PhD Laura Borromeo, Dr. Marta Barbarano and Dr. Muhammad Usman and all the people working for the Laboratory for Provenance study. I am grateful to be introduced to the love of sand and minerals, how much I could learn form a handful of sand to "see a world in a grain of sand"

Many scientific friends worked with me for this thesis. PhD Thomas Baird and Prof. Charles Bristow accompanied me in the Sahara, PhD Shlomy Vainer and Prof. Abi Stone joined for the Kalahari tour. Prof. Helena Van Niekerk, Dr. Lindani Ncube, Prof. Gwenael Jouet, Prof. Germain Bayon and Prof. Pedro Dinis sailed the perilous water of Zambezi River with me.

Prof. Andrew Carter and PhD. Chris Mark, who kindly reviewed this work of thesis, providing suggestive hints and advice for the improvement of the manuscript.

Many thanks to all the students and PhD students at University Milano-Bicocca and University College London, with whom great discussion improved these years.

In conclusion, I am grateful to my friend and family who tolerated and supported me during my studies, and patiently listened to my endless lectures about dune sand.